

Fabrizio Rama

**MODELO CONCEITUAL DA HIDRODINÂMICA DO
TRANSPORTE DE GASOLINA E ETANOL
EM UM AQUÍFERO COSTEIRO RASO**

Tese submetida ao Programa de Pós-graduação em Engenharia Ambiental da Universidade Federal de Santa Catarina para a obtenção do Grau de Doutor em Engenharia Ambiental.

Orientador:
Prof. Dr. Konrad Miotlinski
Coorientador:
Prof. Dr. Henry X. Corseuil
Coorientador:
Prof. Dr. Nilson Guiguer

Florianópolis
2019

Ficha de identificação da obra elaborada pelo autor
através do Programa de Geração Automática da Biblioteca Universitária
da UFSC.

Rama, Fabrizio

Modelo conceitual da hidrodinâmica do transporte de gasolina e etanol em um aquífero costeiro raso / Fabrizio Rama; orientador, Konrad Miotlinski, coorientador, Henry X. Corseuil, coorientador, Nilson Guiguer, 2019.
257 p.

Tese (doutorado) - Universidade Federal de Santa Catarina, Centro Tecnológico, Programa de Pós Graduação em Engenharia Ambiental, Florianópolis, 2019.

Inclui referências.

1. Engenharia Ambiental. 2. Fluxo subterrâneo. 3. Áreas contaminadas. 4. modelagem numérica. 5. Etanol e BTEX. I. Miotlinski, Konrad. II. Corseuil, Henry X. . III. Guiguer, Nilson IV. Universidade Federal de Santa Catarina. Programa de Pós-Graduação em Engenharia Ambiental. V. Título.

Fabrizio Rama

**MODELO CONCEITUAL DA HIDRODINÂMICA DO
TRANSPORTE DE GASOLINA E ETANOL
EM UM AQUÍFERO COSTEIRO RASO**

Esta Tese foi julgada adequada para obtenção do
Título de “Doutor” e aprovada em sua forma final pelo
Programa de Pós-graduação em Engenharia Ambiental
da Universidade Federal de Santa Catarina

Florianópolis, 28 de março de 2019.

Prof.^a Maria Eliza Nagel Hassemer, Dr.^a
Coordenadora do Curso

Banca Examinadora:

Prof. Konrad Miotlinski Dr.
Orientador
Universidade Federal de
Santa Catarina

Prof. Nilson Guiguer, Dr.
Coorientador
Universidade Federal de
Santa Catarina

Prof.^a Alexandra Rodrigues Finotti,
Dr.^a
Universidade Federal de
Santa Catarina

Prof. Davide Franco, Dr.
Universidade Federal de
Santa Catarina

Prof. Adilson Pinheiro, Dr.
Universidade Regional de Blumenau

Prof. Everton de Oliveira, Dr.
Instituto de Geociências e Ciências
Exatas - UNESP - Rio Claro

Alla mia Patatona, a Don Chisciotte,
ad Asterione e ai bivi della vita.

AGRADECIMENTOS

Condensar em poucas linhas os agradecimentos para todas as pessoas que contribuíram, de forma direta ou indireta, neste trabalho, é tarefa quase impossível e capaz ingrata, porque não faz justiça ao papel de cada um nesta aventura. Vou fazer uma síntese muito parcial esperando conseguir passar para o leitor a imensa gratidão que tenho por todas as pessoas envolvidas.

Começo agradecendo o Prof. Konrad Miotlinski, com quem trilhei os últimos dois anos de doutorado, escrevendo 4 artigos e estreitando um vínculo de amizade independente do trabalho acadêmico. Ele foi importante no meu caminho não somente pelas contribuições de conteúdo, em qualidade de orientador, mas também pela atenção as relações e aos pequenos detalhes cotidianos.

Um pensamento especial vai pra o Prof. Henry X. Corseuil, que foi o responsável por eu estar aqui concluindo este doutorado, mas que por problemas de saúde não conseguiu estar aqui concluindo conosco. Mando um forte abraço de apoio para os desafios que está enfrentando neste momento.

Uma menção particular vai para os coautores dos artigos e trabalhos acadêmicos destes últimos anos: Prof. Davide Franco, Débora Toledo Ramos, Juliana Braun Müller. As suas colaborações foram muito profícuas de um ponto de vista profissional e ricas na perspectiva humana, finalizando em amizades sinceras.

Agradeço à principal fonte patrocinadora desta pesquisa, a Petrobras por todo o suporte financeiro, e à UFSC, cuja estrutura permitiu-me desenvolver este trabalho. Agradeço a todas as instituições que forneceram dados e informações para esta pesquisa (INMET, EPAGRI/CIRAM, INFRAERO, etc.) e aos técnicos da Fazenda da Ressacada (CCA) pela sua ajuda prática nas questões de campo.

Também quero agradecer o meu Coorientador Prof. Nilson Guiguer pela formação inicial sobre Feflow e por facilitar a obtenção da licença de estudante na DHI.

Agradeço aos examinadores formais e informais da tese por disponibilizarem seu tempo para revisar, e, portanto, contribuir no melhoramento dos conteúdos deste trabalho.

Quero também agradecer a todos os colegas e amigos do REMA, que contribuíram neste trabalho com conselhos, colaborações, explicações, ajudas e até com risadas descontraídas no momento do café. Bruna, Karina, Jujú, Marcio, Marilda, Renan e todos os demais, vocês foram muito importantes nos meus dias na Ressacada.

Digo “Obrigado, Gracias, Grazie, Merci” de coração...aos muitos amigos sinceros que nestes 5 anos trilharam comigo partes dos caminhos da ilha, do Brasil, do mundo e da vida. Alguns ainda estão aqui em Florianópolis, outros já viajaram para novos portos e novas aventuras, alguns com certeza estarão na sala “torcendo” por mim, outros estarão acompanhando de longe a defesa, alguns infelizmente nos abandonaram antes do tempo, e com outros vamos festejar esta conclusão de doutorado com comida e bebida. Queria que soubessem que apesar de tudo foram, são e sempre vão ser importantes. Com suas diferenças, peculiaridades e contradições... nas nossas divergências e discussões... vocês enriqueceram meu caminho.

Por fim, quero agradecer aos que representam minhas certezas mais profundas, os amparos mais seguros das tempestades, apesar de eu não gostar muitas vezes de admiti-lo: um agradecimento especial vai a meu pai e minha mãe (“Er Baffo” e “Dux”), longes na geografia, mas próximos no carinho; a meu irmão (“Er Panza” alias “Q”) e Dora; a minha querida vó e meu avô que cuidam de mim há 33 anos; e *dulcis in fundo*, a Martina, companheira, conselheira, alegria infinita e luz da manhã...obrigado por existirem!

*“Considerate la vostra semenza:
fatti non foste a viver come bruti,
ma per seguir virtute e canoscenza”.*

(Divina Commedia - Inferno vv. 118-120)

RESUMO

O entendimento do transporte de contaminantes na subsuperfície é uma das questões científicas mais relevantes das últimas décadas. Derramamentos acidentais de produtos podem dissolver e infiltrar rapidamente na zona vadosa e, ao atingir o aquífero, representar um risco para os recursos hídricos. O ambiente subterrâneo é caracterizado por heterogeneidades em diferentes escalas, forçantes hidrológicas e estresses antrópicos que determinam um campo de fluxo altamente variável. Ao analisar o transporte, esta variabilidade põe uma dificuldade prática na compreensão dos mecanismos ativos e constitui um fator de incerteza na análise das plumas. Dentro da situação descrita, o presente trabalho apresenta uma análise dos fenômenos que determinam o fluxo natural subterrâneo na escala de campo. Simultaneamente, o estudo visa destacar os efeitos deste fluxo variável no transporte irregular de plumas de BTEX e etanol. Por conseguinte, se demonstra que o regime hidráulico local representa uma informação central para a escolha de tecnologias de remediação ou planos de monitoramento nas áreas contaminadas. O caso de estudo, situado em um aquífero costeiro, é caracterizado por um lençol freático raso em um clima subtropical úmido. Assim, o trabalho se destaca por abranger um amplo conjunto de fatores na definição do campo de fluxo natural, como: oscilação periódica de maré, ativação dos canais de drenagem, variação de infiltração e recarga, interconexão hidráulica das áreas alagadas e das lentes suspensas. De um ponto de vista metodológico se integram a revisão crítica de bancos de dados históricos, a coleta de novas informações de campo, e o uso de ferramentas numéricas na compreensão conceitual da hidrogeologia regional e das peculiaridades da circulação subterrânea na escala local. A abordagem estatística proposta nas análises permite gerenciar e correlacionar uma elevada quantidade de dados. Os resultados confirmam a elevada variabilidade do fluxo no tempo e no espaço, destacam o processo de recarga como a principal forçante na flutuação do lençol freático e mostram como o nível hidráulico dos receptores impacta o perfil do lençol freático. Sobretudo o retículo de drenagem superficial, ao se ativar, altera por completo o campo de escoamento local, e representa um termo relevante no balanço hídrico da planície. Ao mesmo tempo, a migração e degradação das plumas de BTEX resultam determinadas pelo conteúdo de etanol na fonte e pelo regime de fluxo local. A análise dos centroides das plumas nos experimentos de campo revela uma componente vertical no transporte que precisa ser considerada no gerenciamento de áreas contaminadas. As principais incertezas nas elaborações apresentadas estão relacionadas à

falta de caracterização detalhada das heterogeneidades geológicas do meio poroso. Concluindo, a importância desta pesquisa se deve a sua duplice utilidade: de um lado destacar metodologias e aplicações inéditas para a ciência (teoria), e por outro descrever processos importantes para tomada de decisões em áreas contaminadas (prática).

Palavras-chave: Áreas contaminadas, BTEX, FEFLOW, flutuações carga hidráulica, fluxo local

ABSTRACT

The understanding of contaminant transport mechanisms in the subsurface represented, in the last decades, a relevant issue for scientific community. Accidental spills of products can quickly dissolve and infiltrate the vadose zone and, upon reaching an aquifer, they pose a risk to water resources. The subsoil environment is characterized by heterogeneities at different scales, transient hydrological and anthropogenic stresses of various types that determine a highly variable natural flow field. When analyzing solute transport, this variability poses a practical difficulty in understanding the active mechanisms at different scales, by the non-scalability of the parameters used to describe the problem, and constitutes a factor of uncertainty in the plume analysis. Thus, the present work focus on analyzing the main phenomena that determine natural groundwater flow at field scale. At the same time, this study aims to highlight the impacts of this variable flow on the transport of BTEX and ethanol plumes, demonstrating how the understanding of the local hydraulic regime represents a central information for the choice of remediation technologies or monitoring plans in contaminated areas. The case study is located in a coastal aquifer, characterized by shallow water table and subject to humid subtropical climate. Thus, the work stands out as covering a wide range of factors in the definition of the natural flow field, such as periodic tidal oscillation, activation of drainage channels, variation of infiltration and recharge, hydraulic interconnection of flooded areas and suspended lenses. The proposed approach integrates critical review of historical databases, collection of new field information, and application of numerical tools in the development of a regional conceptual model that explains the peculiarities of the groundwater circulation occurring at local scale. The results: (i) confirmed the high spatiotemporal variability of groundwater flow at the site, (ii) highlighted recharge process as the main force in the water table fluctuation, and (iii) showed how the hydraulic level of the surface receptors (i.e. sea, river) affects water-table shape. Surface drain network, when activated, completely changes the local flow field, representing a factor worthy of greater attention in future works. Migration and degradation of BTEX compounds are controlled by ethanol content in the source and local hydraulic regime. In addition, the analysis of plume centroids in the field experiments showed a relevant vertical component that should be considered in the management of contaminated areas. The major uncertainties in the analysis are related to the lack of detailed characterization of the geological heterogeneities of the porous medium.

Overall, the research have a twofold utility: (1) highlighting new methods for science to understand dissolved contaminants in the environment (theory), and (2) describing active processes in contaminated areas to support decision-makers and governmental entities (practical).

Keywords: Contaminated sites, BTEX, FEFLOW, water-table level fluctuations, local flow

LISTA DE FIGURAS

Figura 1 – Fluxograma completo do trabalho.....	40
Figura 2 – Detalhe da capa do artigo publicado na revista “ <i>International Journal of Environmental Science and Development</i> ”	43
Figura 3 - Detalhe do artigo publicado na revista “ <i>Hydrogeology Journal</i> ”	44
Figura 4 - Detalhe do artigo publicado online na revista “ <i>Journal of Contaminant Hydrology</i> ”.....	44
Figura 5 - Conceptual sketch of a typical soil transect depicting the main processes within two different groundwater regimes: dry (red) and wet (blue).....	54
Figura 6 - Conceptual sketch of a soil transect with a LNAPL spill.....	65
Figura 7 - Conceptual diagrams illustrating difficulty in establishing and instrumenting representative centerline monitoring in different scenarios	83
Figura 8 - Geographical position of the Ressacada Farm.....	113
Figura 9 – (a) Dendrogram. (b) Box plots. (c) Comparative line to bar plot.	117
Figura 10 - Box plot of drainage-by-month to study the seasonality.....	119
Figura 11 - Box plot of drainage-by-depth in each group of piezometers.	120
Figura 12 - Box plot of D rates organized by time since last rain.	121
Figura 13 - Piezometers best fitting curves	122
Figura 14 - Altitude contour plot (a). Scatter plot of D0 against altitude (b).....	123
Figura 15 - Contour line maps of: D0 (a), Db (b) and 80% decay time (c)..	123
Figura 16 - Results of ANOVA and inference of centered statistically-based typical values for drainage in the Ressacada aquifer.....	124
Figura 17 – Location of study area.....	132
Figura 18 - Conceptual model sketches.....	136
Figura 19 - Comparative plot of raw data (grey lines and diamonds), the Low Pass 33 filter signal (black line), and high frequencies residuals (red line).....	139
Figura 20 - (a) Two-dimensional (2D) finite element model setup. (b) Detailed vertical section of the Experimental Area 3	140
Figura 21 - Ultimate specific yield estimation.....	142

Figura 22 - Comparative bar plot between monthly recharge estimates (light bars) and total precipitation (dark bars).....	143
Figura 23 - Statistics boxplot of estimated recharge ratio (RR)	144
Figura 24 - Combined plot of water level fluctuations in the 51-day period.....	146
Figura 25 - Cumulative groundwater balance: (a) scenario 1, (b) scenario 2.....	147
Figura 26 - 2D model verification plot.	148
Figura 27 - Signal reconstruction by harmonic components of (a) South Bay seawater level monitoring, and the (b) PE03 and (c) PM04 high frequency signal.	149
Figura 28 – Graphical abstract describing how migration and biodegradation may affect decreasing of dissolved mass plot.....	157
Figura 29 - Location of experimental sites.	161
Figura 30 - E85 experiment conceptual sketch	163
Figura 31 - Total dissolved mass (%) over time: (a) ethanol, (b) benzene, and (c) BTEX in E85 and E24 experimental sites.....	168
Figura 32 - Plume centroid migration: (a) bromide, (b) ethanol, and (c) BTEX in E24 and E85 sites.....	169
Figura 33 - Plume centroid position and spreading of (a) bromide, (b) ethanol, and (c) BTEX in E24 and E85 sites.	171
Figura 34 - Violin plot with distribution of bromide (salmon) and ethanol (green) concentrations.....	172
Figura 35 - Time series of average dissolved BTEX, water-table levels (dark and grey lines) and daily accumulated recharge (blue columns) within the first 90 days in the E85 site.	173
Figura 36 - Times series of BTCs along the main direction of groundwater flow .	174
Figura 37 - Time series of BTEX BTC along transversal transect.....	176
Figura 38 - Ethanol (circles) and BTEX (triangle) as total organic carbon (TOC) fractions.....	178
Figura 39 - Total mass decay obtained from plume interpolation.....	178
Figura 40 - Concentration of total bacteria (gene copies g ⁻¹) at the source-zone of E85 experiment.	179
Figura 41 - (A) 16S rRNA gene relative abundance (%) of microbial communities. (B) Microbial community respiration mode and aromatic hydrocarbons degraders relative abundance (%).	180

Figura 42 - Location of Ressacada Farm Site.....	192
Figura 43 - Use of field data and information in the development of a comprehensive conceptual model in the site.	195
Figura 44 - Numerical models describing flow and transport.	202
Figura 45 - (a) Statistics of the calibration process for Model A in steady-state; (b) Detail of flow field modification caused by surface drain network.....	203
Figura 46 - Hydraulic head response in different observation points to tidally-driven boundary fluctuations.	204
Figura 47 - (a) Statistics of the calibration process for Model B in steady-state; (b) Detail of advective particle tracking in the experimental areas.....	206
Figura 48 - 2D model verification plot.....	207
Figura 49 - (a) Transient calibration plot for piezometers in the area; (b) plume transport comparison within experiments MNA_B20 and BAA_B20.	210
Figura 50 - Comparison of density ratio effects on plume fingering.	212
Figura 51 - Comparison of fingers behavior with convective and divergence formulation of ADE solved by FEFLOW.	212
Figura 52 – Comparison of Model D simulation (<i>red solid line</i>) and observed evolution (<i>black dots</i>) of total dissolved mass in the experiment MNA_E85.....	214
Figura 53 - Comparison of conservative plumes dispersion after 490 days with transient (a) and steady (b) head boundary conditions.	215
Figura 54 – (a) 3D sketch of hydrogeological conceptual model. (b) 2D sketch of a soil transect (section O-O').	216

LISTA DE QUADROS

Quadro 1- The two-dimensional FEM model input parameters and conditions	141
Quadro 2 - Required information to develop a complete conceptual model.....	197
Quadro 3 - List of numerical exercises towards conceptual model understanding.	200
Quadro 4 - FEM model input parameters and assumptions.....	200

LISTA DE TABELAS

Tabela 1 – Design details of piezometers included in the study	114
Tabela 2 - Descriptive statistics.....	118
Tabela 3 - Piezometers and their design details (piezometers used as observation point in 2D model are in italic).....	133
Tabela 4 - Comparison between discrete and continuous dataset estimations within the 51-day period.....	144
Tabela 5 - Summary of sensitivity analysis results.....	145
Tabela 6 - Comparative tidal analysis (amplitudes with 95% confidence interval). Values in italic are the relevant components.	150
Tabela 7 - Comparative tidal analysis (phases with 95% confidence interval). Values in italic are the relevant components.	150
Tabela 8 - Groundwater flow characteristics from transient analysis.	170
Tabela 9- Estimation of ethanol, benzene and total BTEX first-order degradation rates, and degradation rates with subtracted transport rates.	177
Tabela 10- Estimation of decay rate of bromide mass and main parameters summary for E85 and E24 sites.	177

LISTA DE ABREVIATURAS E SIGLAS

ABNT	Associação Brasileira de Normas Técnicas
ADE	Equação de Advecção-Dispersão
ANOVA	Análise de variância
ANP	Agência Nacional do Petróleo, Gás Natural e Biocombustíveis
AST	American Society for Testing Materials
B20	Misturas de diesel 80% com biodiesel 20%
B100	Biodiesel 100%
BA_	Bioestimulação
BC	Condições de contorno
BDL	Abaixo dos limites de detecção
bgs	Below ground surface
BTC	Breakthrough Curve (curvas de ruptura)
BTEX	Benzeno, Tolueno, Etilbenzeno e Xilenos (Hidrocarbonetos monoaromáticos)
CCA	Centro de Ciências Agrárias
CDF	Função distribuição cumulativa
CETESB	Companhia de Tecnologia de Saneamento Ambiental do Estado de São Paulo
CIRAM	Centro de informações de recursos ambientais e de hidrometeorologia de Santa Catarina
CPTU	Cone penetration tests
CTC	Centro Tecnológico da UFSC
CV	Volume de controle
DEM	Modelo de elevação digital
DHI	Institute for Water and Environment
DL	Limite de detecção
DNAPL	Dense Non-Aqueous Phase Liquids
DTM	Modelo digital do terreno
E10	Misturas de gasolina 90% com etanol 10%
E24	Misturas de gasolina 76% com etanol 24%
E85	Misturas de gasolina 15% com etanol 85%
E95	Misturas de gasolina 5% com etanol 95%
EPA	Environmental protection agency
EPAGRI	Empresa de Pesquisa Agropecuária e Extensão Rural de Santa Catarina
FEFLOW	Finite Element subsurface Flow (Software)
FEM	Método aos Elementos Finitos
FID	Detector por ionização em chama
FPS	Amostra com fase livre
FPZ	Zona de produto livre
GAC	Gerenciamento de áreas contaminadas

GAMA	Groundwater Ambient Monitoring and Assessment Program
GFEM	FEM padrão baseado em Galerkin
GIS, SIG	Sistema de Informação Geográfica
GNSS	Global Navigation Satellite System
HPA	Hidrocarbonetos poliaromáticos
IBGE	Instituto Brasileiro de Geografia e Estatística
INMET	Instituto Nacional de Meteorologia
IPUF	Instituto de Planejamento Urbano de Florianópolis
LNAPL	Light Non-Aqueous Phase Liquids
LoE	Linhas de evidência
LP33	Filtro passa baixo 33
MADE	Macro-Dispersion Experiment
METAR	Rede de Meteorologia do Comando da Aeronáutica
MNA	Atenuação natural monitorada
MP20	Micropurge Flow Cell
MRC	Master Recession Curve
MTBE	Methyl tertiary-butyl ether
MW	Poço de monitoramento
NA	Não analisado
NaN	Not-a-Number
ND	Não detectado
NS	Nash-Sutcliffe
ORP	Potencial de oxido-redução
PDF	Função densidade de probabilidade
PE	Percent Energy
PEST	Model-Independent Parameter Estimation and Uncertainty Analysis
pH	Escala numérica adimensional para medição da acidez
QUIIME	Quantitative Insights Into Microbial Ecology (Software)
REMA	Núcleo Ressacada de pesquisas em Meio Ambiente
RMSE	Root-mean-square error (Erro quadrático médio)
RR	Recharge Ratio (Taxa de recarga)
SE, SC	Coleta de dados
SGB	Sistema geográfico brasileiro
SIRGAS	Sistema de Referência Geocêntrico para as Américas
SNR	Signal-to-Noise Ratio (Relação sinal-ruído)
SW-GW	Surface water-Groundwater
UFSC	Universidade Federal de Santa Catarina
USEPA	Agência de proteção ambiental dos Estados Unidos
UTM	Universal transversa de Mercator
WGS84	World Geodetic System 1984
WMO	Organização meteorológica mundial
WTF	Water-Table Fluctuation method

LISTA DE SÍMBOLOS

K	$[L \cdot T^{-1}]$	Condutividade hidráulica
k_i	$[L^2]$	Permeabilidade intrínseca
ρ	$[M \cdot L^{-3}]$	Densidade
ρ_w	$[M \cdot L^{-3}]$	Densidade da água
μ	$[M \cdot L^{-1} \cdot T^{-1}]$	Viscosidade dinâmica
η	[-]	Porosidade total
S_y, η_e	[-]	Specific yield (Porosidade efetiva)
S_s	[-]	Specific storage (Armazenamento específico)
S	[-]	Aquifer storativity (Coeficiente de armazenamento)
S_r	[-]	Specific retention ou field capacity (retenção específica)
S_{yu}	[-]	Ultimate specific yield (Porosidade efetiva última)
S_{ya}	[-]	Apparent specific yield (Porosidade efetiva aparente)
α	[L]	Dispersividade
α_L	[L]	Dispersividade longitudinal
α_T	[L]	Dispersividade transversal
α_x	[L]	Dispersividade na direção x
D_h	$[L^2 \cdot T^{-1}]$	Tensor genérico de dispersão hidrodinâmica
D_T	$[L^2 \cdot T^{-1}]$	Coeficiente de dispersão hidrodinâmica transversal
D_{ijk}, D_{ij}	$[L^2 \cdot T^{-1}]$	Tensor de dispersão hidrodinâmica projetado em um sistema cartesiano
D_{mx}	$[L^2 \cdot T^{-1}]$	Coeficiente de macro-dispersão na direção x, incluindo efeitos da advecção e da difusão efetiva
δ	[-]	Raço entre tamanho característico dos grânulos e comprimento dos poros em um meio poroso
l	[L]	Tamanho médio dos grãos
D_d	$[L^2 \cdot T^{-1}]$	Coeficiente de difusão em meio aquoso
D_d^*	$[L^2 \cdot T^{-1}]$	Coeficiente de difusão efetiva
T_x	[-]	Tortuosidade do meio poroso na direção x
v, v_s	$[L \cdot T^{-1}]$	Vetor genérico da velocidade linear de fluxo ou velocidade de escoamento
v_i	$[L \cdot T^{-1}]$	Vetor de velocidade linear projetado em uma direção
\bar{v}	$[L \cdot T^{-1}]$	Velocidade linear média no meio poroso
v_x	$[L \cdot T^{-1}]$	Velocidade linear de fluxo na direção x
h	[L]	Carga hidráulica
z	[L]	Altitude ou elevação
p	$[M \cdot L^{-1} \cdot T^{-2}]$	Pressão
ψ_w	[L]	Cabeça de pressão
θ_w	[-]	Conteúdo de umidade ou água
α	[-]	Parâmetro empírico do modelo de umidade (Van Genuchten)

n	[-]	Parâmetro empírico do modelo de umidade (modelo de Van Genuchten)
Δh	[L]	Variação do nível ou carga
Δt	[T]	Variação de tempo
D	[L·T ⁻¹]	Termo de descarga usada no WTF
D_b	[L·T ⁻¹]	Taxa de rebaixamento basal do lençol freático
D_0	[L·T ⁻¹]	Taxa inicial de rebaixamento do lençol freático
D_m	[L·T ⁻¹]	Taxa de rebaixamento média do lençol freático
τ	[T ⁻¹]	Tempo de amortecimento da perturbação
R	[L]	Recarga
RR	[-]	Recharge ratio (Taxa de recarga)
P	[L]	Precipitação acumulada
P_d	[L]	Precipitação acumulada diária
d	[L]	Profundidade do lençol freático
f		Fase
i		Espécie
C	[M·L ⁻³]	Concentração
C_s	[M·L ⁻³]	Concentração de fonte ou sumidouro
q	[L·T ⁻¹]	Taxa de fluxo genérico
q_s	[L·T ⁻¹]	Vazão específica de fonte ou sumidouro
λ	[T ⁻¹]	Coefficiente de degradação de primeira ordem
R_d	[-]	Coefficiente de retardo
s	[M·L ⁻³]	Solubilidade
s_m	[M·L ⁻³]	Solubilidade do composto na mistura
s_w	[M·L ⁻³]	Solubilidade do composto em água
f	[-]	Fração volumétrica do cossolvente
σ	[M·L ⁻³]	Energia de cossolvência
M	[M]	Massa total
t	[T]	Tempo
CV	[L ³]	Volume de controle
UV	[L ³]	Unidade de volume
Pe	[-]	Número de Péclet
Ra	[-]	Número de Rayleigh

SUMÁRIO

1	INTRODUÇÃO	27
1.1	HIPÓTESES	36
1.2	OBJETIVOS	37
1.2.1	Objetivo geral.....	37
1.2.2	Objetivos específicos.....	37
2	ESTRUTURA METODOLOGICA DA DISSERTAÇÃO	39
3	PUBLICAÇÕES	47
3.1	SOLUTE TRANSPORT IN A SPATIALLY AND TEMPORALLY VARIABLE FLOW FIELD: A REVIEW	47
3.1.1	Introduction	49
3.1.2	Factors controlling groundwater flow and solute transport	51
3.1.2.1	Geological	51
3.1.2.2	Hydrological	53
3.1.2.3	Anthropogenic	61
3.1.3	Processes of dissolved solute transport	66
3.1.3.1	Advection and dispersion	66
3.1.3.2	Diffusion.....	70
3.1.4	Physicochemical processes in the shallow subsurface.....	71
3.1.4.1	Dissolution and solubilization	71
3.1.4.2	Volatilization	72
3.1.4.3	Sorption and ion exchange.....	73
3.1.4.4	Degradation	74
3.1.4.5	Additional considerations on NAPL transport	74
3.1.5	Mathematical formulation	75
3.1.5.1	Groundwater flow and solute transport formulas.....	75
3.1.5.2	Hydrodynamic dispersion tensor	79
3.1.6	Flow and process characterization.....	80
3.1.6.1	Modelling conceptualization and execution	80
3.1.6.2	Prospection methods.....	81
3.1.6.3	Site instrumentation	82
3.1.6.4	Groundwater – surface water interactions	84
3.1.6.5	Remaining uncertainties in NAPL characterization	85
3.1.7	Conclusions	87

3.2	SPATIAL AND TEMPORAL ANALYSIS OF NATURAL DRAINAGE IN THE RESSACADA AQUIFER (FLORIANOPOLIS, BRAZIL).....	109
3.2.1	Introduction.....	111
3.2.2	Materials and methods	112
3.2.3	Results.....	116
3.2.4	Conclusion	125
3.3	RECHARGE ESTIMATION FROM DISCRETE WATER-TABLE DATASETS IN A COASTAL SHALLOW AQUIFER IN A HUMID SUBTROPICAL CLIMATE	127
3.3.1	Introduction.....	129
3.3.2	Site description	131
3.3.3	Materials and methods	133
3.3.3.1	Methodology	133
3.3.3.1.1	<i>Discrete-series approach</i>	<i>135</i>
3.3.3.1.2	<i>Continuous analysis and tidal frequency analysis</i>	<i>138</i>
3.3.3.1.3	<i>Numerical FEM model.....</i>	<i>139</i>
3.3.4	Results and discussion	142
3.3.4.1	Recharge estimation: discrete and continuous approach to WTF.....	142
3.3.4.2	Integration of WTF results into the FEM model	145
3.3.4.3	Tidal influence assessment.....	148
3.3.5	Conclusions.....	151
3.4	FLOW FIELD DYNAMICS AND HIGH ETHANOL CONTENT IN GASOHOL BLENDS ENHANCE BTEX MIGRATION AND BIODEGRADATION IN GROUNDWATER	155
3.4.1	Introduction.....	158
3.4.2	Materials and Methods	160
3.4.2.1	Site description.....	160
3.4.2.2	E85 field experiment.....	162
3.4.2.3	Physical and geochemical analysis.....	163
3.4.2.4	Microbial Analysis.....	164
3.4.2.5	Hydrogeological and statistical data processing.....	165
3.4.3	Results and Discussion.....	167
3.4.3.1	Centroid analysis, plume migration and groundwater flow field	167
3.4.3.2	Geochemical footprint of E85 release	171
3.4.3.3	Ethanol and BTEX degradation kinetics	176
3.4.4	Conclusions.....	181

3.5	NUMERICAL MODELLING AS A TOOL TO DEVELOP A CONCEPTUAL HYDROGEOLOGICAL MODEL.....	187
3.5.1	Introduction	189
3.5.2	Methodology.....	191
3.5.2.1	Site description	191
3.5.2.2	Field experiment and monitoring.....	193
3.5.2.3	Groundwater modeling.....	198
3.5.3	Results and discussion	199
3.5.3.1	Model A.....	202
3.5.3.2	Model B.....	205
3.5.3.3	Model C1.....	206
3.5.3.4	Model C2.....	208
3.5.3.5	Model Z.....	210
3.5.3.6	Model D.....	213
3.5.3.7	Hydrogeological conceptual model of Ressacada Aquifer	216
3.5.4	Conclusions	218
4	PRINCIPAIS CONTRIBUIÇÕES	225
5	CONCLUSÕES.....	229
	REFERÊNCIAS	233
	APÊNDICE A – Electronic supplementary material – Recharge estimation from discrete water-table datasets in a coastal shallow aquifer in a humid subtropical climate.....	241
	APÊNDICE B – Supporting Information - Flow field dynamics and high ethanol content in gasohol blends enhance BTEX migration and biodegradation in groundwater.....	244
	APÊNDICE C – Supporting Material - Numerical modelling as a tool to develop a conceptual hydrogeological model	250

1 INTRODUÇÃO

A questão da contaminação do solo e das águas subterrâneas é objeto de grande preocupação nas últimas décadas. A causa desta preocupação é que a maioria dos recursos hídricos de boa qualidade em estado líquido no planeta é proveniente de águas subterrâneas. Mundialmente, o abastecimento para consumo humano depende predominantemente dos aquíferos, sendo que em muitas regiões até 99% da população é abastecida por reservas de águas subterrâneas (WILSON et al., 2013). Assim, eventuais contaminações do solo se traduzem diretamente em graves riscos para a saúde pública. Tendo como objetivo minimizar os danos à população e ao ambiente causados pela existência de áreas contaminadas, os órgãos que possuem a atribuição de administrar os problemas ambientais, devem desenvolver soluções que assegurem o conhecimento das características e dos efeitos das contaminações, a aplicação de instrumentos necessários à tomada de decisão e a definição de medidas e níveis de intervenção adequados (CETESB, 2016). Nos EUA e na Europa as pesquisas sobre transporte de contaminantes em ambiente subterrâneo começaram nos anos 60 e 70, com a definição de conceitos gerais do transporte em meio poroso como dispersão hidrodinâmica, frente da pluma e tempo de chegada (GREEN et al. 1970; BACHMAT; BEAR, 1964; NELSON et al. 1978). No Brasil, a atenção às questões ambientais cresceu na década de 90 e anos 2000, culminando em 2009 na Resolução CONAMA 420, que determina a qualidade do solo em relação a presença de substâncias químicas (CONAMA 420, 2009).

Apesar das fontes poluidoras dos aquíferos estarem ligadas a distintas atividades produtivas (GROUNDWATER FOUNDATION, 2018), neste trabalho foi considerado exclusivamente o setor de petróleo e derivados devido à crescente demanda de combustíveis fósseis e biocombustíveis. Uma vasta literatura foi produzida sobre derivados do petróleo e compostos adicionados nos combustíveis, investigando as possíveis interações recíprocas e os principais efeitos no meio ambiente (CORSEUIL et al., 1998; POWERS et al., 2001; D’AFFONSECA et al. 2008). Particular atenção foi destinada à contaminação dos recursos hídricos devida ao derramamento de combustíveis automotivos (gasolina, diesel), compostos orgânicos móveis, persistentes e tóxicos. Tais produtos são retidos no solo em fase livre (CONAMA 420, 2009), sendo conhecidos como “Light Non-Aqueous Phase Liquids” (LNAPLs) porque apresentam densidades menores da água. Visto a natureza oleosa (alta viscosidade) os LNAPLs migram com dificuldade através dos poros, filtrando verticalmente na zona vadosa como fase livre. Ao atingir o

lençol freático se espalham horizontalmente, de forma irregular, fluuando na parte superior do aquífero e sofrendo os processos de volatilização e dissolução na água subterrânea. Assim, os derramamentos de LNAPLs configuram efeitos negativos para a saúde tanto pelo contato direto, como pela transferência e migração de seus componentes solúveis e voláteis (KAO; WANG, 2001; MCCRAY et al. 2011; BARRY et al., 2002). Dentre os compostos orgânicos procedentes dos derramamentos de LNAPLs, os hidrocarbonetos monoaromáticos (Benzeno, Tolueno, Etilbenzeno e Xilenos - BTEX) e os hidrocarbonetos policíclicos aromáticos (HPA) são os mais amplamente estudados e de principal interesse ambiental, pois possuem maior solubilidade em água, são recalcitrantes e carcinogênicos (SCHIRMER; BUTLER, 2004; LAPINSKIENE; MARTINKUS; REBŽDAITE, 2006). Recentemente, o etanol e biodiesel vêm recebendo mais atenção científica por serem adicionados em percentagens cada vez maiores nos combustíveis fósseis e por impactar o comportamento dos hidrocarbonetos aromáticos no ambiente. Por exemplo, no Brasil, atualmente, há a obrigatoriedade de adição de 10% de biodiesel ao diesel comercial e de 27% de etanol anidro à gasolina (ANP-BMQP, 2018).

Os problemas de vazamentos de LNAPLs em ambiente subterrâneo decorrem principalmente de falhas nos sistemas de armazenamento e distribuição de combustíveis, assim como dos poços de extração e das linhas de distribuição do óleo (ESSAID; BEKINS; COZZARELLI, 2015). Portanto, fontes potenciais de contaminação dos recursos hídricos encontram-se distribuídas em todo o território, desde os terminais aquaviários e petroquímicos nas áreas costeiras que possuem tanques de armazenamento superficial, até os revendedores varejistas de combustíveis (postos de abastecimento) que usam tanques enterrados permanentemente. A maioria destes tanques sofre algum acidente ou ruptura ao longo de sua vida útil, resultando em derramamentos pontuais de combustíveis. Em inglês se usa o acrônimo LUSTs (“leaking underground storage tanks”) para indicar este problema. As reservas mais expostas a este tipo de contaminação são os aquíferos não confinados e superficiais, geralmente em contato com a zona vadosa (não saturada), local onde estes tanques estão instalados. Nos EUA, estima-se a existência de 111.583 revendedores varejistas (US CENSUS BUREAU, 2014) com cerca de 600.000 tanques de armazenamento subterrâneo de combustíveis e 528.521 vazamentos confirmados entre os anos de 1988 e 2015 (USEPA, 2016). Do ponto de vista de recursos hídricos de interesse, estima-se que aproximadamente o 50% de toda a população de EUA se encontra exposta a risco potencial de contaminação por causa de

vazamentos subterrâneos de tanques. Esta percentagem sobe até 99% nas áreas rurais, onde o abastecimento de água potável para população vem exclusivamente de reservas subterrâneas (NADIM et al., 2000; WILSON et al., 2013). No Brasil, somente no estado de São Paulo foram 5.942 áreas contaminadas desde o ano de 2002 até 2017, com 4.543 ocorrências ligadas a combustíveis automotivos, e destas, 4.284 em postos de combustível (CETESB-RAC, 2017). Apesar da falta de um registro detalhado das áreas contaminadas a nível nacional, em todo o país são 40.266 os revendedores varejistas de combustíveis líquidos (ANP-BG, 2015) e cada um destes possui vários tanques subterrâneos de 15 a 60 m³. Adicionalmente, os terminais de distribuição apresentam riscos não desprezíveis para os recursos hídricos e para a saúde humana, levando em consideração a probabilidade de ocorrências de derramamentos (mesmo que menores), mas valores expostos e possíveis danos consideravelmente maiores. Considera-se que, o terminal marítimo Almirante Alves Câmara (TEMADRE), segundo terminal mais importante da Petrobras no Brasil, tem uma capacidade instalada de armazenamento de GLP, álcool, petróleo e derivados da ordem de 500.000 m³, da qual vazaram, respectivamente, cerca de 48.000 L de petróleo bruto (ORGE et al., 2000) e 2.500 L de óleo para a Bahia de Todos os Santos, nos anos de 1992 e 2009. Além disso, derramamentos superficiais em refinarias, terminais e indústrias podem contaminar diretamente o mar ou infiltrar no subsolo, na zona não saturada, atingindo o lençol freático e dissolvendo compostos tóxicos nos aquíferos costeiros.

Quando ocorre um derramamento de alguma substância, inúmeros são os processos de partição e migração ambiental que ocorrem em função das condições e da afinidade química dos compostos. Estas interações determinam o destino final do poluente, assim como os possíveis impactos ambientais (MULLIGAN; YONG, 2004). Em caso de vazamento de combustíveis, os compostos orgânicos se movem e degradam em ambiente subterrâneo na presença da água ou interagindo entre eles, influenciados por diversos processos de transferência de massa (ex. volatilização, dissolução, sorção), transporte (ex. advecção, dispersão, difusão), transformações químicas e biológicas (SCHIRMER; BUTLER, 2004). Tais fenômenos dependem das propriedades químicas dos compostos, do campo de fluxo e escoamento, das condições presentes no local e da escala espacial considerada no estudo. No entanto, mesmo na presença de substâncias pouco solúveis, como os hidrocarbonetos do petróleo, a dissolução é o processo que controla a transferência dos poluentes no meio aquoso, tendo um importante efeito sobre a escala temporal da contaminação (ZHU; SYKES, 2000; HAGGERTY et al.

2004). Somente depois que os componentes estão em fase líquida que se ativam os mecanismos de transporte e degradação propriamente ditos. Em misturas complexas, o processo de dissolução é influenciado pela interação recíproca dos compostos. Assim, a presença conjunta de etanol e gasolina gera um efeito de cossolvência que aumenta o valor de solubilidade dos BTEX, dado pela Lei de Raoult (CORSEUIL; FERNANDES, 1999; POWERS et al., 2001). Uma vez dissolvidos e disponibilizados em fase líquida na água subterrânea, os compostos migram em forma de plumas em função do campo de fluxo local. Contudo, são vários os processos que ocorrem simultaneamente no ambiente subterrâneo e que podem influenciar as condições específicas de fluxo, agindo no transporte e degradação das substâncias dissolvidas. Portanto, fenômenos ativos a uma escala maior (regional ou de bacia) podem impactar o comportamento dos compostos nas áreas contaminadas, modificando o campo de fluxo. Estas alterações, observadas na prática como irregularidades na migração das plumas, podem não encontrar uma explicação se estudados com uma perspectiva exclusivamente local, alimentando assim o campo das incertezas. Impulsionadas por um fluxo irregular e variável as plumas de solutos impactam áreas distantes das fontes de LNAPL, e podem resultar em contaminações de águas de reservas superficiais e subterrâneas (RIVETT; FEENSTRA; CHERRY, 2001; MACKAY et al. 2006). Portanto, visando um entendimento pleno do deslocamento das plumas e dos riscos associados é preciso estudar os mecanismos que determinam as alterações globais e locais do campo de fluxo. Ao mesmo tempo, resulta imperativo avaliar o efeito da variação do fluxo no transporte nos meios porosos, descrito pela equação de advecção e dispersão (BURR; SUDICKY; NAFF, 1994; BARRY et al., 2002).

Ao tratar o aquífero como um corpo único, é possível definir um balanço hídrico regional que descreva a variabilidade do volume armazenado no tempo, e portanto, da carga hidráulica em sua totalidade. Este balanço será definido pelos aportes positivos da recarga devido a infiltração da chuva e dos fluxos entrantes, e pelos aportes negativos dos fluxos pontuais saindo (bombeamentos, drenança entre bacias), da evapotranspiração e do fluxo basal (volume drenado pelos receptores superficiais) (HEALY; COOK, 2002). Um enfoque de bacia permite, portanto, individualizar os processos hidrológicos que são as causas principais da modificação da superfície potenciométrica na escala local. Assim, se fornecem mais ferramentas conceituais para o entendimento do comportamento das plumas de contaminantes observada no campo. Contudo, nos aquíferos não confinados, as interações entre as forçantes

hidrológicas às diferentes escalas e a disposição irregular das heterogeneidades geológicas determinam oscilações locais do nível freático, resultando em um fluxo subterrâneo altamente variável no tempo e no espaço (GOODE; KONIKOW, 1990; DENTZ; CARRERA, 2005). Estas condições determinam modificações transitórias das velocidades das águas subterrâneas (WALKER et al. 2015; MASETTI et al. 2016), dos gradientes hidráulicos naturais (SINGH; RAI; RAMANA, 1991; CUTHBERT 2010), e das direções de escoamento locais (VAN DER KAMP; HAYASHI, 2009; OOSTERWOUD et al. 2017). Por isso, as bacias costeiras e as áreas estuarinas em climas tropicais apresentam um campo de fluxo complexo de se analisar. Lençóis freáticos geralmente rasos e condições de contorno oscilatórias devido ao efeito da maré determinam flutuações e irregularidade na superfície potenciométrica. (ATAIE-ASHTIANI; VOLKER; LOCKINGTON, 2001; MAO et al. 2006; COLOMBANI et al. 2016). De fato as interações entre a distribuição irregular das forçantes climáticas, a limitada profundidade do lençol freático e os nível flutuantes dos corpos hídricos superficiais geram variações no tempo e no espaço das condições na qual é estimado o balanço hídrico do aquífero (POOL; POST; SIMMONS, 2015). Estes ambientes dificultam a definição de um fluxo subterrâneo unívoco nas áreas contaminadas, determinando um campo complexo de escoamento local e resultando em incertezas nas previsões do transporte.

As incertezas estão principalmente relacionadas às interações entre as escalas dos processos investigados, tanto no espaço quanto no tempo (KITANIDIS, 2015). De fato a explicação conceitual dos fenômenos de fluxo e transporte é definida em um meio “contínuo” na escala microscópica (BEAR; CHENG, 2010). As formulações macroscópicas usadas na prática representam médias de efeitos observados experimentalmente. Como lembrado por Molz (2015), qualquer fluido em movimento apresenta somente advecção e difusão, sendo o processo de dispersão um artefato conceitual para explicarmos o fluxo em meios porosos. A presença do coeficiente dispersão hidrodinâmica na equação de advecção-dispersão se deve a nossa incapacidade de reconstruir as irregularidades do campo de velocidade real em todas as escalas (MOLZ, 2015). A nível metodológico, a escalabilidade dos parâmetros de controle do problema de fluxo e transporte (ex. condutividade hidráulica, dispersividade, coeficiente de degradação) dificulta a compreensão dos fenômenos de forma geral (ESSAID; BEKINS; COZZARELLI, 2015). É necessária atenta reflexão nas etapas que levam desde a formulação matemática do meio poroso ideal, até a estimativa dos parâmetros macroscópicos em colunas de laboratório ou na escala de campo

(KITANIDIS, 2015). A mesma caracterização de campo dos parâmetros parece ter uma dependência da escala espacial de investigação (SEBOK et al. 2015).

As incongruências nas escalas temporais das forçantes hidrológicas (horas, dias), das respostas hidráulicas do aquífero (dias, semanas) e do conseqüente transporte de contaminantes (dias, anos) geram também confusão na prática de monitoramento dos fenômenos. Por exemplo, o tempo de resposta do lençol freático a um evento de precipitação depende do processo de infiltração, que por sua vez se relaciona às características e condições da zona vadosa (ex. conteúdo de água, porosidade efetiva), e à distância entre aquífero e superfície. O tipo de resposta no tempo define as condições de fluxo específicas para o transporte no aquífero, cujo resultado é influenciado também pelas propriedades físico-químicas de produtos, água e matriz geológica. Portanto, a evolução das plumas de contaminantes, em termo de variação de concentrações, não apresenta a mesma escala temporal das forçantes hidráulicas (HAGGERTY et al. 2004; DE LOUW et al. 2014). Misturas complexas de substâncias, isótopos, traçadores radioativos e perfis contínuos de temperatura podem ser empregados para definir a escala de tempo dos fenômenos de fluxo e transporte (COOK; HERCZEG, 2000; BRUNNER et al. 2017). Porém, na prática de gerenciamento de áreas contaminadas é mais comum recorrer a informações pontuais de concentração e carga hidráulica. Estas medidas instantâneas são intrinsecamente inapropriadas para descrever as múltiplas escalas temporais dos problemas tratados.

Para lidar com a complexidade dos mecanismos na escala de campo é cada vez mais comum basear à predição do transporte, e a subsequente escolha da tecnologia de remediação, em modelos numéricos. Tais modelos representam uma descrição conceitual aproximada dos sistemas reais, que tomam a forma de uma formulação matemática e podem ser resolvidos por meio de hipóteses simplificativas claras (ANDERSON; WOESSNER; HUNT, 2015). Através destas ferramentas, por meio de simulações e cenários, é possível: (a) integrar dados de campo insuficientes, (b) determinar áreas sensíveis onde concentrar campanhas de medições, (c) validar modelos conceituais, (d) produzir estimativas com um determinado grau de incerteza, (e) montar previsões hipotéticas dos comportamentos futuros (BEAR, 2018). Por isso, a modelagem numérica tornou-se uma metodologia importante no apoio aos processos de planejamento e na tomada de decisões na gestão dos recursos ambientais (BEAR; CHENG, 2010). No processo de identificação e gerenciamento de áreas contaminadas (GAC), os modelos

de fluxo subterrâneo fornecem um apoio analítico para a compreensão preventiva dos mecanismos ativos, e para o controle “*a posteriori*” da qualidade das águas subterrâneas (ASTM D5447-04:2010; ASTM D5609-16:2016; ASTM D5490-93:2014-e1; ASTM D5981-96:2008).

No Brasil, as normas para definição dos passivos ambientais, inspiradas no manual de gerenciamento de áreas contaminadas da CETESB (CETESB-MGAC, 2001), prescrevem o uso de modelos numéricos somente na fase do prognóstico ambiental e no final da etapa da investigação detalhada, e sem muito detalhamento das características destes modelos de fluxo e transporte (ABNT NBR 15515-3:2013). A modelagem ainda não está incluída como prática cotidiana de planejamento e projeto de áreas contaminadas desde suas fases iniciais, nem no gerenciamento preventivo do risco das áreas expostas. Além disso, nota-se que falta na normativa um entendimento explícito da importância das escalas dos fenômenos de fluxo incluídos no modelo numérico de transporte “para simular se as concentrações atingirão receptores em um determinado tempo”.

Tendo em vista a relevância do problema de contaminação e a complexidade dos mecanismos de fluxo e transporte, há inúmeras pesquisas que investigam os processos de migração para melhorar as previsões do comportamento dos combustíveis em escala de campo. A maioria dos estudos foca nos efeitos das heterogeneidades geológicas sobre o espalhamento irregular das plumas (MOLZ et al., 2006; FIORI et al., 2015; SUDICKY; ILLMAN, 2011). Entretanto, pouca atenção foi dedicada à influência dos transientes hidráulicos (tais como infiltração, recarga, descarga) na migração de substâncias dissolvidas nas águas subterrâneas, sobretudo na escala de campo (SCHIRMER et al. 2001; DAVIS et al., 1999). Porém, somente com a caracterização conjunta destes dois fatores de variabilidade em resposta às forçantes climáticas é possível ter um entendimento pleno do fluxo natural e do transporte na escala de campo (DENTZ; CARRERA, 2005; POOL; POST; SIMMONS, 2015; POOL; DENTZ, 2018). Caracterizações hidrogeológicas com inadequada resolução e abrangência, tanto espacial como temporal, podem levar à definição errada das propriedades do fluxo, propiciando planos de monitoramento, estratégias de contenção e tecnologia de remediação não eficazes (SOGA; PAGE; ILLANGASEKARE, 2004). Por esta razão é importante desenvolver experimentos de campo em áreas multidisciplinares, equipadas e caracterizadas detalhadamente, favorecendo a acumulação de extensas bases de dados sobre os processos de fluxo e transporte. Para tratar a complexidade do meio ambiente, os estudos de campo adotam geralmente

assunções sobre subsolo e condições de fluxo, como: (a) isotropia e homogeneidade do meio, (b) campo de fluxo estacionário, (c) lençol freático estático, (d) ausência de interações receptores-aquífero, (e) caracterização hidrogeológica com limitada abrangência espacial e temporal. Estas aproximações facilitam a abordagem conceitual e matemática, mas geram incertezas nos resultados. Cabe destacar que em casos de grande variabilidade do campo de fluxo, tais hipóteses podem comprometer o entendimento geral do problema e as previsões sobre migração das plumas.

O REMA (Núcleo Ressacada de Pesquisas em Meio Ambiente), pertencente ao Centro Tecnológico (CTC) da UFSC, trabalha desde 1996 na Fazenda Experimental da Ressacada (Florianópolis, SC, Brasil) em parceria com a Petrobras, desenvolvendo experimentos em escala de campo e modelos matemáticos sobre o comportamento dos LNAPL no subsolo e a migração das plumas de compostos no aquífero (CORSEUIL et al., 2011; CORSEUIL et al. 2015; RAMOS et al. 2016; FEDRIZZI et al., 2016). Estes experimentos tratam-se de derramamentos subterrâneos monitorados que replicam na escala de campo vazamentos acidentais de combustíveis. No entanto, as condições de contorno destes experimentos são mais definidas em comparação aos derramamentos reais. A evolução das plumas é monitorada por meio de poços multiníveis instalados ao longo da direção principal de escoamento subterrâneo. Na fonte são aplicados traçadores conservativos e misturas de combustíveis (fósseis e biocombustíveis) para testar as interações entre produtos no ambiente natural. Para o desenvolvimento destes estudos foram construídas 11 áreas experimentais, 55 piezômetros, 504 poços de monitoramento multinível e mais de 20.000 amostras de água subterrânea foram coletadas e analisadas ao longo de 20 anos. A base teórica para este tipo de experimentos foi desenvolvida nas experiências da base militar de Borden em Ontario, Canadá (ROBERTS; GOLTZ; MACKAY, 1986; MACKAY et al. 1986; FREYBERG 1986), no campo experimental de Cape Cod em Massachusetts, EUA (GARABEDIAN et al. 1991; LEBLANC et al., 1991, HESS; WOLF; CELIA, 1992), e nos experimentos de macrodispersão (MADE) na base aérea de Columbus em Mississipi, EUA (BOGGS et al., 1992; REHFELDT; BOGGS; GELHAR, 1992; BOGGS; ADAMS, 1992).

Cabe salientar que, diferentemente dos trabalhos desenvolvidos nos EUA, Austrália e Canadá, os experimentos da Ressacada integram as peculiaridades do clima subtropical úmido na migração e degradação dos compostos. Este clima apresenta chuvas intensas e marcadamente variáveis durante todo o ano (MCKNIGHT, HESS, 2000), evidenciando

a importância dos fenômenos hidráulicos transitórios. Uma abordagem estacionária na definição do lençol freático e das características do fluxo subterrâneo (CHIARANDA, 2011; FERNANDES, 2002; COSTA, 2008), pode, nestes casos, comprometer o entendimento do comportamento dos contaminantes no subsolo. De fato, o regime pluviométrico na Fazenda demonstrou ter direta influência nas rápidas variações do lençol freático (SCHNEIDER, 2005). Assim, as prováveis implicações no espalhamento e migração dos compostos sugerem a necessidade de um enfoque mais amplo e completo sobre os mecanismos de fluxo na área (LAGE, 2005).

Além disso, a área de estudo tem uma importância ambiental e socioeconômica relevante para toda a região. Situada na bacia do Rio Tavares, a segunda mais extensa da Ilha de Santa Catarina, contém três unidades de conservação que abrigam duas grandes áreas verdes e um manancial de água doce (IBGE, 2010; CEDAP/EPAGRI, 2015). A elevada pressão antrópica no distrito e a presença de obras de interesse estratégico (ex. Aeroporto Internacional, Base militar) alteram os fenômenos naturais de infiltração e fluxo subterrâneo. Neste quadro, um modelo conceitual dos fenômenos de escoamento da bacia representaria uma ferramenta valiosa de previsão, tutela e gestão para toda a região, e ajudaria na interpretação do transporte local dos contaminantes liberados nos experimentos do REMA.

Neste contexto, este estudo apresenta uma revisão crítica dos dados produzidos pelo REMA em 20 anos de monitoramento sobre o aquífero da Ressacada, visando à construção de um modelo conceitual da circulação subsuperficial na região. A caracterização da região é definida a partir da consolidação de informações históricas, junto às campanhas de medição integrativas e a verificação das redes de monitoramento presentes. A análise dos dados é associada ao desenvolvimento de experimentos numéricos de fluxo e transporte em diferentes escalas, empregados para validar a compreensão dos processos hidrogeológicos, verificar e integrar os dados de campo, e acompanhar a construção do modelo conceitual definitivo do aquífero.

O trabalho tem como finalidade avaliar a influência do regime de fluxo natural na migração subterrânea dos compostos dissolvidos, procedentes de derramamentos de gasolina e etanol. Os experimentos de campo da Ressacada, que representam os casos de estudo específicos, estão localizados em uma região costeira de clima subtropical úmido caracterizada por um aquífero raso, um denso retículo de canais de drenagem e amplas áreas alagadas de mangue. Portanto, a hidrodinâmica subterrânea resulta bastante variável no tempo e no espaço. Este fato

permite investigar as causas que determinam o nível do lençol freático na Fazenda da Ressacada, assim como as velocidades locais, as direções e os gradientes hidráulicos. Todos estes fatores impactam a migração dos contaminantes dissolvidos no aquífero. Para evitar uma caracterização parcial dos mecanismos, o enfoque a nível espacial procede do regional, onde se aplicam as forçantes e se desenvolvem as respostas da bacia, ao local (áreas experimentais) onde a migração das plumas acontece. As escalas temporais consideradas na análise são múltiplas (diária, sazonal, anual, plurianual e por evento). O trabalho se destaca por abranger um amplo conjunto de fatores na definição do campo de fluxo natural, como: oscilação periódica de maré, variação de infiltração e recarga, ativação dos canais de drenagem, interconexão hidráulica das áreas alagadas e das lentes suspensas. Finalmente, além das contribuições de carácter científico geral, outro objetivo é juntar, organizar, verificar e consolidar dados e conhecimento da hidrogeologia da região, para fornecer ferramentas de enquadramento hidrogeológico para as futuras pesquisas.

Cabe salientar que pelas finalidades do presente trabalho os termos “granular” e “poroso” são usados como sinônimos para indicar a natureza solta do meio geológico, composto por grãos de origem sedimentar. Da mesma forma, tendo exclusivamente como foco os aquíferos livres que apresentam lençóis freáticos rasos, os termos “não confinado”, “costeiro”, “livre” ou “raso”, referentes aos corpos hídricos subterrâneos, representam sinônimos no texto.

1.1 HIPÓTESES

Para desenvolvimento do trabalho de pesquisa três hipóteses principais foram formuladas.

- As variações das forçantes hidrológicas influenciam a carga hidráulica do lençol freático no tempo e no espaço. Esta hipótese é verificada com base no monitoramento hidrométrico da Fazenda Experimental da Ressacada, nas séries pluviométricas plurianuais do Aeroporto Hercílio Luz e no conjunto de dados do marégrafo do EPAGRI/CIRAM na Baía Sul.
- As variações do potencial hidráulico do lençol freático, das velocidades e das direções do fluxo subterrâneo influenciam diretamente a migração das plumas de compostos orgânicos. Esta

hipótese é verificada a partir dos múltiplos experimentos de liberação controlada da Fazenda Experimental da Ressacada.

- A migração e atenuação das plumas em condições de fluxo estacionário e transiente resultam divergentes pelo efeito das simplificações introduzidas no regime de escoamento simulado. A hipótese é verificada a partir de experimentos numéricos desenvolvidos em FEFLOW sobre experimentos de campo da Fazenda Experimental da Ressacada.

1.2 OBJETIVOS

1.2.1 Objetivo geral

Este trabalho tem como objetivo geral definir a hidrodinâmica subterrânea no aquífero da Ressacada destacando seus efeitos no transporte de compostos orgânicos em áreas contaminadas por misturas de gasolina e etanol.

1.2.2 Objetivos específicos

Os objetivos específicos deste estudo são:

- OBJETIVO 1: Avaliar a variabilidade dos processos de recarga e descarga como componentes do balanço hídrico do aquífero.
- OBJETIVO 2: Estimar as incertezas ligadas aos processos transientes na definição do campo de fluxo local.
- OBJETIVO 3: Avaliar a influência das variações de velocidade da água subterrânea na migração dos BTEX em áreas contaminadas com gasolina, na presença de diferentes teores de etanol.
- OBJETIVO 4: Construir um modelo conceitual da circulação hídrica subterrânea na região da Ressacada e dos fenômenos ativos nas diferentes escalas.

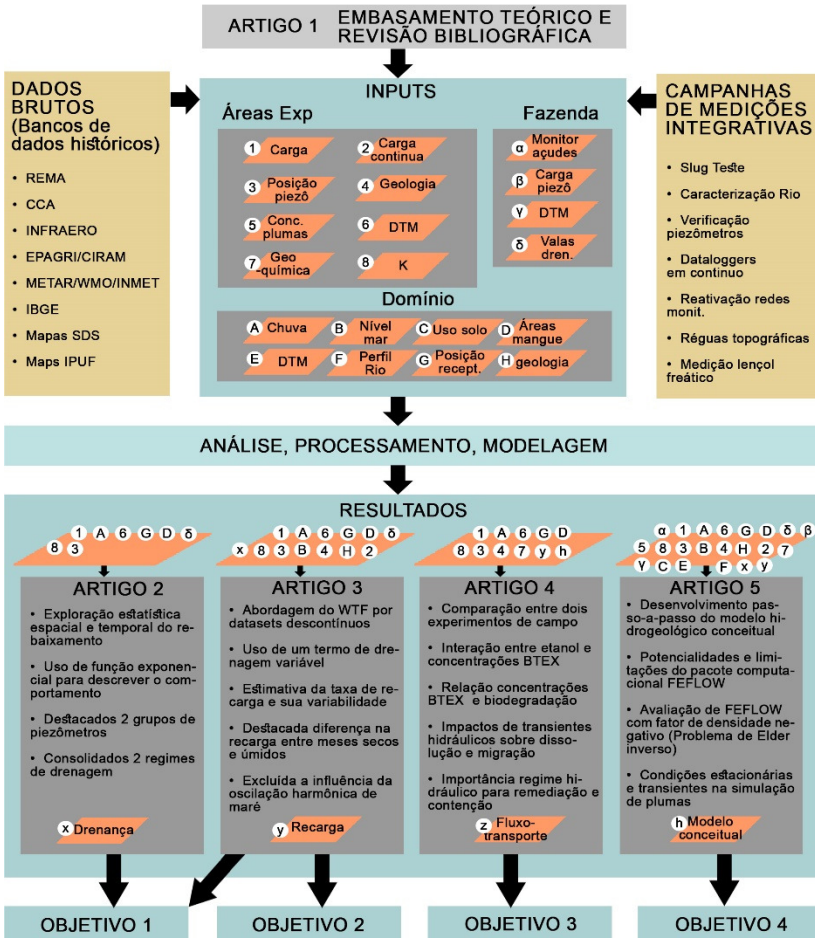
2 ESTRUTURA METODOLOGICA DA DISSERTAÇÃO

Conforme os objetivos especificados, o trabalho foi desenvolvido por etapas independentes, que analisaram aspectos chave do problema. De fato, para identificar e descrever as relações entre a hidrodinâmica do fluxo subterrâneo e o transporte de compostos orgânicos em fase aquosa foi necessário avaliar o balanço hídrico do aquífero e entender os mecanismos ativos sobre o campo de fluxo local. O modelo conceitual hidrogeológico da planície construído nesta pesquisa prevê forçantes hidrológicas e condições de contorno flutuantes na escala regional que, interagindo com as heterogeneidades na escala local, modificam o campo de fluxo no tempo e no espaço e a migração dos compostos nas áreas experimentais. No específico, a ocorrência e variabilidade de quatro mecanismos caracterizaram fortemente o campo de fluxo e o balanço do aquífero costeiro da Ressacada (Fig.5). Trata-se da: (1) flutuação desuniforme do lençol freático devido a recarga que aumenta com a distância dos receptores superficiais; (2) ativação das valas de drenagem que altera a infiltração local; (3) variação do nível nos receptores superficiais que impacta as velocidades no subsolo e os volumes descarregados pelo aquífero; (4) disposição irregular das lentes de argila que podem gerar erros e incertezas na leitura pontual da carga hidráulica, ou modificar o sentido de escoamento local. Portanto, primeiramente foi necessário investigar o processo de recarga e descarga do aquífero nestas condições variáveis e compreender o efeito das oscilações de maré sobre a carga do lençol freático. Em seguida, foi possível definir o efeito destas variações de fluxo no transporte de contaminantes na escala local e finalizar a construção do modelo conceitual de escoamento subsuperficial na região. Como mostrado no fluxograma do projeto (Fig.1), estas etapas confluíram em cinco publicações, cujos resultados visaram atender os quatro objetivos específicos da pesquisa. Portanto, em conformidade ao desenvolvimento do trabalho, a estrutura da tese está organizada em cinco seções, na forma de artigos científicos:

1. Embasamento teórico e revisão bibliográfica (ARTIGO 1)
2. Estudo da taxa de descarga natural do aquífero (ARTIGO 2)
3. Avaliação da recarga vertical e das flutuações de maré (ARTIGO 3)
4. Interação entre fluxo natural e transporte de contaminantes em aquíferos freáticos impactados com gasolina e etanol (ARTIGO4)

5. Aplicação de experimentos numéricos para compreensão conceitual da hidrogeologia regional (ARTIGO 5)

Figura 1 – Fluxograma completo do trabalho. Os símbolos em branco (números e letras nos círculos) permitem o mapeamento do uso dos dados (inputs) nas elaborações dos diferentes artigos, assim como a produção de outputs.



Cabe salientar que, a nível metodológico, todos os inputs para elaborações numéricas e análises estatísticas desenvolvidas no presente trabalho foram gerados a partir de bancos de dados históricos (Dados

brutos - Fig.1) e medições de campo (Campanhas de medições integrativas - Fig.1).

Grande quantidade de informações históricas em múltiplas escalas procedentes de diferentes fontes foram consolidadas e processadas no neste trabalho (ex. banco de dados do REMA, monitoramento da Fazenda do CCA, campanhas geotécnicas da INFRAERO, series pluviométricas da Base Aérea, series de maré do EPAGRI/CIRAM). Estes dados foram subsequentemente organizados em geodatabases em ambiente gis, e estão atualmente disponíveis para futuras pesquisas na área. Vale destacar que trabalhar com conjuntos de dados históricos, dados geralmente não organizados e padronizados, permite manter baixos os custos da pesquisa. Contudo, para que estes dados sejam usados com confiança e eficácia, se requer um oneroso trabalho prévio de consolidação, verificação e homologação. Neste caso, 25-30% do tempo total do projeto foi dedicado a procura, verificação e consolidação de dados históricos. Tal etapa, geralmente esquecida ou pouco valorizada nas pesquisas, representa o fundamento de qualquer avaliação bem-sucedida.

Além do uso de dados históricos, foram planejadas e desenvolvidas campanhas integrativas para caracterização de campo. Uma campanha batimétrica descreveu o trecho do Ribeirão da Fazenda nas proximidades das áreas experimentais. Nesta, foram reconstruídas seis seções do leito fluvial e medida a velocidade do rio com molinete hidráulico à ultrassom para caracterizar as condições de contorno do fluxo subterrâneo (sistema estuarino do Rio Tavares). Ainda, foram realizadas duas campanhas de teste de Slug para avaliar a condutividade hidráulica nas áreas experimentais em diferentes regimes sazonais. Ao mesmo tempo, seguiu-se com o monitoramento manual da carga hidráulica e dos parâmetros físico-químicos do aquífero, uma vez verificadas as condições dos piezômetros instalados na Fazenda da Ressacada (inspeção detalhada dos piezômetros). Além disso, foram instaladas redes integrativas para monitoramento do lençol freático na Fazenda Experimental da Ressacada. Se tratou de dois transdutores de pressão com datalogger para monitoramento em contínuo da carga hidráulica e três réguas topográficas para acompanhamento da ativação da rede de drenagem na Fazenda.

Subsequentemente, para integrar as informações de campo e os dados históricos em um modelo conceitual único e testar o entendimento dos fenômenos foi empregada a modelagem numérica. Modelos numéricos e conceituais foram também usados no direcionamento das investigações de campo para áreas e parâmetros mais sensíveis, visando a otimização constante dos recursos disponíveis no projeto. Ao mesmo tempo, devido ao grande número de dados à disposição, a abordagem para

processamento e análise foi prevalentemente estatística. Assim, na análise dos dados e no desenvolvimento do trabalho foram empregados diferentes pacotes computacionais: FEFLOW (v7.1), PEST (v16.0), Anaconda (Python 2.7), Matlab (R2016a), Statística (v8.0), ArcGis (v10.1). O FEFLOW (desenvolvido pela DHI) é um software consagrado na simulação do campo de escoamento subsuperficial. Esta ferramenta permite gerenciar e resolver as equações de fluxo e transporte para meios porosos parcialmente saturados (DIERSCH, 2014). Tendo um algoritmo de resolução baseado no método dos elementos finitos (FEM), o FEFLOW permite gerenciar domínios de geometria e condições complexa como a área de estudo da Ressacada.

Finaliza-se a estrutura metodológica do trabalho com uma breve síntese dos artigos que constituem o corpo do texto:

1 - Embasamento teórico e revisão bibliográfica (ARTIGO 1): Esta seção apresenta o problema físico de fluxo e transporte em aquíferos naturais na escala de campo. Descreve-se a formulação matemática do problema e os fenômenos físicos considerados nas equações. Ao mesmo tempo se apresentam as especificidades dos aquíferos livres caracterizados por um lençol freático raso. Devido à interação de fatores tais como heterogeneidades geológicas ou periodicidade dos fenômenos e condições hidráulicas, estes reservatórios de água apresentam uma significativa variabilidade do campo de fluxo, tanto espacial quanto temporal. Neste contexto, desenvolve-se uma extensa revisão bibliográfica das irregularidades na migração de contaminantes no subsolo, e suas interações com a hidrodinâmica do fluxo subterrâneo. O objetivo principal desta primeira seção é orientar o leitor sobre a problemática de transporte de solutos em meios porosos, destacando as incertezas que podem ocorrer quando se tem um campo de fluxo variável. Visa-se também apresentar mecanismos e parâmetros tratados nos outros capítulos, criando um vocabulário compreensível sobre a temática. O conteúdo desta seção constitui um artigo submetido para a revista internacional “*Groundwater for sustainable development*”.

Rama, F., Miotlinski, K., Solute transport in a spatially and temporally variable flow field in porous media: A review. Groundwater for sustainable development, (2019). Submitted manuscript.

2 - Estudo da taxa de descarga natural do aquífero (ARTIGO 2): O capítulo apresenta uma extensa análise estatística das taxas de rebaixamento natural da carga hidráulica no aquífero da Ressacada. Por

meio desta abordagem se destaca a variabilidade espacial e temporal do fenômeno de descarga (componente do balanço hídrico do aquífero), propondo justificativas para os diferentes comportamentos dos piezômetros. De fato, a ocorrência conjunta de fatores antropogênicos (ex. valas de drenagem, cobertura e uso do solo) e naturais (ex. intensas precipitações, flutuações de maré, heterogeneidades geológicas) nesta região litorânea determina complexas interações entre superfície e subsolo, resultando em variações da infiltração e irregularidades do perfil hidráulico do aquífero. Os resultados apresentam taxas de rebaixamento distintas em função da condição hidráulica do aquífero e da posição do piezômetro em relação aos receptores superficiais. Além disso, o termo de descarga (D) estimado e consolidado neste capítulo é utilizado na aplicação do Water-Table Fluctuation Method (WTF) para estimar a recarga do aquífero (Seção 3). O conteúdo desta seção representa o artigo publicado na revista internacional “*International Journal of Environmental Science and Development*” em Setembro de 2017 (Fig.2).

Figura 2 – Detalhe da capa do artigo publicado na revista “*International Journal of Environmental Science and Development*”

Manuscript received May 30, 2017; revised July 20, 2017. This work is part of a research and development project in partnership UFSC/UFERSA/Petropolis Brasilero (Petropolis). Additional and improvements in the SCBR (Risk-Based Corrective Solution) mathematical model to support environmental management of Oil/Gas contaminated areas (Contract number: 0050.0006595.15.9).

Fabrizio Rama is with the Núcleo Ressacada de pesquisa em meio ambiente (REMA), Department of Environmental Engineering, Federal University of Santa Catarina (UFSC), Florianópolis, SC, 88040-900 Brazil (e-mail: fabrizio.ama@ufsc.br).

Davide Franco is with Laboratório de Hidráulica Marítima (LAHMAR), Department of Environmental Engineering (UFSC), Brazil (e-mail: franco@ufsc.br).

Henry X. Corseuil is with Núcleo Ressacada de pesquisa em meio ambiente (REMA), Department of Environmental Engineering (UFSC), Brazil (e-mail: henry.corseuil@ufsc.br).

doi: 10.18178/ijesd.2017.8.9.1033

International Journal of Environmental Science and Development, Vol. 8, No. 9, September 2017

Spatial and Temporal Analysis of Natural Drainage in the Ressacada Aquifer (Florianópolis, Brazil)

Fabrizio Rama, Davide Franco, and Henry X. Corseuil

Abstract—This paper proposes an in-depth statistical exploration of the available hydraulic head data concerning the Ressacada aquifer (Florianópolis, Brazil). By means of this

task becomes even more challenging in extreme climate and environmental conditions, on the southern coast of Brazil, where strong and varying precipitations in the presence of

3 - Avaliação da recarga vertical e das flutuações de maré (ARTIGO 3):

Esta seção apresenta a análise detalhada da principal componente de entrada do balanço hídrico do aquífero da Ressacada (recarga). Neste estudo, é abordada a variação da recarga (forçante do fluxo) e das oscilações periódicas de maré (condições de contorno), e os efeitos sobre as flutuações da carga hidráulica do aquífero. Este enfoque pretende destacar a importância dos fenômenos transientes na caracterização do campo de fluxo subterrâneo em um aquífero costeiro. A recarga é estimada através de uma nova abordagem do método da flutuação do lençol freático (WTF), desenvolvida nesta pesquisa para trabalhar com séries descontínuas de cargas hidráulicas que apresentam intervalo de medição irregular (entre 1 e 15 dias). Em contrapartida, o efeito das flutuações das marés sobre os níveis das águas subterrâneas é investigado

por meio de um construtor de componentes harmônicos. O conteúdo desta seção é composto pelo artigo publicado na revista internacional “*Hydrogeology Journal*” em Março de 2018 (Fig.3).

Figura 3 - Detalhe do artigo publicado na revista “*Hydrogeology Journal*”

Hydrogeology Journal (2018) 26:1887–1902
<https://doi.org/10.1007/s10040-018-1742-1>



PAPER



Recharge estimation from discrete water-table datasets in a coastal shallow aquifer in a humid subtropical climate

Fabrizio Rama¹ · Konrad Miotlinski¹ · Davide Franco¹ · Henry X. Corseuil¹

Received: 10 October 2017 / Accepted: 30 January 2018 / Published online: 5 March 2018
 © Springer-Verlag GmbH Germany, part of Springer Nature 2018

4 - Interação entre fluxo natural e transporte de contaminantes em aquíferos freáticos impactados com gasolina e etanol (ARTIGO 4):

A partir do entendimento da variabilidade dos processos que veiculam o fluxo subterrâneo na Ressacada (Seção 2 e 3), este capítulo trata das interações entre campo de fluxo e transporte de compostos dissolvidos.

Figura 4 - Detalhe do artigo publicado online na revista “*Journal of Contaminant Hydrology*”



Journal of Contaminant Hydrology

Available online 11 January 2019

In Press, Accepted Manuscript



Flow field dynamics and high ethanol content in gasohol blends enhance BTEX migration and biodegradation in groundwater

Fabrizio Rama , Débora Toledo Ramos , Juliana Braun Müller, Henry Xavier Corseuil , Konrad Miotlinski 

 Show more

<https://doi.org/10.1016/j.jconhyd.2019.01.003>

Get rights and content

O objetivo é avançar na compreensão dos derramamentos de gasolina e etanol em aquíferos porosos, abordando a contribuição de um campo de fluxo variável na vida útil e no comportamento das plumas. Neste capítulo, que apresenta uma abordagem estatística para processamento dos dados, se adotam análises de tendência, geoquímicas e microbiológicas como linhas de evidências da migração e biodegradação das substâncias (reativas e conservativas). O conteúdo

desta seção consta do artigo publicado na revista internacional “*Journal of Contaminant Hydrology*” em Janeiro de 2019 (Fig.4).

5 - Aplicação de experimentos numéricos para compreensão conceitual da hidrogeologia regional (ARTIGO 5):

Na última seção é ressaltada a importante contribuição da modelagem numérica na caracterização hidrogeológica e no gerenciamento das áreas contaminadas. Nesta, é apresentado, passo a passo, o desenvolvimento do modelo hidrogeológico conceitual do aquífero da Ressacada por meio de experimentos numéricos em diferentes escalas que visam testar o entendimento dos mecanismos observados no campo. Adicionalmente, são destacadas as potencialidades e limitações do pacote computacional FEFLOW na simulação das fontes de contaminação e da hidrodinâmica das plumas em um campo de fluxo variável. O conteúdo desta seção representa um artigo ainda não publicado.

Rama, F., Miotlinski, K., Numerical modelling as a tool to develop a conceptual hydrogeological model. (2019) Unpublished.

3 PUBLICAÇÕES

3.1 SOLUTE TRANSPORT IN A SPATIALLY AND TEMPORALLY VARIABLE FLOW FIELD: A REVIEW

Fabrizio Rama^{(1)*}, and Konrad Miotlinski⁽¹⁾

* Corresponding author

(1) Núcleo Ressacada de pesquisa em meio ambiente (REMA) – CTC - UFSC

Manuscript submitted February 27, 2019

Referência:

Rama, F.; Miotlinski, K. Solute transport in a spatially and temporally variable flow field: A review. *Groundwater for Sustainable Development*, (2019). Submitted manuscript.

Nota ao leitor:

Ajustes de texto e nas figuras foram realizadas em relação ao artigo original para aumentar a precisão da escrita científica e por razões de formato da dissertação sem, no entanto, alterar conteúdo e elementos utilizados nas análises.

Resumo

O transporte de solutos em um campo de fluxo variável no espaço e no tempo, esteve ao centro do debate científico sobre questões ambientais nas últimas cinco décadas. Este fato se deve à capacidade de qualquer composto em fase aquosa de migrar no ambiente subterrâneo, expondo os recursos hídricos à contaminação e, conseqüentemente, representando uma ameaça para saúde pública. Por isso revisamos as técnicas de última geração para caracterizar e modelar o fluxo de águas subterrâneas e os efeitos da não perfeita caracterização da migração dos compostos na escala de campo. Abrangemos uma ampla gama de metodologias, incluindo as técnicas de prospecção e instrumentação local, bem como as questões relacionadas com o alto grau de complexidade dos fenômenos em escala de campo. Os fatores que controlam o fluxo e o transporte nos sistemas naturais são organizados em três classes para conceituar o problema. Em primeiro lugar, as heterogeneidades geológicas em várias escalas são investigadas para explicar a propagação da pluma segundo a dispersão hidrodinâmica e a Lei de Fick. Em segundo lugar, as interações entre as águas superficiais e subterrâneas são discutidas, sendo causa das condições hidrológicas transitórias na subsuperfície. Entre elas, as oscilações das marés, a infiltração no leito fluvial e a dinâmica de recarga

diferencial são fenômenos típicos que afetam o campo de escoamento subterrâneo e, portanto, ao ser incluídos nos modelos numéricos, podem melhorar previsão e compreensão do comportamento dos contaminantes. Em terceiro lugar, os estresses antropogênicos tem efeito no transporte de contaminantes de várias maneiras. Eles podem aumentar a eficiência das tecnologias de remediação, mas também a pressão sobre o sistema natural. Embora as limitações nas teorias matemáticas mais usadas para explicar os processos complexos na subsuperfície já sejam conhecidas, maior integração interdisciplinar entre a caracterização do campo e a modelagem “baseada em processos” ajudaria aprofundar a compreensão geral do problema. A real compreensão dos processos contínuos ativos nas áreas contaminadas está relacionada à análise crítica dos grandes conjuntos de dados produzidos (em sua variedade de extensões e resoluções), juntamente ao uso racional da capacidade computacional a disposição para desenvolver modelos numéricos que respeitem a complexidade do meio ambiente.

Abstract

Solute transport in a spatiotemporal variable flow field has been an environmental concern for the last five decades, due to vulnerability of water resources to contamination and, consequently, public health and environmental risks. We review state-of-art techniques that were applied in full-scale aquifers to characterize and to model natural groundwater flow, and the effects of non-ideal characterization of solutes migration. We cover a wide range of methodologies, including the prospection and site instrumentation techniques as well as the issues related with the high degree of complexity of phenomena at field scale. Factors controlling flow and transport in natural systems are organized in three classes to conceptualize the problem. Firstly, the geological heterogeneity at various scales of analysis has been largely investigated to explain the plume spreading using a Fickian hydrodynamic dispersion. Secondly, the interactions between surface water and groundwater are discussed since they cause transient hydrological conditions in the subsurface. Among them, the tidal oscillations, river streambed infiltration and differential recharge dynamics are typical phenomena that affect groundwater flow field and thereby, if included in numerical models, may improve simulations and understanding of the dissolved contaminant behavior. Thirdly, anthropogenic stress affect the contaminant in many ways. They can improve the efficiency of remediation technologies, but also pollute or exacerbate the pressure over a natural system. Although the limitations in mathematical theories used to explain complex processes in the subsurface are already known, higher interdisciplinary integration between field characterization and process-based modelling help in their thorough understanding. The comprehension of the ongoing full-scale processes in contaminated areas is inherently related with

a critical analysis of large datasets with different data types and resolution scales, along with a rational use of computational capacity to develop relevant numerical models to deepen our understanding of the environment respecting its complexity.

Keywords: Geological heterogeneity, transient hydrological conditions, contamination plumes, NAPL, coastal aquifers

Highlights:

- Phenomena interesting subsurface transport in full-scale conditions were described
- An overview of spatiotemporally variable flow fields in porous media was presented
- Main factors affecting the groundwater flow field are organized in three categories
- Site instrumentation issues and new characterization techniques are presented

3.1.1 Introduction

Solute transport in the subsurface have been extensively studied in the last 50 years in order to develop tools for early warning and efficient remediation in case of incidental spills. Main formulations were developed within the theory of fluid flow in porous media (Freeze, 1969; Nelson, 1966; Green et al., 1970; Hanks et al., 1969), in conjunction with advection-dispersion equation of the solute mass (Bachmat and Bear, 1964; Bredehoeft and Pinder, 1973; Shamir and Harleman, 1967; Guymon et al., 1970). Historically, the evaluation of contaminant spills was based on a distance between the source and the plume front, and the time of the its arrival to receptors (Nelson, 1978a,b). Progressively, more elaborate equations were developed that included mixing due to geological heterogeneity or matrix diffusion (Grisak and Pickens 1980, Małoszewski and Zuber 1985). These equations included a set of diffusion/dispersion coefficients of which the use became a common practice in the groundwater community (Bear 1972; Appelo and Postma, 2005; Molz 2015). Eventually, transient flow conditions in the subsurface (Bear 1972; Bresler, 1973; Rubin 1968) were shown to contribute to the solute spreading and mixing (Kinzelbach and Ackerer, 1986; Rehfeldt and Gelhar, 1992; Dentz and Carrera, 2005) and these effects for practical reasons were embedded into the dispersion coefficients (Cirpka and Attinger, 2003; Dentz and Carrera, 2003).

Predictions on non-ideal solute transport require understanding of the processes that control the movement of water and the dissolved

compounds. This normally necessitates well-controlled experiments and advanced equipment that allows one to monitor spatial and temporal variability in concentrations (Gooday et al. 2008; Jabro et al. 1994; Davis et al. 1999). The results from a number of sites where such experiments were carried out provided an insight into organic contaminant transport in porous media under natural hydraulic gradient: (1) Borden site at the Canadian Forces Base in Ontario, Canada (MacFarlane et al., 1983; Mackay et al. 1986; Sutton and Barker 1985); (2) Cape Cod in Massachusetts, USA (LeBlanc et al., 1991; Hess et al., 1992); and (3) the macro-dispersion experiments (MADE) at Columbus Air Force Base in Mississippi, USA (Boggs et al., 1992; MacIntyre et al., 1993; Julian et al., 2001). These expensive, long-term investigations have substantially contributed to the development of modern contaminant hydrogeology, enhancing our knowledge in full-scale flow phenomena affecting transport of the dissolved compounds (Gelhar et al. 1992) and provided useful data for interpretation and theory development. For instance, Woodbury and Rubin (2000) using the Cape Cod dataset presented a full-Bayesian approach to parameter inference and investigation of scale effects, or Feehley et al. (2000) using the MADE data contributed to the development of dual-domain mass transport theory in aquifers. The knowledge gained from the analysis and understanding of the underlying processes in these sites helped to design other field experiments that addressed specific questions related to chemical or non-chemical subsurface processes. A few examples include monitored natural attenuation of NAPL (Corseuil et al. 2011a,b), natural or human-induced subsurface methanogenesis (Jakobsen and Postma, 1999; Christensen et al. 2000; Fedrizzi et al., 2016), groundwater acidification (Kjøller et al, 2004) or interactions of groundwater with surface water bodies where solutes were used to quantify water fluxes (Batlle-Aguilar and Cook, 2012; Engelhardt et al. 2013). Lessons learned from these full-scale experiments underlined limitations in classical theories of contaminant dispersion and reaction processes in groundwater, allowing the development of new process-oriented paradigm within the hydrogeological research (Sudicky et al. 2010; Sudicky and Illman 2011).

The scope of this review paper is to characterize factors and processes that control solute transport in a highly variable groundwater flow field. Due to the dynamics of the mechanism, the study focuses on the shallow subsurface, sometimes called a critical zone. We present groundwater flow and solute characterization techniques along with mathematical formulation for modelling purposes.

3.1.2 Factors controlling groundwater flow and solute transport

The nature of water flow in the subsurface and subsequent behavior of solute depend on three controlling factors (a) geological, (b) hydrological and (c) anthropogenic ones.

3.1.2.1 Geological

The velocity of groundwater flow depend on hydraulic properties of geological media. Unconsolidated sediments, including sand, gravel and silt are granular and, consequently, are called porous media (Todd and Mays, 2004). In the consolidated formations fractures and karstic features may be developed. This is a major division between the porous, fractured and karstic media, although mixtures of the two or three types are common in subsurface environments.

Porous media consist of different proportion of variable size particles of a particular depositional origin (Eaton, 2006). From a physical point of view, they are classified according to particle size, distribution and texture (relative proportion of sand silt and clay). Since the variations of the physical features are normally encountered at much smaller scale than the distances among the boreholes (Dunkle 2008; Fielding et al. 2009; Zha et al. 2017), or accuracy and precision of the prospective geophysical equipment (Cartwright and McComas, 1968; Stewart and Gay, 1986; Ebraheem et al., 2014), a true three-dimensional knowledge on hydraulic properties is never acquired. However, even a partial characterization of geological medium heterogeneities at field scale required large and expensive campaign. At Cape Cod, seismic investigations and detailed geological surveys were used to define the sand/gravel outwash plain overlying a poorly-permeable crystalline bedrock at the site (LeBlanc et al., 1991). At Borden site, the characterization of the relatively low degree of heterogeneity, composed of medium- to fine-grained sand, required extensive grain-size distribution analyses for a set of 846 samples from 11 undisturbed cores (Freyberg, 1986). The pervasive heterogeneity of Columbus site (Molz et al. 2006) was investigated by numerous core studies, trench studies and a series of smaller scale hydraulic conductivity (K) measurements using borehole flow-meters (Rehfeldt et al., 1992).

Hydraulic conductivity K [$L \cdot T^{-1}$] represents the proportionality constant between hydraulic gradient and groundwater fluxes in a porous medium (Fitts 2012). It is a function of the intrinsic permeability of the porous medium (k_i), bulk density (ρ) and fluid viscosity (μ) (Eq.1)

depending on medium and fluid properties. The Darcy's Law is valid for a limited range of velocity values, where the resistive forces of viscosity predominate, generating a sufficiently slow flow to remain in laminar conditions (Todd and Mays, 2004). The spatial variations in hydraulic conductivity affect local groundwater velocity, resulting in different rates of transport of dissolved contaminants. The injection of water containing bromide and three organic tracers at the MADE site showed asymmetric distribution of concentrations produced between them due to accelerating of groundwater flow along the plume travel path as a result of an increase in the mean hydraulic conductivity (Boggs et al., 1992).

$$K = \frac{\rho g k_i}{\mu} \quad (1)$$

The variations in flow field in fractured and karstic environments are even greater than in the porous media (Sudicky and Frind 1982; Berkowitz, 2002). Groundwater flow is divided between the matrix (or porous structure), fractures and karst (Motyka 1998). Physical apertures available for groundwater flow that are either open or filled with a material of different hydrological properties than the rock matrix (Miotliński et al. 2011). Electromagnetic flow-meters (Molz et al. 1989), geophysical logging and borehole-wall imaging are of great significance to identify open and closed features intersecting the boreholes. (Le Borgne et al., 2007).

Specific yield or effective porosity (η_e) represents the part of porosity that can free drain under atmospheric pressure (Hilberts et al. 2005). It is generally treated as a storage term -independent of time- that accounts for the instantaneous release of water from storage (Healy and Scanlon, 2010). However, in their comprehensive review on recharge estimates, Healy and Cook (2002) underlined that this release is anything but instantaneous or constant in field conditions. Specific yield variability is attributed to natural heterogeneity in geologic materials, different methods used for determining S_y , and, in large part, to the amount of time allotted to the determination (Prill et al. 1965), resulting usually in a limited accuracy in its estimate. For deep water table, when no recharge occurs, the specific yield is equal to its ultimate value that results from the difference between saturation and residual moisture content (Crosbie et al., 2005; Orellana et al., 2012). However, for shallow water table or in cases of recharge, this method may overestimate the specific yield (Cao et al. 2016). Since the relation between water-table fluctuations and

released volumes holds is markedly nonlinear (Nachabe 2002), a transient or apparent specific yield was introduced to represent the behavior of stored water in porous aquifers assuming a transient non-ideal release of water (Childs 1960; Duke 1972). It is worth stressing that, in shallow unconfined aquifers, the response of the water table to input and output fluxes is even controlled by two distinct parameters of effective porosity, drainable and fillable porosity, which are applicable for water table drawdown and rise, respectively (Acharya et al. 2012). These values can be extremely different although hysteresis is neglected, affecting the flow field in response to outer stresses (Acharya et al. 2014). Furthermore, by considering hysteresis in the unsaturated zone, water-retention curves describe a strongly non-linear relation between water content and pressure head, showing a pressure head decreasing (becomes more negative) and a capillary pressure increasing when the water content in the soil decreases (Brooks and Corey, 1966). In other words, the shape of the water-retention curves changes depending upon whether the soil is drying out or wetting (van Genuchten, 1980).

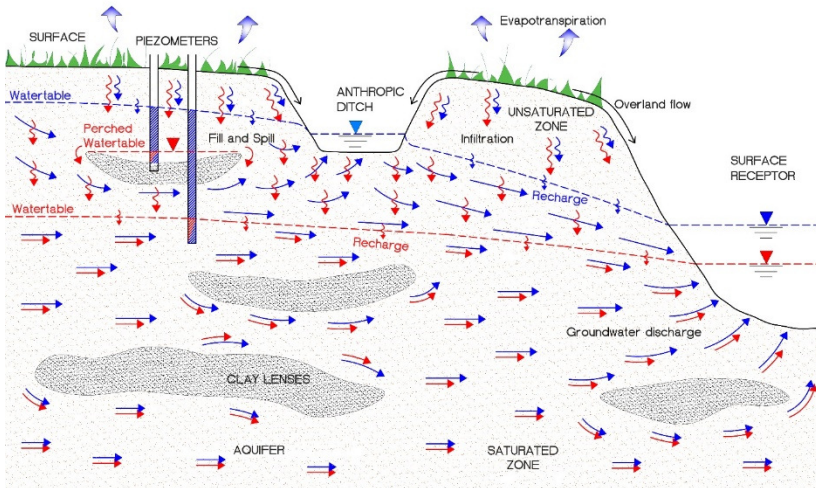
A typical subsurface profile is divided into an unsaturated zone in the upper part and an underlying saturated zone (Fig. 1), which differ for the water content, and thereby the pressure head, in the medium (Fitts, 2012). In the unsaturated or vadose zone, pores are only partially saturated and, with the exception of a small part of the capillary fringe, contain both gases and water (Berkowitz, et al. 2008). The saturated zone represents the aquifer in the strictest sense, which can be imagined, for the objectives of the present review, as a shallow, unconfined and highly variable reserve of pristine water floating over the heavier sea water (for coastal regions) or overlaying an impervious bed rock. The interface at atmospheric pressure that divides these zones is the water table (Freeze and Cherry, 1979), and is represented in the models as a fluctuating free-surface according to inflow and outflow contributions in the basin (Diersch, 2014). While usually studies focused on solute transport in either the saturated zone or the unsaturated zone simplifying the other contribution as boundary conditions, in many full-scale applications it should be relevant to consider both portions of the flow systems together (Cook and Herczeg, 2000, Anderson et al. 2015).

3.1.2.2 Hydrological

Recharge takes place when water is introduced to a groundwater system through infiltration of precipitation, surface or anthropogenic water (Healy and Cook, 2002; Healy and Scanlon, 2010; Bouwer 2002).

The remaining part which does not reach a groundwater system is lost through evapotranspiration (Dickinson, 1984; Shuttleworth, and Wallace, 1985), overland flow (runoff) (Dunne and Black, 1970; De Giesen et al., 2000) and retention above the capillary fringe (interflow) (Feddes et al. 2004; Du et al. 2016). The capillary fringe represents a transition part located on the top of the aquifer above the water table, traditionally assigned to the unsaturated zone, where, despite pores are completely saturated, hydraulic pressure are still negative (Bear, 1972). The thickness of the capillary fringe and the position of water table over time is a principal kind of information to define hydraulic conditions of an unconfined aquifer (Feddes et al. 2004). These conditions affect groundwater movement and velocity (Bear, 1972; Cartwright et al. 2003), and consequently dissolution/migration of organic contaminants (Berkowitz et al. 2004; Brouyère et al. 2004).

Figure 5 - Conceptual sketch of a typical soil transect depicting the main processes within two different groundwater regimes: dry (red) and wet (blue).



Temporal variations in groundwater flow caused by distinct recharge events may affect hydraulic interactions between surface water and groundwater or provoke flooding of poorly permeable layers in the unsaturated zone (Fig.5). The anthropic ditch in Fig. 5 exhibits a hydraulic connection with groundwater only at wet periods, acting as gaining stream on one side and as a losing stream on the other side (Winter et al. 1998), in addition to a preferential drainage of excess groundwater along

the streambed. During dry periods, when aquifer level moves downward, the anthropic ditch remains dry having only a drainage function, and extensively modifies the local subsurface circulation (Luscombe et al., 2016). Even for permanent streams, when water table head decreases leaving streambed disconnected from the aquifer, surface water in the streambed may recharge the aquifer resulting in a modified local flow field (Brunner et al. 2011). Therefore, by reducing preferential surface drainage within the streambed, promising techniques (e.g. trench infiltration) for increasing recharge and minimizing evaporation were developed (Bouwer 2002; Heilweil et al., 2015). In addition, aquifer fluctuations due to flooding causes temporal connection of perched water table with the main aquifer, changing local flow field and infiltration direction. Therefore two piezometers may present extremely different water head in dry and wet periods (respectively, red and blue regime in Fig.5) depending on the activation of small perched aquifers over clay lenses. These examples demonstrate that recharge events may change direction of groundwater flow.

However, the transient hydrological processes are rarely included in large-scale models due to an a priori simplifying assumption of steady-state conditions (Anderson et al. 2015). Lubczyński and Gurwin (2005) provide a detailed evaluation of the complexity of spatiotemporal variable fluxes in a basin balance, and a complete methodology of data acquisition/integration in transient groundwater modelling. Heeren et al., (2010) suggesting that alluvial groundwater in the Ozarks region acts as a transient storage zone, providing a contaminant sink during high stream flow and a contaminant source during stream base-flow. Regional-scale groundwater modelling provide a temporally integrated water balance which is a main tools to effective water management (Shao et al. 2009; Maheswaran et al. 2016; Wang et al., 2009; Zhou and Li, 2011).

Seasonally changing flow acting on a mobile source may result in a temporal variability of contaminant dissolution, flow paths and plume spreading (Davis et al., 1999). Consequently, they cause significant transverse lateral movement, asymmetry and transverse horizontal spreading in plumes dissolved from DNAPL sources (Rivett et al., 2001; Rivett and Allen-King, 2003). Vanderborcht et al. (2000) investigated the effect of flow rate and flow regime on solute transport in sandy-loam and loam, showing an increased dispersivity with increasing flow rate in both soil types and deriving the relation between the dispersivity and the flow rate using an effective flux-weighted average flow rate. Temporal variability in groundwater flow may increase substrate oxygen mixing (Schirmer et al. 2001) resulting in significantly enhanced biodegradation

rates when a differential sorption of electron donor and electron acceptor is assumed (Prommer et al., 2002). Meckenstock et al. (2015) updated the biodegradation concept in contaminated aquifers using the plume fringe concept, transient hydraulic conditions and transport limitations in subsurface. The transient flow was pointed out as source of uncertainties in both field experiment and simulation of plumes migration (Woodward et al., 2016; Abelardo and Nowak, 2018). By analyzing the intrinsic BTEX remediation, Davis et al. (1999) showed a preferential natural attenuation of toluene and o-xylene but underlined highly variable concentrations at individual boreholes, attributed to local hydraulic variations (Davis et al. 1999). Accordingly, Rein et al. (2009) numerically showed that mass discharge and degradation rates based on measurements at observation wells may not be spatially and temporally representative due to transient dynamics of groundwater flow. Simulation results indicated that the transiency of flow is a critical source of uncertainties in field measurements (Rein et al., 2009). In the case of natural (transient) flow field, Rasa et al. (2013b) underlined the importance to properly inform a numerical model with field observations (i.e. temporal moment of conservative tracer BTCs and mass discharge) in the calibration process. Consequently, bromide and heat tracers provided important additional constraints for calibration of hydraulic conductivity and boundary conditions under highly dynamic flow conditions (Ma et al. 2012).

In many arid and semiarid areas, groundwater recharge occurs through water infiltration from intermittent or ephemeral streams during natural flow events (de Vries and Simmers, 2002; Dunkerley, 2008). Batlle-Aguilar and Cook, (2012) showed that during such events, the total infiltration was 33% greater than would have been estimated assuming steady state infiltration rates. Dry antecedent moisture content controlled the transient infiltration rate, by increasing the total infiltrated volume during flow events, but it did not affect the aquifer recharge (Batlle-Aguilar and Cook, 2012). Flow considerations through the unsaturated zone are also important when simulating groundwater flow in humid climates (Hunt et al., 2008), characterized by intense and highly variable rainfalls. Nonetheless, just a few studies focused on the transient behavior of infiltration process in tropical or subtropical climates (Saghravani et al. 2015). In Brazil, for example, a statistically consistent analysis of water table fluctuation to infer recharge was provided by Neto et al. (2016), while a modification of water table fluctuation methods (WTF) was applied to a discrete dataset of hydraulic head in a coastal shallow unconfined aquifer (Rama et al. 2018). The authors highlighted that was

possible to obtain significant information about transient recharge in tropical climate by means of systematic monitoring of water table levels and determine a time gap between the precipitation and aquifer recharge events. In India, Ruiz et al., (2010) showed that a matric storage buffers the groundwater recharge process in a tropical watershed under deciduous forest. Generally, non-linear behavior between recharge, aquifer storage and discharge to surface receptors was found (Wittenberg, 1999; Rama et al. 2017).

Furthermore, recharge events may facilitate contaminant transport from the surface (Bohlke 2002) or may serve as a source of oxygen to react with contaminated aquifers to drive natural attenuation processes (McGuire et al., 2005). By applying first- and higher- order theoretical models to Cape Cod field data, Ezzedine and Rubin (1997) showed the influence of recharge on macro-dispersion, drawing a relation between enhanced lateral spreading and transient recharge. High recharge rates seem to accelerate the process of spreading, acting on the plume acceleration, conditioning observed hydraulic heads and thereby, changing the timescale of the problem (Ezzedine and Rubin, 1997). A theoretical basis for such an analysis was provided by Rubin and Bellin (1994) in which, using a nonlinear transformation of time, the spatial moments computed under the assumption of no recharge can be used to model the effects of recharge.

In addition, surface water bodies (e.g. sea, rivers, lakes, wetlands) are naturally characterized by temporal fluctuations of hydraulic level that affect the unconfined aquifers behavior (Euliss and Mushet, 1996; Hayashi and Rosenberry, 2002; Yan et al., 2010). Since the level of surface receptors and drainage artifacts (e.g. tile-drains, channels, ditches) represents a boundary condition for the groundwater flow and transport formulation (Duchene et al. 1994; Rozemeijer et al. 2010), its variation affects local flow net and total outflow rates (Louw et al. 2013; Colombani et al., 2016; S. Köhne et al., 2006). Rubin (1968) numerically solved the Darcian equation in an unsaturated 2D rectangular domain, considering horizontal infiltration and ditch-drainage, and obtaining a significantly influence on water table descent and total outflow rates. The focus of surface-subsurface interaction studies and models is to improve understanding of transient phenomena affecting groundwater flow field and solute transport (Arnold et al., 1993; Sophocleous 2002; Kollet and Maxwell, 2006). Winter (1999) proposed a large description of streams, lakes, wetlands and groundwater relations, showing as hydrologic processes associated with the surface-water bodies result a major cause of the complex and seasonally dynamic groundwater flow fields. During

rainfall events, ephemeral swamps in peatlands are characterized by a pronounced impact of surface topography and water-table depth on hydraulic inter-connectivity of bogs (Van der Kamp and Hayashi, 2009; Oosterwoud et al. 2017). A “fill and spill” mechanism is used to define aquifer dynamics in wetlands, having groundwater storage in “bowl-shaped” formations in the subsurface and instantaneous releases of water following precipitation events (Tromp-Van Meerveld and McDonnell 2006). Thus, land-cover and land-use changes, along with seasonal precipitation regimes have important implications for the long-term water balance in those complex regions (Hayashi et al. 2016). Moreover, Brunner et al. (2017) presented an extensive review of advances in river-groundwater interactions, highlighting the assimilation of different data types and resolution (Kurtz et al. 2017; Camporese et al. 2009), the development of highly instrumented field sites (e.g. CZO sites in the U.S. and TERENO sites in Germany), ongoing model development (Brunner and Simmons, 2012; Paniconi et al., 2003; Kollet et al. 2010; Partington et al. 2013) and the ultimate integration of models and data (Ramanathan et al. 2010; Liggett et al. 2015) as important future research areas.

Since the late 80s, a few studies focused on tidal influence on groundwater flow, suggesting the inclusion of tides in the models of coastal aquifers (Custodio et al. 1988) and mistrusting in classic Dupuit-Forchheimer (D-F) assumption (Herman et al. 1986). It is worth reemphasizing that D-F approximation assumed: (1) a predominantly horizontal flow, and (2) a negligible vertical hydraulic gradients (Anderson et al. 2015). However, in unconfined aquifers, water table position (i.e. free fluctuating surface) was not a boundary condition but an estimated solution of non-linear formulation of groundwater flow (Anderson et al. 2015), which introduce convergence difficulties. Trying to find a well-defined solution for variable head in BCs, several analytical models approached the problem using: simple vertical interface between ground- and sea-water (Li et al. 2000a); 1D and 2D Boussinesq equation (Li et al. 2000b, 2000c); or a capillarity correction to the shallow flow approximation (Barry et al. 1996; Jeng et al. 2005). They are normally assumed to be for a homogeneous aquifer, with small fluctuations or uniform slope. Li et al. (2000c) described tidally-driven groundwater variations in a L-shaped aquifer, which is an aquifer bounded by two water-land boundaries, exhibiting within the analytical solution the interaction between the cross- and along-shore tidal waves in the aquifer area near the estuary’s entry. In a subsequent paper, Li et al. (2002) improved this formulation obtaining a periodic and more computationally efficient solution. Despite direct tidal oscillations have little outback

propagation in reason of its high frequency, Ataie-Ashtiani et al. (2001) showed a quasi-steady increasing of local water-table level that influence regional run-off rates, while Bakhtyar et al. (2011) suggested a key impact on sediment transport and beach profile changes. Mao et al. (2006) developed a numerical model for a U-shaped aquifer surrounded on three side by the water, demonstrating the importance of the inclusion of tides level in the groundwater flow modelling of an estuarine system. A complex hydrodynamic circulation generally characterizes these coastal aquifers, in which hydraulic heads are described by means of shallow water equations, wave functions and estuarine fluctuations. It worth stressing that in these conditions, by neglecting the contributions of evapotranspiration and recharge, water-table simulations in concomitance with precipitation events, underestimated aquifer fluctuations relative to monitored levels, especially near to the beach where the aquifer was closest to the surface (Mao et al., 2006). Another study on tide-induced groundwater fluctuations in a U-shaped coastal aquifer concluded that the tidal head is most sensitive to the transmissivity and storativity of the aquifer, and least to the damping coefficient of tidal amplitude and wave number along the estuary (F.-K. Huang et al., 2015).

Moreover, where tidal fluctuations affects groundwater levels, variable-density flow must be accounted within the formulation to define solute transport in the subsurface (Diersch and Kolditz, 2002). The processes include intrusion of seawater in coastal aquifers (Gambolati et al. 1999; Pinder and Cooper, 1970; Voss and Souza, 1987), and seasonal variations in salt–freshwater interface (Kim et al., 2006; Heiss and Michael, 2014). The magnitude of tidal stress significantly influenced the biodegradation as it controls the intensity of salt–freshwater mixing, period of exposure of the contaminant to the mixing zone and rate of oxygen delivery to the aquifer (Robinson et al. 2009). Furthermore, seasonal inland changes in groundwater level affect out-flow dynamics and solute transport in a coastal aquifer. Michael et al., (2005) described the oscillations in water exchange between aquifers and ocean, showing a connection between the seasonal hydrologic cycle inland and the saline groundwater system in coastal aquifers, which result in a chemical loading seasonality of coastal waters. Abarca et al. (2013) numerically studied hydrodynamics in a coastal aquifer, focusing on the influence of beach slope and tide level on groundwater discharge. A positive correlation for freshwater discharge and a negative correlation for deep saline discharge with low-tide elevation were found, while high-tide elevation mainly controlled recharge in the intertidal saline cell (Abarca et al., 2013). For mass transport, the finger plume evolution was strongly

affected by tidal fluctuation. Through the changes of hydraulic gradient between the inland boundary and the sea, the water level oscillation affects the time for generating the fingers and the dilution of high concentrations (Liu et al. 2015). In addition, numerical simulations revealed that tidal effects may enhance the attenuation of BTEX compounds in an unconfined near-shore aquifer before their discharge to coastal waters (Robinson et al. 2009).

In a vertical 1D unsaturated flow, root channels and preferential drainage play an important role to define the water content in the soil, and thus, to forecast flow and transport of contaminants (Gerke and Kohne, 2004; Gerke 2006; Hendrickx and Flury, 2001). In an agricultural field in Finland, Warsta et al. (2013) estimated with a 3D distributed numerical model that over 99% of the drainflow originated from the macro-pore system, and drainflow started concomitantly with precipitation indicating preferential flow in the profile. In a specific review, Jarvis (2007) discusses the implications of 'non-equilibrium' flow and transport in large structural pores (i.e. root and earthworm channels, fissures and inter-aggregate voids), showing that high rain intensities increase non-equilibrium of flow in macro-pores, while initial water content generates confounding effects of soil shrinkage and water repellency. Therefore, land use substantially modifies timing and amount of recharge reaching the aquifer (Daly and Porporato, 2005). Zhang and Schilling (2006) studied the effects of land cover on water table, soil moisture, evapotranspiration, and groundwater recharge, showing substantial differences in hydraulic head records from two monitoring wells with grass and bare ground. The varied fraction of infiltration going to recharge reflected the different crops, cultivation practices, irrigation regimes, and soil types in Hebei Plain, China (Wang et al., 2008). Walker et al. 2015 used a simple analytical model to predict impacts of land-use change on catchment water yield by understanding the response time of changes in groundwater discharge to a change in recharge. Neves dos Santos et al., (2016) showed that changes of vegetation cover did not significantly modify the overall conditions for runoff initiation, presenting a similar cumulative flow vs. rainfall response, and implying that soil conditions, such as water content and cracks in unsaturated zone, best explain the flow generation process on the semiarid micro-scale watershed. Field studies from East Africa showed that forest cover loss is accompanied by increases in surface runoff and stream discharge (Guzha et al. 2018). Land cover changes affect moisture content and thereby, evapotranspiration (ET) process (Vivoni et al. 2008), which controls water losses with atmosphere that do not recharge the aquifer (Daly and Porporato, 2005).

Mainly in arid climates, where annual ET budget and total rainfall are comparable, estimating and modelling ET with the inclusion of root water uptake, root distribution, root water compensation, and water and oxygen stress is important for proper assessment of water availability (Campopese et al. 2015). Such information are directly correlated with the kind of plants cultivated and largely change over time and space (Duchemin et al., 2006). Accordingly, because of the decreased ET and increased R, significantly more base flow and chemical loads may be generated from a bare ground watershed compared to a vegetated watershed (Zhang and Schilling, 2006).

3.1.2.3 Anthropogenic

The anthropogenic factors cover both chemical and hydrological elements and include agriculture, chemical storage, pumping and drainage as well as remediation strategies. Hydraulic effects of human activities were studied by Rai et al., (2005), using analytical and numerical solutions of 2D linearized Boussinesq equation, showed that the variations in the rates of recharge, pumping, and leakage have significant effects on the nature of water table fluctuation. Groundwater is discharged through anthropogenic water wells (Scanlon et al. 2003). Monitoring and pumping wells are installed in the aquifer for a wide-range of uses (e.g. water supply, thermal storage, monitoring net). Drainage features include trenches, ditches, drains that are employed to limit local hydraulic heads in the subsurface, by the fast, preferential outflow of water during flooding events, when the water-table levels overcome the drain-bed (Ni and Capart, 2006). In the Ressacada aquifer, Brazil, a dense network of artificial trenches drains the plain, maintaining the water level below the topographic surface in naturally flooded areas (Rama et al. 2018). Irrigation rates and anthropic drainage net alter groundwater fluxes and flow patterns in a complex manner (Bohlke, 2002). Schepper et al. (2015) developed an integrated SW-GW model to describe the impact of shallow tile drainage networks on groundwater flow patterns, and associated transport of chemical species or sediment particles. Kohne and Gerke (2005) showed that preferential flow forced by a tile-drain cannot be fully understood without considering two-dimensional spatial flow dynamics. Luscombe et al. (2016) described how the spatial attributes of the contributing area along the drainage ditch size, morphology and geometry affected flow generation and water storage within shallow peat land catchments.

The active remediation plans refer to affirmative actions developed to remove contaminants from soil or water, which require human intervention (EPA site). Anthropogenic variation of water table level and groundwater flow velocity have a direct impact on solute transport (Boutt and Fleming, 2009). Thus, a multiple pumping-well driven, time-dependent oscillatory flow have improved the containment of injected plumes enhancing the mixing of solutes in porous media with respect to a constant flow (Zhang et al. 2009). The potential of substrate (i.e. sodium acetate) and groundwater mixing by pulse injections was demonstrated in an in-situ biostimulation experiment at the Borden site (Devlin and Barker, 1996). Sposito (2006) theoretically investigated the possibility of inducing chaotic flow field near a recirculation well with time-periodic pumping behavior in order to improve plume removal. Lee et al., (2008) developed a system of injection/withdrawal wells in a doublet arrangement to facilitate lateral spreading and mixing of permanganate (MnO_4^-) in an in-situ remediation scheme. Direct pumping out of dissolved plume volumes (i.e. pump-and-treat) is a widely employed and investigated active technology to deal with contaminated areas (Mackay and Cherry 1989; Berglund, 1997). However, since active remediation schemes can be very expensive to install and operate, the extent of any contamination plume has to be known to minimize pumping of polluted groundwater (Shlomi and Michalak, 2007). Furthermore, to limit the cost of remediation schemes, many works focused in optimizing injection and extraction well placement, along with injected concentrations and pumping rates (Haggerty and Gorelick, 1994; G.H. Huang et al., 2006; Minsker and Shoemaker, 1996). Troldborg et al., (2010) quantified the mass flux through a perpendicular control plane downstream from a NAPL source using multilevel sampling networks, passive flux meters, and integral pumping tests. However, given a slow dissolution process from entrapped NAPL, active remediation schemes are not usually considered effective clean-up methods to deal with not readily mobilized contaminants (Hunt et al. 1988; Nadim et al. 2000; Rivett et al. 2002). In such cases, source flushing with different kind of alcohols (Falta, 1998; Gomez and Alvarez, 2010) can be employed to enhance and accelerate the NAPL dissolution with co-solvency and consequently recover higher amount of dissolved hydrocarbons with groundwater pumping (Jawitz et al., 2000; Brooks et al., 2004; McDowell et al. 2003; McDowell and Powers 2003).

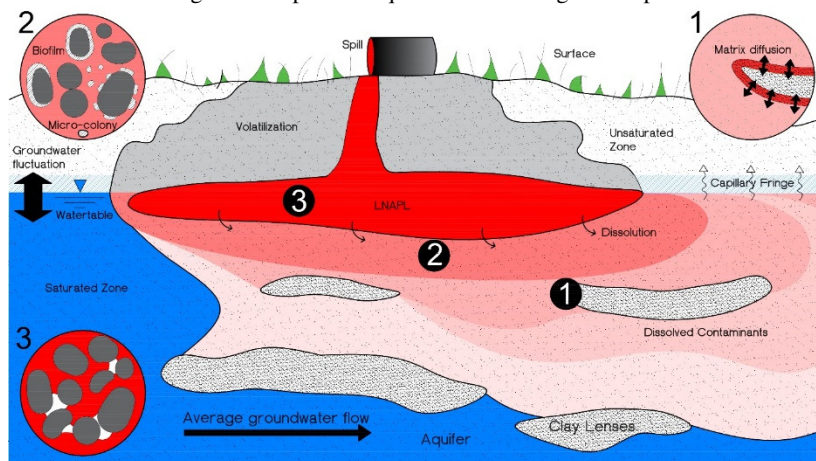
The agriculture sector have a direct impact on chemical quality and recharge rates (Postma et al., 1991; Bohlke, 2002). For this reason, processes affecting nonpoint-source contamination of shallow

groundwater below agricultural land are starting to be analyzed merging recent modeling tools, non-Fickian dispersion algorithms, and advanced characterization methods (Green et al., 2010; Warsta et al., 2013; Colombani et al. 2016). An extended field experiment in a sprinkler-equipped area with monitoring devices showed that transient effects of bidaily irrigations affected conservative transport in shallow unsaturated zone (Butters et al. 1989; Butters and Jury, 1989). Changes in land use or management modify annual nutrient load, having a direct impact on water quality assessment and predictions (Williams et al., 2015). Preferential flow paths along with high recharge rates and long histories of anthropogenic loading in agricultural areas result in increased probability of groundwater pollution with sulfates and phosphates (Johnson and Cole 1980; Simms et al. 1998). Anthropogenic inputs of pesticides, containing arsenic and inorganic nitrogen should be accounted in aquifers and surface receptors adjacent to agricultural areas (Gallagher et al. 1996; Neumann et al. 2010). McMahon et al. (2006) underlined a pesticides accumulation in deep unsaturated zones beneath irrigated croplands overlying the High Plains aquifer. The solutes that involve anthropogenic contaminants can find a passage through the soil column and aquifer and reach sensitive receptors (e.g. groundwater dependent ecosystem, a lake, a river or sea). For example nutrients (Postma et al., 1991; Kröger et al., 2013; Hansen et al., 2017), herbicides (Johnson et al., 2001; J.M. Köhne et al., 2006), pesticides (Reemtsma et al., 2013; Walker et al., 2017) and emerging contaminants (Lapworth et al., 2012; Stuart et al., 2012; Neumann et al. 2010), in spite of their reactivity with porous media and undergoing decay, showed a significant threat to the groundwater environment (Broholm et al, 2001; Berkowitz et al. 2008) and risk for human health (Stuart et al. 2012) and biodiversity. An interesting review about pesticide transport modelling was presented by J.M. Köhne et al. (2009). Here we mostly focus on point contamination sources with short-term loading (Schwartz and Zhang, 2002), because in majority of non-point sources (e.g. from agriculture) with continuous source loading the effects of temporal and spatial variability is blurred. Oil and gas contaminated sites are of the very high risk due to the complex behavior of the contaminant at the unsaturated and saturates zone interface (Lenhard et al., 1989; Oostrom et al. 2003; Dobson et al., 2007).

Groundwater contamination with oil products is often associated with underground storage tank leaks. They can occur within oil or natural gas terminals, manufacturing ports and in common gas stations. There were 530 thousands documented cases of spills in the United States between 1988-2014 (US Census Bureau, 2014). In the São Paulo state,

Brazil, there are 5,200 documented contaminated sites, 3,800 of which are common gas stations. However, petroleum contamination is not limited to the surface spills only. Oil and gas wells, of which there are an estimated 4 million worldwide (Davies et al., 2014), can leak fluids into groundwater due to well integrity failures (Jackson, 2014). In a study of the potential reuse of lands impacted by petroleum releases, the USEPA (United States Environmental Protection Agency) reported that in Oklahoma and Texas alone there are more than 400,000 currently active and 800,000 historically drilled and abandoned oil, natural gas, and exploratory wells (Essaid et al. 2015). Usually, hydrocarbons infiltrate into the subsurface in the form of non-aqueous phase liquids (NAPL), immiscible with water, or directly as dissolved substances (Essaid et al. 2015). NAPL spills contain soluble and volatile components transferred with certain rates to the subsurface air, water, and solid phases, and generally representing a long-term source of contamination (Geller and Hunt, 1993; Peters et al. 1999). Dissolution and mass transfer rates, which depend on the composition of NAPL source along with groundwater flow field, change over time, affecting the concentration of the emanating solute plumes (Molson et al. 2002; Zhang et al. 2007; Brusseau et al. 2008). Unfortunately, in practical cases, a punctual accidental spill involves a complex mixture of substances (Morkin et al. 2000), most of them with unknown chemical composition and actual molecular fraction. Furthermore, the interaction of conjoint factors at field-scale like variability of hydraulic conductivity, spatial or temporal variability of hydraulic gradient, sorption process and vertical advective flux results in a non-ideal transport of dissolved contaminants in groundwater (Brusseau and Srivastava, 1997). For this reason, interpreting observed concentration distributions at field-scale and temporal changes in solute plumes dissolved from a NAPL source is still challenging (Essaid et al. 2015). Experimental and modelling studies demonstrated that a multi-constituent NAPL source evolves with time as components dissolve and volatilize at variable rates (D’Affonseca et al., 2011) resulting in different effluent concentration histories for each constituent. Moreover, once a NAPL reach the aquifer and dissolve, groundwater flow and its variations mainly control plumes migration and shape (Rama et al. 2019). Therefore, solute concentration in organic contaminants plumes will vary over time due to transport and degradation processes forced by the local flow field (Davis et al. 1999; Prommer et al. 2002; Zhang et al., 2009), which is inherently transient.

Figura 6 - Conceptual sketch of a soil transect with a LNAPL spill depicting key transport phenomena for source (dark red area) and dissolved plume fringes (light red shaded areas). (1) Matrix and backward diffusion mechanism through low-permeable layers dominating the long-term persistency of NAPL in the aquifer; (2) Microbial stimulation due to substrate availability (contamination plume) and colony/biofilm development related to the specific micro-scale conditions about porous geometry and flow velocity; (3) Free product zone detail representing an almost fully-saturated NAPL zone floating on the top of the aquifer with an irregular shape.



Thus, temporal distribution of hydrological stresses (e.g. precipitation, tidally-induced oscillation, river flood events) can be readily used to determine the variability of transient groundwater flow field where solute transport occurs and to assess water fluxes through the contamination source (Goode and Konikow, 1990; Dobson et al., 2007). Lumped-parameter and distributed-parameter models, along with field data (e.g. head, fluxes, tracer test) have provided significant insights about timescales of flow and transport processes in the subsurface, allowing more realistic simulation of subsurface complexity (Cook and Herczeg, 2000). However, in practice, the comparison between timescales of hydraulic propagation and response of solute in groundwater is challenging due to the water transit times through the unsaturated zone or retardation mechanisms at water-compound and soil-compound interfaces (Rao et al. 1980; Haggerty et al., 2004; Dobson et al., 2006; Eberhardt and Grathwohl, 2002). Usually in spill containments, the time of interest of a plume evolution do not match with the hydrologic processes affecting such evolution (Cook and Herczeg, 2000). Conversely, unsaturated zone dynamics, buffering transient hydrological

stresses (Feddes et al. 2004), and soil-compound physicochemical interactions, which slow down solute migration relative to groundwater (Brusseau and Srivastava, 1997), should be accounted for the interpretation of field data or modelling results in contaminated areas.

3.1.3 Processes of dissolved solute transport

3.1.3.1 Advection and dispersion

The advection is the movement of dissolved substances with flowing water (Fitts, 2012). This is the mechanism which carries water and associated chemicals through the porous media (Phillips and Castro 2003; Turnadge and Smerdon 2014). The mass flux of a solute due to advection is proportional to the Darcy's velocity and solute concentration, being in terms of rates, the most important transport mechanism in the subsurface (Kitanidis and McCarty, 2012).

The dispersion constitutes a non-steady irreversible mixing of the fluid in which the chemical is contained (Todd and Mays, 2004). In saturated porous media, the actual distribution of groundwater velocity varies significantly both in space and in time. The spatial velocity variations occur at scales ranging from the size of pores on up to the size of channel deposits in a floodplain (Fitts, 2012). The velocity temporal variations affect the direction of longitudinal and transverse spreading. Thus, an elongate solute plume will spread laterally over time with respect to the average flow direction (Goode and Konikow, 1990; Rehfeldt and Gelhar, 1992). The processes dependent on the velocity field represent an averaged formulation of microscopic phenomena over bigger heterogeneous volume, and thereby, a randomly variable flow field at different scales resulting in a wide range of plumes behaviors (MacFarlane et al. 1983; Pool and Dentz, 2018).

Therefore, a macro-dispersion term was introduced to deal with transport in heterogeneous media in full-scale applications (Schwartz, 1977; Gelhar and Axness 1983). Usually, macro-dispersion is treated as pre-asymptotic if the time-rate-of-growth of the second spatial moment of a plume has not stabilized. The travel distance for the controlling parameter, an effective dispersion coefficient, to approach the asymptotic conditions is in the order of 10 correlation lengths (Dagan, 1984). However, the notion of pre-asymptotic behavior does not apply directly to mass transfer models, as the spreading and tailing caused by mass transfer occur only over consistently lower timescales (Zinn and Harvey 2003).

Theoretically, in any fluid flow including groundwater there is only advection and diffusion (Molz, 2015) and other branches of science and engineering different from hydrogeology do not recognize the process of dispersion (Çengel and Cimbala, 2003). The problem is that true velocity field is essentially impossible to calculate or measure and, for this reason, an average approximation like the Darcy's velocity was introduced over a porous volume. Only below this scale, the interaction of actual non-constant fluid velocity in a tortuous fashion and the diffusive transport produce an irreversible mixing called hydrodynamic dispersion (Molz, 2015). Extended field data analysis showed that macro-dispersivity, that quantify spreading of conservative solutes in groundwater due to aquifer heterogeneity, is formation-specific and the modelling of transport cannot be relegated to a unique scaling law (Zech et al., 2015). Actually, this macro-dispersivity should have a constant asymptotic behavior, Fickian in the limit (Fiori et al., 2015), but a necessary condition to reach such limit is that periodicities were stationary. Instability of flow may have a great impact on the transversal macro-dispersion in the asymptotic phase, whereas the anisotropy of the medium plays a significant role only during the pre-asymptotic regime (Bellin et al., 1996). Therefore, under natural conditions, hydraulic gradient oscillations over time prevents transport from converging to well-defined Fickian mechanisms. At Cape Cod site, a field tracer test with bromide and complexed nickel (NiEDTA) showed significant differences in the travel distances needed to reach a constant longitudinal dispersivity (69 and 26 m, respectively), suggesting a spatial or temporal variability in the early time evolution of groundwater solute plumes (Hess et al. 2002). According to Bellin et al. (1996), the dispersion coefficients may change over the years depending on the gradient variation, and therefore the definition of an asymptotic dispersion based on few field data may be difficult/almost impossible. For Molz (2015), since the macro-dispersion concept requires an unrealistically long travel distance or travel time to converge to its Fickian asymptote, its scale-dependent behavior seems to be a "conceptual artefact". Even in laboratory columns under constant flow conditions dispersivity variations due to geochemical reactions were found (Appelo and Postma, 1999).

In the up-scaling of the transport problem from pore-scale to field-scale, studies differentiated spreading, that describes the spatial extent of the dispersed plume, and mixing, that describes the probability of chemical species to mix and react in a moving fluid (Dentz et al. 2011). Kitanidis (1994) underlined the importance to distinguish between spreading and dilution of a plume in groundwater, suggesting that macro-

dispersion coefficient, deduced from tracer tests, are not reliable measures of concentration reduction rates in heterogeneous media. Cirpka et al. (1999) showed that, in highly asymmetric flow models, transverse mixing is often over-represented leading to significant overestimation in the aerobic degradation rates. Such errors are due to the coarse applications of macro-dispersion parameters obtained from the spatial analysis of plume moments, or to numerical dispersion (Cirpka et al. 1999). The dilution index concept for conservative plumes (Kitanidis, 1994) was extended to reactive plumes in heterogeneous media by Chiogna et al. (2011b). An estimation of dilution index for Cape Cod and Border indicated similar values for both sites (0.63 and 0.72, respectively), despite Cape Cod plumes were more stretched and deformed than Borden (Thierrin and Kitanidis, 1994).

By numerical or semi-analytical models and lab-scale experiments, many studies delve into the contribution of advective and diffusive transport to the hydrodynamic dispersion process of solutes, and into the incongruence of conventional Fickian behavior of macro-dispersion coefficient. Cirpka et al. (2006) suggested that even in steady condition of flow the contribution of effective molecular diffusion to transverse dispersion cannot be neglected. This intuition was confirmed by a set of laboratory-scale experiments investigating transverse hydrodynamic dispersion of multi-tracers and its variations in the flow field (Chiogna et al., 2010), which also highlighted a nonlinear relation between dispersion coefficient and average linear velocity against the linear parametric model (Van Breukelen and Rolle, 2012):

$$D_T = \frac{l}{\sqrt{Pe + 123}} v_x + D_d^* \quad (2)$$

where D_T [$L^2 \cdot T^{-1}$] is the vertical transvers hydrodynamic dispersion, l [L] is the porous medium grain size, v_x [$L \cdot T^{-1}$] is the linear groundwater flow velocity in the direction, D_d^* [$L^2 \cdot T^{-1}$] is the effective porous diffusion, or pore diffusion coefficient, Pe is the Péclet number.

Furthermore, transverse mechanical dispersion resulted dependent on the specific diffusion coefficient at the experimental scale (Chiogna et al., 2010). A subsequent study demonstrated that compound-specific transverse mixing of species with different aqueous diffusion coefficients is still significant at field scale, especially in case of low to moderately heterogeneous porous media. The importance of local compound-

dependent effects on the length of simulated plumes in mixing-controlled reactive transport was also underlined (Chiogna et al., 2011a). Such findings were confirmed by Rolle et al. (2013) that showed a relevant influence of diffusive processes (pore channel scale) on the conservative and reactive solute transport (macroscopic scales) using pore-scale modelling, flow-through laboratory experiments, and field-scale numerical modelling based on Borden and Columbus aquifers.

It worth noting that most of this knowledge about the inadequacy of advection-dispersion transport at field scale derives from unsuccessful attempts to explain concentration distributions observed in MADE experiments, at Columbus site, using conventional macro-dispersion concepts (Molz et al. 2006). Gradual understanding of field evidences was built on the realization that neither macro-dispersion, nor hydrodynamic dispersion in general, was playing a dominant role at the MADE site (Zheng and Jiao, 1998; Benson et al., 2001; Zheng and Gorelick, 2003; Liu et al., 2008). Instead, a dual-domain concept (mobile/ immobile zones in close contact) led to conceptually simple simulations that incorporated the measured hydraulic conductivity field (Feehley et al., 2000) and reproduced the primary observed plume characteristics (Molz et al. 2006). Accordingly, a dual-domain mass transfer model resulted more accurate than an advection-dispersion model in describing the early high-concentration peaks and the later low-concentration tails observed in the field (Liu et al. 2010). By examining three stochastic transport models of MADE site, Salamon et al. (2007) highlighted the importance of small-scale heterogeneities in modelling tracer transport. Therefore, most of results from field investigations and modeling analyses suggested that connected networks of small-scale preferential flow paths and relative flow barriers exert dominant control on solute transport processes (Zheng et al. 2011).

In many practical cases, to simplify the solution when dealing with a high variability of parameters, effective field-averaged values are used by elaborating in-site observations (Butters and Jury, 1989, Cirpka and Attinger, 2003). However, some authors question the physical meaning of the effective parameters, suggesting that non-unique parameters would be more characteristic of macro-porous soils (Haws et al., 2005). Carrera et al. (2005) suggests the transformation of raw measurements in order to increase the sensitivity of data to the parameters. For example, using total observed mass instead of individual concentration values when modeling a breakthrough curve in a point or a plume movement (Corseuil et al., 2011a, Guilbeault et al. 2005; Bockelmann et al. 2003), or monitoring

peak concentration evolution and early peak arrival (Woodbury and Rubin 2000, Fiori et al. 2015).

3.1.3.2 Diffusion

In a stagnant solution, a difference in solute concentration between two points activates a net flux of mass from areas of higher to lower concentration, caused by the random Brownian movement of molecules (Appelo and Postma, 2005). This is called molecular diffusion and is governed by the Fick's laws (Fitts, 2012). In steady-state conditions its parameter, a diffusion coefficient, is constant and is directly proportional to the flux of solute mass and the concentration gradient, while in transient conditions the parameter is influenced by the spatial change of concentration and its variation over time (Kitanidis and McCarty, 2012).

The diffusive transport is normally not as important as the advective one (Appelo and Postma, 2005). This is because the diffusion coefficients are orders of magnitude smaller than hydraulic conductivity. Over short time periods diffusive transport equals advective transport, but over longer time periods (and hence also over larger distances) advective flow becomes more and more important (Appelo and Postma, 2005). However, where advective flow is negligible (e.g. in silt, clay lenses), diffusion may be the main transport mechanism (Perkins and Johnson, 1963; Hendry et al. 2017). In some aquifers, matrix and backward diffusion was shown to dominate transport (Chapman and Parker, 2005; Miotliński et al. 2011; Yang et al., 2014).

In some occasions, a groundwater professional needs to determine which process controls the movement of solute, particularly in aquifers where fractures or karstic features occur. If matrix diffusion is unimportant, then the equivalent porous media (Long et al., 1982) can represent the transport of solute in both sedimentary (Larocque et al., 1999, Shapiro and Nicholas, 1989) and crystalline rock aquifers (Hsieh et al., 1985). Where matrix diffusion processes have an important influence on solute concentrations, then introduction of discrete fracture network allows for an explicit characterization of the fracture and matrix properties (Shapiro and Nicholas, 1989, Sudicky and McLaren, 1992, Małozzewski and Zuber, 1993; Miotliński et al. 2011).

The sluggishness of diffusion may limit other processes (Kitanidis and McCarty, 2012). The examples are adsorption and desorption that may take place through very small apertures (Weber and DiGiano, 1996). The rates of some mechanisms may depend on diffusion, since the process-mediating microorganisms need to stay in contact with the porous

matrix (Griebler and Lueders, 2009) where diffusion results dominant in the substrate transport to cells (Hesse et al. 2010; Ramaswami et al. 1997). Similarly, the diffusion of dissolved gases limits the mass transfer of gases at the air-water interface (otherwise, equilibration between the air and gas phases would be practically instantaneous). Thus, in the case of sharp water-table fluctuations that cause surface turbulence, such mass-transfer of gases may be considerably enhanced (Holocher et al. 2003; McKenna and McGillis, 2004; Geistlinger et al. 2010).

The pore water velocity is an important parameter contributing to geochemical reactions including diffusion on the pore scale, although both, high and small water velocities can induce limitations in reactivity or bioavailability of compounds (Molins et al., 2012; Meckenstock et al. 2015). Brusseau (1993) analyzed the influence of seepage velocity at porous scale and intra-particle porosity on solute transport in groundwater, showing an increasing importance of diffusion limitation with the decreasing of flow velocities. Thus, biodegradation resulted availability-limited because microorganisms have consumed the substrate faster than it could be delivered by slow diffusion (Brusseau 1993). For low concentrations and transient flow conditions, Langner et al. (1998) found that degradation rates were higher when water flow was slower, suggesting that molecules needed sufficient time to diffuse into micropores. Thus, the transport time must be long compared to diffusion time, since otherwise molecules may be flushed through the pores without degradation (Langner et al. 1998).

3.1.4 Physicochemical processes in the shallow subsurface

3.1.4.1 Dissolution and solubilization

Macroscopic dissolution rates of NAPL in groundwater depend on their saturation (Miller et al., 1990), position into the mass transfer zone (Geller and Hunt, 1993), product-water interfacial area (J. Huang et al., 2015), groundwater velocity (Powers et al., 1991) and spatial distribution of residual entrapped NAPL (i.e. blobs and ganglia) (Powers et al., 1992, 1994). By analyzing dissolution and mass transfer under field conditions, Frind et al. (1999) showed a flow lines focusing through a dense NAPL source, resulting in a narrow stream tube downstream. In addition, equilibrium concentration are observed only at the center of the effluent plume, suggesting that peaks can be easily missed within the sampling wells at field site (Frind et al. 1999).

Furthermore, given a concomitant presence of ethanol and NAPL in contaminated areas may derive an enhancing of hydrocarbons solubility and saturation concentrations based on Raoult's Law (Corseuil et al., 1998), resulted from the reduction of aqueous phase polarity caused by the hydrophilic compound (ethanol). Such effect is described with a BTEX cosolvency model in ethanol (Powers et al., 2001) that mathematically is expressed by a logarithmic law (Corseuil and Fernandes, 1999):

$$\log(s_m) = \log(s_w) + \sigma f \quad (3)$$

where s_m is the compound solubility in the mixture, s_w is the compound solubility in water, f is the co-solvent volume fraction (ethanol) and σ is the cosolvency energy that accounts for the co-solvent capacity to solubilize the BTEXs.

Solubilization is a mass transfer process that may refer to the dissolution of a chemical from a solid phase into a soluble form (i.e. reverse of precipitation) or the partitioning of a chemical from a non-miscible liquid phase into the aqueous phase (Kitanidis and McCarty, 2012). This NAPL partitioning has generally slow kinetics, because it is controlled by the rate of transport in the aqueous phase (Berkowitz, et al. 2008). Solubilization process is affected by the solubility of compounds or minerals in aqueous phase, which depends on the law of mass action (Appelo and Postma, 2005). The solubility s [$M \cdot L^{-3}$] is a chemical property of a compound that constrains the maximal concentration of its components in aqueous phase (Berkowitz, et al. 2008). In complex mixtures of organic compounds, dissolution process is controlled by Raoult's Law and the saturation aqueous concentration of the individual components depends on numerous factors including the composition of the mixture (Mackay et al., 1991), pressure or temperature (Glynn and Reardon 1990). Raoult's Law actually relates the vapor pressure of each components to the composition of the ideal solution (Raoult, 1886). Thus, if the components are sufficiently similar from a thermodynamic point of view (e.g. BTEX in gasoline), such formulation can be used to predict the soluble concentrations of each compound in a mixture by the product of the aqueous solubility of pure substance, its activity coefficient and its molar fraction in the organic mixture (Eberhardt and Grathwohl, 2002).

3.1.4.2 Volatilization

The volatilization is the movement of a chemical from an aqueous, non-aqueous or solid phase to a gaseous phase (Kitanidis and McCarty, 2012). It is a mechanism acting in the surface or subsurface that reduces the contaminant mass in the soil by the transfer of vaporized contaminants from both saturated and unsaturated zone to the atmosphere (Mercer and Cohen, 1990). The process is a function of the difference between the actual gas pressure of a substance and the gas pressure in equilibrium with its concentration in water. The equilibrium depends on the Henry's law (Appelo and Postma, 2005). Volatilization rates are affected by chemical properties of contaminant (i.e. vapor pressure, solubility in water), environmental conditions (i.e. pollutant concentration, soil moisture content, air movement, temperature) and porous matrix properties (i.e. organic carbon content, porosity, density, clay content) (Lyman et al., 1982). Furthermore, in contrast to NAPL dissolution, mass transfer rates with air-phase decrease with decreasing soil mean grain size (Wilkins et al. 1995). Numerical transport models that include volatilization of organic contaminants are quite complex as there are three physical phases in the subsurface (no-aqueous phase, soluble component, and mobile fraction of a gas phase) (Abriola and Pinder, 1985).

3.1.4.3 Sorption and ion exchange

Sorption and ion exchange are mass transfer processes that results in the partitioning of a chemical from the aqueous phase onto or into a solid phase and retard the movement of contaminants in the subsurface (Kjølner et al., 2004; Kitanidis and McCarty, 2012). Thus, for quantifying retardation, we must consider the effects of adsorption and desorption processes on transport. The phenomenon can be described using sorption isotherms (e.g. linear, Freundlich, Langmuir) that define the relation between sorbed and solute species in a mass balance of a control volume (Appelo and Postma, 2005). It worth stressing that many organic pollutants are hydrophobic, which results in a low affinity for water solutions (polar liquid), preferring dissolve in non-polar liquids. Such contaminants can be readily taken up (absorption) in soil organic matter, depending on their distribution coefficient and partition constant (Karickhoff, 1984). The processes between reactive mineral surfaces and groundwater have been investigated at Cape Cod (Fuller et al. 1996). Adsorption and desorption present an exposure time dependence (Ginn, 2000), along with spatial variability (Allen-King et al., 2006), and variation with lithology (Allen-King et al., 2015). Thus, field-scale variability in sorption was important for explaining transient plume

features (Valocchi et al., 1981; Miralles-Wilhelm and Gelhar, 1996). Spatial variability, along with rate-limited and non-linear sorption phenomena affected transport of dissolved plumes at Borden and Cape Cod sites (Brusseau and Srivastava, 1999). Simulating differential downward movement of lithium and bromide at full-scale (Cape Cod site) required multi-component transport simulations that considered the variable-density of the plume and included lithium sorption (Zhang et al., 1998). Studies highlighted that sorption is controlled by kinetics instead of equilibrium formulations (Thorbjarnarson and Mackay, 1994), especially for short exposure times (Brusseau et al., 1991; Rahman et al., 2004). Effect of kinetic sorption/desorption on transverse mixing under transient flow conditions was mathematically derived by Cirpka (2005), showing that sorption contributes significantly to transverse mixing in flow fields undergoing temporal fluctuations of the flow direction. Thus, complexities of sorption should be accounted in the design of remediation schemes (Essaid et al. 2015).

3.1.4.4 Degradation

Degradation is a process that reduces concentrations and it is governed by chemical reactions often mediated by microorganisms (Jakobsen and Postma, 1999; Christensen et al., 2000). Generally, such activities fix and transform the contaminants, reducing their total amount or their impact in groundwater. The process is coupled with advection, diffusion and dispersion that facilitate the contact between reagents, and its rate in groundwater depends on dispersive mixing phenomena (Maier and Grathwohl, 2006; Cirpka and Valocchi, 2007). The factors that determine the rate at which the process takes place include environmental conditions where the reaction occurs (e.g. light, water, oxygen, temperature, pH), physiological capacity of microorganism to lead the transformation and bioavailability of nutrient (contaminants). The literature studies offer estimates of degradation rates (Appelo and Postma, 2005; Alvarez et al. 1991; Corseuil et al., 1998), which may be helpful in projections, simulations and a design of a remediation technique

3.1.4.5 Additional considerations on NAPL transport

Overall, key controlling phenomena explaining hydrocarbons fate in the subsurface were summarized as follows (Schirmer and Butler 2004): (a) NAPL infiltration in the unsaturated zone; (b) volatilization of NAPL source; (c) dissolution of low soluble free-product zone in contact

with water; (d) mass transfer of dissolved contaminants from source or free-product zone to the aquifer; (e) solute transport in the groundwater (saturated zone); (f) sorption of contaminants to the porous matrix; (g) chemical or abiotic reaction and (h) biological transformation (Fig. 6). In this review we put a particular emphasis on: (1) advection or conservative bulk motion, directly related with groundwater flow and thus, proportional to the seepage velocity obtained with the Darcy's Law; (2) molecular diffusion, caused by a concentration gradient in the aquifer and related with the thermal-kinetic energy of the solute at the microscopic level; and (3) hydrodynamic dispersion, resulted in a local variability of velocity relative to average groundwater flow caused by non-idealities at different scale in the porous medium (Fitts, 2012). The water-soil interface processes were covered elsewhere and they include sorption (Brusseau et al. 1989; Breus and Mishchenko, 2006), biodegradation (Powers et al. 2001; Kobayashi and Rittmann, 1982; Ma et al. 2013) as well as organic compound volatilization in the subsurface (Mercer and Cohen, 1990; Nielsen et al., 1986; Hance 1980).

3.1.5 Mathematical formulation

3.1.5.1 Groundwater flow and solute transport formulas

In addition to a concept development (Fig. 5, 6), a site prospection may require a numerical model, which provides a quantitative framework for synthesizing field information and for verifying complex chemical and hydrogeological processes (Anderson et al., 2015). To interpret or forecast any changes at a site, groundwater professionals use numerical codes that incorporate a set of mathematical equations to represent processes. This is called process-based modelling as opposed to data-driven modelling (Anderson et al., 2015).

The main equations for groundwater flow and solute transport in porous media are derived from the mass balance and conservation principles (Miller et al., 1998). The flow part comes from a pioneering work by Henry Darcy in 1856 on filtration experiments in sand columns (Fitts, 2012). The rate of flow per unit (q) is controlled by hydraulic gradient or hydraulic potential between two points at a line of measurement and the hydraulic conductivity of media (K , as described in Eq.1). Then effective porosity (η_e) is included to calculate pore or linear velocity (v_s) (Eq.4 – Darcy's Equation). Hydraulic head (h) [L] consists in a sum of an altitude term (z) and a pressure head (p) (Post and von Asmuth, 2013).

$$q = -\frac{k_i}{\mu} (\nabla p + \rho g \nabla z) \longrightarrow \quad (4)$$

$$\bar{q} = -K \cdot \frac{\Delta h}{\Delta x} \longrightarrow \bar{v}_s = -\frac{K}{\eta_e} \cdot \frac{\Delta h}{\Delta x}$$

The relation can be directly derived from a simplified momentum balance of the Navier-Stokes equation. In the case of a Newtonian fluid, a porous unconfined aquifer and a non-deformable solid matrix, the microscopic momentum balance is extended and averaged throughout the domain to obtain the "macroscopic" flow in the porous medium (general formulation of fluid motion in space), showing the close relationship between micro and macro scale (Bear and Cheng, 2010). Consequently, a general 3D mass balance equation in an anisotropic saturated porous medium (Eq.5) represents a spatial variation in rate of flow (left side) as a temporal variation in mass storage (right side) for a control volume (CV) (Domenico and Schwartz 1998, p.60):

$$-\left[\frac{\partial(\rho_w q_x)}{\partial x} + \frac{\partial(\rho_w q_y)}{\partial y} + \frac{\partial(\rho_w q_z)}{\partial z} \right] = \frac{\partial(\rho_w \eta)}{\partial t} \quad (5)$$

Thus, the general flow equation (Eq.6) is obtained using the Darcy's specific discharge definition and assuming, a rigid porous matrix and an incompressible fluid with constant density (i.e. pristine groundwater):

$$\frac{\partial}{\partial x} \left(K_{xx} \frac{\partial h}{\partial x} \right) + \frac{\partial}{\partial y} \left(K_{yy} \frac{\partial h}{\partial y} \right) + \frac{\partial}{\partial z} \left(K_{zz} \frac{\partial h}{\partial z} \right) = S \frac{\partial h}{\partial t} \quad (6)$$

Where ρ_w is water density, η is total porosity and S is the aquifer storativity, resulting from a linear combination of specific yield (S_y) and specific storage (S_s). However, given specific yield values order of magnitudes higher than specific storage in unconfined aquifers, S can be approximated with S_y in the aquifer conceptualization. Eventually, in a macroscopic application of this balance, an additional addendum in the right side can be punctual injections or withdrawals. It worth stressing that these formulations employ partial differential equations, which are difficult to solve in their analytical forms (Bear, 1972). For this reason, numerical approaches and simplifying/linearizing solutions (e.g. Boussinesq equation, Dupuit-Forchheimer approximation) are proposed

for many practical cases (Fitts, 2012; Domenico and Schwartz 1998; Bear and Cheng, 2010).

By extending the problem to the vadose zone, the Darcy's flux is integrated into a mass balance of an unsaturated CV (Custodio et al., 1988), where the pore spaces are occupied by two fluid phases: water and air. Therefore, in the case of a non-deformable porous medium, assuming a macroscopic water flow under stationary conditions and a constant air pressure within the pores (atmospheric pressure), Eq. 4 is expressed as a function of moisture content (θ_w) and pressure head (ψ_w) and becomes (Eq.7 - Richards' Equation, 1931):

$$\frac{\partial \theta_w}{\partial t} = \nabla \cdot [K_w \cdot \nabla (z + \psi_w)] \quad (7)$$

However, in the vadose zone all functional relations at the micro-scale were transformed to the macro-scale (Bear and Cheng, 2010), resulting in markedly non-linear relations between pressure (hydraulic head), conductivity and water content head explained by experimental parametric models (Brooks and Corey, 1966; Van Genuchten, 1980). In addition, at the micro-scale, a hysteretic constitutive relations governing variably saturated flow was found (Mualem, 1974, 1976). Thus, a tendency of some variables to have "memory" (i.e. to conserve the properties generated by a previous input) was observed. It worth stressing that in macro-scale applications and modelling, the hysteresis effects of the variables are generally unconsidered, although theoretical studies exist (Albers, 2014).

The transport of dissolved contaminants in the groundwater can be explained by a mass balance of species (i) in a phase (f) for an elemental CV (Barry et al. 2002). Since another variable than flow is defined in the transport problem (concentration of species in aqueous-phase), at least two equations are required to find a finite solution. Thus, in a saturated medium under isothermal conditions, the first equation would be the macroscopic total flux, which combines advection, dispersion, and diffusion processes, while the second relation will be properly the mass balance of dissolved contaminant in the CV (Bear and Cheng, 2010). Summarizing the problem in its general formulation (Eq.8), the advection-dispersion equation for conservative solute transport in porous media is obtained:

$$-\nabla(\eta v_s^f C^{if}) + \nabla(\eta D_h^{if} \nabla C^{if}) = \frac{\partial(\eta C^{if})}{\partial t} \quad (8)$$

where t [T] is time, η is total porosity, v_s [$M \cdot T^{-1}$] is the linear velocity resulting from Darcy's equation, C [$M \cdot L^{-3}$] is the concentration of species (i) in a fluid phase (f), and D_h [$L^2 \cdot T^{-1}$] is the hydrodynamic dispersion tensor.

In organic compounds spills, the aqueous phase is generally diluted and the dissolved solute concentration remains low relative to the total mass (Barry et al. 2002). This is caused by two factors: (a) hydrocarbons having a low solubility, which controls the dissolution of individual compounds in aqueous phase as a direct proportional between saturation and molar fraction (i.e. Raoult's Law), and (b) limited released mass in the source with relatively "low" concentrations with respect to the final contaminated water volume. Even in gasohol (i.e. gasoline and alcohol mixture) spills where the cosolvency effect may enhance BTEX compounds dissolution, the final solution is highly diluted relative to pure product. Therefore, non-dilution effects such as density or viscosity variability are disregarded in this formulation. Consequently, the vector notation in Eq.8, which was independent of the selected coordinate system, is projected into an arbitrary Cartesian coordinate system (x , y , z), resulting in the general equation of 3D transport in a completely saturated anisotropic porous medium for a non-conservative (reactive) solute, incorporating effects of advection, hydrodynamic dispersion (diffusion), source/sink term, decay and sorption-driven retardation:

$$\frac{\partial}{\partial x_i} \left(\eta D_{ij} \frac{\partial C}{\partial x_j} \right) - \frac{\partial}{\partial x_i} (\eta v_i C) - \lambda C + q_s C_s = \frac{\partial(\eta C R_d)}{\partial t} \quad (9)$$

where D_{ij} is the projected hydrodynamic dispersion tensor, v_i [$M \cdot T^{-1}$] is the projected velocity vector, λ is the first-order degradation coefficient [T^{-1}], C_s is the source concentration [$M \cdot L^{-3}$], q_s [T^{-1}] represents the specific source/sink flow, and R_d expresses a storage coefficient (retardation) related with sorption. It worth noting that for an anisotropic flow field with 3D dispersion is not possible to simplify the hydrodynamic tensor in three principal components as in the case of 1D uniform flow. Therefore, the dispersive addendum in Eq.9 results in nine components meanwhile the advective term express three components along the main flow directions.

3.1.5.2 Hydrodynamic dispersion tensor

Hydrodynamic dispersion equation was developed in the general theory of fluid mechanics to introduce the complexity of porous matrix configuration into the transport problem (Bear, 1961; Scheidegger, 1961), accounting for spreading and mixing of plumes at pore- and macro-scale. Since it results as a combined effect of molecular diffusion and mechanical dispersion, in the direction of flow, it is generally approximated proportional to the average Darcy's velocity. Mathematically:

$$D_{ijk} = \alpha_{ijkm} \cdot \frac{\bar{v}_k \cdot \bar{v}_m}{\bar{v}} f(Pe, \delta) \xrightarrow{\text{with}} Pe = \frac{l \cdot \bar{v}}{D_d} \quad (10)$$

where D_{ijk} [$L^2 \cdot T^{-1}$] is the generic hydrodynamic dispersion expressed as a tensor for an anisotropic 3D medium; \bar{v} [$L \cdot T^{-1}$] is the average seepage velocity in the porous medium (derived from the Darcy's equation); Pe is the Péclet number; δ is the ratio of the space of individual pores to the length characterizing their cross-section in a porous matrix; l [L] is the characteristic pores length, and D_d [$L^2 \cdot T^{-1}$] is the coefficient of molecular diffusion of species in aqueous phase. By assuming (Bear and Bachmat, 1967):

$$f(Pe, \delta) = \frac{Pe}{Pe + 2 + 4\delta^2} \quad (11)$$

The effect of tracer transfer by molecular diffusion between adjacent streamlines at the microscopic level is introduced in the transport formulation, although in most practical cases this function is approximated with one. The coefficient α [L] is the dispersivity of the porous medium and it expresses the microscopic configuration of the solid-liquid interface with a fourth-rank tensor (total 81 components with 36 non-zero components in a 3D space). Thus, dispersivity tensor results affected by scale (Rubin et al., 1999; Pickens and Grisak, 1981), saturation (Raouf and Hassanizadeh, 2013) and heterogeneities (Gelhar et al., 1992; Feehley et al. 2000; Harvey and Gorelick, 2000) or whether the solute transport is affected by fractures or karst features (Małozzewski and Zuber, 1985). In an isotropic medium, all the non-zero components of the dispersivity tensor (21) are related to only two parameters: a longitudinal dispersivity (α_L) and a transversal dispersivity (α_T), that usually have a ratio of 10 to 20. In the large-scale natural gradient test at Cape Cod, Massachusetts, longitudinal dispersivity of bromide resulted

much larger than transverse horizontal and vertical dispersivity: 0.96 m, 1.8 cm and 1.5 mm, respectively (Garabedian et al., 1991). Such parameters represents a crucial information to understand a full-scale transport problem, although they are almost impossible to estimate experimentally (Carrera, 1993; Gelhar et al., 1992; Moltz, 2015).

Usually in full-scale models of contaminated areas, a Fickian approach is applied to deal with solute transport in porous media and dispersive effects of advection and molecular diffusion are lumped together in a macro-dispersion coefficient (Eq.12), which represents an averaged term of the dispersion tensor in actual porous media (Hassanizadeh 1986; Harvey and Gorelick, 2000; Bear and Chang, 2010).

$$D_{mx} = \alpha_x \cdot \overline{v_x} + T_x^* \cdot D_d \quad (12)$$

where D_{mx} [$L^2 \cdot T^{-1}$] is the model parameter called macro-dispersion coefficient in the x direction; α_x [L] is the dispersivity in the x direction, v_x is the magnitude of the average linear velocity of flow, T_x^* is the tortuosity of porous matrix in the x direction, and D_d is the aqueous diffusion coefficient. Tortuosity is an experimental value accounting for travel paths, which was empirically related with the formation factor and the effective porosity of the medium (Appelo and Postma, 2005). Sometimes there was a confusion with the conversion of diffusion coefficient in pure water (D_d) to the more useful effective diffusion coefficient in macroscopic porous media (D_d^*) (Appelo and Postma, 2005), represented by the second addendum in the Eq.12. Finally, although lower than the longitudinal macro-dispersion, transverse macro-dispersion coefficient is a widely studied parameter and a relevant source of uncertainty in predicting dissolved contaminants migration, since it affects plume spreading and biodegradation rates (Chiogna et al., 2011a; Schirmer et al. 2001).

3.1.6 Flow and process characterization

3.1.6.1 Modelling conceptualization and execution

By considering a single uniform distribution of pores, single-porosity models are based on Richards' and Darcy's equations (flow formulation) and the advection–dispersion equation (solute transport formulation) (Gerke et al. 2007), while in dual-porosity models (Gerke and VanGenuchten, 1993) micro-pores and macro-pores act as separate

flow regions (Allaire et al. 2002a,b), each characterized by a specific degree of saturation, conductivity, and flux (Larson and Jarvis, 1999). As an alternative a first order mass transfer model can be applied (Feehley et al., 2000, Lu et al., 2011) with two porosity parameters, i.e. mobile and immobile one, as well as a coefficient governing the exchange rate between them (Miotliński et al., 2014). Harvey and Gorelick (2000) used this approach to explain the concentration profiles at the MADE site, pointing to its efficiency in representing the change in mobile dissolved mass with time, the accuracy of peak of the concentration profile, and the profile asymmetry observed in the field. A lack of physical meaning of the parameters, that could be independently measured, in particular the exchange rate coefficient, is believed to be a shortcoming of this approach (Sanford et al., 2017). Nevertheless, its accuracy as well as a relatively low computational effort made it widely used and conceptually extended (Zuber and Motyka, 1998; Fernandez-Garcia and Sanchez-Vila, 2015).

To obtain a fit between observed and modelled results, some authors mix the approaches or use explicit data if they are available. In a forced-gradient tracer test experiment in Tübingen, Germany, peak concentration and time of first arrival were better reproduced by a dual-porosity transport model by including spatial variability of grain size (Riva et al., 2010). In addition, incorporating nonlinear effects in the relationship between hydraulic conductivity and porosity improved a match between the observed and modelled profiles (Riva et al., 2010). Miotliński et al. (2011) used explicit fracture parameters including its porosity to explain the matrix diffusion process in a fractured aquifer. The approach allowed one to obtain a satisfactory fit between the field and model data without the use of the dual-porosity model (Miotliński et al., 2011).

3.1.6.2 Prospection methods

The geophysical methods are useful to evaluate heterogeneity that can potentially contribute to groundwater flow and, subsequently, to solute transport (Paillet and Pedler, 1996, Le Borgne et al. 2007; Shakas et al., 2018). These can be both surface-operated (Cartwright and McComas, 1968; Steward and Gay 1986; Daniels et al., 1998; Ebraheem et al. 2014) and borehole-lowered equipment (Paillet and Pedler, 1996). The techniques together with geological (borehole logging) and hydrogeological (e.g. a push-pull or tracer test) interpretation allow a cost-effective and non-invasive interpretation of permeability contrasts (Le Borgne et al., 2007; Miotliński et al., 2011; Liao et al., 2018). A major

advantage of these techniques is that they may give useful results upon a spill of contaminant and when using with frequency they allow one to trace the contaminant movement. Some borehole techniques are able to determine the exact location of high permeability features, their thicknesses and fracture spatial orientation, and even evaluate the presence of coatings of secondary material. Since a single technique can give ambiguous results, a use of several methods is warranted in order to determine whether fracture flow is significant (Paillet and Pedler, 1996). Muldoon and Bradbury (2005) showed that borehole geophysical logging could be used successfully in the determination of fractured zones in a dolostone aquifer, although a standard pumping test in a large set of observation wells indicated that the aquifer behaved as a porous medium. Recent works presented effective inversion procedures of hydraulic tomography applied to the high resolution characterization of hydraulic conductivity and specific storage heterogeneities at field-scale (Yeh and Liu, 2000; Jiménez et al. 2015)

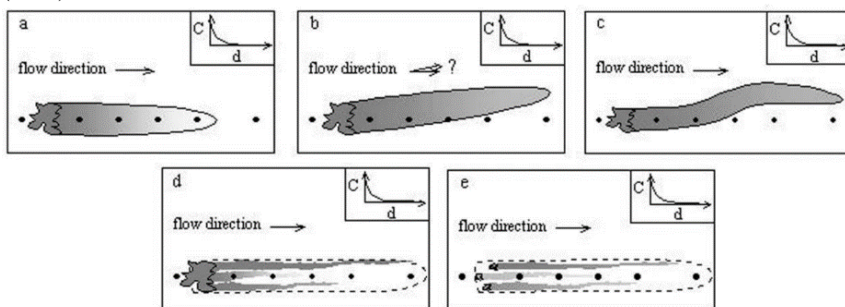
A down-hole electromagnetic flow meter is used to evaluate aquifer heterogeneity in the vertical direction and it gives a quantitative description of flow variability in a water-well, as well as the estimation of hydraulic conductivity over discrete intervals (Molz et al., 1989, Paillet and Pedler, 1996, Le Borgne et al., 2007). Le Borgne et al. (2007) demonstrated that the results from the flow meter analysis were very consistent with the packer tests and borehole geophysical data in identifying preferential flow zones in a fractured aquifer.

3.1.6.3 Site instrumentation

In addition to the spatial non-homogeneity, some processes may vary over time due to the transient nature of hydrological stresses (e.g. rainfalls, tides, river floods). Dynamic flow changes may have similar effects than geological heterogeneity on the plume migration resulting in a significant increase of plume spreading in transverse direction (Kim et al. 2000; Vanderborght et al., 2000; Cirpka and Attinger, 2003). In order to distinguish the effects of spatial heterogeneity and transient mechanisms on the solute distribution over time, a considerable amount of head and concentration measurements is required (Goode and Konikow, 1990). Such datasets are normally collected at field-scale through monitoring networks of piezometers and multi-levels wells, which have to be properly located to account for the plume variability (Chadalavada and Datta, 2008; Rein et al. 2009). Wilson et al. (2004) discussed the challenges related with monitoring well networks for

spatially variable plumes, illustrating the difficulty in establishing and instrumenting a representative centerline under natural conditions (Fig. 7). An earlier contribution by Brusseau (1994) provided an extended description of factors potentially responsible for non-ideal transport of dissolved contaminants under field conditions, which still represents a useful conceptual tool to design a monitoring network. However, recent and substantially more advanced researches are investigating new adaptive strategies for sampling in space and time, including genetic algorithms, systematic model errors estimation, flow-and-transport modeling, ensemble Kalman filtering, and multi-objective evolutionary optimization (Reed et al, 2000; Kollat et al. 2011).

Figure 7 - Conceptual diagrams illustrating difficulty in establishing and instrumenting representative centerline monitoring in different scenarios: (a) uniformly distributed plume in homogeneous, isotropic media, (b) uniformly distributed plume in homogeneous, isotropic media where hydraulic gradient is inaccurately defined, (c) uniformly distributed plume in media with undetected macro-scale heterogeneity (i.e. buried stream channel), (d) non-uniformly distributed plume migrating along preferred flux paths in heterogeneous media, (e) non-uniformly distributed plume generated from heterogeneously distributed sources. Dots represent monitoring wells and insets show resulting concentration vs distance along instrumented transect. Figure and caption obtained directly from Wilson et al. (2004).



Many investigators focused on three-dimensional characterization of heterogeneity deploying high resolution monitoring nets (Guilbeault et al., 2005) or hydraulic topographies with modular, temporarily-emplaced equipment for short-duration tests (Cardiff et al. 2012). A detailed site characterization and an uncertainty evaluation are essential steps for predicting NAPL dissolution and mass flux relationships (Troldborg et al. 2010), as well as for assigning site-specific remediation target values (Soga et al. 2004). At Borden site, Ontario, geostatistical interpretations

of the structure of hydraulic conductivity variations (i.e. variogram) aimed to explain plume spreading at field site (Sudicky, 1986; Woodbury and Sudicky, 1991; 1992). To understand the complex interaction occurring between diffusion, advection and reactions, recent work focus in better characterizing experimental conditions and especially pore-scale domain (Meakin and Tartakovsky, 2009). Promising techniques are being developed for both reactive and non-reactive flow and transport (Alkindi et al., 2010; Fridjonsson et al., 2010; Oostrom et al. 2016). As remembered by Kitanidis (2015), an in-action revolution in materials science, optics, and electronics allowed the production of cost-effective and accurate sensors (e.g. moisture sensors, miniature fiber optic piezometers, and oxygen sensors) contributing to the better definition of field conditions and parameters (Butler et al., 1999; Sakaki et al., 2008; Robinson et al., 2008). Even non-invasive methods based on tracers have been improved to determine NAPL source zone architecture (Rao et al. 2000). Thus, although interpretation is still difficult for multi-component NAPLs in heterogeneous settings, simple source zones can be characterized by partitioning tracer tests. (Boroumand and Abriola, 2015).

3.1.6.4 Groundwater – surface water interactions

To improve the understanding of the variable flow field that connect surface and subsurface, many techniques focus on an accurate recharge estimation. These make a use of hydraulic head (Das Gupta and Paudyal, 1988; Scanlon et al. 2002; Cuthbert, 2010; Crosbie et al. 2005), heat (Rau et al. 2014) and inorganic species data (Egboka et al., 1983; Herczeg and Edmunds, 2000; Xie et al. 2017). Moisture content measurements inform both the timing and volume of groundwater recharge from the surface (Hunt et al., 2008). Therefore, the assumption of constant and instantaneous transfer of infiltration to recharge have to be carefully assessed in the field (Healy and Cook, 2002) and it is inherently not valid for disconnected surface-subsurface systems (Brunner et al., 2011). Hence, streambeds where hydraulic conductivity controls large-scale exchange fluxes with aquifer remain the most challenging sites due to its spatiotemporal variability, and the scale dependency of measurement methods (Boano et al., 2010; Camporeale et al., 2013; Brunner, 2017). High variability of conductivity in the vertical direction have a direct impact on the measurement techniques and modelling approaches in gradient tracer tests (Ptak and Teutsch, 1994). Rosenberry and Pitlick (2009b) highlighted the importance of quantifying

both vertical and horizontal streambed conductivities, showing their relevant local variability, while Sebok et al. (2015) operated at different spatial scales in the measurements, underlining the scale-dependent behavior of conductivity field assessment.

3.1.6.5 Remaining uncertainties in NAPL characterization

In contaminated areas, heterogeneity of conductivity can lead to lateral migration of both LNAPL and DNAPL in the unsaturated zone (Essaid et al, 2015). Many field studies documented the spreading, pooling, and entrapment of non-aqueous phase by low conductive heterogeneities (Dillard et al., 1997; Essaid et al., 1993), and consequently, back diffusion of contaminants (Parker et al. 2008; Chapman and Parker, 2005; Seyedabbasi et al. 2012). Capillary forces affect NAPL relative permeability and make it more difficult to infiltrate into fine-grained layers (J. Huang et al., 2015). In the first MADE experiment, matrix diffusion within low-permeable layers in conjunction with a natural tendency for preferential sampling from permeable regions are used to explain the 21% lower values of sampled aqueous concentrations relative to the soil cores (Boggs and Adams, 1992). Heterogeneity-induced capillarity affects a DNAPL migration against groundwater gradients at the Hyde Park Landfill chemical waste disposal site near Niagara Falls, New York (Osborne and Sykes, 1986). Multiphase flow experiments at lab-scale confirmed such field observations, detailing the unstable NAPL infiltration as a result of pore-scale and macro-scale heterogeneity, along with fluid interactions (Darnault et al., 2001; Glass et al., 2000; Held and Illangasekare, 1995). The field experiments demonstrate that heterogeneities, along with NAPL saturation and groundwater flow affect the dissolution process (Essaid et al 2015). Source zone morphology, determined by the heterogeneity of the formation, controls the post-remediation dissolution behavior of contaminants (Soga et al. 2004). As well biodegradation may change the concentration of dissolved solutes in aqueous phase influencing the interphase mass transfer, which is driven by concentration gradient (Essaid et al., 2003). Furthermore, due to the uncertain total groundwater flux through the source area (Nowak et al., 2010), significant portion of uncertainty in predicting plume migration lies in the initial plume width estimation and source scale (de Barros and Nowak 2010), which have a key influence on expected development, dispersion, dilution and mixing of contaminants (Rubin et al., 1994; Dentz et al.,2000).

Once these contaminants pass to the aqueous-phase, their migration and spreading is affected by conjoint effects of irregular distribution of geological characteristics and hydrological stress apparent at different timescales (Cook and Herczeg, 2000; Dentz and Carrera, 2005; Pool et al. 2015; Zech et al., 2015). In unconfined saturated zones, most of plumes variability is related with heterogeneity of specific yield, along with hydraulic conductivity and macro-dispersion tensors variability (Cirpka et al. 2015; Werth et al. 2006). Especially transversal spreading of dissolved contaminants and sorption/retardation processes seems to be related with the heterogeneous distribution of features in the porous matrix at different scales (Roberts et al. 1986; Brusseau and Srivastava, 1999; Cirpka, 2005). To quantify the impacts of heterogeneity on effective flow, transport and reaction, new up-scaling strategies are being developed from pore-scale to macro-scale (Lichtner and Kang, 2007; Battiato et al., 2009; Battiato and Tartakovsky, 2010; Tyagi et al. 2013). Similarly, the uncertainty related to effective reactive transport models are estimated from a probability density function of the solute concentration (Tartakovsky and Broyda, 2010). Furthermore, reliable non-Fickian models (Berkowitz et al. 2006; Le Borgne et al., 2008; Neuman and Tartakovsky, 2009; Bijeljic et al., 2010) are available nowadays to represent heterogeneity impact on plume spreading. About this, Dentz et al. (2011) proposed a complete review of mixing, spreading and reaction interactions in heterogeneous media. At the same time, transient nature of hydrological stresses over the aquifer results in a wide-varied flow field that increase plume dispersion, substrate oxygen mixing and eventually biodegradation rates of contaminants (Schirmer et al. 2001; Goode and Konikow, 1990; Meckenstock et al., 2015)

Nonetheless, real interactions between geological heterogeneities and transient hydrological processes at different scales remain a critical source of uncertainty in the understanding of solute transport in porous media (Kitanidis 2015). An extensive laboratory-scale experiment, Rolle et al. (2009) tested the influence of steady and transient flow on solute mixing in both homogeneous and heterogeneous porous media, suggesting that changes in groundwater direction only cause local mixing enhancements and their contribution to transverse mixing are generally lower than those caused by geological heterogeneities. By carrying out a tracer experiment with both, conservative and reactive substances, in a quartz sand box of 14 m, Rahman et al. (2005) tried to quantify the vertical transversal mixing in a heterogeneous medium by analyzing concentration profiles. However, the heterogeneities caused a sinuous behavior of plumes, distorting the concentration profiles and leading to

the conclusion that velocity distribution is a mandatory information to estimate transversal mixing (Rahman et al., 2005).

3.1.7 Conclusions

In contaminated areas, an effective monitoring plan or remediation strategy starts with a deep comprehension of spatiotemporal variability of subsurface processes that affect flow field and solute transport at all the scale. Given the complexity of solute behavior in natural porous media, many comprehensive studies with different approaches are reviewed in the paper, including hydrogeology, chemistry, biology, engineering, economy, toxicology. Extended monitoring networks, accurate analysis of available datasets and proper verification of systematic hypothesis by a conceptual model development contribute to this interdisciplinary understanding of non-ideal transport of contaminants in groundwater.

To guarantee an actual usefulness of this paper for both practitioners and researchers, main factors influencing groundwater flow, solute transport and physicochemical processes in shallow aquifers are presented and classified, giving also a simple but rigorous mathematical formulation of the phenomena. The geological, hydrological and anthropogenic factors have a large variability in full-scale experiments, which generally confound our understanding of solutes migration, and make difficult to characterize processes from the simple monitoring of constitutive variables (i.e. hydraulic head, concentration). Further comprehension of fundamental aspects and even some limitation in classical theories are obtained by large field experiment with tracers under natural gradient, usually coupled with numerical models, which together have contributed to the development of modern hydrogeology. For this reason, integrating these contributions in new process-oriented researches and advanced modelling tools can contribute to the rapid improvement of our knowledge, and thereby, the quality of our application in contaminated areas. However, macro-dispersion concept for full-scale aquifers continues to be a controversial subject in contaminant hydrology, many new conceptual models (e.g. dual-porosity, dual-domain mass transfer) are being used to explain transport under natural conditions instead of common advection-dispersion model. These formulations should be routinely included in practical cases to test their performances in “less controlled” conditions than well-instrumented sites.

In addition, a wide-range of prospection methods and technologies is available for hydrogeological characterization, allowing save-time approaches that enhance our comprehension of hydraulic transients and

increase the spatial resolution of measurements. These approaches allow collecting an incredible amount of data, also useful for decision-makers, practitioners and governmental entities dealing with accidental spills. However, such information would firstly require an understanding of data significance, a result interpretation and an uncertainty comprehension. As the risk and regulatory drivers vary with each site, so description and characterization of subsurface phenomena in a site-assessment may require different depth and data comprehensiveness. If requirements change between two sites, our questions, methodologies, analysis, and answers for these two sites will change, implicating different times and resources for the hydrogeological characterization in the site-assessment. For this reason, the interaction between a variable flow field and solute transport in porous media have to be known (and understood) by who develop the contaminated area requirements. The debate about how best to describe solutes migration problem in full-scale experiments, especially under different field conditions, and the role of site-specific flow field in varying such transport in the groundwater is likely to continue for many years, but meantime even the partial advances in our understanding of the problem should be employed in practical cases and spreaded in educational field.

Acknowledgments

This work is part of a research and development project in partnership Universidade Federal de Santa Catarina (UFSC), Fundação de Ensino e Engenharia de Santa Catarina (FEESC) and Petróleo Brasileiro (Petrobras), that we thanks for the financial and material support. We also thanks the PhD student Martina Pacifici (USP, PPGEC) for help in figure design.

References

- Abarca, E., Karam, H., Hemond, H.F., Harvey, C.F., 2013. Transient groundwater dynamics in a coastal aquifer: The effects of tides, the lunar cycle, and the beach profile. *Water Resour. Res.* 49, 2473–2488. <https://doi.org/10.1002/wrcr.20075>
- Abelardo, R.-P., Nowak, W., 2018. Integrating transient behavior as a new dimension to WHPA delineation. *Adv. Water Resour.* 119, 178–187. <https://doi.org/10.1016/j.advwatres.2018.07.005>
- Abriola, L. M., Pinder, G. F. 1985. A multiphase approach to the modeling of porous media contamination by organic compounds: 2. Numerical simulation. *Water Resour. Res.*, 21(1), 19–26, doi:10.1029/WR021i001p00019
- Acharya, S., Jawitz, J.W., Mylavarapu, R.S., 2012. Analytical expressions for drainable and fillable porosity of phreatic aquifers under vertical fluxes from evapotranspiration and recharge. *Water Resour. Res.* 48, 1–15. <https://doi.org/10.1029/2012WR012043>
- Acharya, S., Mylavarapu, R., Jawitz, J., 2014. Evapotranspiration Estimation from Diurnal Water Table Fluctuations: Implementing Drainable and Fillable Porosity in the White Method. *Vadose Zo. J.* 1–13. <https://doi.org/10.2136/vzj2014.04.0048>
- Albers, B., 2014. Modeling the hysteretic behavior of the capillary pressure in partially saturated porous media: A review. *Acta Mech.* 225, 2163–2189. <https://doi.org/10.1007/s00707-014-1122-4>
- Alkindi, A., Al-Wahaibi, Y., Bijeljic, B., Muggerridge, A., 2010. Investigation of longitudinal and transverse dispersion in stable displacements with a high viscosity and density contrast between the fluids. *J. Contam. Hydrol.*
- Allaire, S.E., Gupta, S.C., Nieber, J., Moncrief, J.F., 2002a. Role of macropore continuity and tortuosity on solute transport in soils: 1. Effects of initial and boundary conditions. *J. Contam. Hydrol.* 58, 299–321. [https://doi.org/10.1016/S0169-7722\(02\)00035-9](https://doi.org/10.1016/S0169-7722(02)00035-9)

- Allaire, S.E., Gupta, S.C., Nieber, J., Moncrief, J.F., 2002b. Role of macropore continuity and tortuosity on solute transport in soils: 2. Interactions with model assumptions for macropore description. *J. Contam. Hydrol.* 58, 283–298. [https://doi.org/10.1016/S0169-7722\(02\)00034-7](https://doi.org/10.1016/S0169-7722(02)00034-7)
- Allen-King, R. M., Divine, D. P., Robin, M. J. L., Alldredge, J. R., Gaylord, D. R., 2006. Spatial distributions of perchloroethylene reactive transport parameters in the Borden Aquifer, *Water Resour. Res.*, 42, W01413, doi:10.1029/2005WR003977.
- Allen-King, R. M., Kalinovich, I., Dominic, D. F., Wang, G., Polmanteer, R., Divine, D. 2015. Hydrophobic organic contaminant transport property heterogeneity in the Borden Aquifer, *Water Resour. Res.*, 51, 1723–1743, doi:10.1002/2014WR016161.
- Alvarez, P.J.J., Anid, P.J., Vogel, T.M., 1991. Kinetics of aerobic biodegradation of benzene and toluene in sandy aquifer material. *Biodegradation* 2, 43–51. <https://doi.org/10.1007/BF00122424>
- Anderson, M.P., Woessner, W.W., Hunt, R.J. 2015. *Applied Groundwater Modeling - 2nd Edition - Simulation of Flow and Advective Transport*, Elsevier Inc., Academic Press, ISBN: 9780120581030, p.630
- Appelo, C.A.J., Postma, D., 1999. Variable dispersivity in a column experiment containing MnO₂ and FeOOH-coated sand. *J. Contam. Hydrol.* 40, 95–106.
- Appelo, C.A.J., Postma, D., 2005. *Geochemistry, Groundwater and Pollution - 2nd Edition* CRC Press, Amsterdam, the Netherlands, ISBN 9780415364287, p.647
- Arnold, J.G., Allen, P.M., Bernhardt, G., 1993. A comprehensive surface-groundwater flow model. *J. Hydrol.* 142, 47–69. [https://doi.org/10.1016/0022-1694\(93\)90004-S](https://doi.org/10.1016/0022-1694(93)90004-S)
- Ataie-Ashtiani, B., Volker, R.E., Lockington, D.A., 2001. Tidal effects on groundwater dynamics in unconfined aquifers. *Hydrol. Process.* 15, 655–669. <https://doi.org/10.1002/hyp.183>
- Bachmat, Y., Bear, J., 1964. The general equations of hydrodynamic dispersion in homogeneous, isotropic, porous mediums. *J. Geophys. Res.*, 69(12), 2561–2567, doi:10.1029/JZ069i012p02561.
- Bakhtyar, R., Brovelli, A., Barry, D.A., Li, L., 2011. Wave-induced water table fluctuations, sediment transport and beach profile change: Modeling and comparison with large-scale laboratory experiments. *Coast. Eng.* 58, 103–118. <https://doi.org/10.1016/j.coastaleng.2010.08.004>
- Barry, D.A., Barry, S.J., Parlange, J.Y., 1996. Capillarity Correction to Periodic Solutions of the Shallow Flow Approximation. *Coast. Estuar. Stud.* 50, 496–510.
- Barry, D.A., Prommer, H., Miller, C.T., Engesgaard, P., Brun, A., Zheng, C., 2002. Modelling the fate of oxidisable organic contaminants in groundwater. *Adv. Water Resour.* 25, 945–983. [https://doi.org/10.1016/S0309-1708\(02\)00044-1](https://doi.org/10.1016/S0309-1708(02)00044-1)
- Battle-Aguilar, J., Cook, P.G., 2012. Transient infiltration from ephemeral streams: A field experiment at the reach scale. *Water Resour. Res.* 48, 1–12. <https://doi.org/10.1029/2012WR012009>
- Battiato, I., Tartakovsky, D.M., 2010. Applicability regimes for macroscopic models of reactive transport in porous media. *J. Contam. Hydrol.* <https://doi.org/10.1016/j.jconhyd.2010.05.005>
- Battiato, I., Tartakovsky, D.M., Tartakovsky, A.M., Scheibe, T., 2009. On breakdown of macroscopic models of mixing-controlled heterogeneous reactions in porous media. *Adv. Water Resour.* 32, 1664–1673. <https://doi.org/10.1016/j.advwatres.2009.08.008>
- Bear, J., 1961. On the tensor form of dispersion in porous media. *J. Geophys. Res.* 66.
- Bear, J., 1972. *Dynamics of Fluids in Porous Media*, 764 pp., Elsevier, N. Y.
- Bear, J., Bachmat, Y., 1967. A generalized theory on hydrodynamic dispersion in porous media, in: *Symposium Artificial Recharge and Management of Aquifers*.
- Bear, J., Cheng, A.H.-D. (2010). *Modeling Groundwater Flow and Contaminant Transport*, Springer Science, Vol. 23, ISBN 978-1-4020-6681-8, p.850
- Bellin, A., Dagan, G., Rubin, Y., 1996. The impact of head gradient transients on transport in heterogeneous formations: Application to the Borden Site. *Water Resour. Res.* 32, 2705–2713. <https://doi.org/10.1029/96WR01629>
- Berkowitz, B., 2002. Characterizing flow and transport in fractured geological media: A review. *Adv. Water Resour.* 25, 861–884.
- Berkowitz, B., Cortis, A., Dentz, M., Scher, H., 2006. Modeling non-Fickian transport in geological formations as a continuous time random walk. *Rev. Geophys.* 44(2), <https://doi.org/10.1029/2005RG000178>
- Berkowitz, B., Dror, I., Yaron, B., 2008. *Contaminant Geochemistry*, Springer. <https://doi.org/10.1017/CBO9781107415324.004>
- Berkowitz, B., Silliman, S.E., Dunn, A.M., 2004. Impact of the Capillary Fringe on Local Flow, Chemical Migration, and Microbiology. *Vadose Zo. J.* 3, 534–548.
- Berglund, S., 1997. Aquifer remediation by pumping: A model for stochastic-advective transport with non-aqueous phase liquid dissolution, *Water Resour. Res.*, 33(4), 649–661, doi:10.1029/96WR03853

- Bijeljic, B., Rubin, S., Scher, H., Berkowitz, B., 2010. Non-Fickian transport in porous media with bimodal structural heterogeneity. *J. Contam. Hydrol.*, <https://doi.org/10.1016/j.jconhyd.2010.05.007>
- Boano, F., Camporeale, C., Revelli R., 2010. A linear model for the coupled surface-subsurface flow in a meandering stream. *Water Resour. Res.*, 46, W07535, doi:10.1029/2009WR008317.
- Bockelmann, A., Zamfirescu, D., Ptak, T., Grathwohl, P., Teutsch, G., 2003. Quantification of mass fluxes and natural attenuation rates at an industrial site with a limited monitoring network: A case study. *J. Contam. Hydrol.* 60, 97–121. [https://doi.org/10.1016/S0169-7722\(02\)00060-8](https://doi.org/10.1016/S0169-7722(02)00060-8)
- Boggs, J.M., Adams, E.E., 1992. Field Study of Dispersion in a Heterogeneous Aquifer 4. Investigation of Adsorption and Sampling Bias. *Water Resour. Res.* 28, 3325–3336.
- Boggs, J.M., Young, S.C., Beard, L.M., Gelhar, L.W., Rehfeldt, K.R., Adams, E.E., 1992. Field study of dispersion in a heterogeneous aquifer - 1. Overview and site description. *Water Resour. Res.* 28, 3281–3291. <https://doi.org/10.1029/92WR01756>
- Bohlke, J.-K., 2002. Groundwater recharge and agricultural contamination. *Hydrogeol. J.* 10, 153–179. <https://doi.org/10.1007/s10040-001-0183-3>
- Boroumand, A., Abriola, L. M., 2015. On the upscaling of mass transfer rate expressions for interpretation of source zone partitioning tracer tests. *Water Resour. Res.*, 51, 832–847, doi:10.1002/2014WR015767
- Boutt, D.F., Fleming, B.J., 2009. Implications of anthropogenic river stage fluctuations on mass transport in a valley fill aquifer. *Water Resour. Res.* 45, 1–14. <https://doi.org/10.1029/2007WR006526>
- Bouwer, H., 2002. Artificial recharge of groundwater: hydrogeology and engineering. *Hydrogeol J.* doi:10.1007/s10040-001-0182-4
- Bredehoeft, J. D., Pinder, G. F., 1973. Mass transport in flowing groundwater, *Water Resour. Res.*, 9(1), 194–210, doi:10.1029/WR009i001p00194
- Bresler, E., 1973. Simultaneous transport of solutes and water under transient unsaturated flow conditions, *Water Resour. Res.*, 9(4), 975–986, doi:10.1029/WR009i004p00975
- Breus, I.P., Mischchenko, A.A., 2006. Sorption of Volatile Organic Contaminants by Soils (A Review). *Eurasian Soil Chem.* 39, 1271–1283. <https://doi.org/10.1134/S1064229306120015>
- Broholm, M.M., Rügge, K., Tuxen, N., Højberg, A.L., Mosbaek, H., Bjerg, P.L., 2001. Fate of herbicides in a shallow aerobic aquifer: A continuous field injection experiment (Vejen, Denmark). *Water Resour. Res.* 37, 3163–3176.
- Brooks, M.C., Annable, M.D., Rao, P.S.C., Hatfield, K., Jawitz, J.W., Wise, W.R., Wood, A.L., Enfield, C.G., 2004. Controlled release, blind test of DNAPL remediation by ethanol flushing. *J. Contam. Hydrol.* 69, 281–297. [https://doi.org/10.1016/S0169-7722\(03\)00158-X](https://doi.org/10.1016/S0169-7722(03)00158-X)
- Brooks, R. H., Corey, A. T., 1966. Properties of Porous Media Affecting Fluid Flow. *Journal of the Irrigation and Drainage Division*, 92(2), p.61-90
- Brouyère, S., Dassargues, A., Hallet, V., 2004. Migration of contaminants through the unsaturated zone overlying the Hesbaye chalky aquifer in Belgium: a field investigation. *J. Contam. Hydrol.* 72, 135–164. <https://doi.org/10.1016/j.jconhyd.2003.10.009>
- Brunner, P., Cook, P.G., Simmons, C.T., 2011. Disconnected Surface Water and Groundwater: From Theory to Practice. *Ground Water* 49, 460–467. <https://doi.org/10.1111/j.1745-6584.2010.00752.x>
- Brunner, P., Simmons, C.T., 2012. HydroGeoSphere: A Fully Integrated, Physically Based Hydrological Model. *Ground Water* 50, 170–176. <https://doi.org/10.1111/j.1745-6584.2011.00882.x>
- Brunner, P., Therrien, R., Renard, P., Simmons, C.T., Franssen, H.-J.H., 2017. Advances in understanding river-groundwater interactions. *Rev. Geophys.* 55, 818–854. <https://doi.org/10.1002/2017RG000556>
- Brusseau, M.L., 1991. Application of a multi-process non-equilibrium-sorption model to solute transport in a stratified porous medium. *Water Resour. Res.*, 27 (4), 589–595
- Brusseau, M.L., 1994. Transport of Reactive Contaminants Media in Heterogeneous Porous Media. *Rev. Geophys.* 32, 285–313. <https://doi.org/10.1029/94RG00624>
- Brusseau, M.L., 1993. The Influence of Solute Size, Pore Water Velocity, and Intraparticle Porosity on Solute Dispersion and Transport in Soil. *Water Resour. Res.* 29, 1071–1080.
- Brusseau, M.L., Difilippo, E.L., Marble, J.C., Oostrom, M., 2008. Mass-Removal and Mass-Flux-Reduction Behavior for Idealized Source Zones with Hydraulically Poorly-Accessible Immiscible Liquid. *Chemosphere* 71, 1511–1521. <https://doi.org/10.1016/j.dci.2009.07.003>. Characterization
- Brusseau, M.L., Rao, P.S.C., Gillham, R.W., 1989. Critical Reviews in Environmental Control Sorption nonideality during organic contaminant transport in porous media. *Crit. Rev. Environ. Control* 19, 33–99.
- Brusseau, M.L., Srivastava, R., 1999. Nonideal transport of reactive solutes in heterogeneous porous media - 4. Analysis of the Cape Cod natural-gradient field experiment. *Water Resour. Res.* 35, 1113–1125. <https://doi.org/10.1029/1998WR900019>

- Brusseau, M.L., Srivastava, R., 1997. Nonideal transport of reactive solutes in heterogeneous porous media - 2. Quantitative analysis of the Borden natural-gradient field experiment. *J. Contam. Hydrol.* 28, 115–155. [https://doi.org/10.1016/S0169-7722\(97\)00036-3](https://doi.org/10.1016/S0169-7722(97)00036-3)
- Butler, J.J.J., McElwee, C.D., Bohling, G.C., 1999. Pumping tests in networks of multilevel sampling wells: Motivation and methodology. *Water Resour. Res.*, 35(11), 3553–3560.
- Butters, G.L., Jury, W.A., 1989. Field scale transport of bromide in an unsaturated soil: 2. Dispersion modeling. *Water Resour. Res.* 25, 1583–1589. <https://doi.org/10.1029/WR025i007p01583>
- Butters, G.L., Jury, W.A., Ernst, F.F., 1989. Field scale transport of bromide in an unsaturated soil 1. Experimental methodology and results. *Water Resour. Res.* 25, 1575–1581.
- Camporese, M., Daly, E., Paniconi, C., 2015. Catchment-scale Richards equation-based modeling of evapotranspiration via boundary condition switching and root water uptake schemes. *Water Resour. Res.* 51, 6381–6398. <https://doi.org/10.1002/2014WR016259>
- Camporese, M., Paniconi, C., Putti, M., Salandin P., 2009. Ensemble Kalman filter data assimilation for a process-based catchment scale model of surface and subsurface flow, *Water Resour. Res.*, 45, W10421, doi:10.1029/2008WR007031.
- Camporeale, C., Perucca, E., Ridolfi, L. Gurnell, A. M., 2013. Modeling the interactions between river morphodynamics and riparian vegetation, *Rev. Geophys.*, 51, 379–414, doi:10.1002/rog.20014
- Cao, G., Zheng, C., Simmons, C.T., 2016. Groundwater recharge and mixing in arid and semiarid regions: Heihe River Basin, northwest China. *Acta Geol. Sin.* 90, 971–987.
- Cardiff, M., Barrash, W., Kitanidis, P.K., 2012. A field proof-of-concept of aquifer imaging using 3-D transient hydraulic tomography with modular, temporarily-emplaced equipment. *Water Resour. Res.* 48. <https://doi.org/10.1029/2011WR011704>
- Carrera, J., 1993. An overview of uncertainties in modeling groundwater solute transport. *J. Contam. Hydrol.* 13, 23–48. [https://doi.org/10.1016/0169-7722\(93\)90049-X](https://doi.org/10.1016/0169-7722(93)90049-X)
- Carrera, J., Alcolea, A., Medina, A., Hidalgo, J., Slooten, L.J., 2005. Inverse problem in hydrogeology. *Hydrogeol. J.* 13, 206–222. <https://doi.org/10.1007/s10040-004-0404-7>
- Cartwright, K., McComas, M.R., 1968. Geophysical surveys in the vicinity of sanitary landfills in northeastern Illinois, in: 49th Meeting of the American Geophysical Union. pp. 23–30.
- Cartwright, N., Nielsen, P., Dunn, S., 2003. Water table waves in an unconfined aquifer: Experiments and modeling. *Water Resour. Res.* 39, 1330. <https://doi.org/10.1029/2003WR002185>
- Chadalavada, S., Datta, B., 2008. Dynamic Optimal Monitoring Network Design for Transient Transport of Pollutants in Groundwater Aquifers. *Water Resour. Manag.* 22, 651–670. <https://doi.org/10.1007/s11269-007-9184-x>
- Chapman, S.W., Parker, B.L., 2005. Plume persistence due to aquitard back diffusion following dense nonaqueous phase liquid source removal or isolation. *Water Resour. Res.* 41, 1–16. <https://doi.org/10.1029/2005WR004224>
- Childs, E.C., 1960. The Nonsteady State of the Water Table in Drained Land. *J. Geophys. Res.* 65, 1–3.
- Chiogna, G., Cirpka, O.A., Grathwohl, P., Rolle, M., 2011a. Transverse mixing of conservative and reactive tracers in porous media: Quantification through the concepts of flux-related and critical dilution indices. *Water Resour. Res.* 47, 1–15. <https://doi.org/10.1029/2010WR009608>
- Chiogna, G., Cirpka, O.A., Grathwohl, P., Rolle, M., 2011b. Relevance of local compound-specific transverse dispersion for conservative and reactive mixing in heterogeneous porous media. *Water Resour. Res.* 47. <https://doi.org/10.1029/2010WR010270>
- Chiogna, G., Eberhardt, C., Grathwohl, P., Cirpka, O. a., Rolle, M., 2010. Evidence of compound-dependent hydrodynamic and mechanical transverse dispersion by multitracer laboratory experiments. *Environ. Sci. Technol.* 44, 688–693. <https://doi.org/10.1021/es9023964>
- Christensen, T.H., Bjerg, P.L., Banwart, S. a., Jakobsen, R., Heron, G., Albrechtsen, H.J., 2000. Characterization of redox conditions in groundwater contaminant plumes. *J. Contam. Hydrol.* 45, 165–241. [https://doi.org/10.1016/S0169-7722\(00\)00109-1](https://doi.org/10.1016/S0169-7722(00)00109-1)
- Cirpka, O.A., 2005. Effects of sorption on transverse mixing in transient flows. *J. Contam. Hydrol.* 78, 207–229. <https://doi.org/10.1016/j.jconhyd.2005.05.008>
- Cirpka, O.A., Attinger, S., 2003. Effective dispersion in heterogeneous media under random transient flow conditions. *Water Resour. Res.* 39, 1–15. <https://doi.org/10.1029/2002WR001931>
- Cirpka, O.A., Chiogna, G., Rolle, M., Bellin, A., 2015. Transverse mixing in three-dimensional nonstationary anisotropic heterogeneous porous media. *Water Resour. Res.* 51, 241–260. <https://doi.org/10.1002/2014WR015331>.Received
- Cirpka, O.A., Frind, E.O., Helmig, R., 1999. Numerical simulation of biodegradation controlled by transverse mixing. *J. Contam. Hydrol.* 40, 159–182. [https://doi.org/10.1016/S0169-7722\(99\)00044-3](https://doi.org/10.1016/S0169-7722(99)00044-3)

- Cirpka, O.A., Olsson, Å., Ju, Q., Rahman, M.A., Grathwohl, P., 2006. Determination of transverse dispersion coefficients from reactive plume lengths. *Ground Water* 44, 212–221. <https://doi.org/10.1111/j.1745-6584.2005.00124.x>
- Cirpka, O.A., Valocchi, A.J., 2007. Two-dimensional concentration distribution for mixing-controlled bioreactive transport in steady state. *Adv. Water Resour.* 30. <https://doi.org/10.1016/j.advwatres.2008.10.018>
- Colombani, N., Di Giuseppe, D., Faccini, B., Ferretti, G., Mastrocicco, M., Coltorti, M., 2016. Inferring the interconnections between surface water bodies, tile-drains and an unconfined aquifer-aquitard system: A case study. *J. Hydrol.* 537, 86–95. <https://doi.org/10.1016/j.jhydrol.2016.03.046>
- Cook, P.G., Herczeg, A.L., 2000. *Environmental Tracers in Subsurface Hydrology*, Chap.1 Determining Timescales for Groundwater Flow and Solute Transport, Springer Science, New York, ISBN 978-1-4615-4557-6, p.529
- Corseuil, H.X., Fernandes, M., 1999. Efeito do etanol no aumento da solubilidade de compostos aromáticos presentes na gasolina brasileira. *Rev. Eng. Sanitária e Ambient.* 4, 71–75
- Corseuil, H.X., Hunt, C.S., Santos, R.C.F. dos, Alvarez, P.J.J., 1998. The influence of the gasoline oxygenate ethanol on aerobic and anaerobic btx biodegradation. *Water Res.* 32, 2065–2072
- Corseuil, H.X., Monier, A.L., Fernandes, M., Schneider, M.R., Nunes, C.C., 2011a. BTEX Plume Dynamics Following an Ethanol Blend Release: Geochemical Footprint and Thermodynamic Constraints on Natural Attenuation - Supporting Information. *Environ. Sci. Technol.* 23. <https://doi.org/10.1117/1111.2794018.2>
- Corseuil, H.X., Monier, A.L., Fernandes, M., Schneider, M.R., Nunes, C.C., Do Rosario, M., Alvarez, P.J.J., 2011b. BTEX plume dynamics following an ethanol blend release: Geochemical footprint and thermodynamic constraints on natural attenuation. *Environ. Sci. Technol.* 45, 3422–3429. <https://doi.org/10.1021/es104055q>
- Crosbie, R.S., Binning, P., Kalma, J.D., 2005. A time series approach to inferring groundwater recharge using the water table fluctuation method. *Water Resour. Res.* 41, 1–9. <https://doi.org/10.1029/2004WR003077>
- Custodio, E., Gurgui, A., Lobo Ferreira, J.P., 1988. *Groundwater Flow and Quality Modelling*. <https://doi.org/10.1007/978-94-009-2889-3>
- Cuthbert, M.O., 2010. An improved time series approach for estimating groundwater recharge from groundwater level fluctuations. *Water Resour. Res.* 46, 1–11. <https://doi.org/10.1029/2009WR008572>
- Çengel, Y.A. Cimbala, J.M., 2014. *Fluid Mechanics: Fundamentals and applications – 3rd Edition*, McGraw-Hill Inc., New York, USA, ISBN 978-0-07-338032-2, p.1031
- D’Affonseca, F.M., Prommer, H., Finkel, M., Blum, P., Grathwohl, P., 2011. Modeling the long-term and transient evolution of biogeochemical and isotopic signatures in coal tar-contaminated aquifers. *Water Resour. Res.* 47, 1–22. <https://doi.org/10.1029/2010WR009108>
- Dagan, G., 1984. Solute transport in heterogeneous porous formations, *J. Fluid Mech.*, 145, 151-177
- Daly, E., Porporato, A., 2005. A Review of Soil Moisture Dynamics: From Rainfall Infiltration to Ecosystem Response. *Environ. Eng. Sci.* 22.
- Daniels, J.J., Brower, J., Baumgartner, F., 1998. High Resolution GPR at Brookhaven National Laboratory to Delineate Complex Subsurface Targets. *J. Environ. Eng. Geophys.* 3, 1–5.
- Darnault, C.J.G., DiCarlo, D.A., Bauters, T.W.J., Jacobson, A.R., Throop, J.A., Montemagno, C.D., Parlange, J.Y., Steenhuis, T.S., 2001. Measurement of fluid contents by light transmission in transient three-phase oil-water-air systems in sand. *Water Resour. Res.*, 37(7), 1859–1868, doi:10.1029/2000WR900380
- Das Gupta, A., Paudyal, G.N., 1988. Estimating aquifer recharge and parameters from water level observations. *J. Hydrol.* 99, 103–116. [https://doi.org/10.1016/0022-1694\(88\)90081-9](https://doi.org/10.1016/0022-1694(88)90081-9)
- Davies, R. J., Almond, S., Ward, R. S., Jackson, R. B., Adams, C., Worrall, F., Whitehead, M. A., 2014. Oil and gas wells and their integrity: Implications for shale and unconventional resources exploitation, *Mar. Pet. Geol.*, 56, 239–254.
- Davis, G.B., Barber, C., Power, T.R., Thierrin, J., Patterson, B.M., Rayner, J.L., Wu, Q., 1999. The variability and intrinsic remediation of a BTEX plume in anaerobic sulphate-rich groundwater. *J. Contam. Hydrol.* 36, 265–290. [https://doi.org/10.1016/S0169-7722\(98\)00148-X](https://doi.org/10.1016/S0169-7722(98)00148-X)
- de Barros, F.P.J., Nowak, W., 2010. On the link between contaminant source release conditions and plume prediction uncertainty. *J. Contam. Hydrol.* 116, 24–34. <https://doi.org/10.1016/j.jconhyd.2010.05.004>
- De Louw, P.G.B., Eeman, S., Oude Essink, G.H.P., Vermue, E., Post, V.E.A., 2013. Rainwater lens dynamics and mixing between infiltrating rainwater and upward saline groundwater seepage beneath a tile-drained agricultural field. *J. Hydrol.* 501, 133–145. <https://doi.org/10.1016/j.jhydrol.2013.07.026>
- De Schepper, G., Therrien, R., Refsgaard, J.C., Hansen, A.L., 2015. Simulating coupled surface and subsurface water flow in a tile-drained agricultural catchment. *J. Hydrol.* 521, 374–388. <https://doi.org/10.1016/j.jhydrol.2014.12.035>
- de Vries, J.J., Simmers, I., 2002. Groundwater recharge: An overview of process and challenges. *Hydrogeol. J.* 10, 5–17. <https://doi.org/10.1007/s10040-001-0171-7>

- Dentz, M., Carrera, J., 2003. Effective dispersion in temporally fluctuating flow through a heterogeneous medium. *Phys. Rev. E* 68. doi:10.1103/PhysRevE.68.036310
- Dentz, M., Carrera, J., 2005. Effective solute transport in temporally fluctuating flow through heterogeneous media. *Water Resour. Res.* 41, 1–20. <https://doi.org/10.1029/2004WR003571>
- Dentz, M., Kinzelbach, H., Attinger, S., Kinzelbach, W., 2000. Temporal behavior of a solute cloud in a heterogeneous porous medium 2. Spatially extended injection. *Water Resour. Res.* 36, 3605–3614.
- Dentz, M., Le Borgne, T., Englert, A., Bijeljic, B., 2011. Mixing, spreading and reaction in heterogeneous media: A brief review. *J. Contam. Hydrol.* 120–121, 1–17. <https://doi.org/10.1016/j.jconhyd.2010.05.002>
- Devlin, J. F., Barker, J. F., 1996. Field Investigation of Nutrient Pulse Mixing in an in Situ Biostimulation Experiment. *Water Resour. Res.*, 32(9), 2869–2877. doi:10.1029/96WR01128
- Dickinson, R.E., 1984. Modeling evapotranspiration for three-dimensional global climate models, Geophysical Monograph Series: Climate Processes and Climate Sensitivity.
- Diersch, H. J. G., 2014. *FEFLOW - Finite Element Modeling of Flow, Mass and Heat Transport in Porous and Fractured Media*, Springer, ISBN 978-3-642-38738-8, p.1018
- Diersch, H.J.G., Kolditz, O., 2002. Variable-density flow and transport in porous media; approaches and challenges. *Adv. Water Resour.* 25, 899–944. [https://doi.org/10.1016/S0309-1708\(02\)00063-5](https://doi.org/10.1016/S0309-1708(02)00063-5)
- Dillard, L. A., Essaid, H. I., Herkelrath, W. N., 1997. Multiphase flow modeling of a crude-oil spill site with a bimodal permeability distribution. *Water Resour. Res.*, 33(7), 1617–1632. doi:10.1029/97WR00857.
- Dobson, R., Schroth, M.H., Ostrom, M., Zeyer, J., 2006. Determination of NAPL-water interfacial areas in well-characterized porous media. *Environ. Sci. Technol.* 40, 815–822. <https://doi.org/10.1021/es050037p>
- Dobson, R., Schroth, M.H., Zeyer, J., 2007. Effect of water-table fluctuation on dissolution and biodegradation of a multi-component, light nonaqueous-phase liquid. *J. Contam. Hydrol.* 94, 235–248. <https://doi.org/10.1016/j.jconhyd.2007.07.007>
- Domenico, P.A., Schwartz, F.W., 1998. *Physical and Chemical Hydrogeology*. John Wiley & Sons.
- Du, E., Jackson, C.R., Klaus, J., McDonnell, J.J., Natalie, A., Williamson, M.F., Greco, J.L., Bitew, M., 2016. Interflow dynamics on a low relief forested hillslope: lots of fill, little spill. *J. Hydrol.* 534, 648–658. <https://doi.org/10.1016/j.jhydrol.2016.01.039>
- Duchemin, B., Hadria, R., Erraki, S., Boulet, G., Maisongrande, P., Chehbouni, A., Escadafal, R., Ezzahar, J., Hoedjes, J.C.B., Kharrou, M.H., Khabba, S., Mougenot, B., Olioso, A., Rodriguez, J.-C., Simonneaux, V., A, 2006. Monitoring wheat phenology and irrigation in Central Morocco: On the use of relationships between evapotranspiration, crops coefficients, leaf area index and remotely-sensed vegetation indices. *Agric. Water Manag.* 79, 1–27. <https://doi.org/10.1016/j.agwat.2005.02.013>
- Duchene, M., McBean, E.A., Thomson, N.R., 1994. Modeling of infiltration from trenches for storm-water control. *J. Water Resour. Plan. Manag.* 120, 276–293.
- Duke, H.R., 1972. Capillary properties of soils - Influence upon specific yield. *Trans. ASAE* 15, 688–691.
- Dunkerley, D. L., 2008. Bank permeability in an Australian ephemeral dry-land stream: Variation with stage resulting from mud deposition and sediment clogging. *Earth Surf. Processes Landforms*, 33(2), 226–243
- Dunkle, K.M., 2008. *Hydrostratigraphic and Groundwater Flow Model: Troy Valley Glacial Aquifer*. MSc Thesis, Univ. Wisconsin-Madison, p.236
- Dunne, T., Black, R.D., 1970. An Experimental Investigation Runoff Production in Permeable Soils. *Water Resour. Res.* 6.
- Eaton, T.T., 2006. On the importance of geological heterogeneity for flow simulation. *Sediment. Geol.* 184, 187–201. <https://doi.org/10.1016/j.sedgeo.2005.11.002>
- Eberhardt, C., Grathwohl, P., 2002. Time scales of organic contaminant dissolution from complex source zones: Coal tar pools vs. blobs. *J. Contam. Hydrol.* 59, 45–66. [https://doi.org/10.1016/S0169-7722\(02\)00075-X](https://doi.org/10.1016/S0169-7722(02)00075-X)
- Ebraheem, A.M., Mulla, M.M., Sherif, M.M., Awad, O., Akram, S.F., Al Suweidi, N.B., Shetty, A., 2014. Mapping groundwater conditions in different geological environments in the northern area of UAE using 2D earth resistivity imaging survey. *Environ. Earth Sci.* 72, 1599–1614. <https://doi.org/10.1007/s12665-014-3064-5>
- Egboka, B.C.E., Cherry, J.A., Farvolden, R.N., Frind, E.O., 1983. Migration of contaminants in groundwater at a landfill: A case study. 3. Tritium as an indicator of dispersion and recharge. *J. Hydrol.*, 63 (1/2), 51–80.
- Engelhardt, I., Prommer, H., Moore, C., Schulz, M., Schuth, C., Ternes, T.A., 2013. Suitability of temperature, hydraulic heads, and acesulfame to quantify wastewater-related fluxes in the hyporheic and riparian zone. *Water Resour. Res.* 49, 426–440. <https://doi.org/10.1029/2012WR012604>
- Essaid, H.I., Bekins, B.A., Cozzarelli, I.M., 2015. Organic contaminant transport and fate in the subsurface: Evolution of knowledge and understanding. *Water Resour. Res.* 51, 4861–4902. <https://doi.org/10.1002/2015WR017121>

- Essaid, H.I., Cozzarelli, I.M., Eganhouse, R.P., Herkelrath, W.N., Bekins, B. a., Delin, G.N., 2003. Inverse modeling of BTEX dissolution and biodegradation at the Bemidji, MN crude-oil spill site, *Journal of Contaminant Hydrology*. [https://doi.org/10.1016/S0169-7722\(03\)00034-2](https://doi.org/10.1016/S0169-7722(03)00034-2)
- Essaid, H. I., Herkelrath, W. N., Hess K. M., 1993. Simulation of fluid distributions observed at a crude oil spill site incorporating hysteresis, oil entrapment, and spatial variability of hydraulic properties, *Water Resour. Res.*, 29(6), 1753–1770, doi:10.1029/93WR00370
- Euliss, N.H., Mushet, D.M., 1996. Water-level fluctuation in wetlands as a function of landscape condition in the prairie pothole region. *Wetlands* 16, 587–593.
- Ezzedine, S., Rubin, Y., 1997. Analysis of the Cape Cod tracer data. *Water Resour. Res.* 33, 1–11.
- Falta, R.W., 1998. Using phase diagrams to predict the performance of cosolvent floods for NAPL remediation. *Gr. Water Monit. Remediat. Summer*, 94–102.
- Feddes, R.A., Rooij, G.H.de, Dam, J.C.van, 2004. *Unsaturated-zone Modeling: Progress, Challenges and Applications* Springer-Verlag, Wageningen UR Frontis Series Vol.6, ISBN 978-1-4020-2917-2, p.364
- Fedrizzi, F., Ramos, D.T., Lazzarin, H.S.C., Fernandes, M., Larose, C., Vogel, T.M., Corseuil, H.X., 2017. A Modified Approach for in Situ Chemical Oxidation Coupled to Biodegradation Enhances Light Nonaqueous Phase Liquid Source-Zone Remediation. *Environ. Sci. Technol.* 51, 463–472. <https://doi.org/10.1021/acs.est.6b03604>
- Feehley, C.E., Zheng, C., Molz, F.J., 2000. A dual-domain mass transfer approach for modeling solute transport in heterogeneous aquifers: Application to the Macrodispersion Experiment (MADE) site. *Water Resour. Res.* 36, 2501. <https://doi.org/10.1029/2000WR900148>
- Fernández-García, D., Sanchez-Vila, X., 2015. Mathematical equivalence between time-dependent single-rate and multiple mass transfer models. *Water Resour. Res.* 51, 3166–3180. <https://doi.org/10.1002/2014WR016348>. Received
- Fielding, C.R., Allen, J.P., Alexander, J., Gibling, M.R., 2009. Facies model for fluvial systems in the seasonal tropics and subtropics. *Geology* 37, 623–626. <https://doi.org/10.1130/G25727A.1>
- Fitts, C., 2012. *Groundwater Science- 2nd Edition*, Academic Press, ISBN: 9780123847065, p.692
- Fiori, A., Bellin, A., Cvetkovic, V., De Barros, F.P.J., Dagan, G., 2015. Stochastic modeling of solute transport in aquifers: From heterogeneity characterization to risk analysis. *Water Resour. Res.* 51, 6622–6648. <https://doi.org/10.1002/2015WR017388>
- Freyberg, D.L., 1986. A Natural Gradient Experiment on Solute Transport in a Sand Aquifer: 2. Spatial Moments and the Advection and Dispersion of Nonreactive Tracers. *Water Resour. Res.* 22, 2031–2046.
- Freeze, R. A., 1969. The mechanism of natural ground-water recharge and discharge: 1. One-dimensional, vertical, unsteady, unsaturated flow above a recharging or discharging ground-water flow system, *Water Resour. Res.*, 5(1), 153–171, doi:10.1029/WR005i001p00153.
- Freeze, R.A., Cherry, J.A., 1979. *Groundwater*. Prentice-Hall Inc., Englewood Cliffs, Vol. 7632, p.604.
- Fridjonsson, E.O., Seymour, J.D., Schultz, L.N., Gerlach, R., Cunningham, A.B., Codd, S.L., 2010. NMR measurement of hydrodynamic dispersion in porous media subject to biofilm mediated precipitation reactions. *J. Contam. Hydrol.*
- Frind, E.O., Molson, J.W., Schirmer, M., Guiguer, N., 1999. Dissolution and mass transfer of multiple organics under field conditions: The Borden emplaced source. *Water Resour. Res.* 35, 683–694.
- Fuller, C.C., Davis, J.A., Colston, J.A., Dixon, A., 1996. Characterization of metal adsorption variability in a sand and gravel aquifer, Cape Cod, Massachusetts, USA. *J. Contam. Hydrol.* 2, 165–187
- Gallagher, D.L., Dietrich, A.M., Reay, W.G., Hayes, M.C., Simmons Jr., G.M., 1996. Ground water discharge of agricultural pesticides and nutrients to estuarine surface water. *Groundw. Monit. Remediat.* <https://doi.org/10.1111/j.1745-6592.1996.tb00579.x>
- Gambolati G, Putti M, Paniconi C., 1999. Three-dimensional model of coupled density-dependent flow and miscible salt transport. In: Bear J, Cheng AHD, Sorek S, Quazar D, Herrera I, editors. *Seawater intrusion in coastal aquifers*. Dordrecht: Kluwer Publ. p. 315
- Garabedian, S.P., Leblanc, D.R., Gelhar, L.W., Celia, M.A., 1991. Large-scale natural gradient tracer test in sand and gravel Cape Cod, Massachusetts - 2. Analysis of spatial moment for a non-reactive tracer. *Water Resour. Res.* 27, 14.
- Geistlinger, H., Jia, R., Eisermann, D., Stange, C.F., 2010. Spatial and temporal variability of dissolved nitrous oxide in near-surface groundwater and bubble-mediated mass transfer to the unsaturated zone. *J. Plant Nutr. Soil Sci.* 173, 601–609. <https://doi.org/10.1002/jpln.200800278>
- Gelhar, L.W., Axness, C.L., 1983. Three-Dimensional Stochastic Analysis of Macrodispersion in Aquifers. *Water Resour. Res.* 19, 161–180. <https://doi.org/10.1029/WR019i001p00161>
- Gelhar, L.W., Welty, C., Rehfeld, K.R., 1992. A Critical Review of Data on field-scale dispersion in aquifers. *Water Resour. Res.* 28, 1955–1974.
- Geller, J.T., Hunt, J.R., 1993. Mass transfer From Nonaqueous Phase Organic Liquids in Water-Saturates Porous Media. *Water Resour. Res.* 29, 833–845. <https://doi.org/10.1016/j.biotechadv.2011.08.021>. Secreted

- Gerke, H.H., 2006. Preferential flow descriptions for structured soils. *J. Plant Nutr. Soil Sci.* 169, 382–400. <https://doi.org/10.1002/jpln.200521955>
- Gerke, H.H., Dusek, J., Vogel, T., Koehne, J.M., 2007. Two-dimensional dual-permeability analyses of a bromide tracer experiment on a tile-drained field. *Vadose Zo. J.* 6, 651–667. <https://doi.org/10.2136/vzj2007.0033>
- Gerke, H.H., Kohne, J.M., 2004. Dual-permeability modeling of preferential bromide leaching from a tile-drained glacial till agricultural field. *J. Hydrol.* 289, 239–257. <https://doi.org/10.1016/j.jhydrol.2003.11.019>
- Gerke, H.H., Van Genuchten, M.T. 1993. A dual-porosity model for simulating the preferential movement of water and solutes in structured porous-media. *Water Resources Research* 29, no. 2: 305–319
- Giesen, N.C. van de, Stomph, T.J., Ridder, N. De, 2000. Scale effects of Hortonian overland flow and rainfall-runoff dynamics in a West African catena landscape. *Hydrol. Process.* 14, 165–175.
- Ginn, T. R., 2000. On the distribution of multicomponent mixtures over generalized exposure time in subsurface flow and reactive transport: Theory and formulations for residence-time-dependent sorption/desorption with memory. *Water Resour. Res.*, 36(10), 2885–2893, doi:10.1029/2000WR900170.
- Glass, R.J., Conrad, S.H., Peplinski, W., 2000. Gravity-destabilized non-wetting phase invasion in macro-heterogeneous porous media: Experimental observations of invasion dynamics and scale analysis. *Water Resour. Res.*, 36(11), 3121–3137, doi:10.1029/2000WR900152
- Glynn, P.D., Reardon, E.J., 1990. Solid-Solution Aqueous-Solution equilibria: Thermodynamic theory and representation. *Am. J. Sci.* 290, 164–201.
- Gomez, D.E., Alvarez, P.J.J., 2010. Comparing the effects of various fuel alcohols on the natural attenuation of Benzene Plumes using a general substrate interaction model. *J. Contam. Hydrol.* 113, 66–76. <https://doi.org/10.1016/j.jconhyd.2010.02.002>
- Gooday, R., Anthony, S., Fawcett, L., 2008. A field scale model of soil drainage and nitrate leaching for application in nitrate vulnerable zones. *Environ. Model. Softw.* 23, 1045–1055. <https://doi.org/10.1016/j.envsoft.2007.11.005>
- Goode, D.J., Konikow, L.F., 1990. Apparent dispersion in transient groundwater flow. *Water Resour. Res.* 26, 2339–2351. <https://doi.org/10.1029/WR026i010p02339>
- Green, C. T., Bohlke, J. K., Bekins, B. A., Phillips, S. P., 2010. Mixing effects on apparent reaction rates and isotope fractionation during denitrification in a heterogeneous aquifer. *Water Resour. Res.*, 46, W08525, doi:10.1029/2009WR008903
- Green, D. W., Dabiri, H., Weinaug, C. F., Prill, R., 1970. Numerical modeling of unsaturated groundwater flow and comparison of the model to a field experiment. *Water Resour. Res.*, 6(3), 862–874, doi:10.1029/WR006i003p00862.
- Griebler, C.; Lueders, T., 2009. Microbial biodiversity in groundwater ecosystems. *Freshwater Biol.*, 54, 649–677.
- Grisak, G. E., Pickens, J. F., 1980. Solute transport through fractured media, 1.The effect of matrix diffusion, *Water Resour. Res.*, 16(4), 719–730
- Guilbeault, M.A., Parker, B.L., Cherry, J.A., 2005. Mass and Flux Distributions from DNAPL Zones in Sandy Aquifers. *Ground Water* 43, 70–86.
- Guymon, G. L., Scott, V. H., Herrmann L. R., 1970. A general numerical solution of the two-dimensional diffusion-convection equation by the finite element method, *Water Resour. Res.*, 6(6), 1611–1617, doi:10.1029/WR006i006p01611.
- Guzha, A.C., Rufino, M.C., Okoth, S., Jacobs, S., Nóbrega, R.L.B., 2018. Impacts of land use and land cover change on surface runoff, discharge and low flows: Evidence from East Africa. *J. Hydrol. Reg. Stud.* 15, 49–67. <https://doi.org/10.1016/j.ejrh.2017.11.005>
- Haggerty, R., Gorelick, S.M., 1994. Design of multiple contaminant remediation: sensitivity to rate-limited mass transfer. *Water Resour. Res.* 30(2):435–446
- Haggerty, R., Harvey, C.F., Scherwin, C.F. Von, Meigs, L.C., 2004. What controls the apparent timescale of solute mass transfer in aquifers and soils? A comparison of experimental results. *Water Resour. Res.* 40, 1–13. <https://doi.org/10.1029/2002WR001716>
- Hance, R. J., 1980. Transport in the vapour phase, in 'Interactions Between Herbicides and the Soil', Hance, R., Ed., Academic Press, London.
- Hansen, B., Thorling, L., Schullehner, J., Termansen, M., Dalgaard, T., 2017. Groundwater nitrate response to sustainable nitrogen management. *Nature* 7, 1–12. <https://doi.org/10.1038/s41598-017-07147-2>
- Hanks, R. J., Klute, A., E. Bresler, E., 1969. A numeric method for estimating infiltration, redistribution, drainage, and evaporation of water from soil. *Water Resour. Res.*, 5(5), 1064–1069, doi:10.1029/WR005i005p01064.
- Harvey, C., Gorelick, S.M., 2000. Rate-limited mass transfer or macrodispersion: Which dominates plume evolution at the Macrodispersion Experiment (MADE) site? *Water Resour. Res.* 36, 637–650.
- Hassanizadeh, S.M., 1986. Derivation of basic equations of mass transport in porous media, Part 2 . Generalized Darcy's and Fick's laws. *Adv. Water Resour.* 9, 207–222.

- Haws, N.W., Rao, P.S.C., Simunek, J., Poyer, I.C., 2005. Single-porosity and dual-porosity modeling of water flow and solute transport in subsurface-drained fields using effective field-scale parameters. *J. Hydrol.* 313, 257–273. <https://doi.org/10.1016/j.jhydrol.2005.03.035>
- Hayashi, M., Rosenberry, D.O., 2002. Effects of ground water exchange on the hydrology and ecology of surface water. *Ground Water* 40, 309–316.
- Hayashi, M., van der Kamp, G., Rosenberry, D.O., 2016. Hydrology of Prairie Wetlands: Understanding the Integrated Surface-Water and Groundwater Processes. *Wetlands* 36, 237–254. <https://doi.org/10.1007/s13157-016-0797-9>
- Healy, R.W., Cook, P.G., 2002. Using groundwater levels to estimate recharge. *Hydrogeol. J.* 10, 91–109. <https://doi.org/10.1007/s10040-001-0178-0>
- Healy, R.W., Scanlon, B.R., 2010. Estimating groundwater recharge, Cambridge University Press, Online ISBN: 9780511780745, p.257, <https://doi.org/10.1017/CBO9780511780745>
- Heeren, D.M., Miller, R.B., Fox, G.A., Storm, D.E., Halihan, T., Penn, C.J., 2010. Preferential flow effects on subsurface contaminant transport in alluvial floodplains. *Trans. ASABE* 53, 127–136.
- Heilweil, V.M., Benoit, J., Healy, R.W., 2015. Variably saturated groundwater modelling for optimizing managed aquifer recharge using trench infiltration. *Hydrol. Process.* 29, 3010–3019. <https://doi.org/10.1002/hyp.10413>
- Heiss, J.W., Michael, H.A., 2014. Saltwater-freshwater mixing dynamics in a sandy beach aquifer over tidal, spring-neap, and seasonal cycles. *Water Resour. Res.* 50, 6747–6766. <https://doi.org/10.1002/2014WR015574>. Received
- Held, R. J., Illangasekare, T. H., 1995. Fingering of dense nonaqueous phase liquids in porous media: 1. Experimental investigation, *Water Resour. Res.*, 31(5), 1213–1222, doi:10.1029/95WR00428
- Hendrickx, J.M.H., Flury, M., 2001. Uniform and Preferential Flow Mechanisms in the Vadose Zone, in: National Research Council (Ed.), *Conceptual Models of Flow and Transport in the Fractured Vadose Zone*. The National Academies Press, Washington, DC, pp. 149–187.
- Hendry, M.J., Schmelting, E.E., Barbour, S.L., Huang, M., Mundle, S.O.C., 2017. Fate and Transport of Shale- derived, Biogenic Methane. *Nat. - Sci. Reports* 2–10. <https://doi.org/10.1038/s41598-017-05103-8>
- Herczeg, A.L., Edmunds, W.M., 2000. Environmental Tracers in Subsurface Hydrology, Chap.2 Inorganic Ions as Tracers, Springer Science, New York, ISBN 978-1-4615-4557-6, p.529
- Herman, M.E., Buddemeier, R.W., Stephen, W., 1986. A LAYERED AQUIFER MODEL OF ATOLL ISLAND HYDROLOGY: VALIDATION OF A COMPUTER SIMULATION. *J. Hydrol.* 84, 303–322.
- Hess, K.M., Davis, J.A., Kent, D.B., Coston, J.A., 2002. Multispecies reactive tracer test in an aquifer with spatially variable chemical conditions - Cape Cod, Massachusetts: Dispersive transport of bromide and nickel. *Water Resour. Res.* 38, 119–134. <https://doi.org/10.1029/1999WR900282>
- Hess, K.M., Wolf, S.H., Celia, M.A., 1992. Large-Scale natural gradient tracer test in sand and gravel, Cape Cod, Massachusetts - 3. Hydraulic Conductivity Variability and Calculated Macrodispersivities. *Water Resour. Res.* 28, 18.
- Hesse, F., Harms, H., Attinger, S., Thullner, M., 2010. Linear exchange model for the description of mass transfer limited bioavailability at the pore scale. *Environ. Sci. Technol.*, 44, 2064–2071.
- Hilberts, A.G.J., Troch, P.A., Paniconi, C., 2005. Storage-dependent drainable porosity for complex hillslopes. *Water Resour. Res.* 41, 1–13. <https://doi.org/10.1029/2004WR003725>
- Holocher, J., Peeters, F., Aeschbach-Hertig, W., Kinzelbach, W., Kipfer, R., 2003. Kinetic Model of Gas Bubble Dissolution in Groundwater and Its Implications for the Dissolved Gas Composition. *Environ. Sci. Technol.* 37, 1337–1343.
- Hsieh, P.A., Neuman, S.P., Stiles, G.K., Simpson, E.S., 1985. Field Determination of the Three-Dimensional Hydraulic Conductivity Tensor of Anisotropic Media 2. Methodology and Application to Fractured Rocks. *Water Resources Research* 21 (11), 1667–1676
- Huang, F.K., Chuang, M.H., Wang, G.S., Yeh, H. Der, 2015. Tide-induced groundwater level fluctuation in a U-shaped coastal aquifer. *J. Hydrol.* 530, 291–305. <https://doi.org/10.1016/j.jhydrol.2015.09.032>
- Huang, J., Christ, J.A., Goltz, M.N., Demond, A.H., 2015. Modeling NAPL dissolution from pendular rings in idealized porousmedia. *Water Resour. Res.* 51, 9127–9140. <https://doi.org/10.1002/2014WR016259>
- Huang, G.H., Huang, Y.F., Wang, G.Q., Xiao, H.N., 2006. Development of a forecasting system for supporting remediation design and process control based on NAPL-biodegradation simulation and stepwise-cluster analysis, *Water Resour. Res.*, 42, W06413, doi:10.1029/2005WR004006.
- Hunt, R.J., Prudic, D.E., Walker, J.F., Anderson, M.P., 2008. Importance of unsaturated zone flow for simulating recharge in a humid climate. *Ground Water* 46, 551–560. <https://doi.org/10.1111/j.1745-6584.2007.00427.x>
- Hunt, J.R., Sitar, N., Udell, K.S., 1988. Nonaqueous phase liquid transport and cleanup: 2.Experimetal studies, *Water Resour. Res.*, 24(8), 1259–1269, doi:10.1029/WR024i008p01259.
- Jabro, J.D., Lotse, E.G., Fritton, D.D., Baker, D.E., 1994. Estimation of preferential movement of bromide tracer under field conditions. *J. Hydrol.* 156, 61–71. [https://doi.org/10.1016/0022-1694\(94\)90071-X](https://doi.org/10.1016/0022-1694(94)90071-X)

- Jakobsen, R., Postma, D., 1999. Redox zoning, rates of sulfate reduction and interactions with Fe-reduction and methanogenesis in a shallow sandy aquifer, Rømø, Denmark. *Geochim. Cosm. Acta* 63, 137–151.
- Jarvis, N.J., 2007. A review of non-equilibrium water flow and solute transport in soil macropores: Principles, controlling factors and consequences for water quality. *Eur. J. Soil Sci.* 58, 523–546. <https://doi.org/10.1111/j.1365-2389.2007.00915.x>
- Jawitz, J.W., Sillan, R.K., Annable, M.D., Rao, P.S.C., Warner, K., 2000. In-situ alcohol flushing of a DNAPL source zone at a dry cleaner site. *Environ. Sci. Technol.* 34, 3722–3729. <https://doi.org/10.1021/es9913737>
- Jeng, D.S., Mao, X., Enot, P., Barry, D.A., Li, L., 2005. Spring-neap tide-induced beach water table fluctuations in a sloping coastal aquifer. *Water Resour. Res.* 41, 1–4. <https://doi.org/10.1029/2005WR003945>
- Jiménez, S., Brauchler, R., Hu, R., Hu, L., Schmidt, S., Ptak, T., Bayer, P., 2015. Prediction of solute transport in a heterogeneous aquifer utilizing hydraulic conductivity and specific storage tomograms. *Water Resour. Res.* 51, 5504–5520. <https://doi.org/10.1002/2014WR016402>.Received
- Johnson, A.C., Besien, T.J., Bhardwaj, C.L., Dixon, A., Goody, D.C., Haria, A.H., White, C., 2001. Penetration of herbicides to groundwater in an unconfined chalk aquifer following normal soil applications. *J. Contam. Hydrol.* 53, 101–117.
- Johnson DA, Cole DW, 1980. Anion mobility in soils: relevance to nutrient transport from forest ecosystems. *Environ Int* 3:79–90
- Julian, H., Boggs, J., Zheng, C., Feehley, C., 2001. Numerical simulation of a natural gradient tracer experiment for the natural attenuation study: Flow and physical transport. *Ground Water.* 39(4), p.534–545
- Karickhoff, S.W., 1984. Organic pollutant sorption in aquatic systems. *J. Hydraul. Eng. ASCE* 10(6):707–735.
- Kim, K.-Y., Seong, H., Kim, T., Park, K.-H., Woo, N.-C., Park, Y.-S., Koh, G.-W., Park, W.-B., 2006. Tidal effects on variations of fresh–saltwater interface and groundwater flow in a multilayered coastal aquifer on a volcanic island (Jeju Island, Korea). *J. Hydrol.* 330, 525–542. <https://doi.org/10.1016/j.jhydrol.2006.04.022>
- Kim, K., Anderson, M.P., Bowser, C.J., 2000. Enhanced dispersion in groundwater caused by temporal changes in recharge rate and lake levels. *Adv. Water Resour.* 23, 625–635. [https://doi.org/10.1016/S0309-1708\(99\)00050-0](https://doi.org/10.1016/S0309-1708(99)00050-0)
- Kinzelbach, W., Ackerer, P., 1986. Modélisation du transport de contaminant dans un champ d'écoulement non-permanent. *Hydrogéologie* 2, 197–205.
- Kitanidis, P.K., 2015. Persistent questions of heterogeneity, uncertainty, and scale in subsurface flow and transport. *Water Resour. Res.* 51, 5888–5904. <https://doi.org/10.1002/2015WR017639>
- Kitanidis, P.K., 1994. The concept of the dilution index. *Water Resour. Res.* 30, 2011–2026.
- Kitanidis, P.K., McCarty, P.L., 2012. Delivery and Mixing in the Subsurface: Processes and Design Principles for In Situ Remediation, Springer, SERDP and ESTCP Remediation Technology Monograph Series, ISSN 1869-6864, p.350
- Kjøller, C., Postma, D., Larsen, F., 2004. Groundwater Acidification and the Mobilization of Trace Metals in a Sandy Aquifer. *Environ. Sci. Technol.* 38, 2829–2835.
- Kobayashi, H., Rittmann, B. E., 1982. Microbial removal of hazardous organic compounds, *Environ. Sci. Technol.*, 16 (3), 170A–183A doi:10.1021/es00097a002
- Kohne, J.M., Gerke, H.H., 2005. Spatial and Temporal Dynamics of Preferential Bromide Movement towards a Tile Drain. *Vadose Zo. J.* 4, 79–88. <https://doi.org/10.2113/4.1.79>
- Kohne, J.M., Kohne, S., Simunek, J., 2009. A review of model applications for structured soils: b) Pesticide transport. *J. Contam. Hydrol.* 104, 36–60. <https://doi.org/10.1016/j.jconhyd.2008.10.003>
- Kohne, J.M., Kohne, S., Simunek, J., 2006. Multi-process herbicide transport in structured soil columns: Experiments and model analysis. *J. Contam. Hydrol.* 85, 1–32. <https://doi.org/10.1016/j.jconhyd.2006.01.001>
- Kohne, S., Lennartz, B., Kohne, J.M., Simunek, J., 2006. Bromide transport at a tile-drained field site: experiment, and one- and two-dimensional equilibrium and non-equilibrium numerical modeling. *J. Hydrol.* 321, 390–408. <https://doi.org/10.1016/j.jhydrol.2005.08.010>
- Kollat, J.B., Reed, P.M., Maxwell, R.M., 2011. Many-objective groundwater monitoring network design using bias-aware ensemble Kalman filtering, evolutionary optimization, and visual analytics. *Water Resour. Res.* 47, 1–18. <https://doi.org/10.1029/2010WR009194>
- Kollet, S.J., Maxwell, R.M., 2006. Integrated surface–groundwater flow modeling: A free-surface overland flow boundary condition in a parallel groundwater flow model. *Adv. Water Resour.* 29, 945–958. <https://doi.org/10.1016/j.advwatres.2005.08.006>
- Kollet, S.J., Maxwell, R.M., Woodward, C.S., Smith, S., Vanderborght, J., Vereecken, H., Simmer, C., 2010. Proof of concept of regional scale hydrologic simulations at hydrologic resolution utilizing massively parallel computer resources. *Water Resour. Res.* 46, 1–7. <https://doi.org/10.1029/2009WR008730>
- Kröger, R., Dunne, E.J., Novak, J., King, K.W., McLellan, E., Smith, D.R., Strock, J., Boomer, K., Tomer, M., Noe, G.B., 2013. Science of the Total Environment Downstream approaches to phosphorus management in agricultural

- landscapes : Regional applicability and use. *Sci. Total Environ.* 442, 263–274. <https://doi.org/10.1016/j.scitotenv.2012.10.038>
- Kurtz, W. L., Lapin, A., Schilling, O.S., Tang, Q., Schiller, E., Braun, T., Hunkeler, D., Vereecken, H., Sudicky, E., Krop, P., Hendricks Franssen, H.-J., Brunner, P. 2017. Integrating hydrological modelling, data assimilation and cloud computing for real-time management of water resources, *Environ Modell Softw*, 93, 418–435, doi:10.1016/j.envsoft.2017.03.011.
- Langner, H.W., Inskip, W.P., Gaber, H.M., Jones, W.L., Das, B.S., Wraith, J.M., 1998. Pore Water Velocity and Residence Time Effects on the Degradation of 2,4-D during Transport. *Environ. Sci. Technol.* 32, 1308–1315.
- Lapworth, D.J., Baran, N., Stuart, M.E., Ward, R.S., 2012. Emerging organic contaminants in groundwater: A review of sources, fate and occurrence. *Environ. Pollut.* 163, 287–303. <https://doi.org/10.1016/j.envpol.2011.12.034>
- Larocque, M., Banton, O., Ackerer, P., Razack, M., 1999. Determining karst transmissivities with inverse modelling and an equivalent porous media. *Ground Water* 37 (6), 897–903.
- Le Borgne, T., Bour, O., Riley, M.S., Gouze, P., Pezard, P.A., Belghoul, A., Lods, G., Le Provost, R., Greswell, R.B., Ellis, P.A., Isakov, E., Last, B.J., 2007. Comparison of alternative methodologies for identifying and characterizing preferential flow paths in heterogeneous aquifers. *J. Hydrol.* 345, 134–148. <https://doi.org/10.1016/j.jhydrol.2007.07.007>
- Le Borgne, T., Dentz, M., Carrera, J., 2008. A Lagrangian statistical model for transport in highly heterogeneous velocity fields. *Phys. Rev. Lett.* 101, 090601, <https://doi.org/10.1103/PhysRevLett.101.090601>
- LeBlanc, D.R., Garabedian, S.P., Hess, K.M., Gelhar, L.W., Quadri, R.D., Stollenwerk, K.G., Wood, W.W., 1991. Large-Scale Natural Gradient Tracer Test in Sand and Gravel, Cape Cod, Massachusetts - I. Experimental Design and Observed Tracer Movement. *Water Resour.* 27, 895–910.
- Lee, E.S., Liu, G., Schwartz, F.W., Kim, Y., Ibaraki, M., 2008. Model-based evaluation of controlled-release systems in the remediation of dissolved plumes in groundwater. *Chemosphere* 72, 165–173. <https://doi.org/10.1016/j.chemosphere.2008.01.078>
- Lenhard, R.J., Parker, J.C., Kaluarachchi, J.J., 1989. A Model for Hysteretic Constitutive Relations Governing Multiphase Flow 3. Refinements and Numerical Simulations. *Water Resour. Res.* 25, 1727–1736.
- Li, H., Jiao, J.J., Luk, M., Cheung, K., 2002. Tide-induced groundwater level fluctuation in coastal aquifers bounded by L-shaped coastlines. *Water Resour. Res.* 38, 6-1-6-8. <https://doi.org/10.1029/2001WR000556>
- Li, L., Barry, D.A., Cunningham, C., Stagnitti, F., Parlange, J.Y., 2000a. A two-dimensional analytical solution of groundwater responses to tidal loading in an estuary and ocean. *Adv. Water Resour.* 23, 825–833. [https://doi.org/10.1016/S0309-1708\(00\)00016-6](https://doi.org/10.1016/S0309-1708(00)00016-6)
- Li, L., Barry, D.A., Stagnitti, F., Parlange, J.-Y., 2000b. Groundwater waves in a coastal aquifer: A new governing equation including vertical effects and capillarity. *Water Resour. Res.* 36, 411–420.
- Li, L., Barry, D.A., Stagnitti, F., Parlange, J.Y., Jeng, D.S., 2000c. Beach water table fluctuations due to spring-neap tides: moving boundary effects. *Adv. Water Resour.* 23, 817–824.
- Lichtner, P.C., Kang, Q., 2007. Upscaling pore-scale reactive transport equations using a multiscale continuum formulation. *Water Resour. Res.* 43, W12S15. <https://doi.org/10.1029/2006WR005664>
- Liggett, J.E., Partington, D., Frei, S., Werner, A.D., Simmons, C.T., Fleckenstein, J.H., 2015. An exploration of coupled surface-subsurface solute transport in a fully integrated catchment model. *J. Hydrol.* 529, 969–979. <https://doi.org/10.1016/j.jhydrol.2015.09.006>
- Liu, G., Chen, Y., Zhang, D., 2008. Investigation of flow and transport processes at the MADE site using ensemble Kalman filter. *Adv. Water Resour.* 31, 975–986. <https://doi.org/10.1016/j.advwatres.2008.03.006>
- Liu, G., Zheng, C., Tick, G.R., Butler Jr., J.J., Gorelick, S.M., 2010. Relative importance of dispersion and rate-limited mass transfer in highly heterogeneous porous media: Analysis of a new tracer test at the Macrodispersion Experiment (MADE) site. *Water Resour. Res.* 46, 1–8. <https://doi.org/10.1029/2009WR008430>
- Liu, Y., Jiao, J.J., Luo, X., 2015. Effects of inland water level oscillation on groundwater dynamics and land-sourced solute transport in a coastal aquifer. *Coast. Eng.* 114, 347–360. <https://doi.org/10.1016/j.coastaleng.2016.04.021>
- Long, J.C.S., Remer, J.S., Wilson, C.R., Witherspoon, P.A., 1982. Porous media equivalents for networks of discontinuous fractures. *Water Resources Research* 18
- Lu, Z., Stauffer, P.H., 2012. On estimating functional average breakthrough curve using time-warping technique and perturbation approach. *Water Resour. Res.* 48, 1–11. <https://doi.org/10.1029/2011WR011506>
- Lubczynski, M.W., Gurwin, J., 2005. Integration of various data sources for transient groundwater modeling with spatio-temporally variable fluxes - Sardon study case, Spain. *J. Hydrol.* 306, 71–96. <https://doi.org/10.1016/j.jhydrol.2004.08.038>
- Luscombe, D.J., Anderson, K., Grand-Clement, E., Gatis, N., Ashe, J., Benaud, P., Smith, D., Brazier, R.E., 2016. How does drainage alter the hydrology of shallow degraded peatlands across multiple spatial scales? *J. Hydrol.* 541, 1329–1339. <https://doi.org/10.1016/j.jhydrol.2016.08.037>

- Lyman, W. J., Reehl, W. F., Rosenblatt, D. H. 1982. Handbook of Chemical Property Estimation Methods, Environmental Behavior of Organic Compounds, McGraw-Hill, New York
- Ma, J., Rixey, W.G., Alvarez, P.J.J., 2013. Microbial processes influencing the transport, fate and groundwater impacts of fuel ethanol releases. *Curr. Opin. Biotechnol.* 24, 457–466. <https://doi.org/10.1016/j.copbio.2012.09.005>
- Ma, R., Zheng, C., Zachara, J.M., Tonkin, M., 2012. Utility of bromide and heat tracers for aquifer characterization affected by highly transient flow conditions. *Water Resour. Res.* 48, 1–18. <https://doi.org/10.1029/2011WR011281>
- MacFarlane, D.S., Cherry, J.A., Gilham, R.W., Sudicky, E.A., 1983. MIGRATION OF CONTAMINANTS IN GROUNDWATER AT A LANDFILL: A CASE STUDY I-Groundwater Flow and Plume Delineation. *J. Hydrol.* 63, 1–29.
- MacIntyre, W.G., Boggs, M., Antworth, C.P., Stauffer, T.B. 1993. Degradation kinetics of aromatic organic solutes introduced into a heterogeneous aquifer. *Water Resour. Res.* 29(12), 4045–4051.
- Mackay, D.M., Cherry, J.A., 1989. Groundwater contamination: Pump-and-treat remediation (2of5). *Environ. Sci. Technol.* 23, 7.
- Mackay, D.M., Freyberg, D.L., Roberts, P. V., Cherry, J.A., 1986. A natural gradient experiment on solute transport in a sand aquifer - I. Approach and overview of plume movement. *Water Resour. Res.* 22, 2017–2029. <https://doi.org/10.1029/WR022i013p02017>
- Mackay, D., Shiu, W.Y., Maijane, A., Feenstra, S. 1991. Dissolution of non-aqueous phase liquids in groundwater. *J. Contam. Hydrol.* 8_1., 23–42
- Maheswaran, R., Khosa, R., Gosain, A.K., Lahari, S., Sinha, S.K., Chahar, B.R., Dhanya, C.T., 2016. Regional scale groundwater modelling study for Ganga River basin. *J. Hydrol.* 541, 727–741. <https://doi.org/10.1016/j.jhydrol.2016.07.029>
- Maier, U., Grathwohl, P., 2006. Numerical experiments and field results on the size of steady state plumes. *J. Contam. Hydrol.* 85, 33–52. <https://doi.org/10.1016/j.jconhyd.2005.12.012>
- Maloszewski, P., Zuber, A., 1993. Tracer experiments in fractured rocks. Matrix diffusion and the validity of models. *Water Resources Research* 29 (8), 2723–2735.
- Maloszewski, P., Zuber, A., 1985. On the theory of tracer experiments in fissured rocks with a porous matrix. *J. Hydrol.* 79, 333–358.
- Mao, X., Enot, P., Barry, D. a., Li, L., Binley, a., Jeng, D.S., 2006. Tidal influence on behaviour of a coastal aquifer adjacent to a low-relief estuary. *J. Hydrol.* 327, 110–127. <https://doi.org/10.1016/j.jhydrol.2005.11.030>
- McDowell, C.J., Buscheck, T., Powers, S.E., 2003. Behavior of gasoline pools following a denatured ethanol spill. *Ground Water* 41, 746–757.
- McDowell, C.J., Powers, S.E., 2003. Mechanisms affecting the infiltration and distribution of ethanol-blended gasoline in the vadose zone. *Environ. Sci. Technol.* 37, 1803–1810. <https://doi.org/10.1021/es025976l>
- McGuire, J.T., Long, D.T., Hyndman, D.W., 2005. Analysis of recharge-induced geochemical change in a contaminated aquifer. *Ground Water* 43, 518–530. <https://doi.org/10.1111/j.1745-6584.2005.0040.x>
- McMahon, P. B., Dennehy, K. F., Bruce, B. W., Bohlke, J. K., Michel, R. L., Gurdak, J. J., Hurlbut, D. B., 2006. Storage and transit time of chemicals in thick unsaturated zones under rangeland and irrigated cropland, High Plains, United States, *Water Resour. Res.*, 42, W03413, doi:10.1029/2005WR004417
- Mckenna, S.P., McGillis, W.R., 2004. The role of free-surface turbulence and surfactants in air–water gas transfer. *Int. J. Heat Mass Transf.* 47, 539–553. <https://doi.org/10.1016/j.ijheatmasstransfer.2003.06.001>
- Meakin, P., Tartakovsky, A.M., 2009. Modeling and simulation of pore-scale multiphase fluid flow and reactive transport in fractured and porous media. *Rev. Geophys.* 47, RG3002
- Meckenstock, R.U., Elsner, M., Griebler, C., Lueders, T., Stumpf, C., Aamand, J., Agathos, S.N., Albrechtsen, H.J., Bastiaens, L., Bjerg, P.L., Boon, N., Dejonghe, W., Huang, W.E., Schmidt, S.I., Smolders, E., Sorensen, S.R., Springael, D., Van Breukelen, B.M., 2015. Biodegradation: Updating the Concepts of Control for Microbial Cleanup in Contaminated Aquifers. *Environ. Sci. Technol.* 49, 7073–7081. <https://doi.org/10.1021/acs.est.5b00715>
- Mercer, J.W., Cohen, R.M., 1990. A review of immiscible fluids in the subsurface: Properties, models, characterization and remediation. *J. Contam. Hydrol.* 6, 107–163.
- Michael, H.A., Mulligan, A.E., Harvey, C.F., 2005. Seasonal oscillations in water exchange between aquifers and the coastal ocean. *Nature* 436, 1145–1148. <https://doi.org/10.1038/nature03935>
- Miller, C.T., Christakos, G., Imhoff, P.T., McBride, J.F., Pedit, J.A., 1998. Multiphase flow and transport modeling in heterogeneous porous media: challenges and approaches. *Adv. Water Resour.* 21, 77–120. [https://doi.org/10.1016/S0309-1708\(96\)00036-X](https://doi.org/10.1016/S0309-1708(96)00036-X)
- Miller, C.T., Poirier-McNeill, M.M., Mayer, A.S., 1990. Dissolution of trapped nonaqueous phase liquids: mass transfer characteristics. *Water Resour. Res.* 26 (11), 2783–2793.

- Minsker, B. S., Shoemaker, C. A. 1996. Differentiating a finite element biodegradation simulation model for optimal control. *Water Resour. Res.*, 32(1), 187–192, doi:10.1029/95WR02969.
- Miotlinski, K., Dillon, P.J., Pavelic, P., Barry, K., Kremer, S., 2014. Recovery of Injected Freshwater from a Brackish Aquifer with a Multiwell System. *Groundwater* 52, 495–502. <https://doi.org/10.1111/gwat.12089>
- Miotlinski, K., Dillon, P.J., Pavelic, P., Cook, P.G., Page, D.W., Levett, K., 2011. Recovery of injected freshwater to differentiate fracture flow in a low-permeability brackish aquifer. *J. Hydrol.* 409, 273–282. <https://doi.org/10.1016/j.jhydrol.2011.08.025>
- Miotlinski, K., Postma, D., Kowalczyk, A., 2012. Variable infiltration and river flooding resulting in changing groundwater quality – A case study from Central Europe. *J. Hydrol.* 414–415, 211–219. <https://doi.org/10.1016/j.jhydrol.2011.10.034>
- Miralles-Wilhelm, F., and L. W. Gelhar (1996. Stochastic analysis of sorption macrokinetics in heterogeneous aquifers. *Water Resour. Res.*, 32(6), 1541–1549, doi:10.1029/96WR00791.
- Molins, S., Trebotich, D., Steffel, C.I., Shen, C., 2012. An investigation of the effect of pore scale flow on average geochemical reaction rates using direct numerical simulation. *Water Resour. Res.* 48, 1–11. <https://doi.org/10.1029/2011WR011404>
- Molson, J.W., Barker, J.F., Frind, E.O., Schirmer, M., 2002. Modeling the impact of ethanol on the persistence of benzene in gasoline-contaminated groundwater. *Water Resour. Res.* 38, 4-1-4-12. <https://doi.org/10.1029/2001WR000589>
- Molz, F.J., 2015. Advection, Dispersion and Confusion. *Groundwater* 54, 2–3. <https://doi.org/10.1111/gwat.12383>
- Molz, F.J., Morin, R.H., Hess, A.E., Melville, J.G., Guven, O., 1989. The impeller meter for measuring aquifer permeability variations: Evaluation and comparison with other tests. *Water Resour. Res.* 25, 1677–1683.
- Molz, F.J., Zheng, C., Gorelick, S.M., Harvey, C.F., 2006. Comment on “investigating the Macrodispersion Experiment (MADE) site in Columbus, Mississippi, using a three-dimensional inverse flow and transport model” by Heidi Christiansen Barlebo, Mary C. Hill, and Dan Rosbjerg. *Water Resour. Res.* 42, 1–5. <https://doi.org/10.1029/2005WR004265>
- Morkin, M., Devlin, J.F., Barker, J.F., Butler, B.J., 2000. In situ sequential treatment of a mixed contaminant plume. *J. Contam. Hydrol.* 45, 283–302.
- Motyka, J., 1998. A conceptual model of hydraulic networks in carbonate rocks , illustrated by examples from Poland. *Hydrogeol. J.* 6, 469–482.
- Mualem, Y., 1976. Hysteretical Models for Prediction of the Hydraulic Conductivity of Unsaturated Porous Media. *Water Resour. Res.* 12, 1248–1254.
- Mualem, Y., 1974. A Conceptual Model of Hysteres. *Water Resour. Res.* 1.
- Muldoon, M., Bradbury, K.R., 2005. Site characterization in densely fractured dolomite: comparison of methods. *Ground Water* 43 (6), 863–876
- Nachabe, M.H., 2002. Analytical expressions for transient specific yield and shallow water table drainage. *Water Resour. Res.* 38, 11-1-11–7. <https://doi.org/10.1029/2001WR001071>
- Nadim, F., Hoag, G.E., Liu, S., Carley, R.J., Zack, P., 2000. Detection and remediation of soil and aquifer systems contaminated with petroleum products: An overview. *J. Pet. Sci. Eng.* 26, 169–178. [https://doi.org/10.1016/S0920-4105\(00\)00031-0](https://doi.org/10.1016/S0920-4105(00)00031-0)
- Nelson, R. W., 1966. Flow in heterogeneous porous mediums: 1. Darcian-type description of two-phase systems, *Water Resour. Res.*, 2(3), 487–495, doi:10.1029/WR002i003p00487.
- Nelson, R. W. 1978a. Evaluating the environmental consequences of groundwater contamination: 2. Obtaining location/arrival time and location/outflow quantity distributions for steady flow systems, *Water Resour. Res.*, 14(3), 416–428, doi:10.1029/WR014i003p00416.
- Nelson, R. W. 1978b. Evaluating the environmental consequences of groundwater contamination: 4. Obtaining and utilizing contaminant arrival distributions in transient flow systems, *Water Resour. Res.*, 14(3), 441–450, doi:10.1029/WR014i003p00441.
- Neto, D.C., Chang, H.K., van Genuchten, M.T., 2016. A Mathematical View of Water Table Fluctuations in a Shallow Aquifer in Brazil. *Groundwater* 54, 82–91. <https://doi.org/10.1111/gwat.12329>
- Neumann, R.B., Ashfaque, K.N., Badruzzaman, A.B.M., Ali, M.A., Shoemaker, J.K., Harvey, C.F., 2010. Anthropogenic influences on groundwater arsenic concentrations in Bangladesh. *Nat. Geosci.* 3, 46–52. <https://doi.org/10.1038/ngeo685>
- Neuman, S.P., Tartakovsky, D.M., 2008. Perspective on theories of anomalous transport in heterogeneous media. *Adv. Water Resour.* 32, 670–680. <https://doi.org/10.1016/j.advwatres.2008.08.005>
- Neves dos Santos, J.C., Maia de Andrade, E., Guerreiro, M.J.S., Medeiros, P.H.A., Araújo de Queiroz Palácio, H., Ribeiro de Araújo Neto, J., 2016. Effect of dry spells and soil cracking on runoff generation in a semiarid micro watershed under land use change. *J. Hydrol.* 541, 1057–1066. <https://doi.org/10.1016/j.jhydrol.2016.08.016>

- Ni, W.-J., Capart, H., 2006. Groundwater drainage and recharge by networks of irregular channels. *J. Geophys. Res.* 111, 1–33. <https://doi.org/10.1029/2005JF000410>
- Nielsen, D. R., Van Genuchten, M. Th., Biggar, J. W., 1986. Water flow and solute transport processes in the unsaturated zone. *Water Resour. Res.* 22(9S), 89S–108S, doi:10.1029/WR022i09Sp0089S
- Nowak, W., de Barros, F.P.J., Rubin, Y., 2010. Bayesian geostatistical design: Task-driven optimal site investigation when the geostatistical model is uncertain. *Water Resour. Res.* 46, 1–17. <https://doi.org/10.1029/2009WR008312>
- Oosterwoud, M., van der Ploeg, M., van der Schaaf, S., van der Zee, S., 2017. Variation in hydrologic connectivity as a result of microtopography explained by discharge to catchment size relationship. *Hydrol. Process.* 31, 2683–2699. <https://doi.org/10.1002/hyp.11164>
- Ostrom, M., Hofstee, C., Lenhard, R.J., Wietsma, T.W., 2003. Flow behavior and residual saturation formation of liquid carbon tetrachloride in unsaturated heterogeneous porous media. *J. Contam. Hydrol.* 64, 93–112. [https://doi.org/10.1016/S0169-7722\(02\)00107-9](https://doi.org/10.1016/S0169-7722(02)00107-9)
- Ostrom, M., Mehmani, Y., Romero-Gomez, P., Tang, Y., Liu, H., Yoon, H., Kang, Q., Joekar-Niasar, V., Balhoff, M.T., Dewers, T., Tartakovsky, G.D., Leist, E.A., Hess, N.J., Perkins, W.A., Rakowski, C.L., Richmond, M.C., Serkowski, J.A., Werth, C.J., Valocchi, A.J., Wietsma, T.W., Zhang, C., 2016. Pore-scale and continuum simulations of solute transport micromodel benchmark experiments. *Comput. Geosci.* 20, 857–879. <https://doi.org/10.1007/s10596-014-9424-0>
- Orellana, F., Verma, P., Loheide, S.P., Daly, E., 2012. Monitoring and modeling water-vegetation interactions in groundwater-dependent ecosystems. *Rev. Geophys.* 50 (3). 2011RG000383.
- Osborne, M., Sykes, J., 1986. Numerical modeling of immiscible organic transport at the Hyde Park Landfill. *Water Resour. Res.* 22(1), 25–33, doi:10.1029/WR022i001p00025
- Paillet, F.U., Pedler, W.H., 1996. Integrated borehole logging methods for wellhead protection applications. *Eng. Geol.* 42, 155–165.
- Paniconi, C., Marrocu, M., Putti, M., Verbunt, M. 2003. Newtonian nudging for a Richards equation-based distributed hydrological model. *Adv. Water Resour.*, 26(2), 161–178
- Parker, B.L., Chapman, S.W., Guilbeault, M.A., 2008. Plume persistence caused by back diffusion from thin clay layers in a sand aquifer following TCE source-zone hydraulic isolation. *J. Contam. Hydrol.* 102, 86–104. <https://doi.org/10.1016/j.jconhyd.2008.07.003>
- Partington, D., Brunner, P., Frei, S., Simmons, C.T., Werner, A.D., Therrien, R., Maier, H.R., Dandy, G.C., Fleckenstein, J.H., 2013. Interpreting streamflow generation mechanisms from integrated surface-subsurface flow models of a riparian wetland and catchment. *Water Resour. Res.* 49, 5501–5519. <https://doi.org/10.1002/wrcr.20405>
- Perkins, T.K., Johnston, O.C., 1963. A Review of Diffusion and Dispersion in Porous Media. *Soc. Pet. Eng. J.* 3, 70–84.
- Peters, C.A., Knightes, C.D., Brown, D.G., 1999. Long-Term Composition Dynamics of PAH-Containing NAPLs and Implications for Risk Assessment. *Environ. Sci. Technol.* 33, 4499–4507.
- Phillips, F.M., Castro, M.C., 2003. Groundwater Dating and Residence-time Measurements, in: *Treatise on Geochemistry - Vol.5*. Elsevier, p. 451–497. <https://doi.org/10.1016/B0-08-043751-6/05136-7>
- Pinder, G.F., Cooper, H.H., 1970. A numerical technique for calculating the transient position of the saltwater front. *Water Resour. Res.* 6 3 , 875–882
- Pickens, J. F., Grisak, G.E., 1981. Scale-dependent dispersion in a stratified granular aquifer, *Water Resour. Res.*, 17(4), 1191–1211, doi: 10.1029/WR017i004p01191.
- Pool, M., Dentz, M., 2018. Effects of Heterogeneity, Connectivity, and Density Variations on Mixing and Chemical Reactions Under Temporally Fluctuating Flow Conditions and the Formation of Reaction Patterns. *Water Resour. Res.* 54, 186–204. <https://doi.org/10.1002/2017WR021820>
- Pool, M., Post, V.E.A., Simmons, C.T., 2015. Effects of tidal fluctuations and spatial heterogeneity on mixing and spreading in spatially heterogeneous coastal aquifers. *Water Resour. Res.* 51, 1570–1585. <https://doi.org/10.1002/2014WR016068>.Received
- Post, V.E.A., von Asmuth, J.R., 2013. Review: Hydraulic head measurements-new technologies, classic pitfalls. *Hydrogeol. J.* 21, 737–750. <https://doi.org/10.1007/s10040-013-0969-0>
- Postma, D., Boesen, C., Kristiansen, H., Larsen, F., 1991. Nitrate Reduction in an Unconfined Sandy Aquifer: Water Chemistry, Reduction Processes, and Geochemical Modeling. *Water Resour. Res.* 27, 2027–2045.
- Powers, S.E., Hunt, C.S., Heermann, S.E., Corseuil, H.X., Rice, D., Corseuil, X., Rice, D., Alvarez, P.J.J., 2010. The Transport and Fate of Ethanol and BTEX in Groundwater Contaminated by Gasohol. *Crit. Rev. Environ. Sci. Technol.* 31, 79–123. <https://doi.org/10.1080/20016491089181>
- Powers, S.E., Hunt, C.S., Heermann, S.E., Corseuil, H.X., Rice, D., Corseuil, X., Rice, D., Alvarez, P.J.J., 2001. The Transport and Fate of Ethanol and BTEX in Groundwater Contaminated by Gasohol. *Crit. Rev. Environ. Sci. Technol.* 31, 79–123. <https://doi.org/10.1080/20016491089181>

- Powers, S.E., Abriola, L.M., Weber Jr., W.J., 1992. An experimental investigation of nonaqueous phase liquid dissolution in saturated subsurface systems: steady state mass transfer rates. *Water Resour. Res.* 28 (10), 2691–2705.
- Powers, S.E., Abriola, L.M., Weber Jr., W.J., 1994. An experimental investigation of nonaqueous phase liquid dissolution in saturate subsurface systems: transient mass transfer rate. *Water Resour. Res.* 30 (2), 321–332.
- Prill RC, Johnson AI, Morris DA, 1965. Specific yield – laboratory experiments showing the effect of time on column drainage. *US Geol Surv Water-Supply Paper* 1662-B, 55
- Prommer, H., Barry, D.A., Davis, G.B., 2002. Modelling of physical and reactive processes during biodegradation of a hydrocarbon plume under transient groundwater flow conditions. *J. Contam. Hydrol.* 59, 113–131. [https://doi.org/10.1016/S0169-7722\(02\)00078-5](https://doi.org/10.1016/S0169-7722(02)00078-5)
- Ptak, T., Teutsch, G., 1994. Forced and natural gradient tracer tests in a highly heterogeneous porous aquifer: instrumentation and measurements. *J. Hydrol.* 159, 79–104. [https://doi.org/10.1016/0022-1694\(94\)90250-X](https://doi.org/10.1016/0022-1694(94)90250-X)
- Rahman, M. M., Liedl, R., Grathwohl, P., 2004. Sorption kinetics during macropore transport of organic contaminants in soils: Laboratory experiments and analytical modeling, *Water Resour. Res.*, 40, W01503, doi:10.1029/2002WR001946
- Rahman, M.A., Jose, S.C., Nowak, W., Cirpka, O.A., 2005. Experiments on vertical transverse mixing in a large-scale heterogeneous model aquifer. *J. Contam. Hydrol.* 80, 130–148. <https://doi.org/10.1016/j.jconhyd.2005.06.010>
- Rai, S.N., Manglik, A., Singh, V.S., 2005. Water table fluctuation owing to time-varying recharge, pumping and leakage. *J. Hydrol.* 324, 350–358. <https://doi.org/10.1016/j.jhydrol.2005.09.029>
- Rama, F., Franco, D., Corseuil, H.X., 2017. Spatial and Temporal Analysis of Natural Drainage in the Ressacada Aquifer (Florianopolis, Brazil). *Int. J. Environ. Sci. Dev.* 8, 653–660. <https://doi.org/10.18178/ijesd.2017.8.9.1033>
- Rama, F., Miotliński, K., Franco, D., Corseuil, H.X., 2018. Recharge estimation from discrete water-table datasets in a coastal shallow aquifer in a humid subtropical climate. *Hydrogeol. J.* 26, 1887–1902. <https://doi.org/10.1007/s10040-018-1742-1>
- Rama, F., Ramos, D.T., Müller, J.B., Corseuil, H.X., Miotliński K., 2019. Flow field dynamics and high ethanol content in gasohol blends enhance BTEX migration and biodegradation in groundwater, *J. Contam. Hydrol.*, <https://doi.org/10.1016/j.jconhyd.2019.01.003>
- Ramanathan, R., Guin, A., Ritz, R.W., Dominic, D.F., Freedman, V.L., Scheibe, T.D., Lunt, I.A., 2010. Simulating the heterogeneity in braided channel belt deposits: Part 1. A geometric-based methodology and code, *Water Resour. Res.*, 46, W04515, doi:10.1029/2009WR008111.
- Ramaswami, A.; Ghoshal, S.; Luthy, R. G., 1997. Mass transfer and bioavailability of PAH compounds in coal tar NAPL-slurry systems. 2. Experimental evaluations. *Environ. Sci. Technol.* 31, 2268–2276
- Rao, P.S.C., Annable, M.D., Kim, H., 2000. NAPL source zone characterization and remediation technology performance assessment: Recent developments and applications of tracer techniques. *J. Contam. Hydrol.* 45, 63–78. [https://doi.org/10.1016/S0169-7722\(00\)00119-4](https://doi.org/10.1016/S0169-7722(00)00119-4)
- Rao, P.S.C., Rolston, D.E., Jessup, R.E., Davidson, J.M., 1980. Solute Transport in Aggregated Porous Media: Theoretical and Experimental Evaluation. *Soil Sci. Soc. Am. J.* 44, 1139–1146.
- Raoult, F.-M., 1886. "Loi générale des tensions de vapeur des dissolvants" (General law of vapor pressures of solvents. *Comptes rendus*, 104 : 1430–1433
- Raouf, A., Hassanizadeh, S.M., 2013. Saturation-dependent solute dispersivity in porous media: Pore-scale processes, *Water Resour. Res.*, 49, 1943–1951, doi:10.1002/wrcr.20152
- Rasa, E., Bekins, B.A., Mackay, D.M., de Sieyes, N.R., Wilson, J.T., Feris, K.P., Wood, I.A., Scow, K.M., 2013a. Impacts of an ethanol-blended fuel release on groundwater and fate of produced methane: Simulation of field observations. *Water Resour. Res.* 49, 4907–4926. <https://doi.org/10.1002/wrcr.20382>
- Rasa, E., Foglia, L., Mackay, D.M., Scow, K.M., 2013b. Effect of different transport observations on inverse modeling results: case study of a long-term groundwater tracer test monitored at high resolution. *Hydrogeol. J.* 21, 1539–1554. <https://doi.org/10.1007/s10040-013-1026-8>
- Rau, G.C., Andersen, M.S., Mccallum, A.M., Roshan, H., Acworth, R.I., 2014. Heat as a tracer to quantify water flow in near-surface sediments. *Earth Sci. Rev.* 129, 40–58. <https://doi.org/10.1016/j.earscirev.2013.10.015>
- Reed, P., Minsker, B., Valocchi, A.J., 2000. Cost-effective long-term groundwater monitoring design using a genetic algorithm and global mass interpolation. *Water Resour. Res.* 36, 3731–3741.
- Reemtsma, T., Alder, L., Banasiak, U., 2013. Emerging pesticide metabolites in groundwater and surface water as determined by the application of a multimethod for 150 pesticide metabolites. *Water Res.* 1–11. <https://doi.org/10.1016/j.watres.2013.06.031>
- Rehfeldt, K.R., Boggs, K.M., Gelhar, L.W., 1992. Field Study of Dispersion in a Heterogeneous Aquifer - 3. Geostatistical Analysis of Hydraulic Conductivity. *Water Resour. Res.* 28, 16.
- Rehfeldt, K.R., Gelhar, L.W., 1992. Stochastic analysis of dispersion in unsteady flow in heterogeneous aquifers, *Water Resour. Res.*, 28 (8), 2085–2099

- Rein, A., Bauer, S., Dietrich, P., Beyer, C., 2009. Influence of temporally variable groundwater flow conditions on point measurements and contaminant mass flux estimations. *J. Contam. Hydrol.* 108, 118–133. <https://doi.org/10.1016/j.jconhyd.2009.06.005>
- Riva, M., Guadagnini, L., Guadagnini, A., 2010. Effects of uncertainty of lithofacies, conductivity and porosity distributions on stochastic interpretations of a field scale tracer test. *Stoch. Environ. Res. Risk Assess.* 24, 955–970. <https://doi.org/10.1007/s00477-010-0399-7>
- Rivett, M.O., Allen-King, R.M., 2003. A controlled field experiment on groundwater contamination by a multicomponent DNAPL: Dissolved-plume retardation. *J. Contam. Hydrol.* 66, 117–146. [https://doi.org/10.1016/S0169-7722\(03\)00006-8](https://doi.org/10.1016/S0169-7722(03)00006-8)
- Rivett, M.O., Feenstra, S., Cherry, J. a., 2001. A controlled field experiment on groundwater contamination by a multicomponent DNAPL: Creation of the emplaced-source and overview of dissolved plume development. *J. Contam. Hydrol.* 49, 111–149. [https://doi.org/10.1016/S0169-7722\(00\)00191-1](https://doi.org/10.1016/S0169-7722(00)00191-1)
- Rivett, M.O., Petts, J., Butler, B., Martin, L., 2002. Remediation of contaminated land and groundwater : experience in England and Wales. *J. Environ. Manage.* 65, 251–268. <https://doi.org/10.1006/jema>
- Roberts, P. V, Goltz, M.N., Mackay, D.M., 1986. A Natural Gradient Experiment on Solute Transport in a Sand Aquifer - 3. Retardation Estimates and Mass Balances for Organic Solutes. *Water Resour. Res.* 22, 2047–2058.
- Robinson, C., Brovelli, a., Barry, D. a., Li, L., 2009. Tidal influence on BTEX biodegradation in sandy coastal aquifers. *Adv. Water Resour.* 32, 16–28. <https://doi.org/10.1016/j.advwatres.2008.09.008>
- Robinson, D.A., Campbell, C.S., Hopmans, J.W., Hornbuckle, B.K., Jones, S.B., Knight, R., Ogden, F., Selker, J., Wendroth, O., 2008. Soil moisture measurement for ecological and hydrological watershed-scale observatories: A review, *Vadose Zone J.*, 7(1), 358–389, doi: 10.2136/vzj2007.0143.
- Rolle, M., Chiogna, G., Hochstetler, D.L., Kitanidis, P.K., 2013. On the importance of diffusion and compound-specific mixing for groundwater transport: An investigation from pore to field scale. *J. Contam. Hydrol.* 153, 51–68. <https://doi.org/10.1016/j.jconhyd.2013.07.006>
- Rolle, M., Eberhardt, C., Chiogna, G., Cirpka, O. a., Grathwohl, P., 2009. Enhancement of dilution and transverse reactive mixing in porous media: Experiments and model-based interpretation. *J. Contam. Hydrol.* 110, 130–142. <https://doi.org/10.1016/j.jconhyd.2009.10.003>
- Rosenberry, D.O., Pitlick, J., 2009. Local-scale variability of seepage and hydraulic conductivity in a shallow gravel-bed river. *Hydrol. Process.* 23, 3306–3318. <https://doi.org/10.1002/hyp.7433>
- Rozemeijer, J.C., Velde, Y. Van Der, McLaren, R.G., Geer, F.C. Van, Broers, H.P., Bierkens, M.F.P., 2010. Integrated modeling of groundwater-surface water interactions in a tile-drained agricultural field: The importance of directly measured flow route contributions. *Water Resour. Res.* 46, 1–10. <https://doi.org/10.1029/2010WR009155>
- Rubin, J., 1968. Theoretical Analysis of Two-Dimensional, Transient Flow of Water in Unsaturated and Partly Unsaturated Soils. *Soil Sci. Soc. Am. J.* 32, 607. <https://doi.org/10.2136/sssaj1968.03615995003200050013x>
- Rubin, Y., Bellin, A., 1994. The effects of recharge on flow nonuniformity and macrodispersion. *Water Resour. Res.* 30, 939–948.
- Rubin, Y., Cushey, M.A., Bellin, A., 1994. Modeling of transport in groundwater for environmental risk assessment. *Stoch. Hydrol. Hydraul.* 8, 57–77.
- Rubin, Y., Sun, A., Maxwell, R., Bellin, A., 1999. The concept of block-effective macrodispersivity and a unified approach for grid-scale- and plume-scale-dependent transport. *J. Fluid Mech.* 395, 161–180.
- Ruiz, L. et al., 2010. Water balance modelling in a tropical watershed under deciduous forest (Mule Hole, India): Regolith matrix storage buffers the groundwater recharge process. *Journal of Hydrology*, 380(3–4): 460–472
- Ruiz, L., Varma, M.R.R., Kumar, M.S.M., Sekhar, M., Maréchal, J., Descloitres, M., Riotte, J., Kumar, S., Kumar, C., Braun, J., 2010. Water balance modelling in a tropical watershed under deciduous forest (Mule Hole , India): Regolith matrix storage buffers the groundwater recharge process. *J. Hydrol.* 380, 460–472. <https://doi.org/10.1016/j.jhydrol.2009.11.020>
- Saghravani, S.R., Yusoff, I., Wan Md Tahir, W.Z., Othman, Z., 2015. Comparison of water table fluctuation and chloride mass balance methods for recharge estimation in a tropical rainforest climate: a case study from Kelantan River catchment, Malaysia. *Environ. Earth Sci.* 73, 4419–4428. <https://doi.org/10.1007/s12665-014-3727-2>
- Sakaki, T., Limsuwat, A. Smits, K. M., Illangasekare, T. H., 2008. Empirical two-point alpha-mixing model for calibrating the ECHO2O EC- 5 soil moisture sensor in sands, *Water Resour. Res.*, 44, W00D08, doi:10.1029/2008WR006870
- Salamon, P., Fernández-García, D., Gómez-Hernández, J.J., 2007. Modeling tracer transport at the MADE site: The importance of heterogeneity. *Water Resour. Res.* 43. <https://doi.org/10.1029/2006WR005522>
- Sanford, W.E., Plummer, L.N., Casile, G., Busenberg, E., Nelms, D.L., Schlosser, P., 2017. Using dual-domain advective-transport simulation to reconcile multiple-tracer ages and estimate dual-porosity transport parameters. *Water Resour. Res.* 53, 1–15. <https://doi.org/10.1002/2016WR019469>. Received

- Scanlon, B.R., Healy, R.W., Cook, P.G., 2002. Choosing appropriate techniques for quantifying groundwater recharge. *Hydrogeol. J.* 10, 18–39. <https://doi.org/10.1007/s10040-001-0176-2>
- Scanlon, B.R., Mace, R.E., Barrett, M.E., Smith, B., 2003. Can we simulate regional groundwater flow in a karst system using equivalent porous media models? Case study, Barton Springs Edwards aquifer, USA. *J. Hydrol.* 276, 137–158. [https://doi.org/10.1016/S0022-1694\(03\)00064-7](https://doi.org/10.1016/S0022-1694(03)00064-7)
- Scheidegger, A.E., 1961. General theory of dispersion in porous media. *J. Geophys. Res.* 66. <https://doi.org/10.1029/JZ066i010p03273>
- Schirmer, M., Butler, B.J., 2004. Transport behaviour and natural attenuation of organic contaminants at spill sites. *Toxicology* 205, 173–179. <https://doi.org/10.1016/j.tox.2004.06.049>
- Schirmer, M., Durrant, G.C., Molson, J.W., Emil O. Frind, 2001. Influence of transient flow on contaminant biodegradation. *Groundwater* 39.
- Schumer, R., Benson, D.A., Meerschaert, M.M., Wheatcraft, S.W., 2001. Eulerian derivation of the fractional advection-dispersion equation. *J. Contam. Hydrol.* 48, 69–88. [https://doi.org/10.1016/S0169-7722\(00\)00170-4](https://doi.org/10.1016/S0169-7722(00)00170-4)
- Schwartz, F.W., Zhang, H., 2002. *Fundamentals of Ground Water*. John Wiley and Sons Inc., ISBN: 978-0-471-13785-6, p.592
- Schwartz, F. W., 1977. Macroscopic dispersion in porous media: The controlling factors, *Water Resour. Res.*, 13(4), 743–752, doi:10.1029/WR013i004p00743.
- Sebok, E., Duque, C., Engesgaard, P., Boegh, E., 2015. Spatial variability in streambed hydraulic conductivity of contrasting stream morphologies: Channel bend and straight channel. *Hydrol. Process.* 29, 458–472. <https://doi.org/10.1002/hyp.10170>
- Seyedabbasi, M.A., Newell, C.J., Adamson, D.T., Sale, T.C., 2012. Relative contribution of DNAPL dissolution and matrix diffusion to the long-term persistence of chlorinated solvent source zones. *J. Contam. Hydrol.* 134–135, 69–81. <https://doi.org/10.1016/j.jconhyd.2012.03.010>
- Shakas, A., Linde, N., Le Borgne, T., Bour, O., 2018. Probabilistic inference of fracture-scale flow paths and aperture distribution from hydrogeophysically-monitored tracer tests. *J. Hydrol.* 567, 305–319. <https://doi.org/10.1016/j.jhydrol.2018.10.004>
- Shamir, U.Y., Harleman, D.R.F., 1967. Numerical solutions for dispersion in porous mediums, *Water Resour. Res.*, 3(2): 557–581, doi: 10.1029/WR003i002p00557
- Shao, J.L., Zhao, Z.Z., Cui, Y.L., Wang, R., Li, C.Q., Yang, Q.Q., 2009. Application of groundwater modeling system to the evaluation of groundwater resources in North China plain. *Resources Science* 31, 361–367
- Shapiro, A.M., Nicholas, J.R., 1989. Assessing the validity of the channel model of fracture aperture under field conditions. *Water Resources Research* 25 (5), 817– 828.
- Shlomi, S., Michalak, A.M., 2007. A geostatistical framework for incorporating transport information in estimating the distribution of a groundwater contaminant plume. *Water Resour. Res.* 43, 1–12. <https://doi.org/10.1029/2006WR005121>
- Shuttleworth, W.J., Wallace, J.S., 1985. Evaporation from sparse crops—an energy combination theory. *Q. J. R. Meteorol. Soc.* 111, 839–855.
- Simms JT, Simard RR, Joern BC, 1998. Phosphorus loss in agricultural drainage: historical perspective and current research. *J Environ Qual* 27:277–293
- Soga, K., Page, J.W.E., Illangasekare, T.H., 2004. A review of NAPL source zone remediation efficiency and the mass flux approach. *J. Hazard. Mater.* 110, 13–27. <https://doi.org/10.1016/j.jhazmat.2004.02.034>
- Sophocleous, M., 2002. Interactions between groundwater and surface water: the state of the science. *Hydrogeol. J.* 10, 52–67. <https://doi.org/10.1007/s10040-001-0170-8>
- Sposito, G., 2006. Chaotic solute advection by unsteady groundwater flow. *Water Resour. Res.* 42, 1–6. <https://doi.org/10.1029/2005WR004518>
- Steefel, C.L., DePaolo, D.J., Lichtner, P.C., 2005. Reactive transport modeling: an essential tool and a new research approach for the earth sciences. *Earth Planet. Sci. Lett.* 240, 539–558
- Stewart, M., Gay, M.C., 1986. Evaluation of transient electromagnetic soundings for deep detection of conductive fluids. *Ground Water* 24, 351–356.
- Stuart, M., Lapworth, D., Crane, E., Hart, A., 2012. Science of the Total Environment Review of risk from potential emerging contaminants in UK groundwater. *Sci. Total Environ.* 416, 1–21. <https://doi.org/10.1016/j.scitotenv.2011.11.072>
- Sudicky, E.A., 1986. A natural gradient experiment on solute transport in a sand aquifer: Spatial variability of hydraulic conductivity and its role in the dispersion process. *Water Resour. Res.* 22, 2069–2082. <https://doi.org/10.1029/WR022i013p02069>

- Sudicky, E.A., Illman, W. a. Goltz, I.K., Adams, J.J., McLaren, R.G., 2010. Heterogeneity in hydraulic conductivity and its role on the macroscale transport of a solute plume: From measurements to a practical application of stochastic flow and transport theory. *Water Resour. Res.* 46, W01508 (1-16). <https://doi.org/10.1029/2008WR007558>
- Sudicky, E.A., Illman, W.A., 2011. Lessons Learned from a Suite of CFB Borden History of the CFB Borden Site. *Ground Water* 49, 630–648. <https://doi.org/10.1111/j.1745-6584.2011.00843.x>
- Sudicky, E.A., Frind, E.O., 1982. Contaminant transport in fractured porous media: analytical solutions for a series of parallel fractures. *Water Resour. Res.* 18 6, 1634–1642.
- Sudicky, E.A., McLaren, R.G., 1992. The Laplace transform Galerkin technique for large scale simulation of mass transport in discretely fractured porous formations. *Water Resources Research* 28 (2), 499–514
- Sutton, P.A., Barker, J.F., 1985. Migration and attenuation of selected organics in a sandy aquifer—A natural gradient experiment, *Ground Water*, 23 (1), 10–16
- Sykes, J.F., Pahwa, S.B., Lantz, R.B., Ward, D.S., 1982. Numerical simulation of flow and contaminant migration at an extensively monitored landfill, *Water Resour. Res.*, 18 (6), 1687–1704.
- Tartakovsky, D.M., Broyda, S., 2011 PDF equations for advective–reactive transport in heterogeneous porous media with uncertain properties, *J. Contam. Hydrol.*, <https://doi.org/10.1016/j.jconhyd.2010.08.009>
- Thierrin, J., Kitanidis, P.K., 1994. Solute dilution at Borden and Cape Cod groundwater tracer tests. *Water Resour. Res.* 30, 2883–2890.
- Thorbjarnarson, K.W., Mackay, D.M., 1994. A forced-gradient experiment on solute transport in the Borden aquifer - Transport and dispersion of the conservative tracer. *Water Resour. Res.* 30, 385–399.
- Tyagi, M., Gimmi, T., Churakov, S. V., 2013. Advances in Water Resources Multi-scale micro-structure generation strategy for up-scaling transport in clays. *Adv. Water Resour.* 59, 181–195. <https://doi.org/10.1016/j.advwatres.2013.06.002>
- Todd, D. K., Mays, L. W., 2004. *Groundwater Hydrology - 3rd Edition*, John Wiley and Sons Inc., ISBN: 978-0-471-05937-0, p.656
- Troldborg, M., Nowak, W., Tuxen, N., Bjerg, P. L., Helmig, R., Binning, P. J., 2010. Uncertainty evaluation of mass discharge estimates from a contaminated site using a fully Bayesian framework, *Water Resour. Res.*, 46, W12552, doi:10.1029/2010WR009227
- Tromp-Van Meerveld, H.J., McDonnell, J.J., 2006. Threshold relations in subsurface stormflow: 2. The fill and spill hypothesis. *Water Resour. Res.* 42, 1–11. <https://doi.org/10.1029/2004WR003800>
- Turnadge, C., Smerdon, B.D., 2014. A review of methods for modelling environmental tracers in groundwater: Advantages of tracer concentration simulation. *J. Hydrol.* 519, 3674–3689. <https://doi.org/10.1016/j.jhydrol.2014.10.056>
- United States Census Bureau web site, 2014. Economic Data of Gas Station Industry, Access: 2016 June. Available at: <<https://www.census.gov/econ/isp/sampler.php?naicscode=4471&naicslevel=4#>>
- Valocchi, A.J., Street, R.L., Roberts, P.V., 1981. Transport of ion-exchanging solutes in groundwater: chromatographic theory and field simulation. *Water Resources Research* 17, 1517–1527
- Van Breukelen, B.M., Rolle, M., 2012. Transverse hydrodynamic dispersion effects on isotope signals in groundwater chlorinated solvents plumes. *Environ. Sci. Technol.* 46, 7700–7708. <https://doi.org/10.1021/es301058z>
- van der Kamp, G., Hayashi, M., 2009. Groundwater-wetland ecosystem interaction in the semiarid glaciated plains of North America. *Hydrogeol. J.* 17, 203–214. <https://doi.org/10.1007/s10040-008-0367-1>
- van Genuchten, M.T., 1980. A Closed-form Equation for Predicting the Hydraulic Conductivity of Unsaturated Soils. *Soil Sci. Soc. Am. J.* <https://doi.org/10.2136/sssaj1980.03615995004400050002x>
- Vanderborght, J., Timmerman, A., Feyen, J., 2000. Solute Transport for Steady-State and Transient Flow in Soils with and without Macropores. *Soil Sci. Soc. Am. J.* 64, 1305–1317.
- Vivoni, E.R., Moreno, H.A., Mascaro, G., Rodriguez, J.C., Watts, C.J., Garatuza-Payan, J., Scott, R.L., 2008. Observed relation between evapotranspiration and soil moisture in the North American monsoon region. *Geophys. Res. Lett.* 35, 1–6. <https://doi.org/10.1029/2008GL036001>
- Voss, C.I., Souza, W.R., 1987. Variable density flow and solute transport simulation of regional aquifers containing a narrow freshwater–saltwater transition zone. *Water Resour. Res.* 23 10, 1851–1866.
- Walker, G.R., Gilfedder, M., Dawes, W.R., Rassam, D.W., 2015. Predicting aquifer response time for application in catchment modeling. *Groundwater* 53, 475–484. <https://doi.org/10.1111/gwat.12219>
- Walker, G.W., Kookana, R.S., Smith, N.E., Kah, M., Doolette, C., Reeves, P., Lovell, W., Anderson, D.J., Turney, T.W., Navarro, D.A., 2017. Ecological risk assessment of nano-enabled pesticides: A perspective on problem formulation. *J. Agric. Food Chem.* <https://doi.org/10.1021/acs.jafc.7b02373>
- Wang, L.Y., Han, J.P., Liu, J.R., Ye, C., Zheng, Y.J., Wan, L.Q., Li, W.P., Zhou, Y.X., 2009. Modeling of regional groundwater flow in Beijing plain. *Journal of Hydrogeology and Engineering Geology* 36 (1), 11-19

- Wang, B., Jin, M., Nimmo, J.R., Yang, L., Wang, W., 2008. Estimating groundwater recharge in Hebei Plain, China under varying land use practices using tritium and bromide tracers. *J. Hydrol.* 356, 209–222. <https://doi.org/10.1016/j.jhydrol.2008.04.011>
- Warsta, L., Karvonen, T., Koivusalo, H., Paasonen-Kivekäs, M., Taskinen, A., 2013. Simulation of water balance in a clayey, subsurface drained agricultural field with three-dimensional FLUSH model. *J. Hydrol.* 476, 395–409. <https://doi.org/10.1016/j.jhydrol.2012.10.053>
- Weber, W. J., Jr., DiGiano, F.A., 1996. *Process Dynamics in Environmental Systems*, John Wiley, N. Y
- Werth, C.J., Cirpka, O.A., Grathwohl, P., 2006. Enhanced mixing and reaction through flow focusing in heterogeneous porous media. *Water Resour. Res.* 42, 1–10. <https://doi.org/10.1029/2005WR004511>
- Williams, M.R., King, K.W., Macrae, M.L., Ford, W., Van Esbroeck, C., Brunke, R.I., English, M.C., Schiff, S.L., 2015. Uncertainty in nutrient loads from tile-drained landscapes: Effect of sampling frequency, calculation algorithm, and compositing strategy. *J. Hydrol.* 530, 306–316. <https://doi.org/10.1016/j.jhydrol.2015.09.060>
- Wilson, R.D., Thornton, S.F., MacKay, D.M., 2004. Challenges in monitoring the natural attenuation of spatially variable plumes. *Biodegradation* 15, 359–369. <https://doi.org/10.1023/B:BIOD.0000044591.45542.a9>
- Wilkins, M. D., Abriola, L.M., Pennell, K.D., 1995. An experimental investigation of rate-limited nonaqueous phase liquid volatilization in unsaturated porous media: Steady state mass transfer, *Water Resour. Res.*, 31(9), 2159–2172, doi:10.1029/95WR01677
- Winter, T.C., 1999. Relation of streams, lakes, and wetlands to groundwater flow systems. *Hydrogeol. J.* 7, 28–45. <https://doi.org/10.1007/s100400050178>
- Winter, T.C., Harvey, J.W., Franke, O.L., Alley, W.M., 1998. *Ground Water and Surface Water A Single Resource*, Circular 1139. Denver: Colorado: USGS
- Wittenberg, H., 1999. Baseflow recession and recharge as nonlinear storage processes. *Hydrol. Process.* 13, 715–726. [https://doi.org/10.1002/\(SICI\)1099-1085\(19990415\)13:5<715::AID-HYP775>3.0.CO;2-N](https://doi.org/10.1002/(SICI)1099-1085(19990415)13:5<715::AID-HYP775>3.0.CO;2-N)
- Woodbury A.D., Rubin Y., 2000. A full-Bayesian approach to parameter inference from tracer travel time moments and investigation of scale effects at the Cape Cod experimental site. *Water Resour. Res.* 36(1): 159–171
- Woodbury, A.D., Sudicky, E.A., 1991. The geostatistical characteristics of the Borden aquifer, *Water Resour. Res.*, 27 (4), 533–546.
- Woodbury, A.D., Sudicky, E.A., 1992. Inversion of the Borden Tracer Experiment data: Investigation of stochastic moment models. *Water Resour. Res.* 28, 2387–2398. <https://doi.org/10.1029/92WR01005>
- Woodward, S.J.R., Wöhling, T., Stenger, R., 2016. Uncertainty in the modelling of spatial and temporal patterns of shallow groundwater flow paths: The role of geological and hydrological site information. *J. Hydrol.* 534, 680–694. <https://doi.org/10.1016/j.jhydrol.2016.01.045>
- Xie, Y., Cook, P.G., Simmons, C.T., Partington, D., Crosbie, R., Batelaan, O., 2017. Uncertainty of groundwater recharge estimated from a water and energy balance model. *J. Hydrol.* <https://doi.org/10.1016/j.jhydrol.2017.08.010>
- Yan, Z., Wang, J., Chai, H., 2010. Influence of water level fluctuation on phreatic line in silty soil model slope. *Eng. Geol.* 113, 90–98. <https://doi.org/10.1016/j.enggeo.2010.02.004>
- Yang, M., Annable, M.D., Jawitz, J.W., 2014. Back Diffusion from Thin Low Permeability Zones. *Environ. Sci. Technol.* 49, 415–422.
- Yeh, T.-C.J., Liu, S., 2000. Hydraulic tomography: Development of a new aquifer test method. *Water Resour. Res.* 36, 2095–2105.
- Zech, A., Attinger, S., Cvetkovic, V., Dagan, G., Dietrich, P., Fiori, A., Rubin, Y., Teutsch, G., 2015. Is unique scaling of aquifer macrodispersivity supported by field data? *Water Resour. Res.* 51, 7662–7679. <https://doi.org/10.1002/2015WR017220>
- Zha, Y., Yeh, T.-C.J., Illman, W.A., Onoe, H., Mok, C.M.W., Wen, J.-C., Huang, S.-Y., Wang, W., 2017. Incorporating geologic information into hydraulic tomography: A general framework based on geostatistical approach. *Water Resour. Res.* 53, 2850–2876. <https://doi.org/10.1002/2016WR019185>. Received
- Zhang, C., Werth, C.J., Webb, A.G., 2007. Characterization of NAPL source zone architecture and dissolution kinetics in heterogeneous porous media using magnetic resonance imaging. *Environ. Sci. Technol.* 41, 3672–3678. <https://doi.org/10.1021/es061675q>
- Zhang, H., Schwartz, F.W., Wood, W.W., Garabedian, S.P., Leblanc, D.R., 1998. Simulation of variable-density flow and transport of reactive and nonreactive solutes during a tracer test at Cape Cod, Massachusetts. *Water Resour. Res.* 34, 67–82.
- Zhang, P., Devries, S.L., Dathe, A., Bagtzoglou, A.C., 2009. Enhanced mixing and plume containment in porous media under time-dependent oscillatory flow. *Environ. Sci. Technol.* 43, 6283–6288. <https://doi.org/10.1021/es900854r>
- Zhang, Y.K., Schilling, K.E., 2006. Effects of land cover on water table, soil moisture, evapotranspiration, and groundwater recharge: A Field observation and analysis. *J. Hydrol.* 319, 328–338. <https://doi.org/10.1016/j.jhydrol.2005.06.044>

- Zheng, C., Bianchi, M., Gorelick, S.M., 2011. Lessons learned from 25 years of research at the MADE site. *Ground Water*, 49(5), 649–662. doi:10.1111/j.1745-6584.2010.00753.x
- Zheng, C., Gorelick, S.M., 2003. Analysis of the effect of decimeter-scale preferential flow paths on solute transport. *Ground Water* 41(2), 142–155.
- Zheng, C., Jiao, J.J., 1998. Numerical simulation of tracer tests in heterogeneous aquifer. *J. Environ. Eng.* 124(6), p. 510-516
- Zhou, Y., Li, W., 2011. A review of regional groundwater flow modeling. *Geosci. Front.* 2, 205–214. <https://doi.org/10.1016/j.gsf.2011.03.003>
- Zinn, B., Harvey, C.F., 2003. When good statistical models of aquifer heterogeneity go bad: A comparison of flow, dispersion, and mass transfer in connected and multivariate Gaussian hydraulic conductivity fields. *Water Resour. Res.* 39, 1–19. <https://doi.org/10.1029/2001WR001146>
- Zuber, A., Motyka, J., 1998. Hydraulic parameters and solute velocities in triple-porosity karstic-fissured-porous carbonate aquifers : case studies in southern Poland. *Environ. Geol.* 34, 243–250.

3.2 SPATIAL AND TEMPORAL ANALYSIS OF NATURAL DRAINAGE IN THE RESSACADA AQUIFER (FLORIANOPOLIS, BRAZIL)

Fabrizio Rama^{(1)*}, Davide Franco⁽²⁾, and Henry X. Corseuil⁽¹⁾

* Corresponding author

(1) Núcleo Ressacada de pesquisa em meio ambiente (REMA) – CTC - UFSC

(2) Laboratório de Hidráulica Marítima (LAHIMAR) – ENS - UFSC

Manuscript received May 30, 2017;

revised July 20, 2017; published and print September 8, 2017

Referência:

Rama, F.; Franco, D.; Corseuil, H.X. Spatial and Temporal Analysis of Natural Drainage in the Ressacada Aquifer (Florianópolis, Brazil). *International Journal of Environmental Science and Development*, 2017, 8 (9), 653–660. <https://doi.org/10.18178/ijesd.2017.8.9.1033>

Nota ao leitor:

Ajustes de texto e nas figuras foram realizadas em relação ao artigo original para aumentar a precisão da escrita científica e por razões de formato da dissertação sem, no entanto, alterar conteúdo e elementos utilizados nas análises.

Resumo

Este trabalho propõe uma exploração estatística dos dados de carga hidráulica disponíveis pelo aquífero não confinado da Ressacada (Florianópolis, Brasil), que representam 10 anos de monitoramento dos 13 piezômetros instalados nas áreas experimentais do REMA. Por meio dessa abordagem, o estudo visa obter um quadro completo da drenagem natural no domínio, que está intrinsecamente ligada à taxa de rebaixamento do lençol freático no tempo. Este estudo apoia, portanto, a compreensão geral da relação entre as chuvas e as flutuações do nível freático nesta região costeira, e em específico nas áreas experimentais do REMA. Em uma perspectiva mais ampla, o termo de descarga (definido no texto com D) pode também ser usado como dado de input na aplicação do método do water-table fluctuation (WTF), a fim de explicar o comportamento do escoamento subsuperficial e os fenômenos de recarga. A área de estudo representa um aquífero raso (profundidade do lençol freático entre 0.3 e 2.0 m) cercado por manguezais em uma planície costeira caracterizada por um clima subtropical úmido. Tais características, configuram um domínio complexo para se avaliar os processos de interação

entre águas subterrâneas e superficiais. Além disso, a ocorrência de numerosos fatores antropogênicos e a presença de áreas de interesse estratégico (Ex. Aeroporto Internacional Hercílio Luz, Base aérea militar), dificultam ainda mais a definição da infiltração vertical e do campo de escoamento subsuperficial, dada a presença de uma densa rede de canais de drenagem que constituem uma forma preferencial e transitória de fluxo. A pesar das limitações, os resultados da análise estatística das taxas de rebaixamento dos piezômetros da Fazenda mostram dois comportamentos principais das cargas hidráulicas, que diferem por uma maior ou menor impulsividade das variações tanto em subida que em descida. No texto define-se que esta variação do comportamento depende principalmente da posição do poço ao interno do campo de fluxo geral do aquífero e, portanto, da distância total “piezômetro-receptores superficiais”, tendo os piezômetros mais afastados da condição de contorno superficial como os mais flutuantes do domínio. Aliás cabe ressaltar que por cada grupo de piezômetros, consolidaram-se duas condições típicas de drenagem a partir da ANOVA das taxas, em função da profundidade do lençol freático. Este fato destaca a importância da conteúdo de água do aquífero e do regime pluviométrico (época seca ou úmida) na definição do campo de fluxo e das velocidades locais de escoamento.

Abstract

This paper proposes an in-depth statistical exploration of the available hydraulic head data concerning the Ressacada aquifer (Florianópolis, Brazil). By means of this approach, the study aims to obtain a complete picture of the natural drainage in the domain. This intent supports the understanding of the relationship between rainfalls and aquifer level fluctuations in this coastal region. In a broader perspective, the drainage term can be used in the application of the water table fluctuation method, in order to explain the seepage behavior and recharge phenomena. The chosen study area was a shallow coastal aquifer surrounded by mangrove swamp in a humid subtropical climate region. In view of the cited features, it represented a complex domain to assess both groundwater and surface processes. Besides, the co-occurrence of numerous anthropogenic factors, and the presence of strategic interest areas (International Airport, Military base camp), have further complicated the vertical infiltration and the natural drainage. Finally, results showed two main groups of piezometers with a typical drainage behavior. It seems to depend on the well position in the flow field and, therefore, on the distance from surface receptors. In each group, two distinct drainage conditions were also detached in terms of the water table level.

Keywords: Natural drainage, Spatial analysis, Coastal Aquifer, Water table fluctuation method.

Highlights:

- A statistical exploration of drainage rate in the Ressacada aquifer (coastal shallow unconfined aquifer) was presented
- The evolution of natural drainage over time was described by an exponential function
- Two groups of piezometers with different behaviour of drainage rate was showed
- Two main drainage regimes, dependent to time since the last precipitation, was highlighted for both groups

3.2.1 Introduction

More and more studies in the last two decades have observed the importance of the hydraulic head records in order to understand hydrodynamics of groundwater. The relationship between natural stresses (e.g. rainfalls and tidal oscillations) and water level fluctuations in the aquifer is of primary importance to explain in an effective way the flow field, especially in shallow aquifers [1], and more specific in all unconfined coastal aquifers rounded with oscillating head conditions and characterized with a scarce water table depth or an intense reactivity to changing conditions [2]-[3]. The task becomes even more challenging in extreme climate and environmental conditions, on the southern cost of Brazil, where strong and varying precipitations in the presence of dense mangrove areas would modify the response of groundwater system [4]-[5]. In the described situation, continuous monitoring of the water table could be used both to predict future fluctuations and to establish the recharge of the aquifer [6]: the results obtained so far support its use in different types of technical applications and in different scientific areas [7]-[8]. Nevertheless, generally speaking already available datasets include only discrete measurements of water heads, scattered and irregularly spaced in time. This kind of data, although rarely used, can be a useful source for information and prediction about aquifers if properly mined and processed.

For this reason, among the different methods available in literature, the water table fluctuations (WTF) method was chosen since it provides a valuable tool for interpreting hydraulic head fluctuations over a wide variety of climatic conditions and different time-scales [9]. Despite the flexibility of the method, different limits for its application have been reported in the literature [10] linked to a variety of factors: long-lasting and light rains (due to underestimation of the recharge), daily or weekly fluctuations of the recharge, sampling interval of the hydraulic loads, difficulties in estimating the specific storage and natural decrease rate of

the water table. Focusing on the last point, [11] deals with it through an automatic method that estimates the descent at each moment (MRC), while another study [12], defines the drainage rate (D), as a constant for the entire time and domain, maintaining a statistical approach to estimate its value. In both works a robust and data-driven choice on the drainage term stands out as an important aspect.

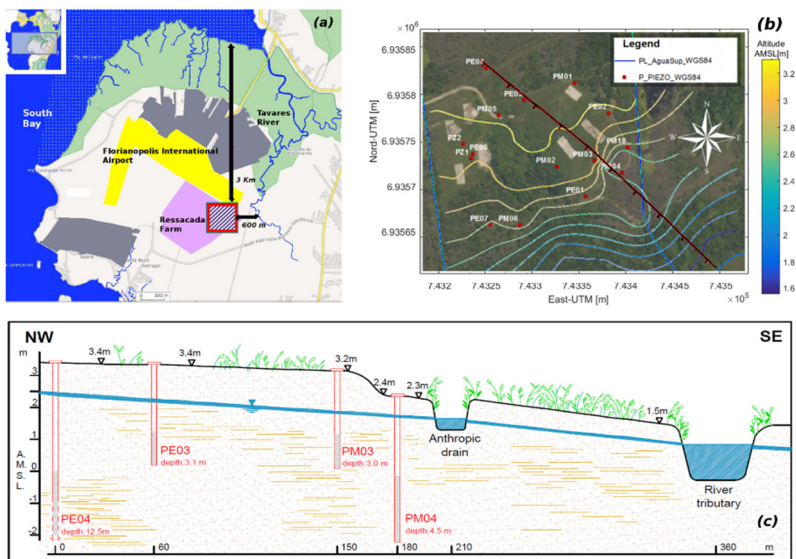
For this reason, the present study aims to analyze and estimate, in a clear and objective way, the decreasing rates of water table levels (all drainage contributes) in the Ressacada aquifer, located in Florianópolis island. Furthering this topic is of great importance for the accurate application of WTF method with a discrete time series approach. The aquifer of the case study is a shallow coastal system located in humid subtropical climate, close to mangrove swamps and a complex estuarine system subject to tides. The paper is based on the exploratory analysis of the water table historical series collected at the Experimental Farm of Ressacada. The possible differences in local response to precipitations (spatial variation) were also investigated by comparing piezometers data in a region considered geologically uniform. The study enhances the knowledge of groundwater dynamics in the area and contributes to design the domain conceptual model, analyzing and reliably defining the drainage term— from a statistical point of view. Furthermore, this allows the application of the WTF method to estimate recharge, corrected with the addition of the drainage contributions.

3.2.2 Materials and methods

The case study is a phreatic aquifer located in the Experimental Farm area of Ressacada, owned by the Federal University of Santa Catarina (UFSC) in the southwest region of Santa Catarina Island, Florianópolis. The whole peninsula is characterized by a flat estuarine system: natural slope between 0 and 3% (excluding trenches and anthropogenic dams), and topography between -0.1 and 4.9 meters above sea level. From a geological point of view, the region is fairly uniform and presents lacustrine deposits with predominance of quartz fine sand with lenses of silt and clay (in general 5-15%), with two main features: a "Intertidal Plain" in the main central part of area and a "Tide Plain" in the boundaries near the shoreline characterized by mangrove swamps [13]. Field studies performed in the farm shown that the soils are characterized by an average total porosity of 36.8% ($\pm 3\%$), also with high values of moisture (20-25%) and saturation percentage in the vadose zone above the static level [14]. In accordance with the description, the aquifer is a

costal shallow system: mean depth of 30-40 m and water table within 0.3 to 2 m to surface, with a very low natural gradient, hydraulically connected to the Tavares River Basin (the second most important on the island) and exposed to intense periodic fluctuations of water levels. It is drained at its boundaries by the South Bay and the Tavares River and at its center by a set of artificial channels, which help to maintain the water table below the topographic surface. The groundwater flow of the study area occurs mainly towards NW-SE, and the natural discharge of aquifer flows to the channels and to the left bank of Tavares River (Fig.8).

Figura 8 - Geographical position of the Ressacada Farm (a) and location of experimental area (dashed square area). Overlapping contour lines on the aerial photo show the topography in the Experimental Area3 (b) and black vertical line indicates longitudinal section. Coordinates refer to WGS 1984 – UTM 22S. Schematic hydrogeological sketch (c).



Meteorologically, the island is defined as humid subtropical climate in the Köppen-Geiger climate classification [15]. Normal rainfall rates varies between 1200 and 1600 mm per year with higher amounts in the months of January to March, and lower between June and August. The rains have an impulsive character with high intensity and outstanding variability. In addition to this common variability, the impacts of periodic precipitation anomalies linked to Southern Oscillation (also known as El

Niño and La Niña), are more pronounced than in Argentina and Uruguay [16]. The rainfall data included in the study refer to daily accumulations (24h on Brasilia local time) and were provided by the Institute of Airspace Control (Ministry of Defense). The station is part of the METAR and WMO network (83899) and is located at Florianopolis Airport (27°40'14 "S - 48°32'50" W) less than 400 meters from the experimental areas. To consolidate this temporal rainfall series, two other datasets were also consulted: an hourly-based dataset from the INMET automatic station in Florianopolis-São José (WMO: 86958), 7 Km away from the first station, and the database of the pluviometric control of Ressacada Farm, that was supplied by the technicians of Agrarian Sciences Center (CCA).

Tabela 1 – Design details of piezometers included in the study

Name (Ref. Code)	Ground altitude AMSL [m]	Well screen depth (top/bottom) [m]	Well case diameter [cm]
PE01	2.83	2.5 / 4.5	5.08
PE02	3.20	2.5 / 4.5	5.08
PE03	3.30	2.5 / 4.5	5.08
PE06	3.10	20.0 / 30.0	10.16
PE07	2.72	11.0 / 13.0	11.43
PM01	3.32	2.5 / 4.5	5.08
PM02	3.25	2.5 / 4.5	5.08
PM04	2.50	2.5 / 4.5	5.08
PM05	3.32	2.5 / 4.5	5.08
PM06	2.88	2.0 / 4.0	5.08
PM18	2.66	1.0 / 3.0	5.08
PZ01	3.12	10.0 / 15.0	5.08
PZ02	3.19	5.0 / 10.0	5.08

For the purposes of the present work, data from 13 piezometers were used, in the time window from 2007 to 2016. All the piezometers are located in experimental area 3 in the Ressacada Farm. Tab.1 presents design information for included ones. Most of piezometers are shallow and intercept phreatic aquifer up to a depth of 4.5 m, except for PZ01, PZ02 and PE06, which reaches respectively 15, 10 and 30 m of depth. The sample intervals are discontinuous and variable in time - from 1 to 60 days in the summer closure - and per each sample location. Therefore, the influence of all phenomena with subdaily signal frequencies (like local astronomical tides, small earthquakes, and Lisse effects) was omitted and will be the object of another collateral work with continuous pressure transducers monitoring water-table levels. During the years, REMA's (Ressacada Environmental Research Group) technicians directly measured the depths of the water table with a manual phreatimeter. Subsequently, raw data were converted to absolute hydraulic head above mean sea level (zero reference was at the ground control point of Imbituba - Nation Sea Level Station) and converted to

millimeters. The justification of the unit is linked to the accuracy of the manual phreatimeter and the resolution of the values in the rainfall data series.

Starting from the hydraulic head, the following values were defined and estimated in every sampling interval: the water levels between consecutive measurements [mm], the sampling interval between these measurements [d] and the changing level rate [$\text{mm}\cdot\text{d}^{-1}$] like the ratio between differenced levels and sampling interval. Cumulative rainfall was also calculated in every sampling interval [mm], as the sum of the precipitations falling between the first day of the interval (included) until the second day of the interval (excluded), and then the uniform cumulated rainfall as ratio between cumulative rainfalls and sampling intervals [$\text{mm}\cdot\text{d}^{-1}$]. After that, the intervals with null accumulated precipitation were isolated and used to determine the only rates related to the drainage processes (defined D in the paper) where no recharge occurs. As evidenced in [12], the D value in the application of time-series approach of the WTF method simplifies, in a “scalar” term, all the water level decreases, which are concomitant, and mostly nonlinear natural processes (evaporation, transpiration, lateral drainage). Far from wanting to provide an indepth explanation of the cited phenomena, the D parameter is designed to help interpreting natural water table trends and dynamics in an area. The drainage rate, although it is a simplification, provides useful and statistically based information by interpreting the dynamics of an aquifer. It is important to highlight that the choice of working with uniform (daily) rates bypasses the large variability in the sampling intervals, allowing spatial and temporal comparisons of measurements.

The authors underline that only the rates in 2 to 7 days of sampling intervals were included in the statistical analysis of drainage term. The upper limit of 7 days was indeed the maximum interval found in the D rates but this agrees with [11] for whom intervals longer than weekly between level data could cause unacceptable underestimations of recharges with the application of WTF. On the other hand, when discarding 1 day spaced data the high amount of noise present in the close-range measurements was significant. This fact depends on the intrinsic limits of discrete precipitation data - cumulated on a daily basis - to explain long-term and continuous phenomena (infiltration and recharge). Therefore, because we could not guarantee the independence of drainage rate from a precipitation prior to the 1-day interval, it was preferred to exclude such data. To verify such a choice, the sample interval distributions (probability density function PDF and cumulative distribution function CDF) were studied for each well (resulting

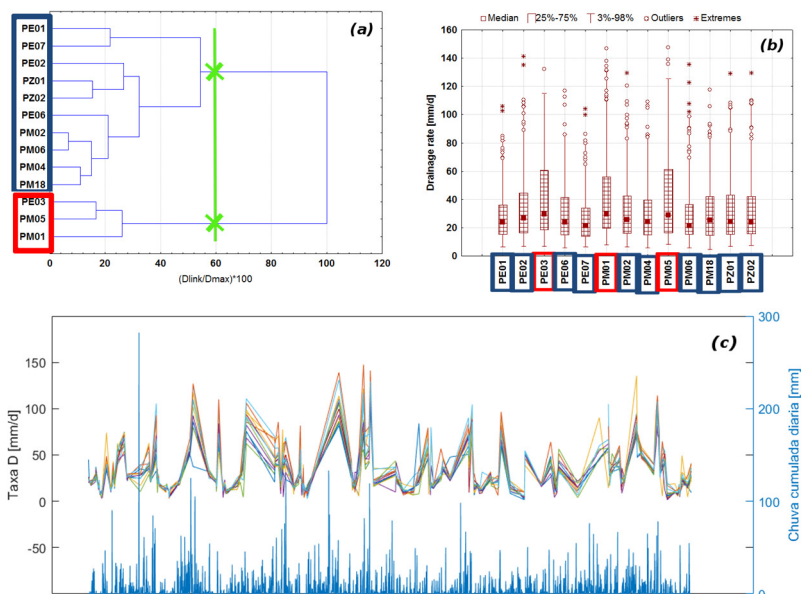
lognormal with median in 4, mean in 4.5 and mode in 3 days). The histograms showed that more than 75% of the data fell within 2 to 4 days and that, by taking out the other intervals, the dataset would have lost approximately 10% of the data: a value considered acceptable given the high number of measurements (800 per piezometer).

The methodology used for analyzing data is based on classical statistical tools: univariate and bivariate statistics were used focusing on the descriptive analysis of the raw head data collected and the drainage rates estimated. First of all position parameters (expected value, median, mode), dispersion (range, standard deviation, quartiles) and data deformation (skewness and kurtosis) were estimated. Then, extreme values and signalized outliers were studied to determine whether to include them or not in the analysis. The next step was to establish discrete histograms and theoretical distributions. Finally, variability in time and space was thoroughly investigated, analyzing the possible presence of different populations in the data. For this exercise, the characteristics of the region were linked to the statistical elaborations with an understanding of the physical part and the dynamics in action in the subsoil. The characteristics of the area, the proximity to the mangrove swamp and the reduced distance from the boundary receptors (approximately 3 km from the South Bay, 2 km from the Ribeirão Bay and less than 500 m from the Tavares River) have a direct influence on surface and groundwater drainage of the region and, therefore, in the statistical response of the aquifer to the rainfalls.

3.2.3 Results

A univariate analysis of raw data was performed to explain their distributions: the histograms of hydraulic head for every piezometer showed gaussian distributions, as opposite to drainage rates that were markedly lognormal. We remark that the commonly negative drainage was convert in a positive term using the absolute value. Following on with descriptive analysis of drainage data organized by piezometer, we found medians between 21 and 27, mean of 26.3 to 36.6 with an error of 2 and standard deviations of 18.6 to 24.8 [$\text{mm}\cdot\text{d}^{-1}$]. Therefore, for an effective and synthetic presentation of the data box-plots were used with a central mark indicating the median, the bottom and top edges of the box indicating the 25th and 75th percentiles and two whiskers reaching the 2.5% percentiles (Fig.9b).

Figura 9 – (a) Dendrogram resulting from cluster analysis of piezometers with consolidated hypothesis of clustering reported in green. (b) Box plots of piezometers D rates: group1 in blue and group2 in red. (c) Comparative line to bar plot depicting decreasing rates within the piezometers (lines) and daily accumulated rain in the area (bars).



At these initial stages all the series were consolidated, analyzing suspect outliers and extreme values to fix them. The congruence was checked by the temporal compliance between high decrease values and rainfall events (Fig.9c). A clustering analysis was performed with the log transformed drainage series and consecutively, with CDFs, using both the complete linkage and the Ward's method (as in Fig.9a). The aim was to identify possibly different population of response of the water level. All the methods converged to similar cluster results, indicating the reliability of the procedure. By having two clustering hypothesis, an analysis of variance (ANOVA) was applied to statistically consolidate the assumptions of two groups instead of three. Then, a physical-based connection between the groups and the variation of hydraulic conductivity was sought (a slug test campaign was performed on all 13 piezometers and interpreted with Winslug® software in December 2016), but it was not possible to consolidate this relationship. Although Group 2 ($6.16E-04 \text{ cm}\cdot\text{s}^{-1}$) has a lower average conductivity than Group 1 ($3.37E-$

03 cm·s⁻¹), Group 1 also includes low conductivity piezometers (e.g. PE07). The conductivity estimation was performed with both Bower-Rice and Hvorslev method, choosing the first one for reported values of hydraulic conductivities.

On the other hand, such analysis underlined that clustering could be related to the altitude of the ground (topography). Therefore, drainage rate series can be aggregated based on the well position in the groundwater flow field and, in particular, by distance to surface receptors that drain the area. In accordance with this idea, Group 1 includes all the piezometers downstream along the main flow direction and Group 2 includes just three “high” piezometers upgradient in the area (as shown in Fig.8). In this simplified description, it is important to highlight the presence of a transition group of piezometers in the middle area, between the high area and down area (e.g. PE02 and PM02).

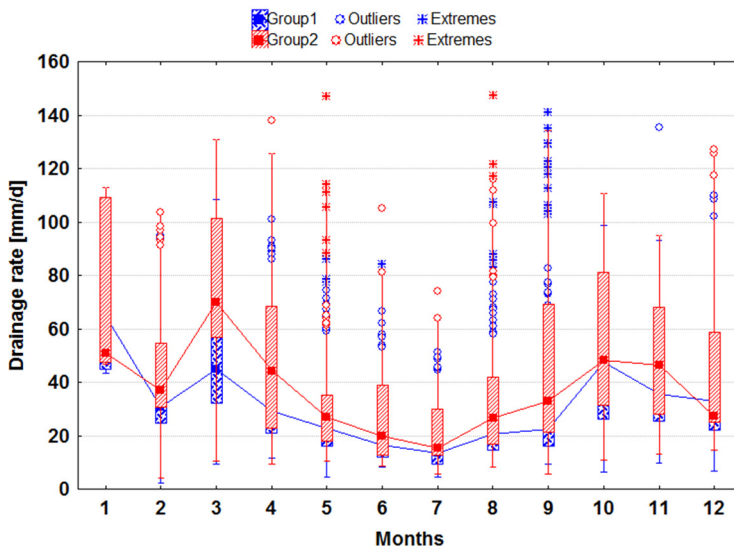
Tabela 2 - Descriptive statistics

	Raw Levels AMSL [mm]	D (Group1) [mm·d ⁻¹]	D (Group2) [mm·d ⁻¹]
Cases (N)	10904	1699	546
Mean	1690.5± 10.3	31 ± 0.6	41.5 ± 1.3
C.I. Mean (95%)	1673.5 / 1707.5	30.1 / 31.9	39.3 / 43.7
Median	1676.5	24	29.5
Stand.Dev. (SD)	279.7	22.9	31.4
C.I. SD (95%)	266.1 / 294.7	22.2 / 23.7	29.7 / 33.4
Mín	865.0	1.7	2.7
Máx	2905.0	141.0	147.5
Quartil (25%)	1505.5	15.4	18
Quartil (75%)	1873.2	39.7	59.3
Skewness	0.2 ± 0.1	1.7 ± 0.1	1.2 ± 0.1
Kurtosis	-0.1 ± 0.2	2.9 ± 0.1	0.7 ± 0.2

For the subsequent statistical analysis, these transition piezometers, with intermediary features, were aggregated in the first group (Fig. 9a). Nevertheless, we have to point out that in some cases their behavior was closer to the piezometers of Group 2. For example, their good compliance in the spatial analysis of basal and initial drainage will be analyzed in Fig. 15. This ambiguity can be explained by the proximity between the two groups and the mild topography of the experimental area: elevation distance between higher and lower piezometer is approximately 1 m. By translating these clustering results into a hydrodynamic conceptual model, we could say that the natural flow is driven by rain infiltration (relevant direction NW-SE), which is stored in the higher central area of the Farm, and is regulated by the hydraulic head of the downstream water bodies or receptors: the farthest piezometers from the receptor bodies also appear the most sensitive with

rainfall showing larger fluctuations and faster rates of decrease. The broader ranges in the D-rates (Tab.2) and the greater depths reached by the groundwater in Group 2 seem to confirm this hypothesis.

Figure 10 - Box plot of drainage-by-month to study the seasonality. Note the large amount of extreme values and outliers also in months with less average rains



In the next stage, drainage trends in the two groups were studied by seasonality and as a function of water table conditions or time elapsed from the last precipitation.

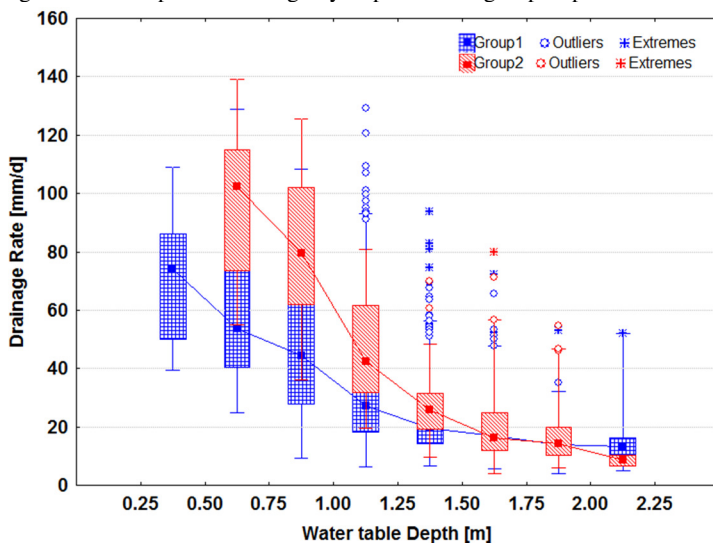
$$\min_x \|F(b, t) - D\|_2^2 = \min_x \sum_i (F(b, t_i) - D_i)^2 \quad (13)$$

Fig.10 shows drainage rates of the groups of piezometers organized per month. This graph shows no temporal or seasonal trend: the spikes in the months of January, March, October and November (months of intense rains and in average much higher decrease rates) do not prevent the presence of extreme values in other months, in conjunction with isolated rains.

Fig.11 presents drainage rates organized by depth to water table and shows, in the case of water level up to 1 meter deep, a drainage 4 or 5 times greater respect to basic. This seems like a head-dependent relationship, as would be expected by Darcy's Law. In addition, decrease

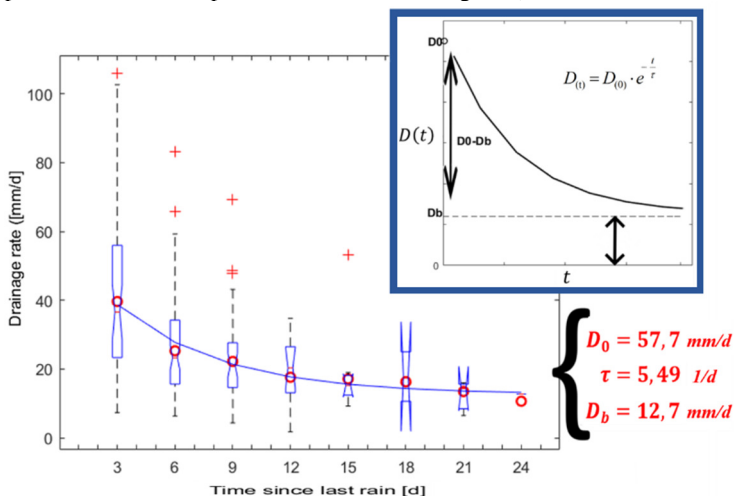
rates seem to reach a kind of asymptote value, similar for both groups, that represents a low-head or “basal” drainage in the area, further away from the last precipitation. This fact suggests a quasi-steady behavior of drainage driven by surface receptors level, which rapidly passes to a precipitation-driven mechanism regulated by the intense increase in aquifer level during rainfall events. By increasing the hydraulic head, a flow with a larger hydraulic gradient and consistent vertical components is activated. Such enhanced decrease rate exhausts in average within 5 days, coming back to the low-head rate. It worth stressing that such decrease rate would be theoretically zero with very long dry periods, having de facto water-table head in equilibrium with surface receptors level. However, in a ten-year period of water level monitoring at the site, a longest period between two precipitation events lasted 24 days and, this idea of low-head drainage refers to our significant time-scale.

Figure 11 - Box plot of drainage-by-depth in each group of piezometers.



Finally, Fig.12 shows drainage box plots organized by time since the last rain. It was observed that the decrease rates had on average higher values soon after the precipitations ended. This fact indicated the possibility of designing an exponential model to explain drainage term against time by fitting a curve above the central position of every box (as they were lognormal distributions, the geometric means was used as central position).

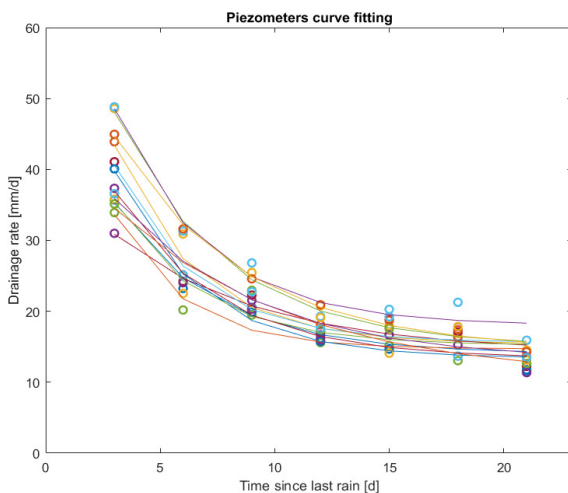
Figura 12 - Box plot of D rates organized by time since last rain; the exponential model built on this formulation and best fit coefficients for whole D dataset (all piezometers of the experimental area studied together).



Through an optimization process, for the whole area and for every piezometer were defined: a basal drainage rate (D_b) [$\text{mm}\cdot\text{d}^{-1}$] as the residual drainage when the rainfall perturbation was shrunk in a monthly time-scale, an Y-intercept of the curve which represents initial rate of decrease after the precipitation event (D_0) [$\text{mm}\cdot\text{d}^{-1}$] and a decay coefficient associated with the perturbation depletion time (τ) [d^{-1}]. Two algorithms were tested to optimize the fitting process: one solving the nonlinear data-fitting problems in least-squares sense (Eq.13), and the other, a robust bisquare fitting that minimizes a weighted sum of squares, where the weight is given depending on how far the point is from the fitted line. The algorithm chosen for fitting our data was the first one, because every point in the data was the central position of distribution already. For this reason we chose a curve that fits the bulk of the data using the usual least-squares approach, without having to minimize the effect of outliers (common in broad dataset but secondary in this case). Therefore, for every piezometer, were found in Eq.13 a vector b of exponential function coefficients (D_0 , τ^{-1} and D_b) that solve the nonlinear fitting problem (Fig. 13), given input data t (chosen time steps) and the observed output D (geometric mean of drainage rates at each step). In the next part of the discussion, we will emphasize the spatial variability of these drainage coefficients.

Regarding the relation between initial decrease rates (D_0) and elevation of the ground, Fig. 14 confirms that the groundwater flows from the “high” zone with more intense decrease rates to “low” area with a less sharp decrease profile. In this sense, PM04 and PM18 represent an exception since follow an inverse trend; these piezometers, in fact, are located near the final receptors (anthropic drain), in the ideal downstream closure sections of groundwater flow. Based on the results, it was observed that the relation of D_0 against elevation loses intensity on the lower part of the area, probably due to the proximity between the plain and the morass area near the river. In addition, Fig. 14 shows a sort of aggregation trend by piezometer position, partially corroborating cluster analysis. Regarding this matter, it should be noted the aggregation of PM02 and PE02 to the light green group, due to the proximity between the piezometers.

Figure 13 - Piezometers best fitting curves on geometric mean values at each time step (found applying the exponential model built previously)



At this step, we were able to design a spatial analysis of the three-coefficient vector b , which was described in Fig. 15. The results confirmed once again the cluster analysis indications and the assumption of an altitude-based cluster. Both contour plots (D_b and D_0 in Fig. 15), showed higher values of drainage near PM1, PE03 and PE02, that was the highest area in accordance with elevation contours (Fig. 14). Nevertheless, the ranges of drainage were consistently different in the two plots: D_0 showed a wide range of values while D_b values were similar in the whole area. In

addition, it should be noted that D_b values for piezometers were close to the low-head drainage for whole area ($12.7 \text{ mm}\cdot\text{d}^{-1}$) and to the limit values found with drainage-by-depth box plots (Fig. 11).

Figura 14 - Altitude contour plot (a) of 200x200m area with the origin in 743215E-6935653N (Coordinates was in GCS WGS 1984 – UTM 22S). Scatter plot of D_0 against the altitude of point (b) confirms a clustering trend by position: higher piezometers (light green), piezometers in the lower plain (light blue), low but also deep piezometers (purple).

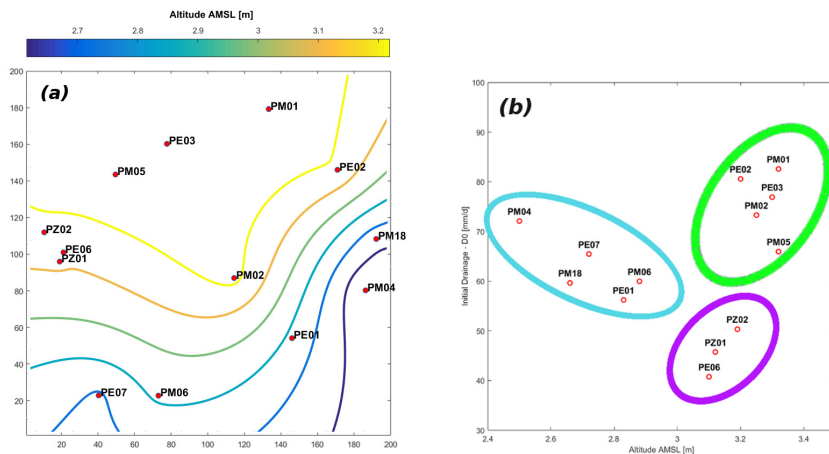
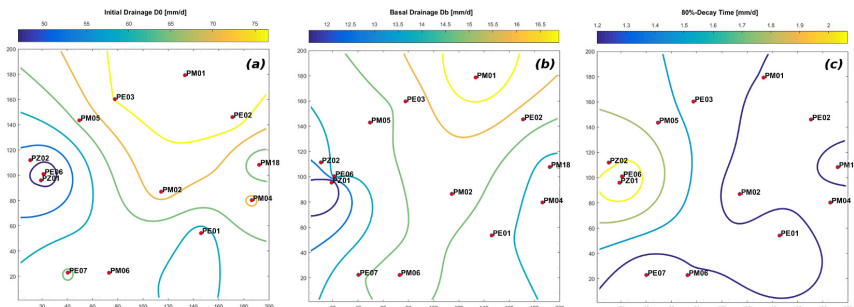


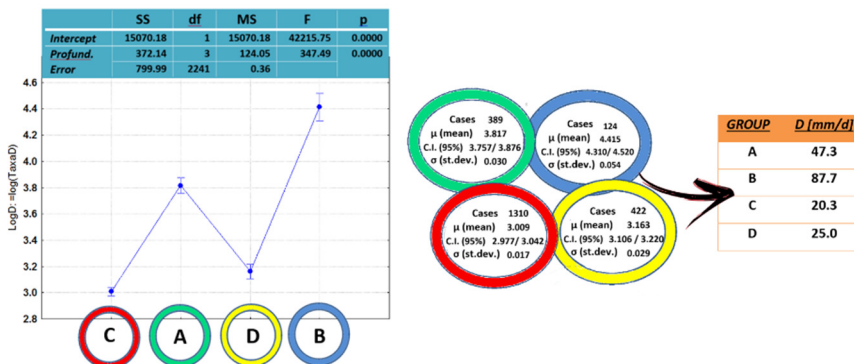
Figura 15 - Contour line maps of spatial variation of coefficient: D_0 (a), D_b (b) and 80% decay perturbation time (c). The 200x200m grid area has the origin in 743215E-6935653N (Coordinates was in GCS WGS 1984 – UTM 22S).



For this reason, D_b can be considered approximately constant in the area and just linked with receptors hydraulic head. On the other hand, contour lines of 80% decay time showed a similar behavior between the

most of piezometers with an approximately constant value of 1 to 1.2 days to attenuate 80% of initial drainage perturbation. An exception of this line of evidence was represented by “deep” piezometers (PE06, PZ01, and PZ02) that showed an attenuation time more than twice the others. About this fact, three hypothesis could be raised: 1) the influence of a sharp variation in the geology due to a less conductive layer in that area; 2) the presence of a multi-layered aquifer system, only intercepted and highlighted by deep piezometers; 3) a leakage from the upgradient anthropic drain that recharges and sustains the local flow during the drainage phase. Spatial distribution of D_0 and D_b in Fig.15 seem to corroborate one of these assumptions.

Figura 16 - Results of ANOVA and inference of centered statistically-based typical values for drainage in the Ressacada aquifer



For each group of piezometers, the study of the spatial and temporal variability in the drainage rates suggested the presence of two data populations in terms of time-elapsd since the last rainfall (depending by hydraulic head). In order to consolidate this hypothesis, another ANOVA was applied to the four cases identified, defining typical values of drainage for each condition: "Case A" was Group1 of piezometers when the depth of the water table was up to 1 m, "Case B" was Group2 in the same condition, "Case C" was the Group1 with water head below 1 m depth and "Case D" was Group2 in this same condition. In the Fig. 16 cases A and B, which represent a high water head condition, shown a considerable distance between the means, which was much more consistent with respect to “low” water table condition (cases C and D). This fact copper-fastened what was highlighted in the whole analysis: the presence of a similar low-head decrease rate (D_b) for all piezometers and

conditions, which represent a site-specific drainage regulated by the receptors water level. The final step defined a reference value of drainage in each of four conditions, estimated from the median values of anti-transformed distribution (orange table in Fig. 16).

3.2.4 Conclusion

A main result of the study was to build an exponential model for the drainage rates in the timeframe, highlighting typical mean values of low-head drainage and initial rate of decrease after the rain event for the whole area (Fig.12). This approach made the big difference between these two values evident. A subsequent spatial analysis of the coefficients allowed the investigation of the relations between the piezometers. Due to the high variability in time and space found for the drainage term in the Ressacada Farm, differentiated values were assumed. These values represent specific aquifer conditions related with the time elapsed since the last rain or with hydraulic head of water table. In making this choice the authors diverged from a single drainage option of [12].

The statistically-based approach of the study allowed the consolidation of two groups of piezometers diverging for elevation and behavior. These findings, in addition of the two aforementioned aquifer conditions, determined four typical values for the drainage term in the Ressacada Farm. Mean values were defined as a function of the position of the piezometers and the aquifer hydraulic head, and represent specific water table conditions. In the "quasi-steady" conditions (low hydraulic heads or far from the rains), drainage values agreed with other studies in similar coastal areas, confirming the validity of the methodology. On the other hand, the underlined high values of cases A and B (high water-table head condition) emphasized the importance of a reliable estimation of the drainage term in the periods of intense rains, for an accurate application of the WTF method in such subtropical area.

Through the aforementioned steps, a comprehensive study of water-table decrease rates in the Ressacada was built, achieving the aim of the paper. Therefore, depending on the accuracy of the recharge estimation we have to achieve, it is now possible to use in the WTF method one of several drainage values found within the study (single mean values for the whole area, groups values or piezometers values).

Acknowledgments

This work is part of a research and development project in partnership UFSC/FEESC/Petróleo Brasileiro (Petrobras): Additions and improvements in the SCBR (Risk-Based Corrective

Solution) mathematical model to support environmental management of Oil&Gas contaminated areas (Contract number: 0050.0096599.15.9).

References

- [1] D. C. Neto, H. K. Chang, and M. T. van Genuchten, "A Mathematical View of Water Table Fluctuations in a Shallow Aquifer in Brazil," *Groundwater*, vol. 54, no. 1, pp. 82–91, 2016.
- [2] J. X. Mao, P. Enot, D. a. Barry, L. Li, a. Binley, and D. S. Jeng, "Tidal influence on behaviour of a coastal aquifer adjacent to a low-relief estuary," *J. Hydrol.*, vol. 327, no. 1–2, pp. 110–127, 2006.
- [3] B. Ataie-Ashtiani, R. E. Volker, and D. A. Lockington, "Tidal effects on groundwater dynamics in unconfined aquifers," *Hydrol. Process.*, vol. 15, no. 4, pp. 655–669, 2001.
- [4] C. E. Braga, I. D. C. Lage, G. Cardoso, and A. Ferreira Damasceno, "O Comportamento Hidroquímico E Hidrodinâmico De Aquífero Sob Influência Do Efeito-Maré," in *XII Congresso Brasileiro de Águas Subterrâneas*, 2002, pp. 1–12.
- [5] I. de C. Lage and C. E. Braga, "Caracterização geológica e hidrogeológica de uma área de manguezal em indústria petroquímica," in *I Simpósio de Hidrogeologia do Sudeste*, 2003, pp. 205–216.
- [6] D. L. Lorenz and G. N. Delin, "A regression model to estimate regional ground water recharge," *Groundwater*, vol. 45, no. 2, pp. 196–208, 2007.
- [7] M. Masetti, D. Pedretti, A. Sorichetta, S. Stevenazzi, and F. Bacci, "Impact of a Storm-Water Infiltration Basin on the Recharge Dynamics in a Highly Permeable Aquifer," *Water Resour. Manag.*, vol. 30, no. 1, pp. 149–165, 2016.
- [8] S. R. Saghravani, I. Yusoff, W. Z. Wan Md Tahir, and Z. Othman, "Comparison of water table fluctuation and chloride mass balance methods for recharge estimation in a tropical rainforest climate: a case study from Kelantan River catchment, Malaysia," *Environ. Earth Sci.*, vol. 73, no. 8, pp. 4419–4428, 2015.
- [9] B. R. Scanlon, R. W. Healy, and P. G. Cook, "Choosing appropriate techniques for quantifying groundwater recharge," *Hydrogeol. J.*, vol. 10, no. 1, pp. 18–39, 2002.
- [10] R. W. Healy and P. G. Cook, "Using groundwater levels to estimate recharge," *Hydrogeol. J.*, vol. 10, no. 1, pp. 91–109, 2002.
- [11] G. N. Delin, R. W. Healy, D. L. Lorenz, and J. R. Nimmo, "Comparison of local- to regional-scale estimates of ground-water recharge in Minnesota, USA," *J. Hydrol.*, vol. 334, no. 1–2, pp. 231–249, 2007.
- [12] R. S. Crosbie, P. Binning, and J. D. Kalma, "A time series approach to inferring groundwater recharge using the water table fluctuation method," *Water Resour. Res.*, vol. 41, no. 1, pp. 1–9, 2005.
- [13] N. O. Horn Filho, A. D. Schmidt, C. Benedet, J. Neves, L. H. F. Pimenta, M. Paquette, and R. Alencar, "Estudo Geológico dos Depósitos Clásticos Quaternários Superficiais da Planície Costeira de Santa Catarina, Brasil," *Gravel*, pp. 41–107, 2014.
- [14] I. de C. Lage, "Avaliação de metodologia para determinação da permeabilidade em meio porosos: Fazenda Ressacada." M.S. thesis, Dept. Geosciences, UFRJ, Rio de Janeiro, Brazil, 2005.
- [15] M. C. Peel, B. L. Finlayson, and T. A. McMahon, "Updated world map of the Köppen-Geiger climate classification," *Hydrol. Earth Syst. Sci.*, vol. 15, no. 3, pp. 259–263, 2006.
- [16] A. M. Grimm, S. E. T. Ferraz, and J. Gomes, "Precipitation Anomalies in Southern Brazil Associated with El Niño and La Niña Events," *J. Clim.*, vol. 11, no. 11, pp. 2863–2880, 1998.

3.3 RECHARGE ESTIMATION FROM DISCRETE WATER-TABLE DATASETS IN A COASTAL SHALLOW AQUIFER IN A HUMID SUBTROPICAL CLIMATE

Fabrizio Rama^{(1)*}, Konrad Miotlinski⁽¹⁾, Davide Franco⁽²⁾,
and Henry X. Corseuil⁽¹⁾

* Corresponding author

(1) Núcleo Ressacada de pesquisa em meio ambiente (REMA) – CTC - UFSC

(2) Laboratório de Hidráulica Marítima (LAHIMAR) – ENS - UFSC

Manuscript received October 10, 2017; accepted January 30, 2018;
published online March 5, 2018; print September 26, 2018

Referência:

Rama, F., Miotlinski, K., Franco, D., Corseuil, H.X., Recharge estimation from discrete water-table datasets in a coastal shallow aquifer in a humid subtropical climate. *Hydrogeology Journal*, 2018, 26 (6), 1887–1902. <https://doi.org/10.1007/s10040-018-1742-1>

Nota ao leitor:

Ajustes de texto e nas figuras foram realizadas em relação ao artigo original para aumentar a precisão da escrita científica e por razões de formato da dissertação sem, no entanto, alterar conteúdo e elementos utilizados nas análises.

Resumo

No texto propõe-se um método para estimar as taxas de recarga por infiltração nos aquíferos não confinados com carga do lençol freático altamente variável. A abordagem desenvolvida pelo autor baseia-se no método do water-table fluctuation (WTF) aplicado às séries temporais de dados, e utiliza medições descontínuas do nível hidráulico subterrâneo. Outros métodos similares requerem dados contínuos com frequências de aquisição elevadas, o que os torna inaplicáveis na ausência de uma rede de monitoramento automático do lençol. A metodologia é aplicada aos dados da Fazenda experimental da Ressacada (SC-Brasil), em um aquífero costeiro raso de clima subtropical úmido, com variações diárias de nível freático de até 1 m após um evento de precipitação. As series de dados (entre 2007 e 2016) representam 10 anos de monitoramento do lençol freático, medidos manualmente a intervalos irregulares (entre 1 e 60 dias) nos 13 piezômetros da Fazenda, preventivamente consolidadas e filtradas. O estudo da recarga e das flutuações do lençol freático visa ter um entendimento dos principais fatores

hidráulicos que afetam no tempo o escoamento subsuperficial na região. Portanto, o efeito das flutuações das marés sobre os níveis das águas subterrâneas é também analisado no capítulo, por meio de um construtor de componentes harmônicos desenvolvido em Matlab, excluindo uma relevante contribuição deste fator nas áreas experimentais. O termo de descarga (D), variável no tempo, foi estimado a partir do estudo do capítulo anterior, e incluído no cálculo da recarga, para amenizar as incertezas da estimativa relacionadas às séries de dados não contínuos de carga hidráulica. A metodologia de cálculo proposta é verificada por meio da comparação dos valores de recargas estimados desta forma e os valores obtidos com séries contínuas de dados, em um intervalo temporal de 51 dias. No texto mostra-se um bom acordo entre as duas abordagens para intervalos amostrais de até 15 dias, apresentando diferenças limitadas nas taxas de recarga (recharge ratios) estimadas. Finalmente, as taxas de recarga estimadas são incorporadas a um modelo numérico de fluxo 2D no estado transiente que descreve um corte longitudinal do aquífero passante pelos piezômetros PE03 e PM04, gerando curvas de nível do lençol com boa concordância entre simulações e dados de campo em 10 anos. Portanto, a abordagem descrita amplia a aplicabilidade do WTF na estimativa da recarga para conjuntos descontínuos de dados com intervalos amostrais variáveis, ajuda na definição de valores de recargas característicos no aquífero da Ressacada baseados sobre robustos dados de campo, e exclui o efeito das oscilações periódicas de maré na variação do lençol freático nas áreas experimentais.

Abstract

A time-series approach to the estimation of recharge rate in unconfined aquifers of highly variable water level is proposed. The approach, which is based on the water-table fluctuation method (WTF), utilizes discrete water-level measurements. Other similar techniques require continuous measurements, which makes them impossible to apply in cases where no data from automatic loggers are available. The procedure is deployed at the Ressacada Farm site, southern Brazil, on a coastal shallow aquifer located in a humid subtropical climate where diurnal water-level variations of up to 1 m can follow a precipitation event. The effect of tidal fluctuations on the groundwater levels is analyzed using a harmonic component builder, while a time-variable drainage term is evaluated through an independent analysis and included in the assessment. The estimated recharge values are compared with those obtained from the continuous measurements showing a good agreement with the approaches for discrete dataset intervals of up to 15 days. Subsequently, the estimated recharge rates are incorporated into a transient groundwater-flow model and the water levels are compared showing a good match. Henceforth, the approach extends the applicability of WTF to non-continuous water-level datasets in groundwater recharge studies.

Keywords: Water-table fluctuation method, Tidal influence, Groundwater recharge/water budget, Numerical modelling, Brazil

Highlights:

- An alternative approach to the WTF method is developed to estimate recharge from non-continuous water-table level datasets
- A variable drainage term D (decreasing with time from last rain) is introduced in the methodology to mitigate uncertainty of sparse series
- A temporally variable recharge in a quite homogeneous coastal aquifer was underlined (43% in average, varying from 36 to 52% on a monthly basis)
- Higher effectiveness of recharge in the dry months with less accumulated rainfall was highlighted
- Effect of tidal fluctuations on groundwater levels in the Ressacada Farm is evaluate negligible

3.3.1 Introduction

Accurate estimation of groundwater recharge is of relevance for different applications related to the assessment of human activity and hydrogeological characterization. It may be critical information to manage changes in groundwater systems effectively (Xiao et al. 2016) and to safeguard scarce resources in arid zones (de Vries and Simmers 2002). Proper estimation of recharge and its variability in time and space is shown to be crucial for both the agricultural sector (Bohlke 2002) and the assessment of fate and transport of solute pollutants (Kim et al. 2000), since it can induce temporal fluctuations in the flow field. Spatial and temporal variability in recharge, as well as preferential flow paths, are key components for assessing aquifer vulnerability to a specific compound (Scanlon et al. 2002). Many investigators deal with the relationship between recharge estimation and numerical groundwater models (Colombani et al. 2016; Sanford 2002), focusing on the main role of vadose flow for simulating recharge (Cao et al. 2016; Heilweil et al. 2015). For a humid climate, Hunt et al. (2008) showed similar timing of recharge but an appreciably different water budget when considering thin unsaturated zones in the simulation. The literature reports a multitude of methods being developed and commonly used to infer recharge (Healy 2010). Recharge is part of the overall infiltration mechanism, when the wetting front reaches the water table, causing its rise. Precipitation is the main contributor to the process, and it is an important factor in the recharge estimation (Shi et al. 2015). Theoretically, in a uniform porous medium with a shallow water table, it can be assumed that a fraction of total precipitation in a time step contributes to the aquifer recharge (Park

and Parker 2008), resulting in a prompt rise of water level in shallow unconfined aquifers (Hilberts et al. 2007). The deeper the water table, the greater the amount of rainfall water held in the unsaturated zone, which in consequence leads to a reduction of the precipitation fraction reaching the water table and to a time lag between the acting force and the water-table rise. Realistically, estimation of groundwater recharge is an iterative process, involving multiple approaches with progressive aquifer-response data collection and resource evaluation (de Vries and Simmers 2002). For this reason, despite this abundance of solutions, assessing the accuracy of any applied method (Healy and Cook 2002) and choosing the most appropriate for given field conditions (Scanlon et al. 2002) is still extremely difficult.

The water-table fluctuation method (WTF) is a widely used method (Masetti et al. 2016; Saghravani et al. 2015) which requires the knowledge of groundwater levels to estimate recharge. Usually applied in an event-basis framework (Delin et al. 2007; Lorenz and Delin 2007), WTF is a simple method applied for unconfined aquifers with a shallow water table and sharp variation in water level. There are three principal requirements for the use of WTF (Healy 2010; Healy and Cook 2002): (1) the applied time step must be as short as possible, (2) an accurate value of specific yield must be used (Acharya et al. 2012; Nachabe 2002), and (3) other possible causes of groundwater head fluctuations not related to recharge must be isolated from the dataset (Neto et al. 2015). In order to estimate recharge useful for aquifer water-balance calculations, a time series approach for WTF has been developed by Crosbie et al. (2005) showing a reliable and well-founded methodology. Nevertheless, its application for continuous datasets presents two major limitations: (1) the empirical estimation for groundwater drainage by a linear function of depth may not properly explain the spatial and temporal variability of the flow field (Cuthbert 2010), and (2) the model requires a continuous and homogeneous level dataset with sufficiently high temporal resolution, at least with hourly records.

Although hydrogeologists constantly deal with a lack of data, there is a tendency to neglect historical databases with incomplete and disjointed information. Nevertheless, discrete records of water-table depth can bring some useful information if they are treated using correct methodologies. This paper extends the application of the time series approach (Crosbie et al. 2005) for discrete hydraulic head datasets. To address this issue, a variable drainage term (D term) may be introduced as an exponential function of the time elapsed from the last rain event, explaining water head reliance of discharge in the time domain. To verify

the whole procedure, recharge estimates from a couple of piezometers are compared with those obtained from continuously monitored water-table series and integrated in a transient 2D vertical flow model. In addition, a harmonic component analysis of high-frequency residual signals is included in the analysis to assess the astronomical tide influence on the groundwater levels in the area, excluding other processes responsible for water-table rises. This contribution aims to clarify the uncertainties in recharge estimates with WTF from discrete records and explains how to extract useful groundwater information from irregular datasets.

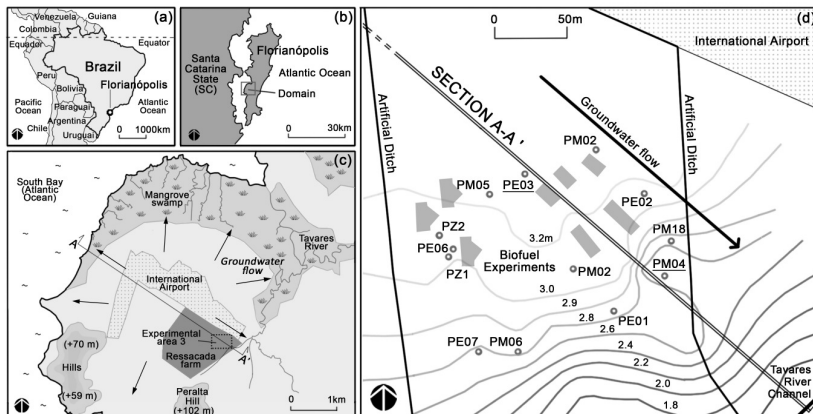
3.3.2 Site description

An unconfined aquifer at the Ressacada Farm experimental site, in the southwestern part of Santa Catarina Island, southern Brazil, is studied (Fig. 17a and 17b). The aquifer, 30-40 m thick, is fairly homogeneous consisting of lacustrine deposits with a predominance of fine quartz sand with lenses of silt and clay (Lage 2005). The total area is 20 km² and the aquifer is laterally adjacent to (1) an Atlantic channel called South Bay to the north and west (Garbossa et al. 2014), (2) the slow curvy estuarine system of the Tavares River surrounded by mangrove swamps to the east, and (3) a compact granite complex of hills to the south (Fig. 17c). The groundwater flow is a result of a very low natural gradient driven by precipitation recharge, and is radial diverging from the domain center to the boundaries.

The ground surface is flat (up to 5 m in elevation) and the average depth to water level varies from 0.3 to 2.0 m. The aquifer constitutes a u-shaped groundwater system (Huang et al. 2015; Mao et al. 2006) which is enclosed on three sides by natural surface water bodies subjected to boundary tidal fluctuations, carried by tidal channels and swamp dynamics. A dense network of artificial trenches in the plain drains the top of the shallow aquifer maintaining the water level below the topographic surface.

From a meteorological point of view, the region is located in the humid subtropical climate zone under the Köppen-Geiger classification (Peel et al. 2006) at the contact of the Atlantic moist tropical and Antarctic polar air masses. The interactions and alternations between the fronts cause rainfall events with high intensity and large variability (Grimm et al. 1998). Precipitation is predominantly in the summer season, and the monitored annual rainfalls varied from 1100 to 2700 mm between years 2007 and 2017. The large variability of rainfall results in large and quick fluctuations of the groundwater levels.

Figura 17 – Location of study area: (a) Map of Brazil; (b) Map of Santa Catarina Island; (c) Study domain at Ressacada Farm Experimental Site, with boundary conditions. Section A-A' indicates the domain transect; (d) Detailed map of Experimental Area No3, depicting: piezometer positions and their names (points), topography with elevation in meters above mean sea level (lines and numbers), and natural attenuation experimental areas (grey areas).



The majority of water level measurements come from the Experimental Area 3 (Fig. 17d), which was historically used to conduct biofuel remediation experiments (Corseuil et al. 2015; Corseuil et al. 2011a). Average hydraulic conductivity values are in the range of 10-3 cm/s. Mean total porosity, measured by gas permoporosimetry, is 0.38 ± 0.01 ($n=31$). The effective porosity (η_e) of the saturated soil is 0.2 (Corseuil et al. 2011b) while the moisture content of the unsaturated zone profile varies from 20 to 25% (Lage 2005). In this part of the aquifer the flow field occurs along section A-A' to the SE, toward the Tavares river (Kobiyama et al. 2011), and is affected by recurring variations in recharge intensity due to: the shallow depth of the water table; the porous highly conductive nature of the deposits; the intermittent, intense and spatially-variable nature of rainfall; and the proximity to boundary receptors. Experimental Area 3 is approximately 3 km from South Bay, 2 km from Ribeirão Bay, and less than 500 m from the Tavares River. Nevertheless, the area is located far away from intensive anthropogenic activities, with no pumping, and steep hydraulic gradients. For these reasons, the aquifer satisfies the conditions to apply the water-table fluctuation method (WTF) for recharge estimations (Healy and Cook 2002) which are: (1) lack of confinement with sharp temporal water level changes; (2) large number

of piezometers to observe water levels; (3) no pumping and no anthropogenic activities that may influence the natural groundwater level over short time scales; (4) a short time lag, and intense and variable rainfall events.

3.3.3 Materials and methods

3.3.3.1 Methodology

A discrete dataset of water levels from 13 piezometers measured from 2007 to 2016 is used in the study (Tab.3). Most of the wells in the area are shallow piezometers that intercept the aquifer up to a depth of 4.5 m, with the exception of PZ01, PZ02 and PE06, which reach 15, 10 and 30 m in depth, respectively. Water-table depths were monitored with a manual phreatimeter at variable recording intervals (1-60 days). In addition, in a shorter time window (from 8 February 2017 to 31 March 2017), PE03 and PM04 are equipped with automatic water-level loggers, recording every 15 min. Both wells are supplied with a vented pressure transducer of a range of 3.5 m with an accuracy of $\pm 0.1\%$. Therefore, the instruments automatically correct the measurements by pressure, to be vented, and by temperature deviation, with a linearizing algorithm of two known points. Hence, the resulting total error is in the order of ± 2 mm.

Tabela 3 - Piezometers and their design details (piezometers used as observation point in 2D model are in italic)

Name (Ref. Code)	Ground elevation ^a , MSL ^b [m]	Well screen depth (top/bottom) [m]	Well screen elevation ^c , MSL (top/bottom) [m]	Well case diameter [cm]
PE01	2.83	2.5 / 4.5	0.3 / -1.7	5.08
PE02	3.20	2.5 / 4.5	0.7 / -1.3	5.08
<i>PE03</i>	3.30	2.5 / 4.5	0.8 / -1.2	5.08
PE06	3.10	20.0 / 30.0	-16.9 / -26.9	10.16
PE07	2.72	11.0 / 13.0	-8.3 / -10.3	11.43
PM01	3.32	2.5 / 4.5	0.8 / -1.2	5.08
PM02	3.24	2.5 / 4.5	0.7 / -1.3	5.08
<i>PM04</i>	2.50	2.5 / 4.5	0.0 / -2.0	5.08
PM05	3.32	2.5 / 4.5	0.8 / -1.2	5.08
PM06	2.88	2.0 / 4.0	0.9 / -1.1	5.08
PM18	2.66	1.0 / 3.0	1.7 / -0.3	5.08
PZ01	3.12	10.0 / 15.0	-6.9 / -11.9	5.08
PZ02	3.19	5.0 / 10.0	-1.8 / -6.8	5.08

^a Ground elevation: values obtained with a Geodetic total station (distance accuracy of 5mm and angular de 2")

^b MSL: elevation above Mean Sea Level (zero reference at the ground control point of Imbituba Sea Level Station)

^c Well screen elevation: equal to Ground elevation minus Well screen depth

The water-table fluctuation method (WTF) is based on the premise that water-table rises are due solely to vertical rainfall infiltration (Healy and Cook 2002). Therefore, in a time step Δt , a total amount of recharge R [mm] is mathematically defined as:

$$R = S_y \times \frac{\Delta h}{\Delta t} \quad (14)$$

where S_y is the specific yield [% by volume], and Δh is the maximum registered water level change [mm] in a time step Δt . A recharge ratio RR [%] is:

$$RR = \frac{R}{P} \quad (15)$$

where P is the total amount of rainfall [mm] in the same time step Δt . The P represents total precipitation including events not contributing to water level rises, whereas R refers to the sum of all level rises in the same period. In accordance with Eqn (14), all the components in the groundwater budget that are not storage (like evapotranspiration, net subsurface flow or baseflow) are supposed null during the recharge process. The time lag between the arrival of the infiltrated water and its redistribution to all the components is place-specific and determines the reasonable time step to be applied in the method. Therefore, over cumulative time intervals (months or years), all the contributions that are not accounted in the recharge term, like evapotranspiration losses and surface runoff during the precipitation, are lumped in $(1-RR)$, with RR defined in Eqn (15).

Using the WTF, recharge values are inferred in variable time steps along a time window of 10 years. A variable drainage rate and variations of S_y with depth are included in the evaluation. The time series approach by Crosbie et al. (2005) is modified to handle discrete datasets with irregularly spaced data. This is to handle heterogeneity of datasets which made it difficult to directly compare one-by-one data using statistical methods available in the time-series analysis (Neto et al. 2015).

The paper follows three main stages. In the first part, the recharge values are estimated on the basis of water level fluctuations using a sparse, discontinuous and time-variable dataset with time intervals varying from 1 to 60 days. In the second part, the estimates are compared with the continuous time-series approach (Crosbie et al. 2005). Finally, in order to verify the assumptions, test the conceptual model and calculate

water balances, a numerical model was built with a finite element method (FEM), the FEFLOW code (Diersch 2014).

3.3.3.1.1 Discrete-series approach

Discrete and irregularly spaced records of water-table levels are used to automate the estimation of monthly-accumulated recharge. In accordance with the work of Shi et al. (2015), which indicates precipitation as the most important factor controlling the daily and monthly WTF recharge estimates, the following conditions are applied in the approach:

$$R_{\Delta t_i} = (\Delta h_i + D\Delta t_i) \times S_{ya} \quad \xrightarrow{\text{if}} \quad \sum_{\Delta t_i} P_d > 0 \quad \text{and} \quad (\Delta h_i + D\Delta t_i) > 0 \quad (16)$$

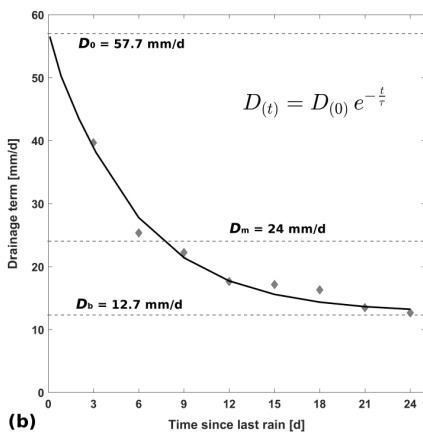
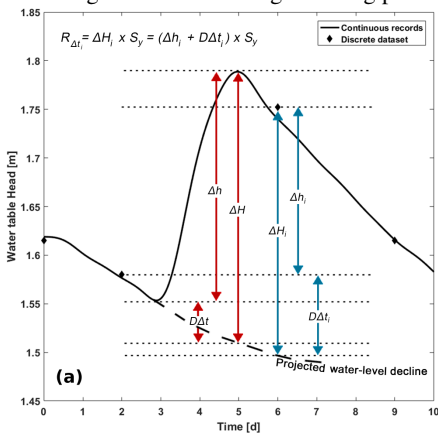
where Δh_i represents the ‘differenced water level’ in each interval [mm], that is the difference in water head between two consecutive records, D is the drainage rate [mm/d] or D term, Δt_i is the interval time length [d], P_d is the daily accumulated precipitation [mm], and S_{ya} is the apparent specific yield [% by volume], estimated by Eqn (18). Subscript i represents all intervals available in the dataset. Hence, the recharge value in Eqn (16) is estimated in the rainy intervals solely, and is corrected by all drainage contributions lumped in the D term, including the moisture content of the unsaturated zone. The term substitutes, at each interval, the drawing of the “antecedent recession curve” that the well hydrograph would have followed in the absence of the rise-producing precipitation (Healy and Cook 2002, Fig.18a), in analogy with the Master Recession Curve approach (Delin et al 2007).

The methodology is divided into five basic steps. Firstly, the series are synchronized and the measurements are consolidated to remove errors or outliers. In order to avoid underestimation of recharge (Delin et al. 2007) sampling intervals longer than 15 days are excluded, losing only 1% of records. Therefore, the resultant average sampling interval used in the procedure is 3-4 days. Secondly, the raw depth dataset is converted to absolute hydraulic head above mean sea level. Thirdly, the difference in water levels between consecutive measurements (Δh_i) is defined. Then, the amount of rainfall in each interval [mm] is calculated as the sum of the daily precipitation (P_d) between the first day and the second to last day of the interval as in Eqn (17).

$$P_{\Delta t_i} = \sum_{\Delta t_i} P_d \quad \xrightarrow{\text{is}} \quad \sum_{d=1}^{N-1} P_d \quad \text{with} \quad (\Delta t_i = t_1, t_2, \dots, t_N) \quad (17)$$

Finally, accumulated precipitation is used to divide the time-series: intervals with null accumulated precipitation are isolated and used to determine the rates related to the drainage processes where no recharge occurred, while intervals with positive accumulated precipitation are used to infer the recharge itself.

Figure 18 - Conceptual model sketches: (a) Definition of the water-table fluctuation method (WTF) for continuous (red arrows) and discrete (blue arrows) datasets: ΔH_i represent the total water-table rise in the interval, whereas Δh_i is defined on the water level measurements; (b) Exponential model (equation) fitted on field data to assess the D term as a function of the time elapsed since the last rainfall. Solid line is the mean function obtained from the fitting curves of 13 piezometers, grey diamonds represent for each time step the mean drainage value for the whole dataset, D_0 is the average initial drainage after a rainfall event, D_m is the median drainage and D_b is the average low-head drainage for long periods without rain.



(b)

As derived analytically by Cuthbert (2010) groundwater drainage in a flat unconfined aquifer is a transient function depending on the distance from (a) the surface receptor and (b) water-table head. The water head dependency of drainage (D term) in the Ressacada Farm site is explained as an empirical exponential function with respect to time for a period of 10 years (from 2007 to 2016) (Rama et al. 2017). Since a linear relationship between saturated volume and groundwater discharge at quasi-steady-state conditions was suggested (Walker et al., 2015), it was proposed to group the rates into classes representing time elapsed since the last rain event. In order to simplify the procedure these averaged values are used in the discrete approach of WTF to infer recharge. Thus, upper and lower drainage values in a significant time-scale obtained from the average best-fit curve for the whole area are: 12.7 mm/d for the low-head drainage of the aquifer in dry periods, and 57.7 mm/d immediately after a rainfall event, when the hydraulic head of the aquifer is high (Fig. 18b). As shown in Fig. 18b, low-head drainage indicates the water table decreasing rate after 24 days with no rain, since dry periods never overstepped 25 days in 10 years of monitoring. In the continuous approach of WTF, a constant D term is set up to 24 mm/d, equal to the median of the whole distribution of drainage rates.

An apparent specific yield (S_{ya}) represents the storage of water controlled by capillary forces above the water table, assuming a transient non-ideal release of water (Child 1960, Duke 1972). Mathematically, for a layered soil S_{ya} is defined as (Crosbie et al. 2005):

$$S_{yu} = (\eta - S_r) \quad \rightarrow \quad S_{ya} = S_{yu} - \frac{S_{yu}}{\left[1 + (\alpha \times d)^n\right]^{1-\frac{1}{n}}} \quad (18)$$

where η is the total porosity, S_r is the specific retention, also known as field capacity [% by volume], d is the mean depth of the water table in the time step [cm], and S_{yu} is the ultimate specific yield [% by volume]. To determine S_{ya} a nonlinear relation between soil moisture and specific yield is assumed, supposing pressure distribution at equilibrium at each step. Given the spacing of the sampling intervals and a quick reaction of the water table to the rainfall, this strategy seems reasonable. S_{yu} represents a steady specific yield without influence of depth. Soil specific parameters of the Van Genuchten moisture model (α and n) are adopted from the Hanford sediment (Echin and Hopmans 1993) which exhibits similar characteristics and behavior with the Ressacada soil. In order to estimate S_{yu} , the procedure by Armstrong and Narayan (1998) is

automated for a discrete dataset, obtaining ultimate specific yield from the groundwater level changes versus the accumulated precipitation plot (Fig. 21). To assess Syu, only the water level declines in the last 50 cm of recorded depths in each piezometer are used. This corresponded to the water-table depth of at least 1.5 m. Therefore, only the low-head drainage value of 12.7 mm/d is applied to lower records. Finally, multiplying the differenced water level series corrected with the drainage term by the Sya, the recharge in each interval is inferred and aggregated in a monthly recharge at the Ressacada farm.

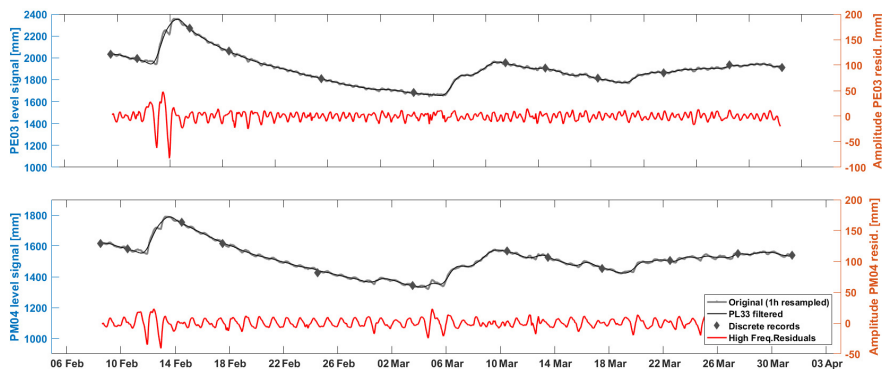
3.3.3.1.2 Continuous analysis and tidal frequency analysis

In the second stage, the discrete-series approach is compared with the continuous-series analysis proposed by Crosbie et al. (2005). The analysis is performed for the datasets PE03 and PM04 in a 51-day time window, from 8 February 2017 to 31 March 2017 (Fig.19), using both manually collected records (discrete and variably-spaced data) as well as datalogger series (continuous and homogeneously-spaced data). The two piezometers are chosen to be located along the main groundwater flow direction and exhibit the highest difference in the water-table variability.

To manage continuous datasets, water level records are firstly resampled to 1-h rate using a Doodson filter (Pugh 1987). This is followed by a data synchronization for the period from 8 February 2017 at 15:00:00 to 31 March 2017 at 09:00:00, to obtain 1,220 hourly records. In a congruence analysis, errors, spikes and noise are removed. To isolate periodic components with high frequencies, a Low Pass 33 filter (LP33) is subsequently applied (Emery and Thomson 2001). Finally, in order to separate tidal influence from other periodic contributions (evapotranspiration, atmospheric pressure variation, etc), a frequency analysis is carried out with a Matlab based UTide code (Codiga, 2011) on the residual signal (red lines in Fig. 19). The harmonic component builder allowed one to identify the signal contribution at tidal frequencies from time series, including groundwater records. In addition, UTide is run on the sea level series, monitored in the South Bay, comparing the identified significant components with the PE03 and PM04 results. The significance of each component is attributed to the amplitude of the signal, based on the accuracy of the sensors and the Signal-to-Noise Ratio (SNR) with a modified Rayleigh criterion, while their relative importance is controlled by the Percent Energy (PE) contributing to the signal reconstruction (Codiga 2011). The SNR value of 6 and a minimum PE of 0.5% are adopted. The sea levels in the South Bay are monitored by an OTT/RLS

radar level sensor (accuracy of 3.5 mm, sampling frequency of 5 min) and are provided by EPAGRI/CIRAM (Agricultural research and extension company / Information center for environmental resources and hydrometeorology).

Figura 19 - Comparative plot of raw data (grey lines and diamonds), the Low Pass 33 filter signal (black line), and high frequencies residuals (red line) for (a) PE03 and (b) PM04 in the 51-day period. The residual signal is analyzed with UTide Codiga 2011) to assess astronomical tide influence on the water table.



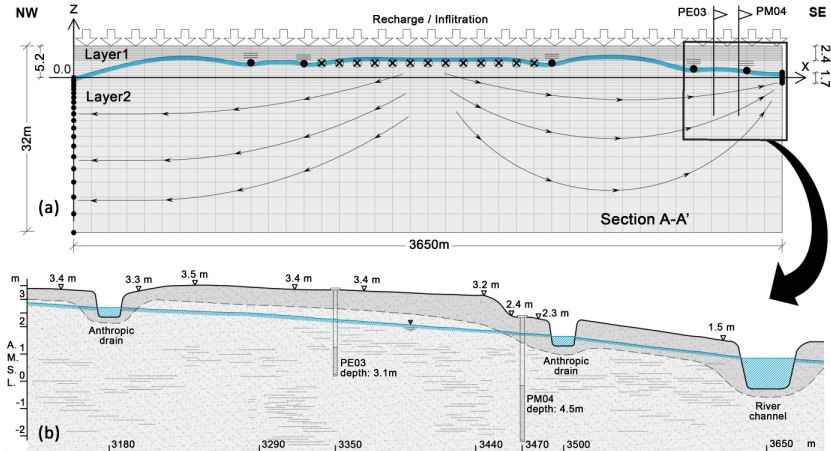
3.3.3.1.3 Numerical FEM model

In the last stage, a 2D vertical finite element model is constructed in order to integrate obtained recharge estimates in a transient simulation of the flow field. The model domain of 3650 m and 32 m in length and height, respectively, is divided into 18,154 rectangular elements (58 rows and 313 columns), regularly spaced in the horizontal direction every 11.7 m and with irregular spacing in the vertical direction. In the top 5.2 m of depth, the spacing is equal of 0.4 m and then increased gradually by about 5.5% until the bottom. The elevation $z = 0$ m refers to the mean average sea level. At the elevation $z = 2.4$ m the domain is divided into two layers of different hydraulic properties to reflect the existence of a superficial layer of finer geologic material rich in organic matter.

Constant-head boundary conditions (Dirichlet-type BC) are used to represent surface water bodies: South Bay on the left side ($x = 0$ m; $z = 0$ m), and Tavares River on the right ($x = 3650$ m; $z = 0.8$ m). In addition, five “seepage face” BCs are introduced within the domain to represent partially penetrating artificial ditches at an elevation $z = 2.8$ m ($x = 944, 1236$ and 2460 m), at $z = 2$ m ($x = 3180$ m), and at $z = 1.2$ m ($x = 3500$ m) (Fig.20). Conceptually, a seepage face corresponds to a

constant-head BC, which is combined with a maximum flux constraint equal to zero, allowing a free outflow of water from the model. To reproduce a parallel trench influencing the flow field, but located outside of the simulation domain, a Cauchy flow BC constrained with a null max-flow rate is used (Diersch 2014). This condition allowed for the performance of a distance-dependent drain in the central part of the domain from $x = 1294$ m to $x = 2402$ m at an elevation $z = 3.4$ m. Finally, recharge is represented by a fluid-flux BC on the top elements, which is a time-variable inflow condition. These values express volumes of water travelling through the unsaturated zone to the water table, solved by Richard's Law and regulated by a modified van Genuchten moisture model. The details of the model set up are presented in Quad.1.

Figure 20 - (a) Two-dimensional (2D) finite element model setup along Section A-A' (Fig.17c), used to test the recharge estimation methodology in Stage 3. Filled dots represent the head boundary condition (BC), dots with lines above are constrained-head BC (seepage face), encircled crosses indicate Cauchy-type BC with flow constraint, lines with arrows show groundwater flow paths, blue line is the water-table position, and flags are observation points (piezometer locations). (b) The detailed vertical section of the Experimental Area 3 (Fig.17d), showing ground elevation and water-table position.



The model is calibrated using a trial-and-error method with the following criteria: (1) modeled hydraulic conductivity values should not deviate from the field-derived values by more than $\pm 15\%$; (2) hydraulic conductivity values are adjusted for the steady-state comparing simulated levels with the average of monitored hydraulic heads; (3) the initial

condition of hydraulic head for transient-state is obtained by a single calibrated steady-state run; (4) unsaturated-flow porosity of layer 1 for the transient-state should not deviate by more than $\pm 15\%$ from the average of Sya estimates; (5) unsaturated-flow porosity of layer 2 and Richard's model parameters are adjusted using a fixed RR into the range established with the WTF estimates in PM04 and PE03, equal to 43% of monitored precipitation (Tab.4, Fig.23); (6) daily recharge values in transient-state must not exceed precipitation; (7) approximation of hydraulic heads never oversteps minimal targets of 0.85 for the Nash-Sutcliffe (NS) efficiency coefficient, 10% of total observed head range for root-mean-square error (RMSE), and 10 cm of absolute error in comparison to field data (Anderson et al. 2015).

Quadro 1- The two-dimensional FEM model input parameters and conditions

FEM parameter ^a	Symbol	Value [unit]	Reference
<i>Model parameters for "Calibrated scenario"</i>			
Saturated conductivity	K	3.2 (layer1) / 8.5 (layer2) [m/d]	Lage (2005) / Field data
Unsaturated flow porosity	η_e	0.067 (layer1) / 0.13 (layer2) [-]	WTF estimation / Calibration
Specific storage coeff.	S_0	0	Diersch (2014)
Maximum saturation	ss	1	
Residual saturation	sr	0.25	WTF method / Field data
<i>Modified van Genuchten parametric model</i>			
Pore-size distribution index	n	2.2 [-]	Diersch (2014)
Fitting coefficient	α	2.8 [1/m]	
Fitting exponent	m	0.55 [-]	
Fitting exponent	δ	1 [-]	
<i>FEM - 2D mesh consisting of 18,154 quadrangle elements (313 × 58)</i>			
Domain	X vs Z	3650 vs 32 [m]	Conceptual model
Vertical space increment	Δz	$0.4 + (5.5\% \Delta z_{i-1})$ [m]	
Horizontal space increment	Δx	11.661 [m]	
Initial time-step size	Δt_0	0.001 [d]	
RMS ^b error tolerance (AB/TR)	ζ	0.001 [-]	
Simulation time period	t_{end}	52 [d]	

^a FEM: Finite Element Method model, design by the FEFLOW code (DHI)

^b RMS: Root mean square

Therefore, once the model results satisfactorily represent transient hydraulic head data, scenarios with different recharge are constructed:

1. recharge equal to 43% of daily precipitation, statistically inferred from rainfall records, and input parameters in compliance with Quad.1 (it is called also "calibrated scenario"),

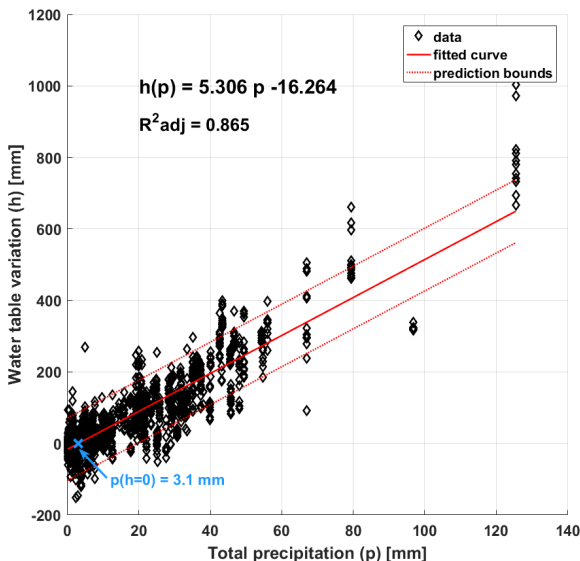
2. recharge assessed with the continuous-series method of WTF (Section ‘Discrete-series approach’),
3. steady constant recharge equal to 2.15 mm/d (43% of average precipitation in the 51-day period),
4. recharge equal to 43%, with a constant unsaturated-flow porosity for the whole domain, equal to 0.188 (measure of S_{yu} estimated as the inverse of the slope of the line of best fit in Fig. 5).

3.3.4 Results and discussion

3.3.4.1 Recharge estimation: discrete and continuous approach to WTF

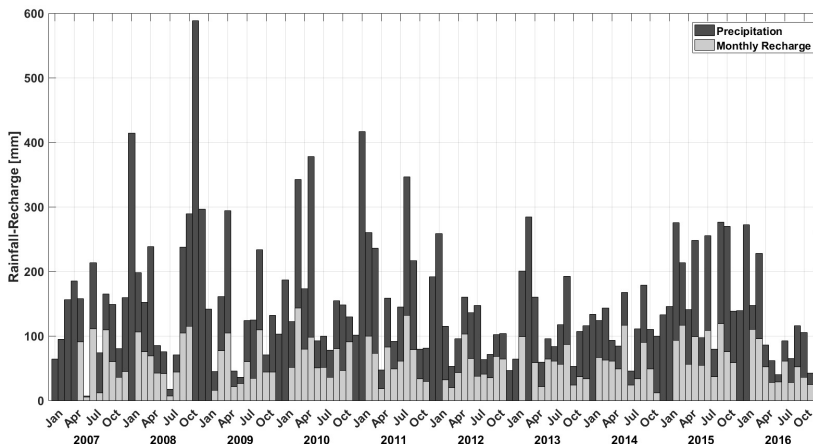
The water level variations versus accumulated rainfall for each interval show a linear correlation (Fig. 21). The inverse of the slope of the fitting line in the graph gives the value of S_{yu} equal to 0.188 (95% confidence bounds from 0.185 to 0.192), which agrees with the field S_y assessment (Corseuil et al. 2011b).

Figure 21 - Ultimate specific yield estimation using the regression best fit (red line and equation) in a precipitation vs water-table fluctuation plot. R^2_{adj} is the degree-of-freedom adjusted coefficient of determination for the typed equation. Dotted lines show the prediction interval for a non-simultaneous new observation with 95% level of certainty.



All water losses (i.e. soil moisture variation, evapotranspiration and run-off) are assumed to be included in the part of the rainfall that falls below the threshold value (x -intercepting value in blue Fig. 21). This means that on average only accumulated precipitation above 3.1 mm (2.5 to 3.7 mm with 95% confidence interval) has an evident influence on the Ressacada groundwater levels.

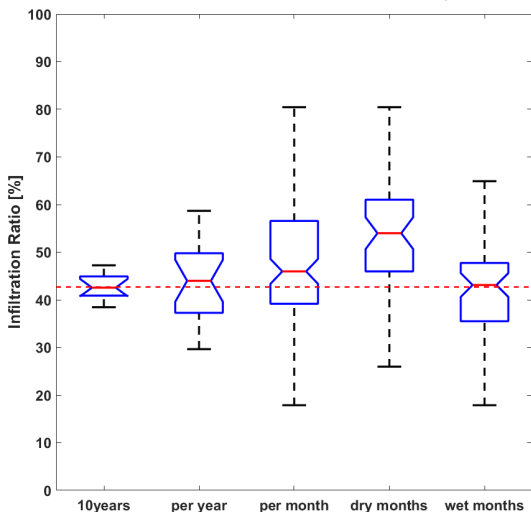
Figura 22 - Comparative bar plot between monthly recharge estimates (light bars) and total precipitation (dark bars). Recharge bars are average values between the 13 piezometers.



The estimates of average monthly recharge for the whole area show an outstanding variability (Fig.22). There is no constant or directly proportional relation between monthly precipitation and recharge which has a three-fold explanation: firstly, in rainy months the intense runoff, due to the temporal proximity of precipitation events to each other, has less contribution to a water-table rise; secondly, recurrent flooding events during the intense precipitation periods reduces groundwater recharge; finally, swamp areas near the Tavares River modify hydraulic head to boundary receptors for long periods resulting in a reduced capacity for aquifer drainage, and hence, storage capacity. It should be highlighted that, since months with no available water level records are excluded from the analysis, no bar of recharge is shown in the graph for these months

For the discrete dataset of thirteen piezometers the total recharge in 10 years varies from 5634 to 6957 mm which constitutes from 38.5% to 47.2% of precipitation, respectively; this is on average 43% of RR in the area (Fig. 23).

Figura 23 - Statistics boxplot of estimated recharge ratio (RR) for different time periods. Red lines express median value of distribution; blue boxes indicate the 25th and 75th percentiles, while dashed whiskers extend to the most extreme data points. Red dashed line show 43% (median RR in 10 years).



The values of monthly recharge sums indicate that average annual recharge varies between 536 to 885 mm/year, respectively, for the driest and wettest year, whereas the annual recharge range (difference between maximum and minimum value) between all the piezometers is on average 230 mm. Therefore, average recharge ratios are in the range of 35.9-51.6%, resulting in a wider range of RR than the 10-years analysis. It should also be emphasized that the years with more accumulated rainfall show the lower RR values. This suggests that the effectiveness of recharge decreases with the increase of precipitation, due to an enhanced saturation of pores. The effect is widely referred to as “fill and spill” systems (Tromp-van Meerveld and McDonnel 2006). The implication is that dry winter months show on average markedly higher RR, whereas during the rainy months RR is lower.

Tabela 4 - Comparison between discrete and continuous dataset estimations within the 51-day period

Dataset	Accumulated column [mm]	Recharge Ratio [%]
Precipitation	260	-
PE03 Discrete WTF	146	56.2
PE03 Continuous WTF	136	52.3
PM04 Discrete WTF	90	34.6
PM04 Continuous WTF	81	31.2

Recharge estimates for the continuous datasets during a 51-day time span are 136 and 81 mm for PE03 and PE04, respectively. The recharge estimate in the same period for the discrete datasets are 146 and 90 mm, for PE03 and PE04, respectively, showing a good agreement between the approaches (Tab.4).

Tabela 5 - Summary of sensitivity analysis results

S_{yu} (RR) ^a [% by volume]	D term (RR) ^a [mm/d]
0.188 (0.430)	Initial values: 12.7 – 57.7 ° (0.430)
0.13 (0.302)	Constant low-head value: 12.7 (0.357)
0.2 (0.464)	No correction with D term: (0.248)
0.2 constant ^b (0.794)	Constant average value: 20.7 (0.441)
	Higher piezometer: 15.2–66.2° (0.483)
	Lower piezometer: 9.6 – 35.9° (0.390)

^a RR in brackets is the average recharge ratio between all piezometers, calculated as the ratio of total recharge in 10 years and total accumulated precipitation

^b Constant specific yield equal to field assessment (Corseuil et al. 2011)

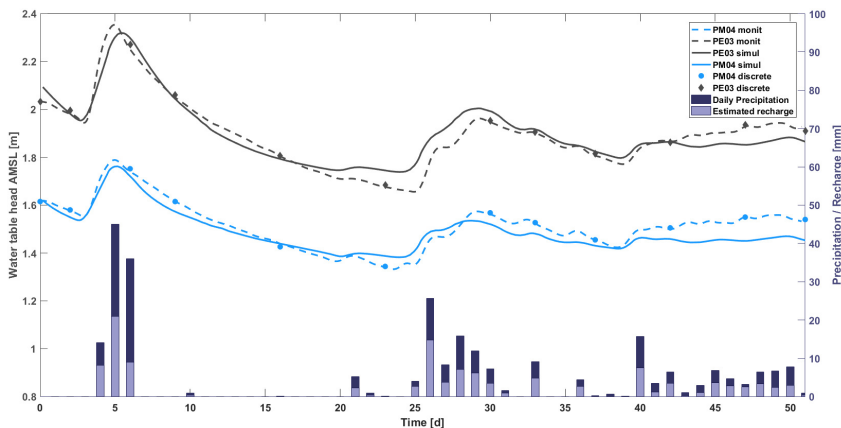
^c Respectively, final and initial drainage rate in an exponential D function of 25 days without rain, namely 24-dry-days and 0-dry-days drainage.

The sensitivity analysis of inferred recharge ratios (RRs) to the model parameters is summarized in Tab.5. RRs in brackets refer to the whole 10-year time period for the different S_{yu} values and D term. The recharge estimates with WTF exhibit a linear relationship with S_{yu} value, as shown in Eqn. 18. Nevertheless, if S_{yu} is constant (no S_{ya} decline at the surface) recharge estimates increase dramatically. This observation confirms the finding by Child (1960) indicating an overestimation of recharge if a constant S_y is used instead of a non-steady value. In addition, the model seems to be very sensitive to the drainage term, highlighting the importance of its accurate assessment. The D term has increasing influence depending on the larger time step between the records. Similarly, uncertainties on the real recession hydrograph intensify their relevance in the final estimation. For this reason, the authors suggest to use head-variable D values up to one week, adopting a fixed low-head or median D value for time intervals overstepping one week.

3.3.4.2 Integration of WTF results into the FEM model

Observed and simulated water head values in PM04 and PE03 show a good agreement (Fig.24), with a NS coefficient of 0.87 and a RMSE of 5 cm. Solid lines in the graph represent calibrated simulation with parameters as in Quad.1 and RR equal to 43% of daily precipitation (scenario 1).

Figura 24 - Combined plot showing water level fluctuations in the 51-day period. Dashed lines represent continuously monitored piezometer levels while solid lines are the calibrated asset (scenario 1). The bar plot shows recorded precipitation (dark purple bars) and daily estimated recharge values (lilac bars)

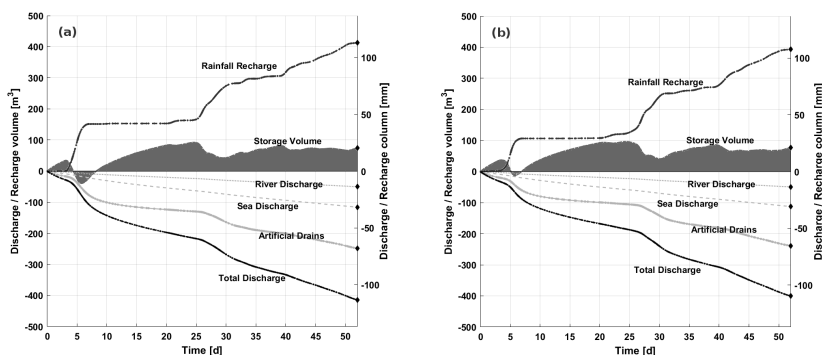


Recorded precipitation and water-table variation (dashed lines) indicate a generally fast response of the Ressacada aquifer to infiltration (8-24 h). The distribution of simulated levels (solid lines) indicates a similar timing in recharge in agreement with findings by Hunt et al. (2008). In addition, the comparison of records from two piezometers exhibits greater distance between the two lines during a rainfall event and immediately after it, with a scarce increase of PM04 levels compared with levels at PE03. This behavior demonstrates the spatially different recharge in the area, with greater fluctuations in areas further away from the boundary receptors.

The numerical model allows one to compare water budget components between the estimated recharge with WTF and different FEM scenarios. Comparative analysis of the water columns at the end of the simulation (Fig. 25) shows a good agreement in the water budgets with the WTF estimates (Tab.4). Although the NS coefficient on the water-table head decreases from 0.87 to 0.76 passing from scenario 1 to scenario 2 (Apêndice A – Fig.ESM1, ESM3), water volumes at the end of the simulation are very close in both runs. It suggests that prior estimation of recharge with WTF prevents a long trial-and-error process to assess the recharge with the numerical model, also providing a robust theoretical basis for its values. The difference in the shapes of the Rainfall Recharge curves (Fig. 25) emphasizes that effectiveness of recharge is

related to the precipitation distribution: first, a more intensive rainfall event (day 4 to 6) has less estimated RR than 43% and the curve grows less, whereas the second event (day 25 to 31), less rainy and more distributed in time, exhibits a higher RR than the average value of 43%.

Figura 25 - Transient cumulative groundwater balance: (a) scenario 1, (b) scenario 2. Storage filled curves exhibit storage contribution to flow and discharge.

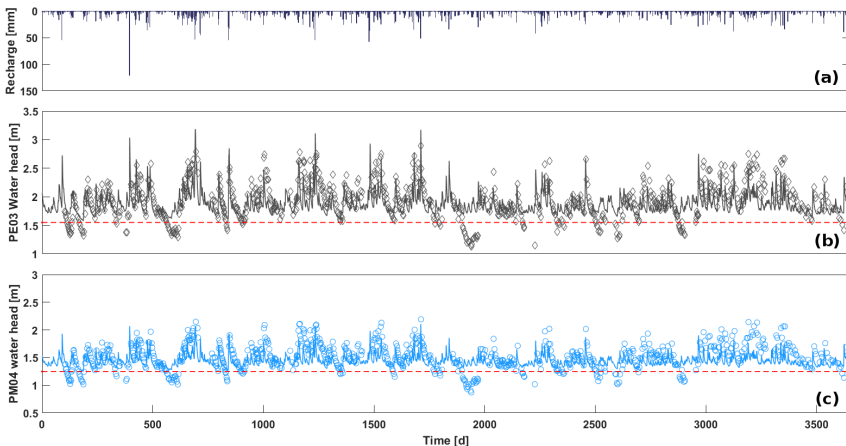


The calibrated scenario 1 was also tested using a transient unsaturated flow porosity in layer 1 equal to the estimated S_{ya} , as described in section ‘Discrete-series approach’ (Apêndice A – Fig. ESM2). Here, the water budget exhibits sharper curves in response to changing parameters along the simulation, with a higher contribution of storage volume to flow between days 9 and 25. Nonetheless, the total approximation of simulated levels results in a NS coefficient of about 0.77. It should be highlighted that the storage contribution to flow at the end of 51 days remains similar in all the scenarios, except with a constant unsaturated-flow porosity equal to S_{yu} (scenario 4). By running this scenario (Apêndice A – Fig. EMS1, ESM2), hydraulic levels, and hence, water discharge budgets show a pronounced sensitivity to the parameter, with a drastic mismatch in the peak of hydrographs (absolute error more than 15 cm), although the simulation NS efficiency coefficient remains about 0.8. This explains the sensitivity of recharge estimates using WTF to the value of S_{yu} (Tab.5). Finally, by running the “steady recharge” run (scenario 3), simulated steady-state levels converge to the average of the transient hydraulic head in scenario 1, with also good agreement in the entire water budget at the end of the simulation (Apêndice A – Fig. ESM2).

Using scenario 1, model verification is run on a 10-year-long discrete dataset of groundwater levels for PE03 and PM04 (Fig. 26). The

resulting water table shows a good model agreement for the majority of water level values, except for low water levels for which modeled values are overestimated. The head-BC assigned on Tavares River is meant to represent a natural dynamic system with sharp level fluctuations over time. In accordance with the head-dependent relationship of Darcy's Law, the BCs define in the model the hydraulic gradient for nodes where flow occurs, mostly in long periods without rainfall. This behavior implicates a progressively slower flow as the water table approaches an equilibrium state with the BCs. However, dry periods determine lower levels in the river too, resulting in a faster decrease of groundwater levels in the field, which are impossible to simulate with fixed values of BCs. Therefore, the authors suppose that the deviation could be reduced with the use of a time-variable boundary condition at the river cells rather than a time-constant value. Nevertheless, the deviation from the field data occurs in periods of null recharge only, and, hence, it is of a low significance for long-term recharge estimation.

Figure 26 - 2D model verification plot: comparison between simulated (solid lines) and monitored levels dataset (symbols) in a 10-year-long simulation that used calibration parameters, for (a) Recharge, (b) PE03, (c) PM04. The red dashed lines (lower head value reached by simulation in each piezometer) show that simulated lines never decrease under fixed values related to the river BC, losing accuracy to explain low groundwater levels.

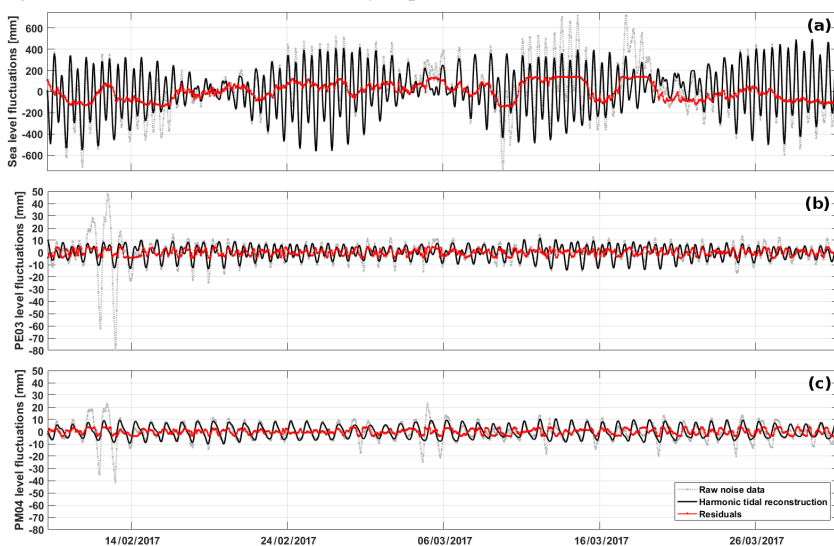


3.3.4.3 Tidal influence assessment

Frequency decomposition of the groundwater-level signals indicates an only marginal tidal influence on PE03 and PM04 hydraulic

head in comparison to the other aperiodic stresses, such as rainfall infiltration (Fig. 19). In fact, the absolute value of the reconstructed signals remains confined within 12.2 mm (sygizial tides) and -9 mm (quadrature tides). Nevertheless, analysis of harmonic components on the high frequency residuals allows a quantitative assessment of tidal influence on PE03 and PM04 hydraulic head.

Figura 27 - Signal reconstruction by harmonic components of (a) South Bay seawater level monitoring, and the (b) PE03 and (c) PM04 high frequency signal. In each graph a comparison of raw high frequencies records (grey dotted lines), tidally reconstructed signal (black solid line) and non-tidally explained residuals (red line) is shown.



Since the tide estimation uses a 51-day time series, 35 harmonic components are identified. However, when applying significance limits ($\text{SNR}=6$ and $\text{PE}>0.5\%$), only eight of those components are shown to be relevant in the South Bay signal and only two in the groundwater level records. Astronomical tide assessment on the South Bay shows that 73.6% of the sea level records are explained by high-frequency periodic contribution, while the other 26.4% is due to other meteorological stresses. In the same way, astronomical tide components explain 33.2% and 49.9% of residual signals after LP33 application, on PE03 and PM04, respectively (Fig. 27). It should be noted that PM04 is 180 m away from the river channel, while PE03 is 300 m away (Fig. 20).

This fact indicates a higher percentage of tidal influence on the signal of the closest piezometer to the river and suggests that only a small part of the tidal perturbation in the South Bay influences water head in the inland piezometers. Most of higher frequency components seem to be smoothed out by pressure propagation in porous media, in accordance with the main theory of incompressible flow: the higher the component frequency, the greater the attenuation in a dissipative media.

Tabela 6 - Comparative tidal analysis (amplitudes with 95% confidence interval). Values in italic are the relevant components (namely SNR \geq 6, PE \geq 0.5%, and Ampl. \geq 3.5mm).

Tidal Component		SouthBay (OUT)			PM04 (IN1)				PE03 (IN2)			
Name	Freq. (cl/hr) ^c	Ampl. (mm)	Ampl. Error (mm)	Perc. Ener. ^a	Ampl. (mm)	Ampl. Error (mm)	Perc. Ener. ^a	Atten ^b PM04	Ampl. (mm)	Ampl. Error (mm)	Perc. Ener. ^a	Atten ^b PE03
Q1	0.037	<i>26.6</i>	<i>11.3</i>	<i>0.8%</i>	0.9	0.3	1.2%	96.6%	0.9	0.3	1.2%	96.5%
O1	0.039	<i>117.0</i>	9.7	<i>15.6%</i>	0.3	0.3	0.1%	99.8%	1.3	0.3	2.4%	98.9%
K1	0.042	<i>42.4</i>	<i>10.4</i>	<i>2.1%</i>	7.8	<i>0.3</i>	<i>85.6%</i>	<i>81.7%</i>	<i>4.8</i>	<i>0.3</i>	<i>32.4%</i>	<i>88.6%</i>
N2	0.079	<i>39.2</i>	8.2	<i>1.8%</i>	0.1	0.2	0.0%	99.6%	0.3	0.3	0.2%	99.1%
M2	0.081	<i>193.0</i>	8.2	<i>42.8%</i>	0.2	0.2	0.1%	99.9%	0.3	0.3	0.1%	99.8%
S2	0.083	<i>166.0</i>	8.6	<i>31.5%</i>	1.7	0.3	3.9%	99.0%	<i>5.8</i>	<i>0.3</i>	<i>47.3%</i>	<i>96.5%</i>
M3	0.121	<i>24.4</i>	7.1	<i>0.7%</i>	0.2	0.2	0.0%	99.3%	0.1	0.2	0.0%	99.7%
M4	0.161	<i>23.0</i>	8.1	<i>0.6%</i>	0.1	0.2	0.1%	99.4%	0.1	0.2	0.0%	99.6%

^a Perc. Ener. Percent of energy (PE) that contributes to the signal reconstruction as the ratio between component energy, gauge of potential energy of sea level, and total energy of the reconstructed signal.

^b Atten. is the attenuation of the component in comparison of the South Bay signal. It is calculated by 100 minus the ratio of component amplitude in the piezometer and in the sea-level gauge.

^c cl/hr means cycles per hour. It is a frequency unit that implicate a 1/3600 cl/hr for a frequency of 1 hertz.

Tabela 7 - Comparative tidal analysis (phases with 95% confidence interval). Values in italic are the relevant components.

Tidal Component		SouthBay (OUT)			PM04 (IN1)				PE03 (IN2)			
Name	Freq. (cl/hr)	Pha (°)	Pha Err.	SNR (RM) ^a	Pha (°)	Pha Err.	SNR (RM) ^a	Δ Pha ^b PM04 (h)	Pha (°)	Pha Err.	SNR (RM) ^a	Δ Pha ^b PE03 (h)
Q1	0.037	<i>56</i>	<i>21</i>	<i>22</i>	159	22	34	-7.7	273	22	29	-16.2
O1	0.039	73	5	<i>560</i>	191	81	3	-8.5	347	15	73	-19.6
K1	0.042	<i>150</i>	<i>13</i>	<i>64</i>	<i>166</i>	2	<i>2300</i>	<i>-1.1</i>	<i>221</i>	<i>4</i>	<i>780</i>	<i>-4.7</i>
N2	0.079	<i>145</i>	<i>13</i>	<i>89</i>	359	417	2	-7.5	96	44	6	1.7
M2	0.081	79	3	<i>2100</i>	172	58	5	-3.2	145	58	5	-2.3
S2	0.083	83	3	<i>1400</i>	122	10	150	-1.3	<i>99</i>	<i>9</i>	<i>1700</i>	<i>-0.5</i>
M3	0.121	<i>174</i>	<i>18</i>	<i>46</i>	99	82	1	1.7	223	158	1	-1.1
M4	0.161	<i>99</i>	<i>21</i>	<i>31</i>	276	95	3	-3.1	113	147	1	-0.2

^a SNR (RM) Signal-to-Noise Ratio with modified Rayleigh criterion.

^b Δ Pha Phase delay between the offshore component in the South Bay and the same component in the piezometer

In addition, comparative analysis on K1, that is the only relevant component greater than sensors accuracy (Ampl \geq 3.5mm) in both PE03 and PM04, indicates that perturbations decrease moving inwards (Tab. 6 and 7). PE03 showed an attenuation rate higher than PM04, which

conserves more amplitude. At the same time, the PE03 signal had more phase delay than PM04. This observation confirms the findings of Mao et al. (2006) and is due to the tidal perturbation pathway, which moves from the estuary along the course of the river towards the center of the domain. Nevertheless, other non-relevant components (S2 and O1) exhibit an opposite behavior. This may be due to an additional interaction of the PM04 signal with the water level in the artificial trench close by, where no tidal effects are observed.

3.3.5 Conclusions

The paper describes the use of a time-series approach for WTF, with discrete and irregularly spaced water-level datasets. The application of WTF allowed one to estimate the groundwater recharge from sparse head records in an aquifer with a shallow water table and sharp fluctuations. The methodology represents an improvement on WTF, increasing its application possibilities. The introduction of a time-variable drainage term and the definition of the differenced water levels based on monitored precipitation allowed one to moderate the recharge underestimation with increasing time steps. Hence, the results in the 51-day time window show good agreement with the results of the Crosbie et al. (2005) method. For the water level dataset between 2007 and 2017, the estimated amount of recharge is on average 43% of precipitation, showing a higher effectiveness of recharge in the “dry” months with less accumulated rainfall. Subsequently, estimated recharge values are integrated into a 2D finite element model that agrees with observed water level records. Solely low water levels are overestimated in the simulation, probably due to the constant-head BC in the river, suggesting the possibility to introduce a variable-in-time condition to better reproduce dry periods with deeper water table.

The application of WTF is limited to changes in groundwater levels over time due to rainfall infiltration only. This condition is confirmed to be reasonable at the Ressacada Farm site, by analyzing tidal influence on groundwater levels and absolute values of the residual high-frequency signal in the piezometers, which was usually less than 2 cm of amplitude. Since WTF was shown to be very sensitive to the specific yield, its value is assessed in the paper with a statistically-based framework that integrates punctual field measures. The main requirement of the proposed procedure is to allocate all the accumulated precipitation of each interval to the last day of the interval, as if total rainfall infiltrates and recharges the aquifer at the same time. As the sampling intervals

increase, the underestimation of recharge using the cumulative approach increases. This limitation is mitigated by introducing a variable D term to account for the water volume that leaves the aquifer in the same time interval. Finally, another important issue is related to the representativeness of the catchment as a whole. The uniform geological setting made the extrapolation of the relevant processes outside of the head monitoring area possible. Nonetheless, it is warranted to incorporate data from outside of the farm site, most of all in the center of the domain, in order to establish representative values for the watershed.

Acknowledgements

The authors want to acknowledge FEESC and Petróleo Brasileiro (Petrobras) for the financial and material support that made this study possible and DHI Group for providing a MIKE Powered by DHI license file to use FEFLOW. We thank also the Institute of Airspace Control (ICEA) and National Institute of Meteorology (INMET) for providing valuable precipitation data, all the technicians of Agrarian Sciences Center (CCA) for their support in the field data collection, Dr. Luis H.P. Garbossa for help obtaining sea-level records from the EPAGRI/CIRAM gauge station in the South Bay, and the PhD student Martina Pacifici (USP, PPGEC) for help in figure design. Finally, the manuscript benefited from suggestions from two anonymous reviews and comments/discussions with Sue Duncan (Technical Editorial Advisor of Hydrogeology Journal) for which we are most grateful.

References

- Acharya S, Jawitz JW, Mylavarapu RS (2012) Analytical expressions for drainable and fillable porosity of phreatic aquifers under vertical fluxes from evapotranspiration and recharge. *Water Resour Res* 48:1–15. doi: 10.1029/2012WR012043
- Anderson MP, Woessner WW, Hunt RJ (2015) *Applied groundwater modelling* 2nd Edition. Elsevier Inc. p.564 ISBN 978-0-12-058103-0
- Armstrong D, Narayan K (1998) *Using groundwater responses to infer recharge*. CSIRO, Australia. ISBN 0-643-06286-6
- Bohlke J-K (2002) Groundwater recharge and agricultural contamination. *Hydrogeol J* 10:153–179. doi: 10.1007/s10040-001-0183-3
- Cao G, Scanlon BR, Han D, Zheng C (2016) Impacts of thickening unsaturated zone on groundwater recharge in the North China Plain. *J Hydrol* 537:260–270. doi: 10.1016/j.jhydrol.2016.03.049
- Childs EC (1960) The Nonsteady State of the Water Table in Drained Land. *J Geophys Res* 65:1–3.
- Codiga DL (2011) *Unified Tidal Analysis and Prediction Using the UTide Matlab Functions*. Technical Report 2011-01. Graduate School of Oceanography, University of Rhode Island, Narragansett, RI. 59pp. <ftp://www.po.gso.uri.edu/pub/downloads/codiga/pubs/2011Codiga-UTide-Report.pdf> Cited: 05 March 2017
- Colombani N, Di Giuseppe D, Faccini B, et al (2016) Inferring the interconnections between surface water bodies, tile-drains and an unconfined aquifer-aquitard system: A case study. *J Hydrol* 537:86–95. doi: 10.1016/j.jhydrol.2016.03.046
- Corseuil HX, Gomez DE, Schambeck CM, et al (2015) Nitrate addition to groundwater impacted by ethanol-blended fuel accelerates ethanol removal and mitigates the associated metabolic flux dilution and inhibition of BTEX biodegradation. *J Contam Hydrol* 174C:1–9. doi: 10.1016/j.jconhyd.2014.12.004

- Corseuil HX, Monier AL, Fernandes M, et al (2011a) BTEX plume dynamics following an ethanol blend release: Geochemical footprint and thermodynamic constraints on natural attenuation. *Environ Sci Technol* 45:3422–3429. doi: 10.1021/es104055q
- Corseuil HX, Monier AL, Fernandes M, et al (2011b) BTEX Plume Dynamics Following an Ethanol Blend Release: Geochemical Footprint and Thermodynamic Constraints on Natural Attenuation - Supporting Information. *Environ Sci Technol* 23. doi: 10.1117/1111.2794018.2.
- Crosbie RS, Binning P, Kalma JD (2005) A time series approach to inferring groundwater recharge using the water table fluctuation method. *Water Resour Res* 41:1–9. doi: 10.1029/2004WR003077
- Cuthbert MO (2010) An improved time series approach for estimating groundwater recharge from groundwater level fluctuations. *Water Resources Research* 46(9), 46:1-11. DOI: 10.1029/2009WR008572
- da Silva MLB, Corseuil HX (2012) Groundwater microbial analysis to assess enhanced BTEX biodegradation by nitrate injection at a gasohol-contaminated site. *Int Biodeterior Biodegrad* 67:21–27. doi: 10.1016/j.ibiod.2011.11.005
- de Vries JJ, Simmers I (2002) Groundwater recharge: An overview of process and challenges. *Hydrogeol J* 10:5–17. doi: 10.1007/s10040-001-0171-7
- Delin GN, Healy RW, Lorenz DL, Nimmo JR (2007) Comparison of local- to regional-scale estimates of ground-water recharge in Minnesota, USA. *J Hydrol* 334:231–249. doi: 10.1016/j.jhydrol.2006.10.010
- Diersch H-JG (2014) FEFLOW - Finite Element Modeling of Flow, Mass and Heat Transport in Porous and Fractured Media. Springer-Verlag Berlin Heidelberg, p.996 ISBN 978-3-642-38738-8
- Duke HR (1972) Capillary properties of soils - Influence upon specific yield. *Trans ASAE* 15:688–691.
- Eching SO, Hopmans JW (1993) Optimization of Hydraulic Functions from Transient Outflow and Soil Water Pressure Data. *Soil Sci Soc Am J* 57:1167–1175
- Emery WJ, Thomson RE (2001) Data analysis methods in physical oceanography. Second and revised edition. Elsevier. B.V. Amsterdam
- Garbossa LHP, Vanz A, Fernandes L, et al (2014) Modelling and Validation of the Santa Catarina Island Bays Hydrodynamics Based on Astronomic Tides and measured Tides. 11th Int Conf Hydroinformatics 8. doi: 10.13140/2.1.5123.6163
- Grimm AM, Ferraz SET, Gomes J (1998) Precipitation Anomalies in Southern Brazil Associated with El Niño and La Niña Events. *J Clim* 11:2863–2880. doi: 10.1175/1520-0442(1998)011<2863:PAISBA>2.0.CO;2
- Healy RW (2010) Estimating groundwater recharge. Cambridge University Press, Cambridge p.245 ISBN 978-0-521-86396-4. Available at: <https://www.cambridge.org/core/terms>. <https://doi.org/10.1017/CBO9780511780745.001> Cited: 12 September 2017
- Healy RW, Cook PG (2002) Using groundwater levels to estimate recharge. *Hydrogeol J* 10:91–109. doi: 10.1007/s10040-001-0178-0
- Heilweil VM, Benoit J, Healy RW (2015) Variably saturated groundwater modelling for optimizing managed aquifer recharge using trench infiltration. *Hydrol Process* 29:3010–3019. doi: 10.1002/hyp.10413
- Hilberts AGJ, Troch PA, Paniconi C, Boll J (2007) Low-dimensional modeling of hillslope subsurface flow: Relationship between rainfall, recharge, and unsaturated storage dynamics. *Water Resour Res* 43:1–14. doi: 10.1029/2006WR004964
- Huang FK, Chuang MH, Wang GS, Yeh H Der (2015) Tide-induced groundwater level fluctuation in a U-shaped coastal aquifer. *J Hydrol* 530:291–305. doi: 10.1016/j.jhydrol.2015.09.032
- Hunt RJ, Prudic DE, Walker JF, Anderson MP (2008) Importance of unsaturated zone flow for simulating recharge in a humid climate. *Ground Water* 46:551–560. doi: 10.1111/j.1745-6584.2007.00427.x
- Kim K, Anderson MP, Bowser CJ (2000) Enhanced dispersion in groundwater caused by temporal changes in recharge rate and lake levels. *Adv Water Resour* 23:625–635. doi: 10.1016/S0309-1708(99)00050-0

- Kobiyama M, Bortolotto NL, Tanaka SI (2011) Relatório Hidrológico da Fazenda experimental da Ressacada (Hydrological report of the Ressacada experimental farm). Centro de Ciências Agrárias, UFSC, Available: <http://fazenda.ufsc.br/descricao-fisica/hidrologia/> Cited: 01 October 2017
- Lage I de C (2005) Avaliação de metodologias para determinação da permeabilidade em meios porosos: Fazenda Ressacada (Evaluation of methodologies for determination of permeability in porous media: Ressacada Farm). UFRJ. Rio de Janeiro. MSc Thesis.
- Lorenz DL, Delin GN (2007) A regression model to estimate regional ground water recharge. *Ground Water* 45:196–208. doi: 10.1111/j.1745-6584.2006.00273.x
- Mao X, Enot P, Barry D a., et al (2006) Tidal influence on behaviour of a coastal aquifer adjacent to a low-relief estuary. *J Hydrol* 327:110–127. doi: 10.1016/j.jhydrol.2005.11.030
- Masetti M, Pedretti D, Sorichetta A, et al (2016) Impact of a Storm-Water Infiltration Basin on the Recharge Dynamics in a Highly Permeable Aquifer. *Water Resour Manag* 30:149–165. doi:10.1007/s11269-015-1151-3
- Nachabe MH (2002) Analytical expressions for transient specific yield and shallow water table drainage. *Water Resour Res* 38:11-1-11-7. doi: 10.1029/2001WR001071
- Neto DC, Chang HK, van Genuchten MT (2016) A Mathematical View of Water Table Fluctuations in a Shallow Aquifer in Brazil. *Groundwater* 54:82–91. doi: 10.1111/gwat.12329
- Park E, Parker JC (2008) A simple model for water table fluctuations in response to precipitation. *J Hydrol* 356:344–349. doi: 10.1016/j.jhydrol.2008.04.022
- Peel MC, Finlayson BL, McMahon TA (2006) Updated world map of the Köppen-Geiger climate classification. *Hydrol Earth Syst Sci* 15:259–263. doi: 10.1127/0941-2948/2006/0130
- Pugh DT (1987) Tides, surges and mean sea level. John Wiley and Sons. Swindon, UK. ISBN 0-471-91505-X
- Rama F, Franco D, Corseuil HX (2017) Spatial and temporal analysis of natural drainage in the Ressacada aquifer (Florianópolis, Brazil). *IJESD Vol.8(9)*: 653-660 ISSN: 2010-0264, doi: 10.18178/ijesd.2017.8.9.1033
- Saghravani SR, Yusoff I, Wan Md Tahir WZ, Othman Z (2015) Comparison of water table fluctuation and chloride mass balance methods for recharge estimation in a tropical rainforest climate: a case study from Kelantan River catchment, Malaysia. *Environ Earth Sci* 73:4419–4428. doi: 10.1007/s12665-014-3727-2
- Sanford W (2002) Recharge and groundwater models: An overview. *Hydrogeol J* 10:110–120. doi: 10.1007/s10040-001-0173-5
- Scanlon BR, Healy RW, Cook PG (2002) Choosing appropriate techniques for quantifying groundwater recharge. *Hydrogeol J* 10:18–39. doi: 10.1007/s10040-001-0176-2
- Shi X, Vaze J, Crosbie R (2015) The controlling factors in the daily and monthly groundwater recharge estimation using the water table fluctuation method [online]. In: 36th Hydrology and Water Resources Symposium: The Art and Science of Water. ACT, Barton, Australia. <http://search.informit.com.au/documentSummary?dn=824177714642772;res=IELENG>. Accessed: 1 October 2017
- Tromp-van Meerveld HJ, McDonnell JJ (2006) Threshold relations in subsurface stormflow: 2. The fill and spill hypothesis. *Water Resources Research* 42. W02411. doi:10.1029/2004WR003800
- Walker GR, Gilfedder M, Dawes WR and Rassam DW (2015) Predicting Aquifer Response Time for Application in Catchment Modeling. *Groundwater* 53(3), 475-484. DOI: 10.1111/gwat.12219
- Xiao H, Wang D, Hagen SC, et al (2016) Assessing the impacts of sea-level rise and precipitation change on the surficial aquifer in the low-lying coastal alluvial plains and barrier islands, east-central Florida (USA). *Hydrogeol J* 1791–1806. doi: 10.1007/s10040-016-1437-4

3.4 FLOW FIELD DYNAMICS AND HIGH ETHANOL CONTENT IN GASOHOL BLENDS ENHANCE BTEX MIGRATION AND BIODEGRADATION IN GROUNDWATER

Fabrizio Rama^{(1)*}, Débora Toledo Ramos⁽¹⁾, Juliana Braun Müller⁽¹⁾, Henry X. Corseuil⁽¹⁾, and Konrad Miotlinski⁽¹⁾

* Corresponding author

(1) Núcleo Ressacada de pesquisa em meio ambiente (REMA) – CTC - UFSC

Manuscript received October 13, 2018; Received in revised form December 21, 2018; Accepted January 9, 2019; Published online February 21, 2019

Referência:

Rama, F., Ramos, D.T., Müller, J.B., Corseuil, H.X., Miotlinski, K., Flow field dynamics and high ethanol content in gasohol blends enhance BTEX migration and biodegradation in groundwater. *Journal of Contaminant Hydrology*, 2019. <https://doi.org/10.1016/j.jconhyd.2019.01.003>

Nota ao leitor:

Ajustes de texto e nas figuras foram realizadas em relação ao artigo original para aumentar a precisão da escrita científica e por razões de formato da dissertação sem, no entanto, alterar conteúdo e elementos utilizados nas análises.

Resumo

Os derramamentos de gasolina e etanol, embora superficiais, podem descer facilmente no solo e, à medida que os contaminantes se dissolvem nas águas subterrâneas impactar os receptores sensíveis. Cabe salientar que as formulações de gasolina são comumente misturadas com etanol, tanto no Brasil quanto a nível mundial, para aliviar questões ambientais e econômicas associadas aos combustíveis fósseis. No entanto, a quantidade de etanol e o regime hidráulico do fluxo subterrâneo podem afetar significativamente a dinâmica e a vida média das plumas de BTEX, que se desprendem das fontes NAPL. Por conseguinte, no estudo são monitoradas no tempo (5 e 10 anos) duas liberações na escala de campo de volumes de gásóleo com diferente teor de etanol (E85 e E24), a fim de avaliar as dinâmica de migração e degradação das plumas de etanol e BTEX no subsolo da Ressacada. O objetivo é avançar no entendimento dos processos de transporte de compostos dissolvidos em aquíferos granulares, nos casos de derramamentos de gasolina e etanol, delineando a contribuição do campo de fluxo subterrâneo na migração das plumas. Abordagens estatísticas, geoquímicas, microbiológicas e análises de

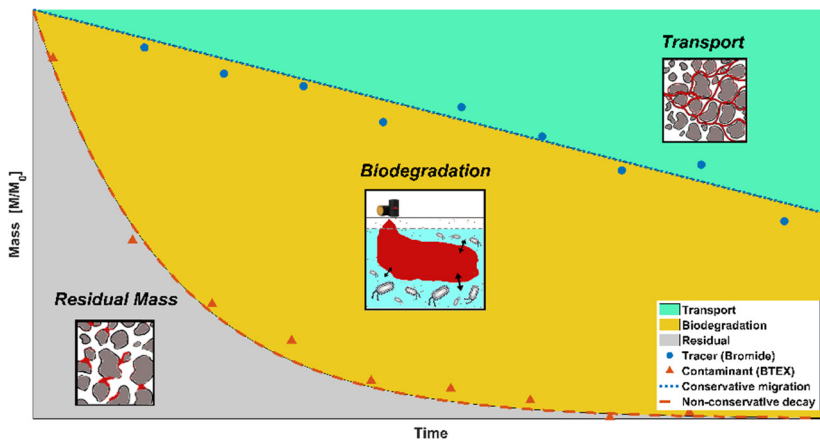
tendência são empregadas para estimar a influência do fluxo sobre o transporte nos dois derramamentos, assim como as taxas de biodegradação associadas. As plumas de etanol e BTEX no aquífero são caracterizadas a partir das curvas de ruptura (BTC) ao longo da direção de fluxo, pelas posições do centro de massa, pelas taxas de espalhamento, e pelo decaimento da massa total. A estimativa da taxa de deslocamento das plumas de brometo é usada para definir a contribuição do fluxo natural na dissolução e migração de todas as substâncias em solução nas áreas. Os resultados revelam que, em locais contaminados por gasóleo, um elevado conteúdo de etanol, juntamente a um fluxo natural mais rápido e dinâmico, exerce uma sorta de “lavagem” da fonte NAPL, aumentando a dissolução e migração (vertical e horizontal) de BTEX, com consequentes concentrações elevadas nas águas subterrâneas. A maior quantidade de etanol na área E85 determina uma elevada e imediata dissolução dos BTEX e da relativa biodisponibilidade dos compostos em relação à área E24, produzindo um aumento das taxas de biodegradação no aquífero através do efeito de cosolvência e da diluição do fluxo metabólico. Por outro lado, uma vez dissolvidos, os hidrocarbonetos do petróleo migram em forma de plumas conforme a velocidade de escoamento local e as variações do campo de fluxo. Portanto, a definição e o equilíbrio desses dois fatores (migração e biodegradação) são cruciais para estabelecer de maneira apropriada o destino e o transporte de contaminantes na escala de campo. Ao mesmo tempo estes resultados sugerem que o regime hidráulico deve ser previamente caracterizado, espacial e temporalmente, para apoiar as tomadas de decisões sobre planos de monitoramentos e tecnologias de remediação para derramamentos de gasolina e etanol.

Abstract

Gasohol spills may easily descend through the soil column down and impact sensitive receptors as contaminants dissolve into the groundwater. Gasoline formulations are commonly blended with ethanol to alleviate environmental and economic issues associated with fossil fuels. However, the amount of ethanol added to gasoline and the groundwater hydraulic regime can significantly affect BTEX plume dynamics and lifespan. In this study, two long-term (5 and 10 years) field-scale gasohol releases with ethanol contents of 85% (E85) and 24% (E24), respectively, were assessed to discern the different dynamics undergone by gasohol blends. Statistical, geochemical, microbiological and trend approaches were employed to estimate the influence of groundwater flow variations on ethanol and dissolved BTEX transport, and the associated biodegradation rates of different gasohol blend spills. Ethanol and BTEX groundwater flow were quantified in terms of breakthrough curve characteristics, plume centroid positions and spreading, source depletion and mass degradation rates. In addition, bromide migration was evaluated to address the contribution of flow-driven dissolution. Results

revealed that the high amount of ethanol along with a fast and dynamic flow exerted a flushing behavior that enhanced BTEX dissolution, migration (vertical and horizontal) and concentrations in groundwater. The higher amount of ethanol in E85 enhanced BTEX dissolution (and bioavailability) relative to E24 site and led to faster biodegradation rates, which can be explained by the cosolvency effect and metabolic flux dilution. Therefore, flow field dynamics and high ethanol content in gasohol blends enhance BTEX migration and biodegradation in gasohol-contaminated sites. The balance of these factors is crucial to determine fate and transport of contaminants in field sites. These findings suggest that hydraulic regime should be spatially and temporally characterized to support decisions on appropriate monitoring plan and remedial strategies for gasohol spills.

Figura 28 – Graphical abstract describing how migration and biodegradation may affect decreasing of dissolved mass plot.



Keywords: Transient flow, dissolution, BTEX, plume spreading, biodegradation rate, transport

Highlights:

- Two long-term controlled gasohol releases (E85 and E24) were monitored
- High amount of ethanol in E85 increased BTEX concentrations in groundwater
- Elevated BTEX concentrations led to higher degradation rates (relative to E24)
- Recharge and water-table fluctuations enhanced BTEX dissolution and migration
- Hydraulic regime supports decisions on proper monitoring and remediation strategies

3.4.1 Introduction

Gasohol spills by accidental or incidental releases may readily descend through the soil column and pollute the subsurface. The dissolution of highly toxic and recalcitrant organic compounds present in gasoline can pose serious threats to human health and groundwater resources, as they are transported away from the source and can potentially reach sensitive receptors. Ethanol was primarily added to gasoline to replace MTBE (methyl tertiary-butyl ether) and reduce the environmental impacts related with MTBE high solubility and low biodegradation rates (Powers et al., 2001). Consequently, the incidence of ethanol-gasoline blends contamination increased as MTBE was phased out. The fate and transport of the organic compounds in the subsurface are generally affected by several processes such as volatilization, dissolution, advection, dispersion, diffusion, sorption and biological transformations (Schirmer and Butler, 2004). Moreover, the presence of ethanol and gasoline in fuel storage facilities or contaminated areas can also affect their degradation and mobility in groundwater and thus, must be addressed to predict the fate of multiple organic compounds in dynamic aquifers (Molson et al. 2002). High ethanol concentrations (above 10%) can exert a cosolvency effect on organic compounds present in gasoline formulations, including priority contaminants such as monoaromatic hydrocarbons (benzene, toluene, ethyl-benzene, xylenes, known as BTEX) and increase their dissolution into the aqueous phase (Powers et al. 2001; Corseuil et al., 2004). This can lead to a fast and complete dissolution of NAPLs (Non-Aqueous Phase Liquids) source, resulting in higher groundwater downgradient concentrations of recalcitrant and carcinogenic compounds (e.g. benzene) (Brooks et al., 2004) that thereby, increase the associated risk of exposure.

The effect of ethanol on gasoline spills in the subsurface has been extensively studied and the main observed features can be summarized as follows: (1) cosolvency of several gasoline components (e.g. BTEX) enhancing their solubility in aqueous-phase and remobilizing pre-existing NAPLs (McDowell et al. 2003; Falta et al. 1998; Jawitz et al., 2000); (2) collapse of capillary fringe, which influences the vertical migration velocity and the lateral distribution of the free-product zone (Henry and Smith, 2002; Yu et al. 2009); (3) preferential ethanol biodegradation followed by the depletion of favorable electron acceptors (e.g. O_2 , NO_3^- , Fe^{3+} , etc.) and lower BTEX biodegradation rates (Corseuil et al., 1998; Mackay et al., 2006); (4) decreasing sorption-related retardation of hydrocarbons (Da Silva and Alvarez, 2002); (5) microbial biostimulation

and growth inhibition at high ethanol concentrations ($10 \text{ g}\cdot\text{L}^{-1}$), (Capiro et al., 2008; Rasa et al., 2013). In addition to this, some studies underlined a preferential retention of ethanol in vadose zone and into capillary fringe due to the partitioning to the pore-water (McDowell and Powers, 2003). Nevertheless, McDowell and Powers (2003) carried out their studies under stationary water table, whereas natural water table fluctuations cause capillary fringe mixing (Fetter, 2001) and may further release retained ethanol. These confounding effects may be mitigated under laboratory conditions (Gomez et al. 2008, Yu et al. 2009). However, laboratory studies are unable to reproduce a complex natural environment or account for field site-specific conditions and phenomena. To discern the effect of ethanol in gasohol blends on aromatic hydrocarbons biodegradation, Freitas et al. (2011) carried out field experiments of contaminant spills without ethanol (E0), as well as in gasohol mixtures with 10% (E10) and 95% (E95) of ethanol. The results demonstrated that BTEX biodegradation rates in groundwater were lower for high ethanol gasohol blends due to depletion of available dissolved oxygen, whilst for the no-ethanol spill and the low ethanol content blend no significant effect on BTEX biodegradation rates was observed. Conversely, Gomez and Alvarez (2010) used a numerical model to study the effects of five alcohols on the natural attenuation of benzene and claimed that high-ethanol content fuels (i.e. E85) result in smaller, shorter-lived benzene plumes in groundwater when compared to low-ethanol blends (i.e. E10). Corseuil et al. (2011a) observed a short-lived inhibitory effect of ethanol and acetate on BTEX biodegradation, demonstrating that monitored natural attenuation (MNA) can be a viable remediation strategy to deal with gasohol residual sources (E24). Corseuil et al. (2015) demonstrated the potential benefits of augmenting the electron acceptor pool with nitrate to accelerate ethanol removal mitigate its inhibitory effects on BTEX compounds and speed up their biodegradation. Lastly, Steiner et al. (2018) showed that for gasohol blends with low-ethanol content (i.e., 10%), MNA can provide slightly higher BTEX degradation rates compared to nitrate biostimulation, provided that the aquifer geochemical conditions offer a sufficient electron acceptor pool for aromatic hydrocarbons biodegradation.

Field studies normally conduct limited spatial and temporal hydrogeological characterization of groundwater that can be conducive to unreliable monitoring plans and negatively affect remediation strategies. Shallow aquifers, which are commonly affected by contamination, often exhibit a significant temporal variability in water level position, thickness of unsaturated and capillary zones and directions of groundwater flow

which may affect migration, dissolution and biodegradation rates (Davis et al. 1999; Prommer et al. 2002; Zhang et al., 2009). Rein et al. (2009) showed through numerical simulations that transient flow conditions represent a critical source of uncertainties in field measurements, as they are conducive to significant temporal fluctuations of the contaminants concentration in the monitoring wells. Dobson et al. (2007) demonstrated that water-table fluctuations in contaminated aquifers increased the elution of dissolved LNAPL components and thus, enhanced the risk of exposure of downgradient receptors. In addition, water-table fluctuations along with transient changes in groundwater direction and flow focusing into highly permeable heterogeneities are claimed to be the main drivers for solute mixing, especially for transverse plume spreading (Werth et al., 2006; Rolle et al., 2009). Since biodegradation rates may be controlled by the mixing process, which supports interchanges between electron donor and acceptor (Cirpka et al. 1999), recharge events may result in higher biodegradation rates by means of groundwater fluctuations and oxygen mixing (Schirmer et al., 2000). Although limited attention has been given towards transient hydraulic effects in full-scale experiments, they can have an overriding significance for monitoring plans and remediation strategies for gasohol spills.

In this contribution, two long-term (5 and 10 years) controlled releases of gasohol blends (E85 and E24) were monitored to discern the role exerted by groundwater flow dynamics on ethanol/BTEX plumes migration and degradation rates. This work aims to advance the current understanding on gasohol spills with different ethanol content and overall site remediation by addressing the contribution of groundwater flow field and site-specific transport rates on ethanol and BTEX plume dynamics and lifespan.

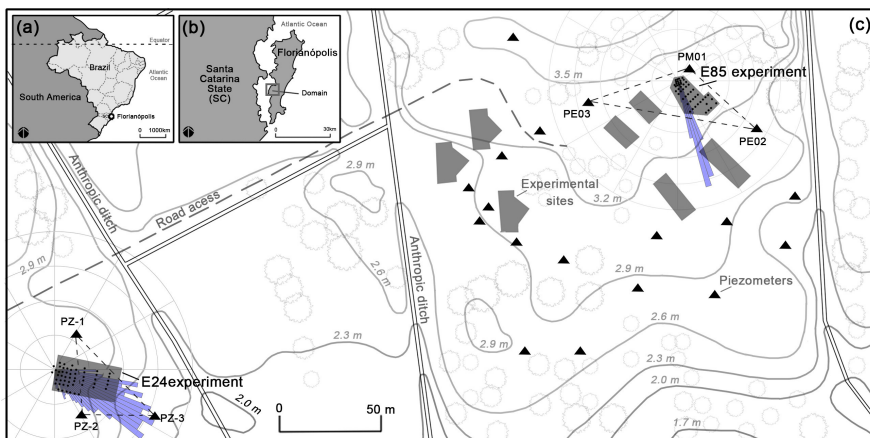
3.4.2 Materials and Methods

3.4.2.1 Site description

The controlled releases of gasohol blends were carried out at Ressacada Experimental Farm, in Florianópolis, Santa Catarina, Brazil (latitude 27°30'S, longitude 48°30'W) (Fig. 29). The climate is humid subtropical with average groundwater temperature of 22 °C and mean annual precipitation varies from 1,100 to 2,700 mm·y⁻¹. Rainfall is highly variable and more intense during the summer season. The study area represents a shallow coastal aquifer (30–40 m thick) with an average depth to water level in the range of 0.3 to 2.0 m, featured by sharp and

quick transient fluctuations driven by rainfall events (Rama et al., 2017). The aquifer is located in a flat coastal plain (up to 5 m in elevation) of about 20 km², enclosed by surface water bodies. Nevertheless, the tidal fluctuations have negligible influence on water-table levels when compared to rainfall infiltration (Rama et al., 2018). A dense net of rivers, ponds and anthropogenic ditches controls groundwater drainage in the plain (Fig. 29).

Figura 29 - Location of experimental sites: (a) map of Brazil; (b) map of Florianópolis; (c) detailed map of the E24 and E85 experimental sites depicting the monitoring wells (black points), local directions of groundwater flow estimated according to the method described in Section 2.5 (light blue polar diagram), piezometers positions (black triangles) and designations (e.g. PE03, PZ-1, etc.), surface elevation above mean sea level (light grey isolines and numbers in *italic*) and other field experiments (grey polygons).



The aquifer is composed of unconsolidated deposits of lacustrine and marine fine quartz sands with hydraulic conductivity values in the range of 10⁻³ to 10⁻⁴ cm.s⁻¹ (Lage, 2005). Irregularly distributed lenses of silt and clay are present in the plain and mangrove swamps areas are located at surface water receptors. The typical subsurface sample contains about 90% of sand, 3% of silt and 7% of clay, although higher silt and clay contents (up to 20%) were observed in several samples (Lage, 2005). The average organic matter content in the top layer (0.82 m depth) is 1.16% and decreases in a vertical direction (from 2 to 4 m depth) to 0.06% (standard deviation of 0.03%) (Fernandes, 2002).

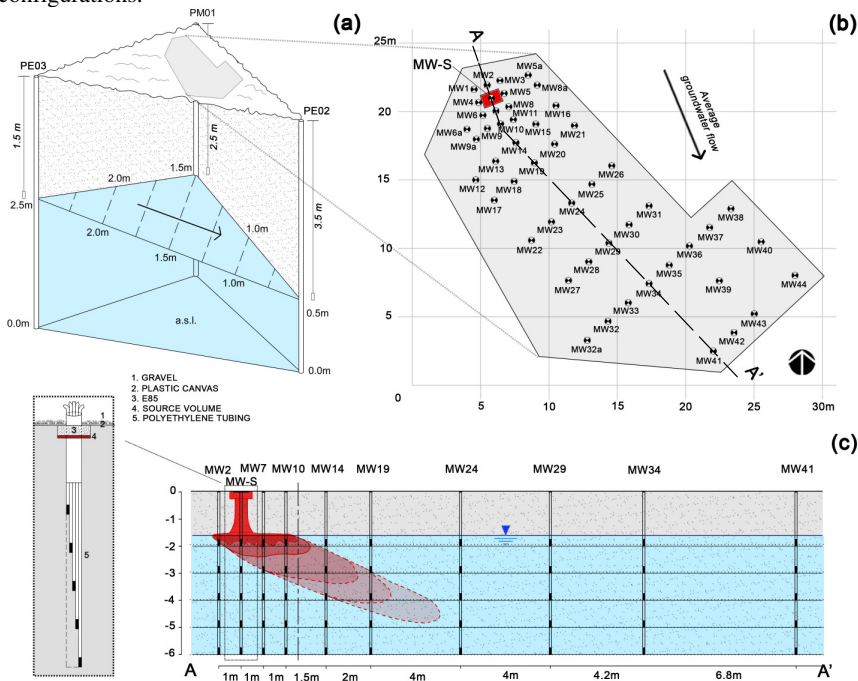
3.4.2.2 E85 field experiment

The experiment was established by releasing 200L of E85 (85% ethanol and 15% gasoline v/v) and 2.5 kg of the conservative tracer - potassium bromide (previously diluted in the 200L-blend) into an excavated pit of 1.5 x 1.0 x 0.25 m in the unsaturated zone (Fig. 30). When the experiment started (September 8, 2010), the water-table depth was 1.6 m below ground surface (bgs) or 1.35 m below the bottom of the excavation pit. The area was monitored with a total of 50 multilevel (2, 3, 4, 5 and 6 m bgs) monitoring wells (MW). Groundwater sampling was conducted using a peristaltic pump connected to each level by a polyethylene tubing (Fig. 30b). The wells were installed downgradient to the source of contamination (NW-SE). The free-product zone (FPZ), which represents the free NAPL “floated” on the top of the aquifer as a result of infiltration process, extends beyond the source zone affecting a larger area (bright red area in Fig. 30c). A recharge ratio of 43% of precipitation varies from 36 to 52% on a monthly basis (Rama et al., 2018). Groundwater background geochemical conditions were: pH 4.9 +/- 0.2; specific conductance 0.04 +/- 0.008 $\mu\text{S}\cdot\text{cm}^{-1}$; redox potential 191 +/- 60 mV, bromide 0.05 +/- 0.03 mg L^{-1} and phosphate 0.09 +/- 0.03 mg L^{-1} . Background electron acceptors concentrations and shifts over time are available in the Apêndice B (Tab.S1).

An adjacent field experiment with E24 (24% ethanol and 76% gasoline v/v) located at a distance of 400 m (Fig.29c) was used to provide insight into the different dynamics undergone by gasohol blends with a different ethanol content (85% and 24%), source position relative to the water table (135 and 0 cm, for E85 and E24 respectively) and local flow field conditions. This experiment started in 1998 with the release of 100L of E24 blend into a 1.5 x 1.0 x 1.5 m pit (Corseuil et al., 2011a). Both experimental sites were covered with a plastic impermeable canvas overlaid by coarse uniform gravel to avoid direct rainfall infiltration.

The mean hydraulic conductivity values estimated with slug tests were $8.81\times 10^{-4}\text{cm}\cdot\text{s}^{-1}$ and $1.1\times 10^{-4}\text{cm}\cdot\text{s}^{-1}$ (Corseuil et al., 2011b) at E85 and E24, respectively. The average hydraulic gradient at E24 (0.011 +/- 0.0041 m/m) was approximately two times higher than at E85 (0.0067 +/- 0.0018 m/m). Saturated effective porosity was 0.2 (Corseuil et al., 2011b) and 0.28 (Müller et al., 2017) at E24 and E85, respectively. These data were used to calculate the local seepage velocities by applying the Darcy's law.

Figura 30 - E85 experiment conceptual sketch: (a) geometrical interpretation of water-table inclination and groundwater flow direction; (b) position of 50 multilevel monitoring wells (circles), source area (red rectangle) and the mask adopted for the plume interpolation (grey area); (c) A-A' transect with conceptual gasohol distribution and detailed sketch of monitoring well with sampling depths configurations.



3.4.2.3 Physical and geochemical analysis

The E85 biodegradation and migration were monitored through ethanol and BTEX concentrations and their anaerobic metabolites, acetate and methane. Background groundwater geochemical conditions were determined at sampling events conducted at 160 and 41 days before the release. After E85 was released, 15 sampling events (SE) were conducted over 1,540 days: the first 10 SE (sampling interval 1 to 15 days) aimed to monitor source depletion and mass-transfer mechanisms, while SE 11 to 15 (sampling interval 6-12 months) focused on plumes migration. Oxidation-reduction potential (ORP), pH and dissolved oxygen were measured on site using a Micropurge Flow Cell (MP20) and a peristaltic pump (Millipore Easy-Load model XX80EL000). Bromide and acetate

were analyzed by ion chromatography using a Dionex ICS-3000 equipped with a conductivity detector (Software Chromeleon PN 6.40), an AS4A-SC column, with two eluents: sodium carbonate and sodium bicarbonate (APHA, 1992). BTEX, ethanol and methane were measured by gas chromatography with a HP 6890 II chromatographer coupled with a HP 7694 headspace auto sampler and a flame ionization detector (FID). A methyl-siloxane capillary column, HP 1 (30 m × 0.53 mm × 2.65 μm) was used. Samples were collected into capped sterile glass vials without headspace to prevent volatilization losses. Detection limits were as follows: bromide (0.1 mg.L⁻¹), acetate (1 mg.L⁻¹), ethanol (1 mg.L⁻¹), methane (10 μg.L⁻¹) and BTEX (1 μg.L⁻¹). Free-phase NAPL samples or free-product samples (FPS) indicate water samples that show visible dual-phase or a BTEX concentration above aqueous saturation limits, and for this reason were not accounted in the dissolved mass.

Transient hydraulic gradients and directions were estimated from the triangulation of the closest hydraulic head records in both experiments to allow a reliable flow field reconstruction over time (Fig. 30a). Water level was monitored by a manual phreatimeter with variable recording intervals (1–60 days). Saturated hydraulic conductivity was estimated from two slug test campaigns in different seasons (summer and autumn). Bouwer and Rice method was utilized to interpret the data and to determine hydraulic conductivity (Butler, 1997).

3.4.2.4 Microbial Analysis

Real-time quantitative polymerase chain reaction (qPCR) was used to estimate the concentration of total Bacteria to evaluate bacterial growth and Archaea (groups Crenarchaeota and Euryarchaeota), which includes methanogens. A total of 5 sampling events before (background) and after the release (72; 918; 1,161 and 1,532 days after the release) were conducted at the E85 site. For DNA extraction, 1L of groundwater was collected and samples were subsequently filtered with a 0.22 mm Millipore membrane filter (Sartorius Stedim Biotech, Gottingen, Germany). DNA was extracted using a MoBio Power Soil™ (Carlsbad, CA) kit, following the manufacturer's protocol. Primer sequences and PCR assays details can be found elsewhere (Ramos et al., 2013). Next-generation sequencing (16S rRNA gene sequencing) were conducted for E85 experiment (MW-23 at 1,161 days after the release and MW-25 and source at 1,532 days) to characterize microbial populations profile at the site. Briefly, Illumina Miseq platform was used for the sequencing of regions V3 and V4 that were amplified by PCR. Bioinformatics was

conducted by the Quantitative Insights Into Microbial Ecology (QUIIME, v1.9.0, <http://qiime.org/index.html>) software and Greengenes was used as database to obtain taxonomic information. Details are described in Müller et al. (2017).

3.4.2.5 Hydrogeological and statistical data processing

Different lines of evidences (LoE) were used to discern the ongoing predominant biotic and abiotic processes in the experimental sites. Accordingly, in order to associate plume migration, maximum concentration occurrences and flow field variations, geometrical rules were applied to triangulate information from monitored head records, simplifying the unconfined aquifer with a plane. As depicted in Fig.30a, the plane was defined by passing through three points to establish the dip angle and direction (strike + 90°), which represent the water-table inclination and the direction of groundwater flow, respectively. In addition, geochemical and microbial analyses were employed to evaluate the different dynamics undergone by E85 and E24 blends in groundwater. An exploratory analysis on concentrations was conducted for the conservative tracer (bromide), organic contaminants (ethanol and BTEX) and main metabolites (methane and acetate). The dataset was previously transformed to deal with the large amount of data assigned as below the detection limit (BDL) or non-detected values (ND).

Means and standard deviations for each series were calculated from a linear regression of expected normal scores (Z-scores) (Gineval and Splitstone, 2003). The methodology consists in a linear regression of the known standard concentrations, firstly converting the ranks of the data into cumulative percentiles. Observations from a normal distribution tend to fall on a straight line when plotted against their Z-Scores, even for ND values. Thus, the fitting line intercept indicate the mean of distribution, while the slope of the line gives the standard deviation. Such values were used to fix NDs data following the same distribution of the raw data (Fig. S1 - Apêndice B). Hence, a normal distribution was applied to NDs in the dataset.

The cosolvency model was applied to distinguish the BTEX free-product from the dissolved-phase in full-scale experiments with high-ethanol blends (Corseuil and Fernandes, 1999; Powers et al., 2001). The model states that ethanol (a hydrophilic compound) can reduce the polarity of aqueous phase, modifying the solubility of hydrocarbons in groundwater systems and enhancing the saturation concentration based on Raoult's law. Detailed information about the calculus of the saturation

concentration of BTEX at E85 site is available in the Apêndice B (Tab. S2).

The dissolution and persistence of ethanol and BTEX in groundwater, as well as the production of their corresponding metabolites (acetate and methane) were graphically depicted on the breakthrough curves of concentration (BTC). Plume stability and trend analysis for bromide, ethanol and BTEX were built using MATLAB to assess sites under natural attenuation with a well-established and consistent monitoring over a given time frame (Ricker, 2008). The method is applied only to dissolved contaminants and corresponds to a combination of graphical and statistical analysis, based on the spatial interpolation of data from multilevel monitoring wells in the experimental site, aiming to define isocontour maps for every compound, depth levels and SE. This allows the calculation of dissolved mass in every SE by summing results per level. Detection limits (DL) were used to contour plumes for each compound. While a 35×30×5.5 m domain was applied for E24 area, a 33×33×7 m domain was used for the interpolation of E85 data, both deploying a regular grid spacing of 0.1×0.1×0.25 m. A mask was adopted to limit extrapolated values out of the monitored sites (Fig. 30b). Raw concentration data were log transformed to obtain normal distribution and reduced coefficient of variation (ratio of standard deviation and mean) and kriging interpolator was used to plot contour maps.

The zero-order momentum of concentration over time was used to estimate total dissolved mass at the site. Plume centroid position was obtained by the estimation of first-order momentum. A plume center of mass represents the centroid of interpolated contour plume. Conceptually, it is a mass weighed-mean of every unit volume along three main directions (Freyberg, 1986; Dentz et al., 2000). The position of mass centroid was chosen to represent plume migration less sensitive to heterogeneous spatial distribution of contaminants. Finally, neglecting the local-scale mixing, the estimation of central second-order spatial moments provided direct plume-spreading information (Cirpka, 2002). Therefore, in order to quantify combined impacts of groundwater flow and the ethanol cosolvency in both areas, plumes lifespan (normalized dissolved mass, centroid position, distance to source, spreading) were plotted over time. Total accuracy of the method was equal to maximum mass recovery of dissolved bromide (about 66% of initial released mass). The mass losses can be related to experimental limitations, such as spacing between monitoring wells and depth levels, gaps between sampling events or spatial interpolation efficiency.

The linear fitting (zero-order kinetics) of bromide mass decrease was used to represent migration of compounds (forced by groundwater flow field) beyond the assumed mask. Site-specific transport rates were estimated by dividing bromide zero-order fitting rates for the total bromide mass released. First-order kinetics are commonly used to describe BTEX and ethanol degradation rates in aquifers, by fitting dissolved masses versus time to an exponential decay model (Alvarez and Illman, 2006, Corseuil et al., 2015; Steiner et al., 2018). Nonetheless, these rates do not discern between migration and biodegradation processes. Thus, biodegradation rates were obtained by subtracting transport rates (bromide advective-dispersive transport-related) from the reactive compounds first-order degradation rates. Finally, ethanol and BTEX biodegradation rates were determined after the onset of ethanol and BTEX degradation.

3.4.3 Results and Discussion

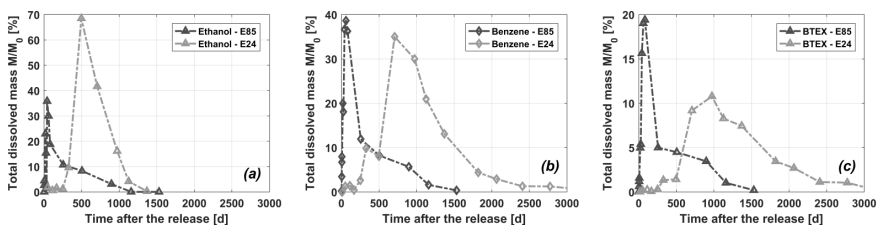
3.4.3.1 Centroid analysis, plume migration and groundwater flow field

The ethanol content in different gasohol blends can markedly affect aromatic hydrocarbons dissolution into the groundwater. Accordingly, in E85 plot BTEX compounds exhibited a faster and enhanced dissolution relative to E24 (Fig. 31). This was attributed to the cosolvency effect exerted by high dissolved mass of ethanol (≈ 50 kg) that thereby enhanced aromatic hydrocarbons dissolution and resulted in high BTEX plume concentrations (≈ 20 mg L⁻¹). The fast ethanol and BTEX dissolution into the groundwater was evidenced by the peak of dissolved mass after 42 and 83 days, respectively (Fig. 31a and Fig. 31c). This implies that high concentrations of dissolved BTEX can rapidly migrate away from the source zone, enhancing the potential risk to downgradient sensitive receptors. In contrast, BTEX compounds dissolution and corresponding aqueous average concentrations were significantly lower in E24 site (≈ 5 mg L⁻¹), as ethanol content was probably not high enough (less than 15 kg) to exert cosolvency effect. The E24 site showed a typically slow dissolution of aromatic hydrocarbons (Corseuil et al., 2011a), reaching a maximum dissolved mass at 1,000 days following the release, which corresponded to the half of the observed percentage for BTEX in E85 plot (Fig. 31c). Thus, although the amount of gasoline released in E24 (76L) was 2.5 times higher than in E85 (30L), BTEX compounds exhibited an opposite trend by rapidly (after 83 days) reaching peak dissolved concentrations and dissolved mass percentage in

E85 site, due to the cosolvency effect exerted by the high ethanol content in the gasohol blend.

The cosolvency effect was more apparent for the higher molecular weight and less soluble BTEX compounds (ethyl-benzene and xylenes), while benzene presented similar maximum dissolved percentage in both E24 and E85 sites (Fig. 31b). Thus, BTEX plot showed that 12% of initial mass was dissolved in E24 while such percentage increased to about 20% in E85 (Fig. 31c). This behavior is justified by the ratio of the saturation concentration (enhanced by the cosolvency) to the original compound solubility (Tab.S2 - Apêndice B). Such a ratio, which increased with the molecular weight, indicates the effect of the cosolvency on enhancing the maximum solubility of the compound and results in significantly higher dissolved mass for ethyl-benzene (3.7) and xylenes (3.8) relative to benzene (1.9). Hence, the difference in the maximum dissolved mass between E24 and E85 was more pronounced for ethyl-benzene and xylenes than benzene.

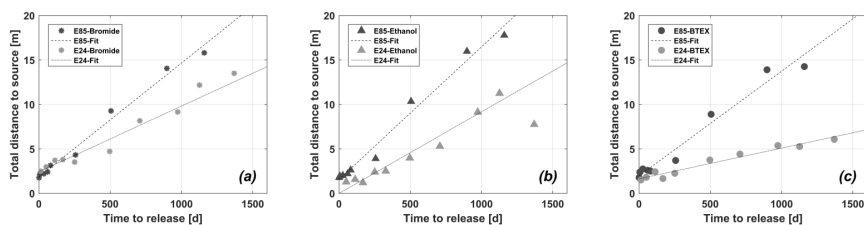
Figura 31 - Total dissolved mass (%) over time: (a) ethanol, (b) benzene, and (c) BTEX in E85 and E24 experimental sites.



Contaminant plumes are typically formed after compounds dissolve into the groundwater and their behavior (e.g. position, geometry) is highly dependent on the hydraulic regime (Dobson et al., 2007). Accordingly, at E85 the BTEX, ethanol and bromide plumes migrated concomitantly, at similar velocities (between 4.5 and 6.2 m·y⁻¹) and followed the local groundwater flow direction, moving faster in horizontal and downward directions, as evidenced by the close position of centroids (Fig. 32 and Fig. 33). Conversely, at E24 the bromide, ethanol and BTEX plumes followed different migration pathways (Fig. 33). The ethanol plume velocity was similar (3.0 m·y⁻¹) to bromide (2.6 m·y⁻¹) but significantly higher than BTEX (1.2 m·y⁻¹), which is probably due to a sorption-related retardation of hydrocarbons (Fig. 32). Therefore, at E24 the BTEX plume exhibited a limited migration of plume centroid (5 m away from the source) when compared to E85 (15 m) during the

same timespan (Fig. 32c). The different dynamics undergone by BTEX, ethanol and bromide plumes in E85 and E24 sites was consistent with the average seepage velocities (Tab.1). In addition, a direct correlation between water-table levels and seepage velocity was observed for both experimental sites (Fig. S2 and Fig. S3 - Apêndice B), which was attributed to the periodic increase of hydraulic gradients due to the intense and prolonged rainfall events (Rama et al., 2018). This led to transient accelerations in the transport of contaminants, as the gradients are directly proportional to the seepage velocity. Thus, ethanol apparently exerted influence on BTEX compounds dissolution in the source zone that was conducive to high groundwater concentrations, while plume dynamics were predominantly affected by hydraulic effects and groundwater flow.

Figura 32 - Plume centroid migration: (a) bromide, (b) ethanol, and (c) BTEX in E24 and E85 sites. Dotted fitting lines represent plume centroid velocity.



The larger variability in groundwater direction and hydraulic gradient enhanced transversal spreading of plumes. Accordingly, despite the lower seepage velocity at E24, the bromide plume showed an enhanced dispersion relative to E85 (Fig. 33a) which is reflected by more dynamic groundwater flow (Tab. 8). These findings agreed with Bellin et al. (1996), who showed a plume dispersion affected by instability of the hydraulic gradient over time. Likewise, the total range of directions in E24 reached 90°, whereas in the E85 site it was limited to 30° (Fig.29c). The E85 site was characterized by a slower shift of flow direction, with long periods (2-6 months) in which groundwater flow presented homogeneous deviations from the average direction. Low water levels were highly correlated with negative deviations of groundwater direction, as opposed to the higher levels that were associated with positive deviations (Fig. S2 - Apêndice B), suggesting an existence of a low-conductivity layer in the aquifer, which is probably dipped towards the east. Comparatively, in the E24 experiment, a more pronounced and quicker variability in the flow direction was observed (Fig. S3 - Apêndice B). The data suggests a random rotation of groundwater direction during

intense rainfall events (with no evident correlation with hydraulic heads), which was likely attributed to the position of the finer and, consequently, less conductive material in the E24 site.

Heterogeneities in permeability along with impulsive precipitation and differences in land use led to a different infiltration regime and thus, a local variability in transient groundwater flow directions and recharge. It is worth highlighting that as little as 10-15% of fine material admixture in a soil profile is enough to confer a low-permeability character of the porous medium (Mitchell, 1976). Thus, despite its geological homogeneity at regional-scale, the existing clay content in the site (up to 20%) is sufficient to significantly influence the local flow field and the migration of compounds. In addition, the close relation between small low-permeability lenses and, hydrodynamic dispersion (Werth et al., 2006) or back diffusion of contaminants (Chapman and Parker, 2005; Yang et al., 2014) has been shown. This is also consistent with the enhanced plume spreading in the E24 relative to E85 site (Fig. 33).

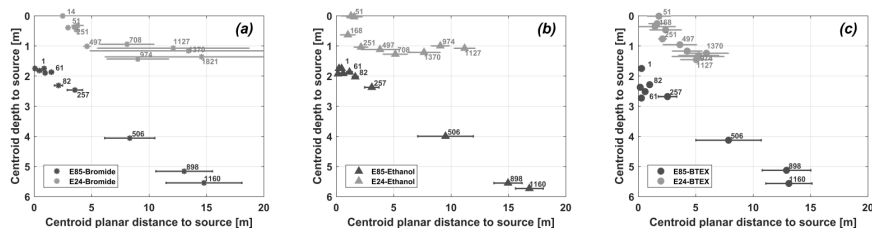
Tabela 8 - Groundwater flow characteristics from the transient analysis.

	E85	E24
Precipitation [mm/y]: Range	1600 - 2200	
Recharge [%]: Mean (range)	43% (39 - 55%)	
Hydraulic conductivity [cm/s]	8.81×10^{-4}	1.1×10^{-3}
Saturated effective porosity [-]	0.28	0.2
Average water-table level [m]: Range	1.0 - 2.9	1.3 - 3.1
Gradient [m/m]: Mean (std. dev.)	0.0067 (0.0018)	0.0114 (0.0041)
Direction [degrees]: Mean (std. dev.)	161.2° (10°)	127.7° (30°)
Seepage velocity [m/y]: Mean (std. dev.)	6.7 (0.8)	2.0 (1.0)

The sharp water-table fluctuations may prevent the retention of dissolved compounds within and above the capillary fringe. The E85 mass center moved vertically very quickly when compared with the E24 site (Fig. 33). For example, at the E85 site between 257 and 506 days from release, the ethanol centroid moved more than 1.5 m downwards and 7 m in a horizontal direction away from the source, while BTEX plume migrated 1 meter vertically and about 5 m horizontally. Such high velocities of contaminants vertical transport is likely due to the sudden water-table oscillations (recharge-related) that literally drag solutes downward, similar to a natural “vertical flushing” of the source zone. Conversely, in E24 site, the consistently lower conductivity of E24 (relative to E85) limited compounds transport, as evidenced by the low bromide (> 1.5 m downwards over 1821 days) and ethanol (> 1 meter downwards over whole monitoring period) centroid vertical migration (Fig. 33). Nevertheless, since the amplitude of water-table fluctuations

was similar in both sites (Fig. S2 and Fig. S3 - Apêndice B), the aquifer in E24 probably discharged laterally the flow related to the high hydraulic heads, as is the case for wetlands (Hayashi et al., 2016). Thus, the high variability of groundwater direction at the E24 may be caused by a hanged up “fill and spill” system (Tromp-van Meerveld and McDonnel, 2006) with an irregular groundwater connectivity. It is worth noting that the influence of vertical infiltration from precipitation events was dismissed, as both sites were covered with plastic impermeable canvas and gravel. Therefore, the plumes behavior is attributed to the combined effects of natural Darcy’s flow with “bottom-up” variations in water-table levels. The field data show that the transient flow regime directly affected spreading and position of the contaminants plumes (Davis et al., 1999). The flow field assessment indicated that the water-table plane in both experiments rotates in time, depending on the condition of recharge, heterogeneities and soil saturation. The faster and more regular groundwater flow in the E85 site seemed to be mainly related to the precipitation regime, while the highly variable flow field in the E24 site was probably forced to a lateral movement by hanged clay lenses and geological heterogeneities.

Figure 33 - Plume centroid position and spreading of (a) bromide, (b) ethanol, and (c) BTEX in E24 and E85 sites. Symbols represent centroid vertical and horizontal location (m) relative to source, bars show planar plume spreading (m) over time and numbers above the bars represent the time (days) after the release.

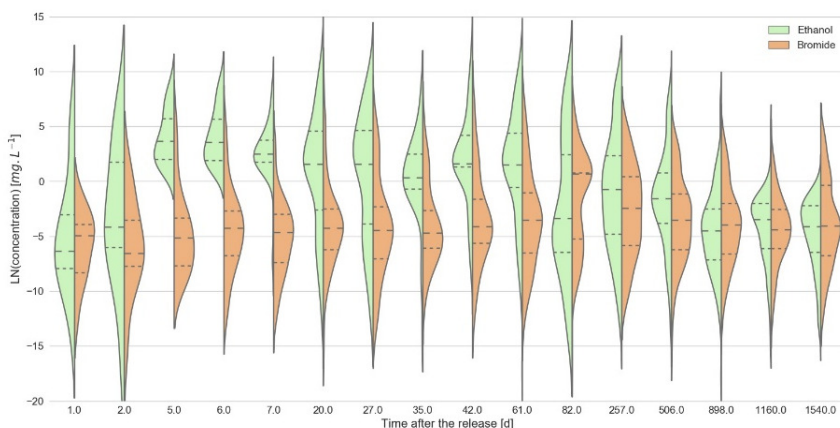


3.4.3.2 Geochemical footprint of E85 release

The statistical analysis depicted a lognormal distribution of ethanol and bromide concentrations at each sampling event for E85 plot (Fig.34). Violin plots median values showed the faster dissolution of ethanol that peaked only 5 days after the release, while bromide maximum dissolution occurred 83 days after the release. Since bromide and the gasohol blend were released together, such differences reflect the higher aqueous solubility of ethanol relative to bromide. In addition, violin plots revealed

a smoother variation of bromide shapes over time relative to the highly irregular ethanol distribution. This can be attributed to the conservative behavior of bromide as opposed to the highly biodegradable ethanol.

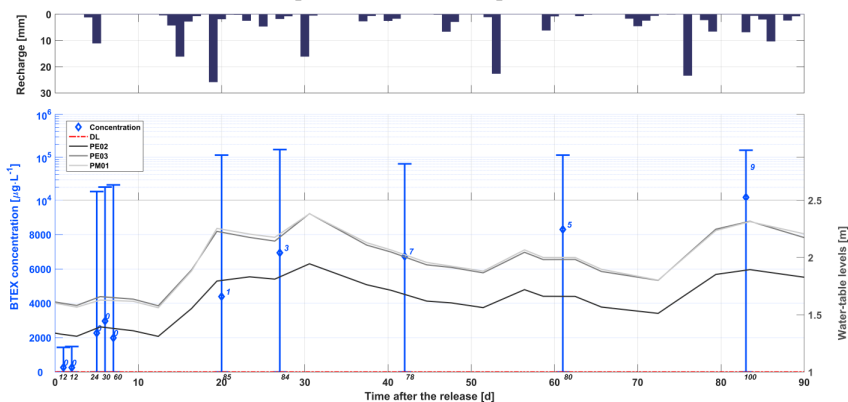
Figure 34 - Violin plot with distribution of bromide (salmon) and ethanol (green) concentrations. Loosely dashed lines represent the median, densely dashed lines are the interquartile intervals, while the shape of violins depicts the distribution.



A highly variable water table may enhance BTEX dissolution from the source or the free-product zone (FPZ), and the subsequent outcome would be a vertical downward migration of contaminants as the water table descends. In gasohol spills, the dissolved ethanol, which “floats” on the top of an aquifer, can remobilize retained BTEX in the vadose zone (McDowell et al. 2003; Falta, 1998). This seems to be the case of the E85 source area, as the high dissolved concentrations of BTEX coincided with the increase in water level and the intense recharge events (Fig. 35). The contaminants (ethanol and BTEX) rapidly reached the water table moving vertically 1.3 m in one day (Fig. 33). Such fast migration was attributed to the root channels and other preferential transport pathways (Jarvis 2007), which along with the high solubility of ethanol facilitates the movement. The high amount of ethanol could have also reduced the sorption of hydrocarbons, contributing to the vertical transfer of BTEX as well (Da Silva and Alvarez, 2002). During the initial water level increase (between 5 and 6 days after the release), the average concentration of BTEX in the aqueous-phase increased about 10 times, whereas after 20 days, a pronounced rising of aquifer water table resulted in a pulse enhanced concentration up to three-fold. Lastly, between 42 and 83 days after the release, average concentrations of BTEX doubled and maximum

values per sampling event continued to increase because of the high hydraulic head of the aquifer (Fig. 35). Thus, data confirmed a correlation between rainfall-driven processes (e.g. recharge, water-table variation) and the increasing dissolved BTEX concentrations in the source zone (Tab.S3 - Apêndice B).

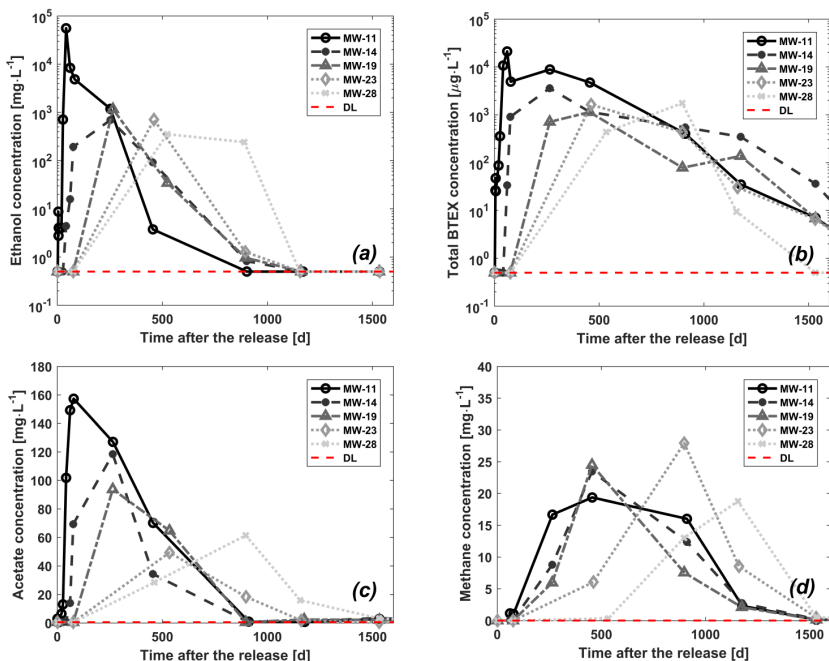
Figura 35 - Time series of average dissolved BTEX, water-table levels (dark and grey lines) and daily accumulated recharge (blue columns) within the first 90 days in the E85 site. The blue diamond markers represent mean values of concentration; errorbars show the range of concentrations; blue numbers represent the total of BTEX free-phase samples (FPS) in each sampling event, dashed red lines represent the detection limit and black numbers correspond to the total samples collected.



The combined effects of ethanol and aquifer fluctuation must be carefully accounted in sites impacted by gasohol spills as they can accelerate dissolution process and may compromise remediation plans based on the slow transfer hypotheses of persistent LNAPL sources that generally results in long-lasting contaminations. Free-phase product sample (FPS) occurrences started 18 days after the release, when the water table reached 2.25 m above sea level (0.7 m depth underneath the source), underlining a correlation between aquifer oscillation and NAPL migration. Hence, after 42 days, dual-phase samples collected at 3 m depth were dragged down with water table descent (between 27 and 42 days). In addition, groundwater samples highlighted a remarkable lateral migration of NAPL, probably due to the collapse of capillary fringe exerted by the high amount of ethanol. Twenty-five FPS were detected between 20 and 83 days after release in different wells (MW-F, MW-2, MW-5, MW-7, MW-8, MW-10, and MW-11). If they were accounted within the source region, in only 42 days, the initial spill area increased from 1.5 m² in the vadose zone to at least 5.6 m² of FPZ on the top of

saturated zone. These findings suggest that high ethanol content blends can lead to the fast NAPL mobilization due to ethanol-driven cosolvency and collapse of capillary fringe, resulting in large and irregular FPZs. However, despite the complexity of FPZ dissolved ethanol/BTEX compounds in the E85 site exhibited a comparable plume evolution (Fig. 32 and Fig. 33), showing similar and uniform shapes, which is consistent with Yu et al. (2009) observations. Therefore, our data demonstrate that ethanol content or transiency of groundwater flow exerts a larger influence on dissolved plume behavior when compared to the geometry of the contamination source.

Figure 36 - Times series of BTCs along the main direction of groundwater flow: MW-11 (source zone), MW-14 (3.7 m from source), MW-19 (5.7 m from source), MW-23 (10 m from source) and MW-28 (14 m from source). Each graph represents average concentrations in the vertical profile ($n=5$) of ethanol (a), total BTEX (b), acetate (c) and methane (d).

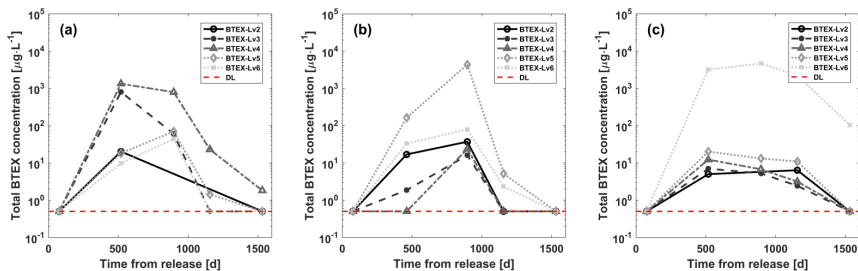


BTEX mass transfer in the E85 site was similar to an ethanol flushing of the source (Jawitz et al., 2000; Brooks et al., 2004). To exemplify, BTEX was readily transferred to the aqueous phase (the peaks occurred between 40 and 85 days) and exhibited low persistence, reaching

concentrations ($7 \mu\text{g}\cdot\text{L}^{-1}$) close to remediation goals within 1,600 days after release. Comparatively, such low source-zone concentrations were observed at the E24 site only after 5,000 days following the release. Although the highly soluble ethanol generally dissolves earlier than BTEX (Corseuil et al., 2011a) as a result of the limited aqueous solubility of the aromatic compounds, the breakthrough curves (BTC) in E85 plot showed peak concentrations of both ethanol and BTEX at the beginning of the experiment. As compounds migrated away from the source, peak concentrations of ethanol and BTEX were concomitantly detected in the MWs located in the main groundwater flow direction, demonstrating their concurrent dissolution and migration (Fig. 36). Likewise, centroid locations also indicated a pronounced migration of ethanol and BTEX plumes in E85 site (Fig. 32, Fig. 33), which is coherent with compounds enhanced dissolution exerted by the site hydraulic effects and the high ethanol content of the gasohol blend. The decrease in ethanol and BTEX concentrations was accompanied by the production of their anaerobic metabolites acetate and methane, thus providing evidence of ethanol and BTEX biodegradation (Fig. 36c, 36d).

The flow field characteristics can predict the migration of dissolved contaminants plumes and thereby support the decision on the most appropriate monitoring strategy. Contaminants concentration per sampling level indicated a sinking process of the dissolved compounds in the E85. The source-zone wells revealed high contaminants concentration at the upper level (2 m bgs), whereas at distant monitoring wells (MW-23 and MW-28 – located at 10 and 14 m away from the source, respectively) contaminants concentrated on the deeper levels (5 and 6 m bgs). Likewise, as previously mentioned in Section 3.1, the same phenomenon was observed for the E24 site, although it was less pronounced. The vertical drift is directly associated with the local flow field that contributes to a downward movement of the compounds. In addition, a plume inspection along a transect located 14 m away from the source shows the highest concentrations at 4 m bgs from the western boundary (MW-27 in Fig. 37a) and 6 m bgs from the eastern boundary (MW-31 in Fig. 37c). This nonhomogeneous distribution of concentrations is probably caused by a low permeability formation dipped towards the east that corroborates the anti-clockwise rotation of the main groundwater direction during dry periods (Apêndice B). Such changes in plume direction could be predicted with a time-series analysis of the flow field at contaminated sites. This underscores the importance of conducting a thorough hydrogeological assessment to properly select groundwater monitoring wells and track contaminants plume migration.

Figura 37 - Time series of BTEX BTC along transversal transect (14 m to source) from western to eastern boundary: MW-27 (a), MW-29 (b), MW-31 (c) organized per sampling depth to ground (Lv = level in meters bgs).



3.4.3.3 Ethanol and BTEX degradation kinetics

The faster dissolution of BTEX observed in the E85 site relative to E24 was attributed to the higher amount of ethanol that exerted cosolvency effect (Fig. 31). Accordingly, both BTEX and ethanol mass peaked at 85 days after the release (Fig. 39), thus demonstrating a similar dissolution dynamics. Degradation rates were determined after the onset of ethanol and BTEX biodegradation and, as they peaked concomitantly, similar initial timeframes were considered in the calculations (Tab.9). Unlike E85, in the E24 site, BTEX concentrations peaked after 970 days and the onset of their biodegradation was observed only after ethanol depletion (Fig. 39). It is worth noting that control experiments with gasoline alone would be useful to quantitatively discern the effects of ethanol.

The conservative tracer (bromide) zero-order mass decrease was used to represent migration of dissolved compounds forced by groundwater flow field at both experimental sites and to estimate transport rates. Results revealed a transport rate three times higher in E85 (0.242 y^{-1}) than E24 (0.092 y^{-1}) (Tab.10), which coincided with the flow field analysis (Section 3.1). This difference in mass decrease transport-related follows the ratio of seepage velocities between the sites, which can potentially avoid confounding effects in the estimation of contaminants biodegradation rates, since the area with faster flow (E85) also presented higher fitted decay rates. It worth stressing that fitted mass degradation values for ethanol and BTEX (Tab.9) agreed with results reported by other studies that used different methodologies (Corseuil et al.,2011a; Corseuil et al.,2015; Ramos et al.,2016; Steiner et al.,2018).

After subtracting specific transport rates from the reactive compounds degradation, the resulting first-order biodegradation rates were: ethanol 1.104 y^{-1} (E85) and 1.076 y^{-1} (E24), benzene 0.836 y^{-1} (E85) and 0.674 y^{-1} (E24) and in average for total BTEX 0.816 y^{-1} (E85) and 0.401 y^{-1} (E24) (Tab.9). These values are consistent with the range of rates reported elsewhere for ethanol and BTEX compounds (Alvarez et al. 1991; Corseuil et al., 1998). Therefore, the enhanced dissolution of BTEX in E85 site led to higher biodegradation rates relative to BTEX in E24 site.

Tabela 9- Estimation of ethanol, benzene and total BTEX first-order degradation rates, and degradation rates with subtracted transport rates and quality summary for E85 and E24 sites.

Compound (Site)	Time frame [y ⁻¹]	First-order degradation rates (95% Conf. Bounds) [y ⁻¹]	Degradation rates with subtracted transport rates [y ⁻¹]	R ²	n
Ethanol (E85)	0.1-4.2	1.346 (0.551 - 2.141)	1.104	0.959	7
Ethanol (E24)	1.4-4.1	1.168 (0.590 - 1.756)	1.076	0.969	5
Benzene (E85)	0.2-5.2	1.078 (0.891 - 1.266)	0.836	0.997	7
Benzene (E24)	2.7-10.5	0.766 (0.643 - 0.890)	0.674	0.995	10
BTEX (E85)	0.2-5.2	1.058 (0.553 - 1.582)	0.816	0.981	7
BTEX (E24)	2.7-10.5	0.493 (0.403 - 0.584)	0.401	0.967	10

Tabela 10- Estimation of decay rate of bromide mass and main parameters summary for E85 and E24 sites.

Tracer (Site)	Timeframe [y ⁻¹]	Zero-Order fitting rate (95% Conf. Bounds) [g.y ⁻¹]	Initial released mass [g]	Transport rate [y ⁻¹]	R ²	n
Bromide (E85)	2.5-5.2	406.6 (203.9 - 609.6)	1,678	0.242	0.974	4
Bromide (E24)	2.7-10.5	61.6 (53.4 - 69.7)	670	0.092	0.974	10

The higher BTEX biodegradation rates in E85 (relative to E24 site) could be attributed to the metabolic flux dilution phenomenon, as it predicts that removal rates are proportional to the fraction of the available substrates in the mixture (Lovanh and Alvarez, 2004). Accordingly, the metabolic flux dilution in E85 was evaluated at the source zone (MW-11) and compared with source zone (SW4) at E24 site (Corseuil et al., 2015). The enhanced dissolution (and availability) of BTEX in E85 site increased their source zone fraction in the mixture (ethanol/BTEX), as opposed to the lower dissolved BTEX concentrations and corresponding fraction in the mixture in E24 site (Fig. 38). Therefore, higher biodegradation rates were observed for BTEX in E85 site, which was likely due to their enhanced fraction in the mixture relative to E24 site. This is consistent with metabolic flux dilution that considers the simultaneous degradation of multiple substrates with compound-specific

degradation rates being proportional to their relative abundance in the mixture.

Figure 38 - Ethanol (circles) and BTEX (triangle) as total organic carbon (TOC) fractions in the mixture for E85 (MW11 – source zone) and E24 (SW4 – source zone) experiments.

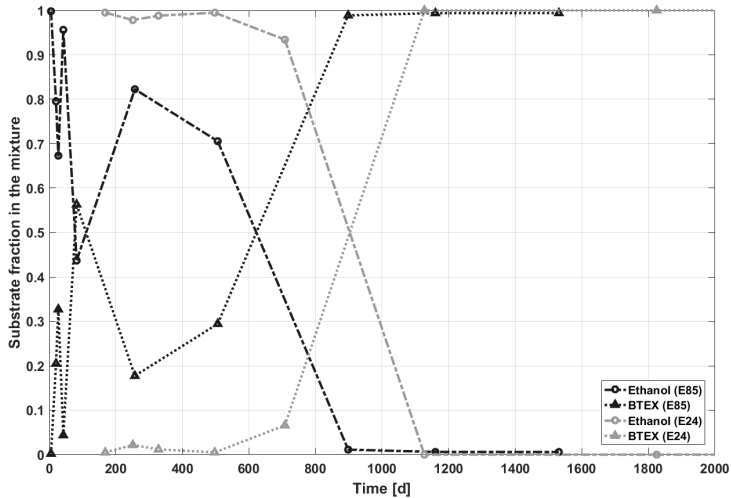
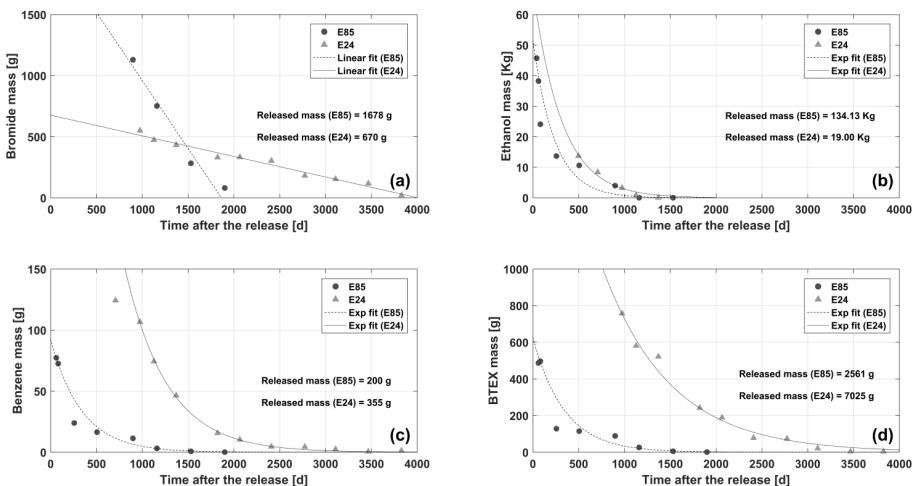
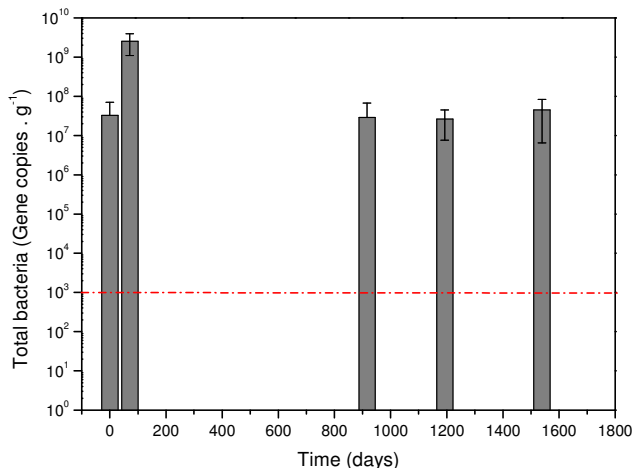


Figure 39 - Total mass decay obtained from plume interpolation for E24 and E85 sites: (a) linear fitting for bromide mass evolution, (b) exponential fitting for ethanol, (c) dissolved benzene and (d) total BTEX.



The higher removal rates observed for the E85 site are coherent with the stimulation of biomass and specific hydrocarbon degraders. Accordingly, after 72 days following the release total biomass growth increased up to 2 orders of magnitude ($\approx 2.5 \times 10^9$ gene copies g^{-1}) relative to the background concentration at the source-zone ($\approx 3 \times 10^7$ gene copies g^{-1}). This is consistent with the organic compounds infiltration and dissolution into the groundwater, as they were likely used as substrates for microbial growth. The migration of dissolved contaminants away from the source (Fig. 40 and Fig. 41) was reflected by the decrease in total biomass source-zone concentration at 918 days after the release, reaching a condition similar to the background (2.9×10^7 gene copies g^{-1}) that was observed until the end of the monitoring period (4.5×10^7 gene copies g^{-1} at 1,532 days after E85 release) (Fig. 40). Thus, although contaminants were partly consumed as substrates, the transport was likely the driving force as evidenced by the plume migration over the site, which justifies the return towards the original (unpolluted state) baseline microbial condition at the source zone.

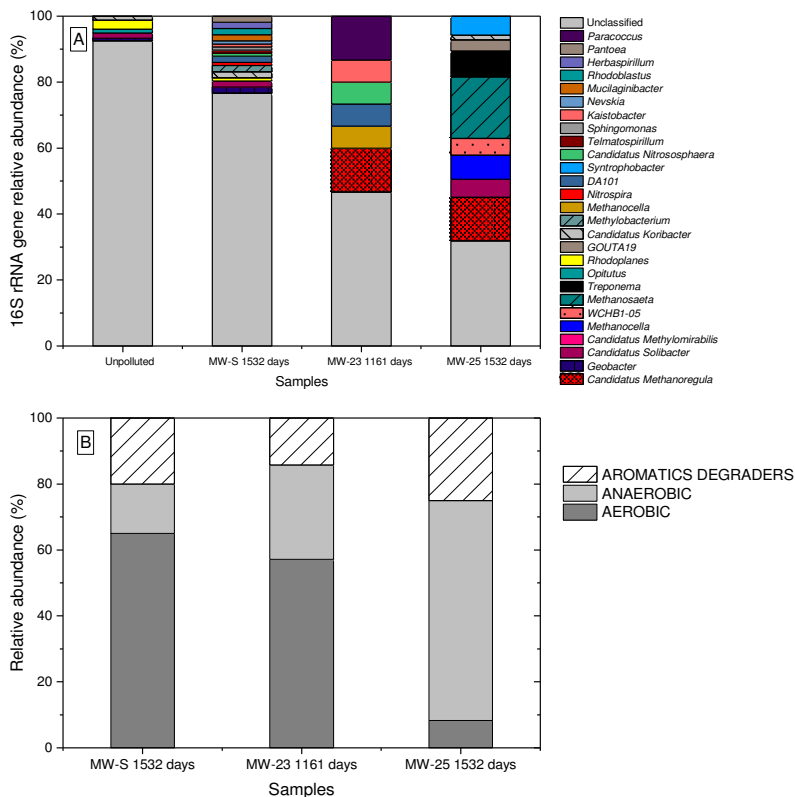
Figura 40 - Concentration of total bacteria (gene copies g^{-1}) at the source-zone of E85 experiment. Detection limit (dashed red lines) for total bacteria analysis was 103 gene copies g^{-1} .



Likewise, sequencing results revealed the presence of aromatic hydrocarbons degraders (Gouta 19, Treponema, WCHB1-05, Kaistobacter, Geobacter, Rhodoplanes, Sphingomonas) at the monitoring wells evaluated (MW-S, MW-23 and MW-25) (Fig. 41A and Fig. 41B), which is coherent with their exposure to BTEX compounds.

Anaerobic genera dominated wells MW-23 and MW-25, which was likely due to the presence of residual concentrations of BTEX (132 and 241 $\mu\text{g}\cdot\text{L}^{-1}$) that generally depletes the available dissolved oxygen and leads to the establishment of anaerobic zones, as evidenced by the negative ORP values (-36 and -1 mV) and methane production (8.5 and 4 $\text{mg}\cdot\text{L}^{-1}$). Comparatively, the source-zone microbial profile at 1,532 days was mainly composed by aerobic genera which can be supported by the absence of BTEX compounds at the source after 1,532 days, the positive ORP value (+ 222 mV) and methane concentration below the detection limit ($< 10 \mu\text{g}\cdot\text{L}^{-1}$).

Figura 41 - (A) 16S rRNA gene relative abundance (%) of microbial communities at E85 experiment at background (unpolluted) well, MW-S (source-zone), MW-23 and MW-25. Charts depict microbial genera with a relative abundance of $> 0.7\%$. (B) Microbial community respiration mode and aromatic hydrocarbons degraders relative abundance (%) in MW-S at 1532 days, MW23 at 1161 days and MW25 at 1532 days (without depicting unclassified genera).



Detailed information about the metabolism and respiration mode of the microbial genera detected in E85 site is available in the Apêndice B (Tab.S4). These findings provide converging lines of evidence of BTEX migration over the site and biodegradation thus, indicating that molecular biology can be used as a complementary tool for groundwater pollution monitoring, as communities shift according to the transient flow and geochemical conditions encountered at the site.

3.4.4 Conclusions

Spills of gasohol blends into phreatic aquifers subject to high recharge rates and sharp water-table fluctuations can undergo enhanced migration and degradation. Transient variations in groundwater flow velocity and direction, caused by the changes in recharge as well as geological heterogeneity, can enhance source dissolution, resulting in greater plume spreading and migration. This has significant implications for effective monitoring of groundwater pollutants and plume dynamics and lifespan. In controlled gasohol spills at Ressacada, Brazil, the sharp water-table fluctuations observed in E85 site dragged the compounds downwards, showing a fast vertical migration, while this effect was less pronounced in E24 site due to the lower hydraulic conductivity and the position of low-conductivity layers. Specific migration of bromide plumes showed significant differences in transport rates between the E85 (faster) and E24 (slower) sites, despite the fact that both sites are located at neighboring areas (400 m of distance). The higher seepage velocity in E85 relative to E24 resulted in a faster horizontal migration of plume center of mass (15 and 5 m, for E85 and E24, respectively), which underscores the critical influence of local flow field in contaminated sites assessment and the importance of subtracting flow-driven rates from the decay rates obtained by fitting field data to isolate biodegradation rates.

The high amount of ethanol in E85 site exerted cosolvency effect on BTEX and thereby enhanced their dissolution (within 85 days) and average concentrations (up to 20 mgL⁻¹) in groundwater. The high concentrations of BTEX led to faster degradation rates relative to E24 site and BTEX and ethanol were biodegraded concomitantly as opposed to the often observed ethanol preferential biodegradation. This was likely attributed to the metabolic flux dilution phenomenon as the relative biodegradability of a compound in a mixture of alternative substrates is often concentration-dependent and the degradation rates are proportional to their fraction in the substrates mixture. Therefore, BTEX and ethanol were biodegraded at similar rates. Comparatively, in E24 site BTEX

dissolution was significantly slower (maximum after 1000 days) and the onset of BTEX dissolution and biodegradation was only observed after ethanol depletion. Accordingly, BTEX degradation rates were slower (0.401 y^{-1} relative to 0.816 y^{-1}) and mass depletion was delayed (after 3800 days relative to 1600 days following the release) relative to E85 site. Total biomass was stimulated as ethanol and BTEX dissolved into the groundwater and shifts in microbial communities were driven by the transient flow and geochemical groundwater conditions at the E85 site. Thus, although the high amount of ethanol (in E85 site) enhanced BTEX dissolution, it led to fast degradation rates that speeded up BTEX compounds biodegradation, while their migration was determined by the local groundwater flow.

Overall, the practical implication of this work is that the groundwater flow field and high ethanol content in gasohol blends can significantly affect plume dynamics and lifespan, especially at sites under high recharge rates or fast groundwater flow. Accordingly, E85 site, due to a faster groundwater flow, showed an increased migration of contaminants relative to E24 (2.6 times higher), but also exhibited higher biodegradation rates (2.0 times higher), whilst E24 demonstrated a lower plume mobility and longer-lasting contamination due to the reduced biodegradation rates relative to E85. These factors must be carefully accounted to estimate the risk for downgradient receptors and to support decisions on monitoring plans and remedial actions. Simplified approaches that focus solely on a single component of the balance (e.g. degradation kinetics) cannot thoroughly assess plume behavior, especially in highly fluctuant or heterogeneous aquifers.

Acknowledgments

The authors want to acknowledge Fundação de Ensino e Engenharia de Santa Catarina (FEESC) and Petróleo Brasileiro (Petrobras) for the financial and material support (Project contract number: 0050.0096599.15.9). We also thank the technical staff from the Ressacada Experimental Farm and the REMA group for the field monitoring of water quality, and the PhD candidate Martina Pacifici (USP, PPGEC) for her help with the figure design. Finally, we thank Professor Dr. Timothy Vogel (Université de Lyon) for the Illumina Miseq sequencing.

References

- Alvarez, P.J.J., Anid, P.J., Vogel, T.M., 1991. Kinetics of aerobic biodegradation of benzene and toluene in sandy aquifer material. *Biodegradation* 2, 43–51. <https://doi.org/10.1007/BF00122424>
- Alvarez, P.J.J., Illman, W.A., 2006. *Bioremediation and natural attenuation: Process fundamentals and mathematical models*. John Wiley & Sons, Inc. p.604. <https://doi.org/10.1017/CBO9781107415324.004>
- American Public Health Association (APHA), 1992. *Standard methods for the examination of water and wastewater*, American Public Health Association, American Water Works Association and Water Pollution Control Federation, Washington, DC.

- Bellin, A., Dagan, G., Rubin, Y., 1996. The impact of head gradient transients on transport in heterogeneous formations: Application to the Borden Site. *Water Resour. Res.* 32, 2705–2713. <https://doi.org/10.1029/96WR01629>
- Brooks, M.C., Annable, M.D., Rao, P.S.C., Hatfield, K., Jawitz, J.W., Wise, W.R., Wood, A.L., Enfield, C.G., 2004. Controlled release, blind test of DNAPL remediation by ethanol flushing. *J. Contam. Hydrol.* 69, 281–297. [https://doi.org/10.1016/S0169-7722\(03\)00158-X](https://doi.org/10.1016/S0169-7722(03)00158-X)
- Butler, J. J. Jr., 1997. *The Design, Performance, and Analysis of Slug Tests (1st Edition)*. CRC Press. p.262. ISBN 9781566702300
- Cápiro, N.L., Da Silva, M.L.B., Stafford, B.P., Rixey, W.G., Alvarez, P.J.J., 2008. Microbial community response to a release of neat ethanol onto residual hydrocarbons in a pilot-scale aquifer tank. *Environ. Microbiol.* 10, 2236–2244. <https://doi.org/10.1111/j.1462-2920.2008.01645.x>
- Chapman, S.W., Parker, B.L., 2005. Plume persistence due to aquitard back diffusion following dense nonaqueous phase liquid source removal or isolation. *Water Resour. Res.* 41, 1–16. <https://doi.org/10.1029/2005WR004224>
- Cirpka, O.A., 2002. Choice of dispersion coefficients in reactive transport calculations on smoothed fields. *J. Contam. Hydrol.* 58, 261–282. [https://doi.org/10.1016/S0169-7722\(02\)00039-6](https://doi.org/10.1016/S0169-7722(02)00039-6)
- Cirpka, O.A., Frind, E.O., Helmig, R., 1999. Numerical simulation of biodegradation controlled by transverse mixing. *J. Contam. Hydrol.* 40, 159–182. [https://doi.org/10.1016/S0169-7722\(99\)00044-3](https://doi.org/10.1016/S0169-7722(99)00044-3)
- Corseuil, H.X., Fernandes, M., 1999. Efeito do etanol no aumento da solubilidade de compostos aromáticos presentes na gasolina brasileira. *Rev. Eng. Sanitária e Ambient.* 4, 71–75.
- Corseuil, H.X., Gomez, D.E., Schambeck, C.M., Ramos, D.T., Alvarez, P.J.J., 2015. Nitrate addition to groundwater impacted by ethanol-blended fuel accelerates ethanol removal and mitigates the associated metabolic flux dilution and inhibition of BTEX biodegradation. *J. Contam. Hydrol.* 174C, 1–9. <https://doi.org/10.1016/j.jconhyd.2014.12.004>
- Corseuil, H.X., Hunt, C.S., Santos, R.C.F. dos, Alvarez, P.J.J., 1998. The influence of the gasoline oxygenate ethanol on aerobic and anaerobic btx biodegradation. *Water Res.* 32, 2065–2072.
- Corseuil, H.X., Kaipper, B.I.A., Fernandes, M., 2004. Cosolvency effect in subsurface systems contaminated with petroleum hydrocarbons and ethanol. *Water Res.* 38, 1449–1456. <https://doi.org/10.1016/j.watres.2003.12.015>
- Corseuil, H.X., Monier, A.L., Fernandes, M., Schneider, M.R., Nunes, C.C., Do Rosario, M., Alvarez, P.J.J., 2011a. BTEX plume dynamics following an ethanol blend release: Geochemical footprint and thermodynamic constraints on natural attenuation. *Environ. Sci. Technol.* 45, 3422–3429. <https://doi.org/10.1021/es104055q>
- Corseuil, H.X., Monier, A.L., Fernandes, M., Schneider, M.R., Nunes, C.C., 2011b. BTEX plume dynamics following an ethanol blend release: Geochemical footprint and thermodynamic constraints on natural attenuation - Supporting Information. *Environ. Sci. Technol.* 23. <https://doi.org/10.1117/1111.2794018.2>
- Da Silva, M.L.B., Alvarez, P.J.J., 2002. Effects of Ethanol versus MTBE on Benzene, Toluene, Ethyl-benzene, and Xylene Natural Attenuation in Aquifer Columns. *J. Environ. Eng.* 128, 862–867. [https://doi.org/10.1061/\(ASCE\)0733-9372\(2002\)128:9\(862\)](https://doi.org/10.1061/(ASCE)0733-9372(2002)128:9(862))
- Davis, G.B., Barber, C., Power, T.R., Thierrin, J., Patterson, B.M., Rayner, J.L., Wu, Q., 1999. The variability and intrinsic remediation of a BTEX plume in anaerobic sulphate-rich groundwater. *J. Contam. Hydrol.* 36, 265–290. [https://doi.org/10.1016/S0169-7722\(98\)00148-X](https://doi.org/10.1016/S0169-7722(98)00148-X)
- Dentz, M., Kinzelbach, H., Attinger, S., Kinzelbach, W., 2000. Temporal behavior of a solute cloud in a heterogeneous porous medium 2. Spatially extended injection. *Water Resour. Res.* 36, 3605–3614.
- Dobson, R., Schroth, M.H., Zeyer, J., 2007. Effect of water-table fluctuation on dissolution and biodegradation of a multi-component, light nonaqueous-phase liquid. *J. Contam. Hydrol.* 94, 235–248. <https://doi.org/10.1016/j.jconhyd.2007.07.007>
- Falta, R.W., 1998. Using phase diagrams to predict the performance of cosolvent floods for NAPL remediation. *Gr. Water Monit. Remediat.* Summer, 94–102.
- Fernandes, M., 2002. *Atenuação natural de aquífero contaminado por derramamento de gasolina*. PhD thesis. UFSC. Universidade Federal de Santa Catarina, Florianópolis, Brazil. p.233

- Fetter, C.W., 2001. *Applied Hydrogeology* (4th edition). Prentice Hall. Upper Saddle River, NJ, USA. p.624. ISBN13 9780130882394
- Freitas, J.G., Mocanu, M.T., Zoby, J.L.G., Molson, J.W., Barker, J.F., 2011. Migration and fate of ethanol-enhanced gasoline in groundwater: A modelling analysis of a field experiment. *J. Contam. Hydrol.* 119, 25–43. <https://doi.org/10.1016/j.jconhyd.2010.08.007>
- Freyberg, D.L., 1986. A Natural Gradient Experiment on Solute Transport in a Sand Aquifer: 2. Spatial Moments and the Advection and Dispersion of Nonreactive Tracers. *Water Resour. Res.* 22, 2031–2046.
- Gineval, M.E., Splitstone, D.E., 2003. Statistical tools for environmental quality measurement. Chapter 5: *Procedures for Dealing with Censored Data*. Chapman & Hall CRC. p.256. ISBN 1-58488-157-7
- Gomez, D.E., Alvarez, P.J.J., 2010. Comparing the effects of various fuel alcohols on the natural attenuation of Benzene Plumes using a general substrate interaction model. *J. Contam. Hydrol.* 113, 66–76. <https://doi.org/10.1016/j.jconhyd.2010.02.002>
- Gomez, D.E., De Blanc, P.C., Rixey, W.G., Bedient, P.B., Alvarez, P.J.J., 2008. Modeling benzene plume elongation mechanisms exerted by ethanol using RT3D with a general substrate interaction module. *Water Resour. Res.* 44, 1–12. <https://doi.org/10.1029/2007WR006184>
- Hayashi, M., van der Kamp, G., Rosenberry, D.O., 2016. Hydrology of Prairie Wetlands: Understanding the Integrated Surface-Water and Groundwater Processes. *Wetlands* 36, 237–254. <https://doi.org/10.1007/s13157-016-0797-9>
- Henry, E.J., Smith, J.E., 2002. The effect of surface-active solutes on water flow and contaminant transport in variably saturated porous media with capillary fringe effects. *J. Contam. Hydrol.* 56, 247–270. [https://doi.org/10.1016/S0169-7722\(01\)00206-6](https://doi.org/10.1016/S0169-7722(01)00206-6)
- Jarvis, N.J., 2007. A review of non-equilibrium water flow and solute transport in soil macropores: Principles, controlling factors and consequences for water quality. *Eur. J. Soil Sci.* 58, 523–546. <https://doi.org/10.1111/j.1365-2389.2007.00915.x>
- Jawitz, J.W., Sillan, R.K., Annable, M.D., Rao, P.S.C., Warner, K., 2000. In-situ alcohol flushing of a DNAPL source zone at a dry cleaner site. *Environ. Sci. Technol.* 34, 3722–3729. <https://doi.org/10.1021/es9913737>
- Lage, I. de C., 2005. Avaliação de metodologias para determinação da permeabilidade em meios porosos: Fazenda Ressacada. MSc Thesis. UFRJ, Universidade Federal de Rio de Janeiro, Brazil. p.119
- Lovanh, N., Alvarez, P.J.J., 2004. Effect of ethanol, acetate, and phenol on toluene degradation activity and tod-lux expression in *Pseudomonas putida* TOD102: evaluation of the metabolic flux dilution model. *Biotechnology and Bioengineering* 86 (7), 801–808. doi:10.1002/bit.20090.
- Mackay, D.M., de Siewes, N.R., Einarsen, M.D., Feris, K.P., Pappas, A.A., Wood, I.A., Jacobson, L., Justice, L.G., Noske, M.N., Scow, K.M., Wilson, J.T., 2006. Impact of Ethanol on the Natural Attenuation of Benzene, Toluene, and o-Xylene in a Normally Sulfate-Reducing Aquifer. *Environ. Sci. Technol.* 40, 6123–6130. <https://doi.org/10.1021/es060505a>
- McDowell, C.J., Buscheck, T., Powers, S.E., 2003. Behavior of gasoline pools following a denatured ethanol spill. *Ground Water* 41, 746–757.
- McDowell, C.J., Powers, S.E., 2003. Mechanisms affecting the infiltration and distribution of ethanol-blended gasoline in the vadose zone. *Environ. Sci. Technol.* 37, 1803–1810. <https://doi.org/10.1021/es0259761>
- Mitchell, J.K., 1976. *Fundamentals of Soil Behavior*. John Wiley & Sons, Inc. New York, 422p.
- Molson, J.W., Barker, J.F., Frind, E.O., Schirmer, M., 2002. Modeling the impact of ethanol on the persistence of benzene in gasoline-contaminated groundwater. *Water Resour. Res.* 38, 4-1-4-12. <https://doi.org/10.1029/2001WR000589>
- Müller, J.B., Ramos, D.T., Larose, C., Fernandes, M., Lazzarin, H.S.C., Vogel, T.M., Corseuil, H.X., 2017. Combined iron and sulfate reduction biostimulation as a novel approach to enhance BTEX and PAH source-zone biodegradation in biodiesel blend-contaminated groundwater. *J. Hazard. Mater.* 326, 229–236. <https://doi.org/10.1016/j.jhazmat.2016.12.005>
- Powers, S.E., Hunt, C.S., Heermann, S.E., Corseuil, H.X., Rice, D., Corseuil, X., Rice, D., Alvarez, P.J.J., 2001. The Transport and Fate of Ethanol and BTEX in Groundwater Contaminated by Gasohol. *Crit. Rev. Environ. Sci. Technol.* 31, 79–123. <https://doi.org/10.1080/20016491089181>

- Prommer, H., Barry, D.A., Davis, G.B., 2002. Modelling of physical and reactive processes during biodegradation of a hydrocarbon plume under transient groundwater flow conditions. *J. Contam. Hydrol.* 59, 113–131. [https://doi.org/10.1016/S0169-7722\(02\)00078-5](https://doi.org/10.1016/S0169-7722(02)00078-5)
- Rama, F., Franco, D., Corseuil, H.X., 2017. Spatial and Temporal Analysis of Natural Drainage in the Ressacada Aquifer (Florianopolis, Brazil). *Int. J. Environ. Sci. Dev.* 8, 653–660. <https://doi.org/10.18178/ijesd.2017.8.9.1033>
- Rama, F., Miotlinski, K., Franco, D., Corseuil, H.X., 2018. Recharge estimation from discrete water-table datasets in a coastal shallow aquifer in a humid subtropical climate. *Hydrogeol. J.* 26, 1887–1902. <https://doi.org/10.1007/s10040-018-1742-1>
- Ramos, D.T., da Silva, M.L.B., Chiaranda, H.S., Alvarez, P.J.J., Corseuil, H.X., 2013. Biostimulation of anaerobic BTEX biodegradation under fermentative methanogenic conditions at source-zone groundwater contaminated with a biodiesel blend (B20). *Biodegradation* 24, 333–341. <https://doi.org/10.1007/s10532-012-9589-y>
- Ramos, D.T., Lazzarin, H.S.C., Alvarez, P.J.J., Vogel, T.M., Fernandes, M., do Rosário, M., Corseuil, H.X., 2016. Biodiesel presence in the source zone hinders aromatic hydrocarbons attenuation in a B20-contaminated groundwater. *J. Contam. Hydrol.* 193, 48–53. <https://doi.org/10.1016/j.jconhyd.2016.09.002>
- Rasa, E., Bekins, B.A., Mackay, D.M., de Siewes, N.R., Wilson, J.T., Feris, K.P., Wood, I.A., Scow, K.M., 2013. Impacts of an ethanol-blended fuel release on groundwater and fate of produced methane: Simulation of field observations. *Water Resour. Res.* 49, 4907–4926. <https://doi.org/10.1002/wrcr.20382>
- Rein, A., Bauer, S., Dietrich, P., Beyer, C., 2009. Influence of temporally variable groundwater flow conditions on point measurements and contaminant mass flux estimations. *J. Contam. Hydrol.* 108, 118–133. <https://doi.org/10.1016/j.jconhyd.2009.06.005>
- Ricker, J.A., 2008. A practical method to evaluate ground water contaminant plume stability. *Gr. Water Monit. Remediat.* 28, 85–94. <https://doi.org/10.1111/j.1745-6592.2008.00215.x>
- Rolle, M., Eberhardt, C., Chiogna, G., Cirpka, O. A., Grathwohl, P., 2009. Enhancement of dilution and transverse reactive mixing in porous media: Experiments and model-based interpretation. *J. Contam. Hydrol.* 110, 130–142. <https://doi.org/10.1016/j.jconhyd.2009.10.003>
- Schirmer, M., Butler, B.J., 2004. Transport behaviour and natural attenuation of organic contaminants at spill sites. *Toxicology* 205, 173–179. <https://doi.org/10.1016/j.tox.2004.06.049>
- Schirmer, M., Durrant, G.C., Molson, J.W., Frind, E.O., 2000. Influence of transient flow on contaminant biodegradation. *Ground Water* 39, 276–282.
- Steiner, L.V., Ramos, D.T., Liedke, A.M.R., Serbent, M.P., Corseuil, H.X., 2018. Ethanol content in different gasohol blend spills influences the decision-making on remediation technologies. *J. Environ. Manage.* 212, 8–16. <https://doi.org/10.1016/j.jenvman.2018.01.071>
- Tromp-Van Meerveld, H.J., McDonnell, J.J., 2006. Threshold relations in subsurface storm-flow: 2. The fill and spill hypothesis. *Water Resour. Res.* 42, 1–11. <https://doi.org/10.1029/2004WR003800>
- Werth, C.J., Cirpka, O.A., Grathwohl, P., 2006. Enhanced mixing and reaction through flow focusing in heterogeneous porous media. *Water Resour. Res.* 42, 1–10. <https://doi.org/10.1029/2005WR004511>
- Yang, M., Annable, M.D., Jawitz, J.W., 2014. Back Diffusion from Thin Low Permeability Zones. *Environ. Sci. Technol.* 49, 415–422.
- Yu, S., Freitas, J.G., Unger, A.J.A., Barker, J.F., Chatzis, J., 2009. Simulating the evolution of an ethanol and gasoline source zone within the capillary fringe. *J. Contam. Hydrol.* 105, 1–17. <https://doi.org/10.1016/j.jconhyd.2008.11.006>
- Zhang, P., Devries, S.L., Dathe, A., Bagtzoglou, A.C., 2009. Enhanced mixing and plume containment in porous media under time-dependent oscillatory flow. *Environ. Sci. Technol.* 43, 6283–6288. <https://doi.org/10.1021/es900854r>

3.5 NUMERICAL MODELLING AS A TOOL TO DEVELOP A CONCEPTUAL HYDROGEOLOGICAL MODEL

Fabrizio Rama^{(1)*}, and Konrad Miotlinski⁽¹⁾

* Corresponding author

(1) Núcleo Ressacada de pesquisa em meio ambiente (REMA) – CTC - UFSC

Referência:

Rama, F., Miotlinski, K., Numerical modelling as a tool to develop a conceptual hydrogeological model. (2019) Unpublished.

Nota ao leitor:

O conteúdo desta seção representa um artigo não publicado que será reorganizado para submissão em revista internacional após da integração das contribuições da banca examinadora.

Resumo

Apesar das melhorias na precisão dos equipamentos e nas técnicas de monitoramento, a compreensão dos processos na escala de campo continua sendo uma questão desafiadora em hidrogeologia. A caracterização de um site é uma atividade cara e demorada que normalmente resulta em muitas menos informações das necessárias. No entanto, ferramentas numéricas podem ser aplicadas eficientemente em várias fases de uma investigação hidrogeológica, auxiliando na construção e atualização de um modelo conceitual preliminar. Elas fornecem uma estrutura quantitativa para sintetizar informações de campo e para verificar processos hidrogeológicos complexos. Assim, uma boa relação custo-benefício nas tomadas de decisões em questões ambientais pode muitas vezes depender de modelos numéricos. Para abordar esta questão, este trabalho apresenta o desenvolvimento sistemático de um modelo conceitual para uma bacia hidrográfica do litoral em um clima subtropical úmido, caracterizada por precipitações intensas e variadas, e marés oceânicas. Um conjunto de experimentos numéricos é empregado para testar a compreensão dos processos naturais e sugerir campanhas integrativas de campo. Os processos naturais relacionados com o fluxo de águas subterrâneas e o transporte de solutos na subsuperfície são verificados a diferentes escalas e incluídos, se apropriado, no modelo hidrogeológico geral. Por consequência, o escoamento subterrâneo das colinas pode ser excluído enquanto a recarga é reconhecida como principal mecanismo do balanço hídrico. Por outro lado, a carga hidráulica e suas flutuações nos receptores superficiais (Ex. mar, rio e drenos), confirmaram ter um impacto significativo no perfil do lençol freático em toda a bacia. Ao apresentar informações detalhadas de configuração sobre o desenvolvimento

dos modelos, são descritas as aplicações e discutidas as limitações à luz dos dados de campo disponíveis e dos objetivos específicos de pesquisa.

Abstract

Despite the improvement of the field equipment accuracy and site instrumentation techniques, the understanding of processes at field scale remains a challenging issue for hydrogeological applications. A site characterization is an expensive and time-consuming activity that normally results in much less information that is needed. However, numerical models can be applied efficiently at various phases of a hydrogeological investigation, helping in updating a preliminary conceptual model. They provide a quantitative framework for synthesizing field information and for verifying complex hydrogeological processes. Thus, a cost-effective decision-making process related with environmental issues may often rely on numerical models. To address this issue, this contribution presents a systematic development of a conceptual model for a coastal hydrogeological basin in a humid subtropical climate affected by intensive precipitation and ocean tides. A set of numerical experiments is employed to test the understanding of natural processes and suggest integrative field campaigns. The natural processes related with groundwater flow and solute transport in the subsurface are verified at different scales and included, if appropriate, in the hydrogeological conceptual model. Consequently, the subsurface runoff from hills can be excluded, when recharge is recognized as main process affecting the overall water balance. On the other hand, a hydraulic head position and its temporal oscillation at surface receptors such as sea, river, and drains confirmed to have a significant impact on the water-table elevation throughout the groundwater basin. By presenting detailed setup information on the model development, applications are showed and limitations are discussed in the light of available field data and specific research objectives.

Keywords: groundwater flow field, coastal aquifer, tropical climate, FEFLOW, conceptual model

Highlights:

- A step-by-step hydrogeological conceptual model of the Ressacada aquifer was developed
- Importance of a multi-numerical model approach in the conceptualization process was underlined
- Potential and limitations of FEFLOW in forecasting plume dynamics in a variable flow were described
- A sensitivity analysis of modified inverse Elder problem was presented
- Use of steady and transient BCs in transport modelling was described

3.5.1 Introduction

The subsurface, similarly to other natural systems, is a complex environment. We gain a knowledge about it through an observation and interpretation of information which is collected using various techniques from the land surface or under the ground (Chamine et al., 2015). The superficial data include variations in topographic relief (Wade 1935), lithology (Dewandel et al., 2006), soil texture (Skempton, 1953), and vegetation (Eberhardt and Latham, 2000) or dimensions in surface water bodies as well as temporal changes of river flow (Harrington et al., 2013; Devos et al., 2015). The underground data refer geologically to spatial variations in lithology, grain distribution, fractures and karst features, while hydrologically include water levels, flow velocities, pumping rates and tracer concentrations.

From a methodological point of view, subsurface data are divided into (a) “hard-core” information obtained from the surface and from boreholes and (b) indirect information from the geophysical and hydrogeological inverse modelling (Linde et al., 2015). All of them supplement each other, but they have their own caveats. For example, boreholes are quite expensive to drill and the logs give one-dimensional information only, while the geophysical and hydrogeological techniques, although capable of providing a two- or three-dimensional image of the subsurface, are often non-unique (Li and Oldenburg, 1996; McKenna et al., 2003; Renard 2005). In an aquifer, measurement of hydraulic attributes and interpretation techniques, typically based on pumping tests, provide only averaged values of actual properties around the wells (Riva et al. 2010; Sanchez-Vila et al. 2006). As a result, our knowledge of a geological setting or a groundwater system in three dimensions is always uncertain (Nilson et al., 2007; Doherty and Welter 2010; Randle et al. 2018). Such uncertainty is due to the innate scarcity of data to characterize a full-scale system, where variables continuously varying in a not-well known “continuum” (Bear and Cheng, 2010; Enemark et al., 2019). Of course, uncertainty can be reduced through refinement or application of other techniques of field investigation. Nevertheless, since a management process is a cost-benefit judgment, additional funds for a refined geological prospection (Cherry et al., 1996), geoelectrical transects (Kirsch and Yaramanci, 2009) or long-lasting pumping tests (Miotliński et al., 2011) may not be available. Therefore, modelling can be helpful to gain insight on actual phenomena using available information and resources. A numerical groundwater model followed by conceptual modelling provides a quantitative framework for synthesizing field

information and verifying complex hydrogeological processes (Barnett et al., 2012; Anderson et al., 2015).

A conceptual model is a qualitative representation of a groundwater system based on geological, geophysical, hydrological, hydrogeochemical, climatic and other ancillary information (Anderson et al. 2015). It provides a systematic and internally consistent explanation of boundaries, properties and processes relevant to the research question, linking hydrogeological characterization with numerical modelling (Enemark et al., 2019). Therefore, a properly constructed conceptual model includes all available information from a specific site, but may also drive information from similar settings (Sudicky 1986; Motyka, 1998). For example, a conceptual model can be progressively updated upon numerical modelling (Konikow, 2011; Francés et al., 2014).

A numerical model is a freely selected and appropriately simplified version of real phenomena taking place within a domain, which simulates the system's input–output relationships by using a mathematical formulation (Bear, 2018). This implicates an appropriate level of reduction and idealization of the real world (i.e. conceptualization) where the most important processes are emphasized and the subordinate processes are dropped (Diersch, 2014). For example, a profile model is a 2D vertical slice (simplification) of a real groundwater system, oriented parallel to a groundwater flow path (Anderson et al., 2015). Profile models can be used to study regional groundwater flow in cross sections (e.g. Toth, 1962; Cardenas, 2008; Winter, 1976) and hyporheic interchange beneath a stream (e.g. Woessner, 2000; Brunner et al. 2009), instead of creating complex 3D models. Thus, modelling procedure can be organized in three main stage (Diersch, 2014): (1) a model conceptualization or description of the system, which includes assumptions and simplifications; (2) a mathematical representation of this conceptual model in the form of numerical schemes and discrete solution techniques, because mathematical model is often not amenable to analytical solution; (3) a computational realization of the model in the form of a simulation software. All these steps entail errors and hypotheses that must be constantly checked.

Models that describe flow and transport in porous media can be applied at various phases of hydrogeological investigation and have essentially three main purposes: (i) to organize and test our understanding of physical mechanisms within a considered domain (Freeze and Witherspoon, 1967; Boano et al., 2014); (ii) to forecast future scenarios (Herckenrath et al., 2011; Guillaume et al., 2016), enabling the prediction of the specific perturbation-response behavior (forward modelling); and

(iii) to hindcast past conditions (Clement, 2011) or determine significant properties/parameters through an optimization process that involves minimization of the deviations between observations and model-based predictions (backward/inverse modelling or history matching). This can be used as basis for cost-effective decision-making on environmental issues, although modelers need to be aware of model's limitations and uncertainty, openly informing them to stakeholders (Doherty and Simmons, 2013). Indeed, not accounting for conceptual model uncertainties or limitations can largely underestimate total uncertainty, giving false confidence in model results (Bredehoeft 2005).

This contribution deals with a step-by-step development of a conceptual model of a complex hydrogeological system applying a multi-model approach. Thus, an ensemble of different conceptualizations (i.e numerical experiments) is considered in the modelling process to verify assumptions and physical phenomena in the scarcity of available field data, showing a cost-effective way to deal with field complexity. The case study is a shallow coastal aquifer located in a humid subtropical climate, enclosed by mangrove swamps and an estuarine system, under influence of intensive rainfall events and strong ocean tides (Ressacada, Florianopolis, Brazil). A number of conceptual issues are addressed numerically, including process verification, mapping or quantification of groundwater balance. Following the modelling exercises with a detailed description on model development we show the applications and discuss limitations based on available field information and the research objectives.

3.5.2 Methodology

This section concerns a general description on the site, field experiments and modelling software to address the objective.

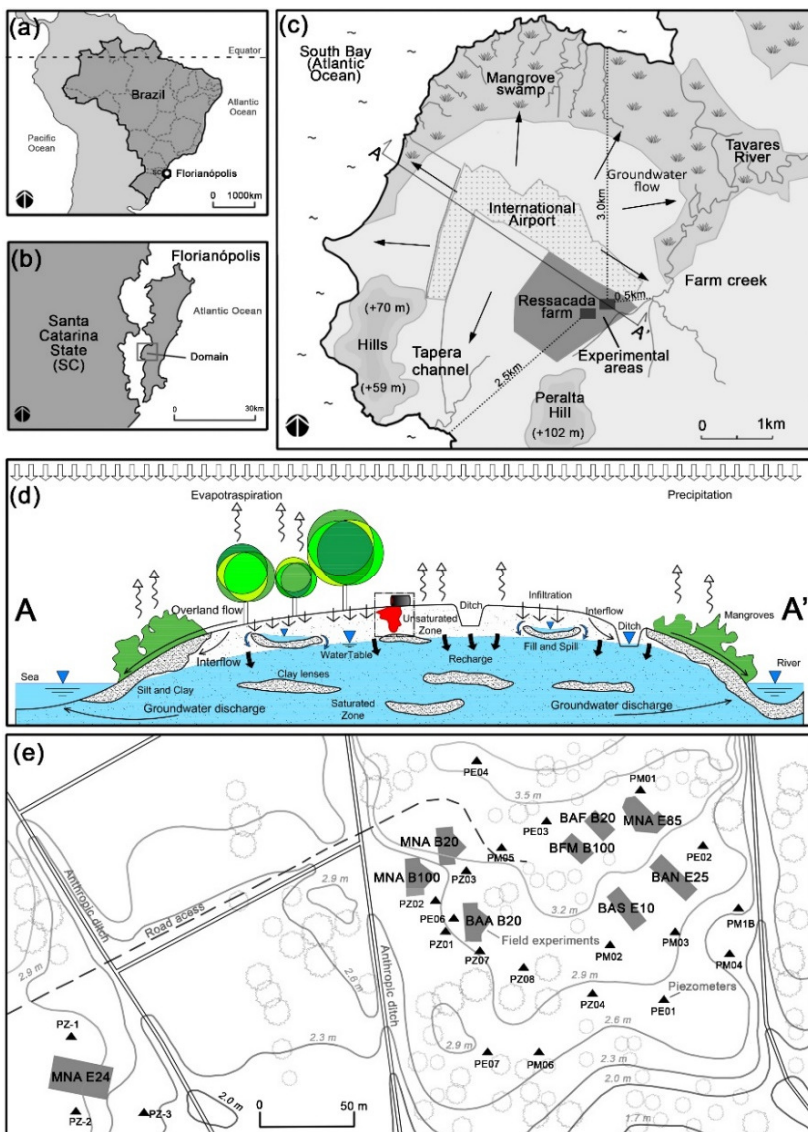
3.5.2.1 Site description

The site is located in a flat depositional plain of about 20 km² in the south-western part of Santa Catarina Island, Florianopolis, Brazil (27°41'06.28"S; 48°32'38.81"O) (Fig.42b). The region is characterized by a humid subtropical climate, with high intensity and large variability of precipitation (1100 to 2700 mm/y between 2007 and 2017). The aquifer is of lacustrine and marine depositional environments, characterized by fairly homogeneous deposits with a predominance of fine quartz sand and

the presence of extended silt and clay areas, rich in organic matter (Lage 2005). The ground surface in the plain is up to 5 m in elevation, while peripheral hills of about 100 m are located in the south and west. The average depth to water table varies from 0.3 to 2.0 m. A dense network of artificial trenches and tidal channels drains the top of the shallow aquifer. The surface basin can be divided in two-subdomains: (1) the west side of Tavares River and Farm Creek, a slow curvy estuarine system surrounded by mangrove swamps that drains most of east and south part of domain (Rama et al. 2018), and (2) Tapera Channel, an anthropogenic surface water system that collects drained water from ditches in the south-west part of domain and the International Airport area. Both surface systems flow into an Atlantic Ocean channel called South Bay (Garbossa et al. 2014), which surround the whole domain to north and west.

The hydrological system of Tavares River defines east and south-east boundaries, and a compact granite complex of hills encloses the south (Fig.42c). The coastal unconfined aquifer, 30–40 m thick to crystalline bedrock, constitutes a quite homogeneous “u-shaped” system surrounded on three sides by surface water bodies (Rama et al. 2017). These receptors represents groundwater flow boundaries, characterized by tidal oscillation and flood event propagation. In addition, peripheral areas in the domain are covered by mangrove swamps and generally flooded with brackish water. Thus, land use within the plain results Atlantic forest (23%), grassland (18.5%), urban area (32%), and mangrove swamp (26.5%). The Ressacada Farm is located in the central part of the plain, near the International Airport (Fig.42c), covering an area of 1.7 km² where field experiments take place. It is managed by agricultural science department (CCA) and REMA research group, owned by Federal University of Santa Catarina (UFSC). The land use in the Farm is organized in cultivated and arable lands (41%), swamps and mangroves (17%) native vegetation (dense ombrophylous forest, 14%), unused land or pastures (26%) and experimental areas (2%) (CCA, 2016).

Figura 42 - Location of Ressacada Farm Site: (a) map of Brazil; (b) map of Santa Catarina Island; (c) study domain at Ressacada Farm Experimental Site, with boundary conditions. Section A–A' indicates a longitudinal transect; (d) Conceptual scheme along A-A' transect exhibiting principal phenomena in the region; (e) Detailed map of experimental areas at Ressacada Site, depicting piezometers positions (black triangles) and designations (e.g. PE03, PZ-1, etc.), surface elevation above mean sea level (light grey isolines and numbers in *italic*) and monitored field experiments (grey polygons).



3.5.2.2 Field experiment and monitoring

Two large experimental areas (Area1 and Area3) covering totally 31,000 m² in the east part of the Ressacada Farm (Fig.43) were used to

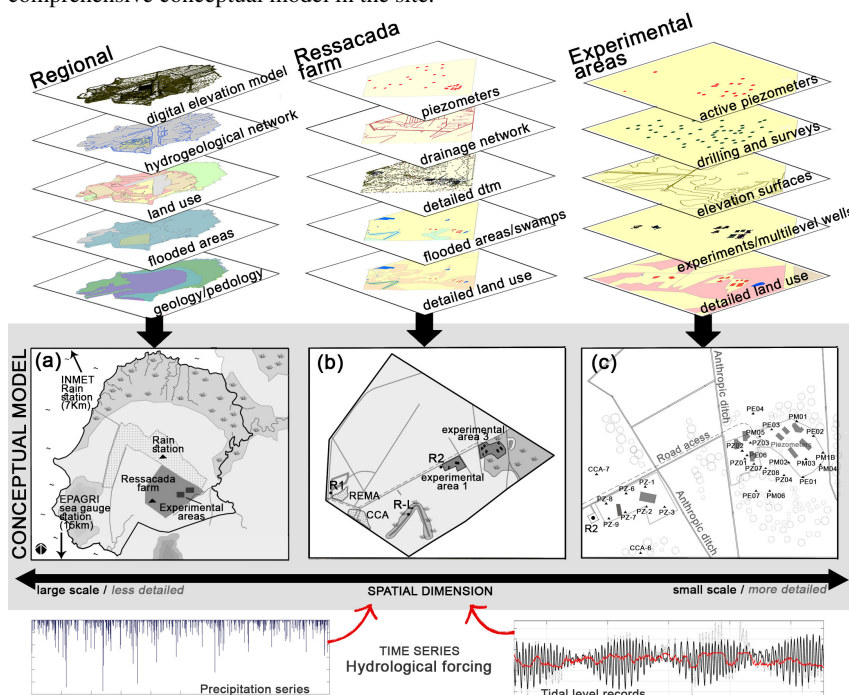
carry out controlled experiments of fuel/biofuel spills into the ground. From 1998, these areas host 11 long-term field experiments on monitored natural attenuation (MNA) and biostimulation (BA_) (Fig.43). Each field experiment has common features: (a) a product source, released as a single slug into an excavation within the saturated or vadose zone; (b) a conservative tracer release (i.e. bromide), spilled with the product; (c) multilevel monitoring wells with 4-5 sampling levels (about 50 per experiment); (d) plastic canvas and protective gravel overlain the whole experiment area to avoid vertical infiltration and approximate horizontal flow conditions in the subsurface. The details of the experiments are summarized in Supporting Material (Tab.SM1). The experiments were focused on different blends of conventional fuels (i.e. gasoline, diesel) and biofuels (i.e. ethanol, biodiesels), investigating cosolvency of hydrocarbons with ethanol (Corseuil and Fernandes, 1999; Corseuil et al. 2004), NAPL source weathering (Ramos et al., 2013; Steiner et al. 2018) and degradation rates of dissolved plumes (Corseuil et al. 2011a,b; Corseuil et al. 2015) at field scale. Rama et al. (2019) suggested that hydraulic regime should be spatially and temporally characterized to support decisions on appropriate monitoring plan and remedial strategies for gasohol spills, because groundwater flow velocity and transient processes consistently contribute to plume spreading and solute migration in full-scale experiments.

In the experimental areas, hydraulic head and water quality monitoring has been performed since 1998 using 55 observation wells and piezometers, 27 of which still existing. The head measurements and samples for water quality are taken at irregular interval from 1 to 60 days depending on the phase of a spill. Some piezometers are equipped with automatic level loggers since 2016. Also, 16 shallow piezometers were installed in the rest of Ressacada Farm since 2012 monitoring the water table shape. Finally in 2016, 3 staff (head) gauges in aluminum were placed in the reservoir ponds to check hydraulic levels evolution in the surface drain network (Fig.43). The complete list of the equipment is given in Supporting Material (Tab.SM2).

Between 2002 and 2007, to understand the spatial distribution of geological features a set of drilling campaigns (Lage, 2005) along with geophysical examinations (i.e. Self-potential monitoring and Vertical Electric Soundings) were conducted in Experimental Area 3 (Esteves, 2000, 2002; LEBAC/FUNDUNESP, 2007). In addition, a number of field and laboratory tests have been accomplished to the hydrogeological characterization of the site. Saturated hydraulic conductivity was estimated from four large slug test campaigns, testing different years and

seasons (Supporting Material – Tab.SM3). Average hydraulic conductivity are in the range of $10^{-3}/10^{-4}$ cm/s, varying from 10^{-2} to 10^{-5} cm/s. Multiple granulometry and X-ray diffraction analysis were used to define particle-distribution and grain size in every experiment, along with mineral proportion in the soil. Furthermore, 31 soil samples collected at regular intervals during two deep probes were encapsulated and tested to determine porosity and permeability. Mean total porosity, measured by gas permo-porosimeter, is 0.38 ± 0.01 over 31 samples (Lage 2005). The effective porosity (η_e) of the saturated layer is 0.2 (Corseuil et al. 2011b), while the moisture content of the unsaturated zone profile varies from 20 to 25% (Lage 2005).

Figura 43 - Use of field data and available information in the development of a comprehensive conceptual model in the site.



In the center of the plain, around the new terminal of the International Airport, 210 independent geotechnical surveys were carried out in 2010 (Engevix / Infraero). Provided information about perforations are divided between percussion drillings, cone penetration tests (CPTUs), withdrawals from Shelby samplers and infiltration tests. The material

includes also geological profiles and stratigraphic columns reaching up to 35 meters deep. Thus, for the purposes of the present study such a depth, which agreed with the PE06 column within the Farm, was considered the horizontal impenetrable bottom of the unconfined aquifer.

The sea-level records have been collected since 2013 by an OTT/RLS radar level sensor located in a gauge station in the South Bay coast, 15 km far from the domain (Fig.43). This is carried out and provided by EPAGRI/CIRAM (Agricultural Research and Extension Company/Information Center for Environmental Resources and Hydrometeorology).

In five streambed sections along the Tavares River and Farm Creeks a bathymetric study was done in 2017. Streamflow velocity was measured in every section by an interpolation of about 10-15 punctual measurements with an ultrasonic propeller current-meter (LaHiMar, ENS/UFSC). Since the surface water bodies at the plain are exposed to a tidal oscillation, the flux inverts twice a day of up to about 3 km from the river outlet. The river/estuarine characterization aim to define an eastern boundary condition for the Ressacada aquifer, in term of water level and flow rate. Since feature changes occur at the river junctions, Tavares River system can be simplified with three pseudo-homogeneous traits for geometry and flow rate: (a) a curvy and slow Tavares estuarine trait, with larger (20 to 40 m) and deeper (more than 5 m) sections; (b) a regular Farm Creek trait with 10-15 m large sections maximum 3 meters deep; and (c) a small and straight channel trait with decreasing dimensions (5 m large and 1.5 m deep) and increasing ramifications. At the Farm Creek trait, about 300 m far from experimental areas, the surface water system can be described in average by a 25 m² section with a flow rate of 1.5-2 m³/s. Information about river system characterization are summarized in the Supporting Material (Fig.SM1).

To define the regional topography, a digital elevation model (DEM) was set up using ArcGis (Johnston et al., 2001; Ormsby et al, 2004). Coarse elevation model of Ressacada plain is based on the integration of detailed aerial surveys (1:10.000) from IPUF (Florianopolis Urban Planning Institute), a free-access DEM (1:50.000) from IBGE (Brazilian Institute of Geography and Statistics) and digital maps (1:50.000) from EPAGRI/CIRAM. Final model is obtained by refining the central part of the plain where the Ressacada Farm is located with other three planialtimetric surveys: (i) a 1:500 map of the two experimental areas in the Farm including 1000 levelled points, committed in 2009 by REMA to LineDraw Topografia; (ii) a 1:1000 map of 581855 m² in the new terminal area adjacent the Farm, including 3200 levelled

points, committed by INFRAERO and executed by Engevix Engenharia S/A in 2010; and (iii) a GNSS (global navigation satellite system) campaign of 3500 points in the Ressacada farm developed by Agrarian Sciences Center (CCA) in 2012 resulting in a 1:2500 topographic map. The final result was a DEM with about 20000 points, average resolution of 1 meter, georeferenced with datum SIRGAS2000 and cartographic projection UTM22S. According with the zero-elevation reference of Brazilian Geographical System (SGB) (Resolução IBGE-R.PR 1/2005), sea-level gauge of Imbituba/SC is used as vertical reference.

Quadro 2 - Required information to develop a complete conceptual model for the site.

INFORMATION CLASS	TYPE	SOURCE/METHOD	QUALITY ^a
Elevation (DTM)	Surface character. ("hard-core")	Surveys / GIS maps	5
Surface drain network	Surface character. ("hard-core")	Surveys / GIS maps	3
Geology / feature geometry	Subsurface character. ("hard-core")	Drilling / Geophysics / Surveys	1
Hydraulic conductivity	Material property (flow)	Pump Test / Slug Test / Literature	3
Aquifer Storage	Material property (flow)	Pump Test / Literature	-
Specific yield / porosity	Material property (flow-transport)	Pump Test / Laboratory / Literature	1
Groundwater flow	Material property (flow-transport)	Flow meter / Literature	-
Recharge / Discharge rate	Boundary condition (flow-transport)	Tracer Test / Monitoring network / Literature	1
Density distribution	Fluid property (transport)	Field sampling / Laboratory / Literature	2
Dispersivity	Material property (transport)	Tracer Test / Laboratory / Literature	-
Organic matter distribution	Material property (transport)	Laboratory / Literature	1
Hydraulic heads	Monitoring data (flow)	Monitoring network / Maps	3
Water chemistry	Monitoring data (transport)	Field sampling / Laboratory / Literature	4
Product characteristics	Contaminant property (transport)	Laboratory / Literature	5
Soil chemistry	Material property (transport)	Field sampling / Laboratory / Literature	2

^a Quality column indicates an evaluation of available data for each class in the site

The precipitation in the region is monitored by using 3 different meteorological stations: (1) a METAR and WMO station located at the International Airport (83899), less than 400 meters far from the experimental areas, and provided by the Institute of Airspace Control (Ministry of Defense); (2) an INMET and WMO automatic station in Florianopolis-São José (86958), 7 Km to the North-East from the first station, used to integrate and validate series; and over shorter time-periods

(3) a manual rain gauge installed in the Ressacada Farm, supplied by the CCA technicians.

Non-homogeneity of data sources and field information required a careful pre-process work to understand of main phenomena governing groundwater flow and to extrapolate information in the whole plain based on Ressacada Farm data. Processed information are organized in databases developed in a GIS environment, which are used in the construction of conceptual model proceeding from the whole region to the experimental areas (Fig.43). Focusing in the modelling process, raw data are part of information classes, theoretically required to develop a complete conceptual model of the aquifer (Quad.2).

3.5.2.3 Groundwater modeling

FEFLOW was used to solve flow and transport problem (Diersch, 2014). This tool is capable of simulating processes in a partially saturated porous medium by a multidimensional finite element method (FEM) for complex geometric and parametric situations including variable fluid density, variable saturation, free surface, multispecies reaction kinetics, non-isothermal flow, and multidiffusive (thermohaline) effects (Diersch, 2014). FEFLOW is a closed and proprietary software with a robust graphical user interface, which is a reference in groundwater modelling (Trefry and Muffels, 2007).

A FEM was preferred to a finite difference modelling at Ressacada for the irregular and complex nature of spatial discretization (e.g. variably anisotropy, thin clay lenses, complex boundaries). In addition, FEFLOW has an algorithm using a variably saturated formulation that considers saturated and unsaturated zone as a continuum and solves the main equations for the pressure head (saturation) on the whole domain (Diersch, 2014). This fact allows to manage in a rigorous way the free surface problem (i.e. Ressacada unconfined aquifer) resulting in a more consistent solution for water table position (Anderson et al. 2015). An accurate simulation of water table as a free fluctuating surface is challenging because requires a fine representation of vertical flow and a non-linear BC. Furthermore, a consistent boundary flux method is used in FEFLOW, accounting for total inflow/outflow to estimate the water budget error (Diersch, 2014). Such error should be less than 1%, ideally less than 0.1% (Konikow, 1978), to consider a numerical model to be of acceptable accuracy (Anderson et al. 2015).

The advection-dispersion equation (ADE) in FEFLOW (Eq.19) results from the transformation of the microscopic balance equation

defined in the continuum to the macroscopic level using averaging theorems (Diersch, 2014). Eq.19 is solved for C (concentration), and depend on D (hydrodynamic dispersion tensor), v (velocity vector), λ (first-order degradation coefficient), C_s (source/sink concentration), q_s (specific source/sink flow), and R_d (retardation).

$$\frac{\partial(C R_d)}{\partial t} = \nabla(D \cdot \nabla C) - \nabla(v C) - \lambda C + q_s C_s \quad (19)$$

In order to find a solution, different boundary conditions (BC) can be required in the defined domain: Dirichlet type (prescribed head), Neumann type (prescribed flux), Cauchy type (prescribed head and flux), or Well-type condition. Each BC may have an associated constraint to limit the use of such condition (Diersch, 2014). An example is a seepage face, which acts as the prescribed-head boundary condition if hydraulic head in an aquifer is higher than in the node with the condition, but is inactive if the hydraulic head in the aquifer is lower than in the said node. Thus, a set of conditions, along with specific material parameters, mathematically define a problem formulation that can be a hyperbolic, parabolic or elliptic PDE depending on the processes to be simulated. It worth stressing that in subsurface transport of solutes most of the cases result in second-order PDE's, which can be effectively solved by the standard Galerkin-based FEM (GFEM) developed and optimized in FEFLOW.

The general mathematical software packages such as MATLAB (<https://it.mathworks.com>) and Python (<https://www.python.org/>) were coupled with FEFLOW to develop specific subroutines or to manage and format field data. PEST (Model-Independent Parameter Estimation and Uncertainty Analysis) was used for the parameter optimization (Doherty, 2015). The procedure for parameter optimization with PEST included absolute levels, temporal variations and spatial differences in hydraulic head. Spatial head differences are useful to calibrate vertical conductivity, increasing the signal-to-noise ratio of the raw level data (Doherty and Hunt, 2010, p.13). Temporal head differences, which are more effective than absolute hydraulic heads to calibrate transient models, can be calculated from a singular time-series (Doherty and Hunt, 2010, p.13).

3.5.3 Results and discussion

The hydrogeological model of the Ressacada aquifer was developed by a multi-model approach. Thus, many conceptualizations

with different model complexity were tested, until reaching a mechanisms enable that enable an acceptable representation of the reality. Accordingly, a number of numerical experiments were developed to address particular groundwater uncertainties, integrating available field data (Quad.3). The areas of domain varied in each case depending on the objectives and included phenomena (Fig. 44).

Quadro 3 - A list of numerical exercises towards conceptual model understanding.

Objective	Model
Verify the role of anthropic drain network in control water-table level within the plain	A
Create a preliminary groundwater level map	A
Assess the effect of physical mechanisms on water balance in order to exclude these of lowest relevance	A
Determine the role drain/fillable porosity (specific yield) and its sensitivity in water-table head calibration	B
Calibrate a preliminary regional groundwater flow field using heads, directions of groundwater flow and travel times (advective particle tracking)	B
Verify the recharge rate estimated by Water-Table Fluctuation method (Rama et al., 2018)	C1
Determine the influence of vertical recharge and surface receptors levels on water-table shape and position	C1
Evaluate the influence of acetate injection on flow field modification and solute transport in the BAA_B20 experiment	C2
Verifying FEFLOW software for a density-driven flow and transport problem with negative density ratio (ethanol)	Z
Explore the viscosity effects and verify the importance of density ratio in a density-driven flow problem	Z
Determine the differences in plume transport between steady and transient prescribed-head type boundary conditions	D

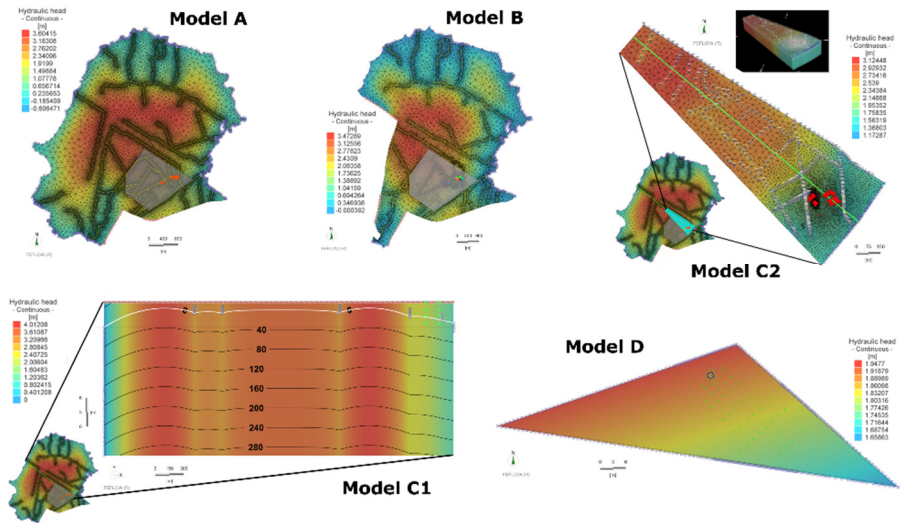
Quadro 4 - FEM model input parameters and assumptions.

FEM parameter	[unit]	Model A	Model B	Model C1	Model C2	Model D	Model Z
Dimensionality	[-]	3D	3D	2D (vertical)	3D	3D	2D (vertical)
Problem class	[-]	Transient flow	Transient flow	Transient flow	Transient transport	Transient transport	Transient transport
Flow formulation	[-]	Saturated (unconf.)	Saturated (unconf.)	Unsat. (Richards)	Saturated (unconf.)	Unsat. (Richards)	Saturated (unconf.)

Transport formulation	[-]	-	-	-	Convective form	Convective form	Convective and Divergence
Domain dimensions	X·Y [m ²] - Z[m]	20812000-32	15792000-32	(3650x1)-32	793600-32	1300-32	(600x1)-600
No of mesh elements (nodes)	[-]	1095990 (592170)	693322 (374880)	18154 (18526)	610392 (320125)	553248 (290136)	54530 (55008)
No of layers	[-]	14	14	-	24	32	-
Mesh type	[-]	Triang.	Triang.	Quadrang.	Triang.	Triang.	Quadrang.
RMS ^b error tolerance	[%]	0.001 (AB/TR)	0.001 (AB/TR)	0.001 (AB/TR)	0.001 (AB/TR)	0.003 (FE/BE)	0.001 (FE/BE)
Simulation time period	[d]	365	365	3653	365	1545	9125
Saturated conductivity	K _{xx} - K _{yy} - K _{zz} [m/d]	Top layers: K _{xx} = 2.16 (surface) / 8640 (river, drains) Otherwise: K _{xx} = 3.9 (sand) K _{xx} = 2K _{zz}	Top layers: K _{xx} = 0.5 (mangrove) / 3.75 (surface) / 8000 (river, drains) Otherwise: K _{xx} = 8 (sand) K _{xx} = 5K _{zz}	K _{xx} = 3.2 (layer1) / 8.5 (layer2)	K _{xx} = 3.08 (layer1) / 5 (layer2) K _{xx} = 3K _{zz}	K _{xx} = 1 K _{xx} = 3K _{zz}	1-1-1
Specific yield	[-]	0.2	Top layers: 0.05 (mangrove) / 0.13 (surface) / 0.08 (river, drains) Otherwise: 0.188 (sand)	0.067 (layer1) / 0.13 (layer2)	0.2	0.188	0.2
Total porosity	[-]	-	-	-	0.38	0.38	0.38
Specific storage coeff.	[l/m]	10 ⁻⁴	10 ⁻⁴	0	10 ⁻⁴	10 ⁻⁴	10 ⁻⁴
Fluid density	[g/m ³]	-	-	-	999793 (constant)	999793 (variable with concentr.)	999793 (variable with concentr.)
Density ratio	[-]	-	-	-	0	-0.211	-0.05/ -0.5
Fluid viscosity (type)	[kg/m/d]	-	-	-	97.1 (constant)	70 (variable)	60 / 240 (constant)
Dispersivity (Long.-Transv.)	[m]	-	-	-	1 – 0.1	1 – 0.1	5 – 5
Henry constant	[-]	-	-	-	0	0	0
Decay-rate	[1/d]	-	-	-	0	0 – 0.003	0 / 0.003
Molecular diffusion	10 ⁻⁹ [m ² /s]	-	-	-	1	1	0.6 / 2.8

^b RMS: Root mean square

Figura 44 - Numerical models describing flow and transport in the Ressacada Farm.



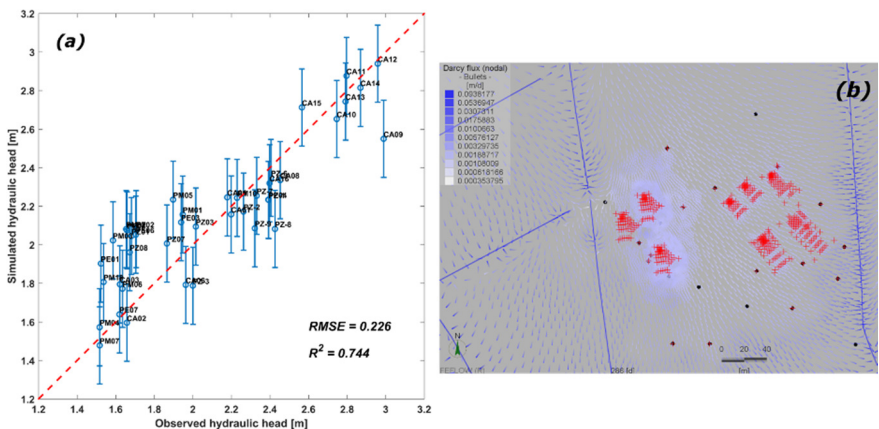
3.5.3.1 Model A

The model A had the purpose of: (a) developing a regional groundwater level map of the Ressacada plain, (b) exploring the role of anthropic drain network in control water-table level, and (c) defining principal mechanisms in the aquifer water balance that will be included in transport modelling.

A large-scale 3D transient model of the saturated flow was chosen to represent the groundwater hydrodynamic within the basin. However, the model was calibrated with averaged steady conditions of water table. Detailed setup information are in Quad.4. A regional model was preferred to a local one in order to control the role of physical boundaries in the hydrogeological system and the evaluation of water balance. The boundaries respect the hydrological limits of the aquifer: Tavares River and Estuary on the east site; South bay on the north, west and southwest; and granite hill group on the south. By organizing geological information described at Section 2.2, five typical geological classes or facies with different parameters were defined in the domain: (1) embankment materials; (2) mangrove swamp soil (silt/sand rich in organic matter); (3) crystalline bedrock (compact granite); (4) fine quartzitic sand; (5) silt and clay lenses. The lithological classes are included in the model as homogeneous and isotropic layers with irregular extension and thickness.

This conceptualization results in a large and complex model incorporating a majority of natural phenomena observed at the site. Water level records of South bay are used to define sea-boundary fluctuations over time. Different values of prescribed-head BC are set along Tavares River to characterize flow regime and water elevation in the three pseudo-homogeneous traits. Spatial and temporal variations of recharge rate are applied on a daily basis by using precipitation records and defining three classes of land use (i.e. grass, forest, urban). A seepage face condition (i.e. prescribed-head BC with a max-flow rate constrain) is applied along to the drain streambeds and describes the aquifer drainage by the anthropic trench network in the plain. A no-flux boundary is set in the south, with the exception of the section that receives surface run-off from emerging granite hills beyond the boundary (Fig. 42). Data from 2014 are chosen for inform the model with field information and run a 1-year case.

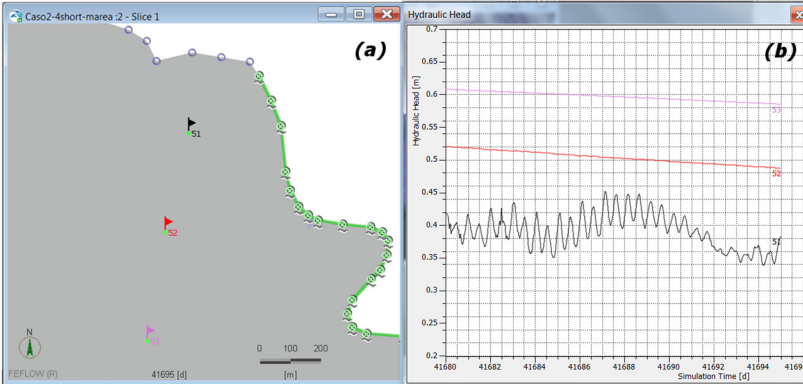
Figure 45 - (a) Statistics of the calibration process for Model A in steady-state using average values of piezometer records; (b) Detail of flow field modification (Darcy flux vectors) caused by surface drain network (seepage face condition).



Consequently, although the calibration of hydraulic head gave a good fit for steady conditions (Fig. 45a), the numerical model resulted slow and unstable. The time and cost of designing process along with the running time made almost impossible concluding transient calibration and parameter optimization. Thus, performance and uncertainty analysis with such a complex model are simply unviable due to the computational effort. In addition, given a strong non-linearity of free surface problem in an unconfined aquifer, the model showed convergence difficulties in early

modelling steps (e.g. steady state runs). Such limitations were amplified by a complex geometry and a rushed parameters choice (e.g. irregular domain shape, special BCs, pinched layers, large range of conductivity). Therefore, the set of “assumptions” was inappropriate to develop a useful and manageable model of groundwater flow in the region (Bear, 2018).

Figura 46 - Hydraulic head response in different observation points to tidally-driven boundary fluctuations (first and third type BC): (a) location and BCs, (b) head plot.



Nonetheless, the model A underlined the importance of surface receptors levels for the water-table position, even though direct perturbation of boundary levels dampen fast and interest a limited hinterland area. Diurnal fluctuations of sea level (40 to 100 cm) affect the aquifer level at a distance of up to 300 meters from the coast (Fig. 46). However, long-term modifications of average sea level should mainly influence the groundwater flow in the region. Moreover, the drainage network affects the aquifer by: (1) lowering water levels up to 2 meters, (2) changing local direction of groundwater flow (Fig. 45b), (3) reducing five times the average residence time of water in the experimental areas. Conversely, other components of water budget, including recharge from the hills have a negligible effect on water budget (<1%).

Overall, the model A was useful to confirm existence of a shallow water table with a radial groundwater flow from the domain center, mainly driven by recharge and hydraulic levels at the boundaries. The local water-table shape, and thereby groundwater velocity, were controlled by preferential flow through the drainage network. This fact highlights that automatic level monitoring within Farm Creek system and total out-flow measures from the drain network would be crucial information to integrate monitoring network of the Ressacada aquifer.

3.5.3.2 Model B

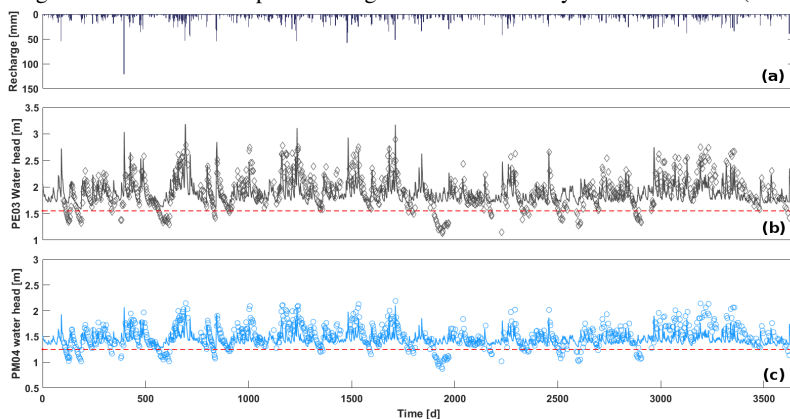
The objectives of the model B were: (a) to determine the importance of drain/fillable porosity (i.e. specific yield) and its sensitivity in the hydraulic head calibration, and (b) to calibrate a preliminary regional groundwater flow using heads and groundwater travel times.

The model B was a simplified version of the model A by removing from the domain the right side of Tapera Channel and the impervious granite hills in the south west (Fig.42c). As proved by model A, this part resulted with no contribute to the groundwater flow at the Ressacada Farm and negligible for the whole water-budget. Furthermore, by removing the granite feature, a large hydraulic conductivity contrasts were avoided and, consequently, numerical stability was improved. The Tapera Channel streambed represents the new western boundary of the domain, defined by a seepage face condition on the top layer and a no-flux condition on the others layers. This results in a groundwater flow parallel to the western boundary, as expected in the reality. Meanwhile, seepage face condition allows draining water excess at the top of the aquifer. In addition, since hills run-off in the south showed very little influence on the flow field in the model A, this in-flow BC is suppressed (Fig. 44). Model B setup is available in Quad.4.

Despite these changes, the model B still runs slow in transient mode, resulting unable to be optimized by an inverse formulation using PEST. Similar to the model A, the hydraulic head calibration was obtained for steady averaged levels (Fig. 47a) resulted from a statistical analysis of piezometer records (Supporting Material – Tab.SM4). Introduced “simplifications” are still in a lack of necessary conceptual hypotheses to describe the groundwater flow in the system effectively and with low computation effort (Diersch, 2014). However, the particle tracking was efficiently deployed during the runs to calibrate flow direction and velocity in the field experiments using a manual trial-and-error approach. In general, a simple hydraulic head calibration is not able to constrain a unique and well-posed saturated flow solution in an unconfined aquifer. (Anderson et al. 2015). Even for a trial-and-error approach, many different field information should be used during a calibration process (Hunt et al. 2006), especially head, fluxes and residence times (Haitjema, 2006). In this case, the comparison of qualitative information such as plume directions with advective particle tracking in the model allowed calibrating a preliminary flow field in the region that explained local transport (Fig. 47b). Specific field measures with flow-meters or a well-to-well tracer test in the experimental areas

The model C1 is a profile transient flow model, developed from the assumption of a recharge-driven flow in the plain. It is developed along a longitudinal transect passing through two piezometers (PE03 and PM04) and crossing towards NW-SE the whole domain of model A (Fig. 44). The boundaries are on South Bay and Farm Creek basin, respectively. Therefore, this model have the advantage to avoid fixing a watershed position, and thereby a natural gradient for the aquifer flow, defining water-table shape directly from recharge dynamics (prescribed in-flow BC), surface receptors level (prescribed head BC) and anthropic ditches drainage (prescribed head BC with a maximum flow-rate constrain). Given the importance of vadose zone effects to simulate sharp and sudden changes in water-table levels, Richard's equation was preferred to the saturated flow formulation. More details are available in Quad.4.

Figure 48 - 2D model verification plot: comparison between simulated (solid lines) and monitored levels dataset (symbols) in a 10-year-long simulation that used calibration parameters, for (a) recharge, (b) PE03, (c) PM04. The red dashed lines (lower head value reached by simulation in each piezometer) show that simulated lines never decrease under fixed values related to the river BC, losing accuracy to explain low groundwater levels. Caption and figure obtained directly from Rama et al. (2018).



Model C1 aimed to describe water-table fluctuations in the experimental areas, demonstrating their dependence on recharge and surface drainage. Hydraulic heads are calibrated using continuous records from two points over 52 days and verified in transient state with discontinuous records over 10-year (Rama et al. 2018). Additional qualitative information in the center of Ressacada Farm are extrapolated from level records of three piezometer (CCA9 – CCA11 – CCA12), even

though out from longitudinal transect. Conversely, groundwater fluxes and velocities was neglected in the calibration. Optimized parameters were specific yields and conductivities, organized in two homogeneous geological layers. In addition, Farm Creek BC (prescribed-head) was tested with PEST code, confirming to be a very sensitive information for water-table shape and surface drainage activation.

Numerical results helped to verify typical recharge rate in the Ressacada Farm (in average 43% over 10 years) estimated with the water table fluctuation method (Rama et al. 2018). The water-table shape along the transect was efficiently characterized, allowing also to establish watershed position based on aquifer water budget. This information can be used to reduce domain extension in the transport problem, positioning the BC on the watershed instead of the sea. Finally, the calibration process underline the role of receptor levels and ditches streambed position in the definition of water-table shape. A detailed field characterization of receptors along with a dense vertical discretization in the model are crucial to reproduce the infiltration front over time.

3.5.3.4 Model C2

The main objective of the model C2 was: (a) evaluate the influence of injections on groundwater flow and solute transport in the BAA_B20 experiment.

Model C2 was a 3D expansion of the profile model C1, which represented its central axis. Thus, a truncated pyramid with a quadrangular base was developed by passing through Experimental Area 3 and including eight of eleven field experiments in the site. Such 3D domain have its boundaries at the hydrological watershed in the center of the plain and at the Farm Creek system, resulting in a recharge-driven natural gradient with slightly diverging groundwater flow and no fluxes through the lateral boundaries. The dense network of ditches was reproduced by an accurate DTM of about 4125 elevation points, along with the application of a seepage face condition on their streambed. Given its smaller extension, model C2 was consistently more efficient and faster to run than model A, also maintaining the principal phenomena of groundwater flow in the area. However, given a more complex domain than model C1, saturated flow formulation is preferred to simulate transient transport instead of Richard's equation. Recharge was forced with a 1-year series of precipitation from April 2009, applying the average ratio verified with model C1 (43%). Detailed setup information of model C2 are available in Quad.4.

It worth noting that a simple 2D areal model was excluded to be incompatible with flow processes in the Ressacada farm (e.g. intense recharge, sharp water-table fluctuations, oscillating boundaries). Two-dimensional areal models use the Dupuit-Forchheimer (D-F) approximation that assumes: (1) a predominantly horizontal flow, and (2) a negligible vertical hydraulic gradients (Anderson et al. 2015). Hence, it is inaccurate near the discharge face and close to the water table, and thereby, inappropriate tool to establish flow field variations in contaminated areas with shallow aquifers. Hydraulic head results from areal 2D and 3D models would coincide only at distances greater than $2.5d$ from a hydraulic feature (e.g. subsurface watershed, pumping well, surface receptors) and $5d$ from a system boundary (BC) that causes vertical fluxes (Haitjema, 2006):

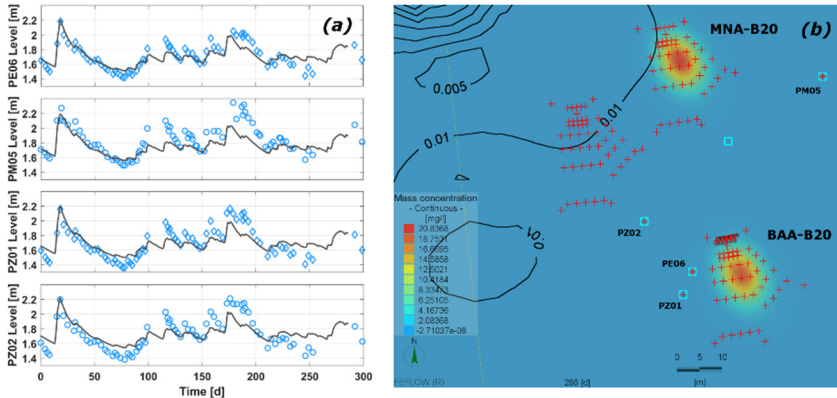
$$d = b \sqrt{\frac{K_h}{K_v}} \quad (20)$$

with b representing aquifer thickness, K_h horizontal conductivity and K_v vertical conductivity. Whereas d is about 50-60 m in the Ressacada, the experiments would have to be more than 130-260 meter far from any other hydraulic features in the Farm.

By comparing the behavior of dissolved plumes at MNA_B20 and BAA_B20 experiments, model C2 delved into the impacts of injections on the dilution and migration of contaminants. The hypothesis was that 25 Lt of acetate injected as a pulse every week in five multilevel wells, up-gradient to a B20 source, had a direct impact on the dissolved contaminants movement, enhancing their migration. Nonetheless, the effects of injections in the BAA_B20 area resulted negligible, and dissolved plumes in both experiments moved at the same velocity within the simulations (Fig. 49b). This fact suggested that other processes should be used to explain plume behavior in these areas, as for example the distribution of low conductive layers in the subsurface. In addition, the model C2 was easier to handle than the model A, readily calibrated in transient flow (Fig. 49a), but too complex to be optimized in a transport simulation using an inverse approach techniques such as PEST. Indeed, 1-year simulation of transport problem lasted about 1 day to run, preventing optimization processes based on many runs. Parameters optimization is conducted for the steady flow problem, also including groundwater fluxes and velocities information estimated from solute plume migration in the experiments. Optimized hydraulic conductivities show slightly different values with model C1, related to the adoption of a

constant specific yield and a different groundwater flow formulation in the problem solution. This fact suggests pumping test appropriateness to assess the actual long-term storage response in the aquifer.

Figure 49 - (a) Transient calibration plot for piezometers in the area; (b) plume transport comparison within experiments MNA_B20 and BAA_B20.



3.5.3.5 Model Z

The model Z, a two dimensional box model, aimed to: (a) verifying FEFLOW for a density-driven flow and transport problem with negative density ratio (ethanol), (b) assessing the importance of density ratio value in a density-driven flow problem; and (c) exploring the viscosity effects.

The model Z represents a numerical experiment with no field data to calibrate that investigated the density-driven flow by an inversion of modified solute Elder problem (Xie et al. 2010). More setup details of this model are available in Quad.4. Model Z aims to test FEFLOW simulating a density-driven flow for an ethanol spill, since no prior works assessed its performance on this problem. Essentially, this model represents the first demonstration of a density-driven problem, with negative density ratios and including viscosity effects, developed within FEFLOW software. A sensitivity analysis is developed over the main parameters. Such information will be used to develop a 3D density-driven model with an ethanol spill, including recharge dynamics, source area at the top of the model, reactive transport (i.e. first-order decay and linear diffusion).

Established by Elder (1967) as both laboratory and numerical experiments on thermal convection in porous layers, the Elder problem is a widely accepted example of free convection phenomena (Prasad and

Simmons, 2003). This original formulation was modified repeatedly in order to describe solute transport of salt blobs (Xie et al. 2010) or reactive transport (Post and Prommer, 2007). Mainly, the vertical domain extent was increased from 150 m to 600 m (Xie et al. 2010), the molecular diffusion coefficient was drastically decreased, and the fixed-concentration BC at the bottom of the model was changed into a no-flux BC to represent porous aquifers with limited permeability and low solute removal rate through the aquifer base (Post and Prommer, 2007). The model Z include all these previous improvements and flip the squared domain over. It was composed by a vertical 2D domain of 600 x 600 meters with a 300 m source of ethanol within the center of bottom boundary and no flux through the boundaries. The conventional groundwater flow equation (saturated medium) was used to solve the transport problem activated by a concentration-driven density gradient. In this configuration, the domain represents a homogeneous and isotropic medium with a dynamic viscosity as a nonlinear function of ethanol concentration and density described by a polynomial formulation (Jamshidzadeh et al. 2013). The importance to include viscosity effects into a density-driven flow model was highlighted by Ophori (1998). A fine grid (3 x 1.3 m elements) within a 150 m width band near to the source allows convergence of the model even changing fluid conditions to test the parameters sensitivity, especially the diffusion coefficient. Such grid was designed to produce a low Péclet number ($Pe < 1$), which minimizes perturbations from inadequate mesh elements. Pe represents a ratio of convective transport to dispersive/diffusive transport (Voss and Souza, 1987). The previous work underlined that free convection is initially characterized by a boundary layer occurrence as a result of diffusion in the source, which reaching a critical thickness, becomes unstable and breaks up into solute fingers (Wooding, 1969; Diersch and Kolditz, 2002). Therefore, a critical zone for the numerical stability in the model Z was the bottom part of the domain near the fix source, which for this reason was refined. In order to simulate a pure free solute convection, the dimensionless Rayleigh number (Ra) was used as an indicator of the onset of instabilities. Practically, high Ra values define full-convective fluid movement, and a constant value within two runs preserves a constant fluid speed.

The sensitivity analysis was presented by a visual/graphical comparison of colored continuous plumes, mainly describing behavior of density ratio, viscosity effects and molecular diffusion coefficient. Results confirmed that blobs creation and evolution strongly depend on the density ratio within the domain (Fig. 50), while viscosity effects result

negligible (Supporting Material - Fig.SM2). Dynamic viscosity was tested for 60, 120, and 240 [kg/m/d] encompassing a wider range than in actual ethanol spills. As expected, variations in the diffusion coefficient affected model stability by modifying fingers and blobs formation and velocity. Low diffusion values resulted in instability occurrences close to the concentration interface that spread in the whole domain quickly.

Figure 50 - Comparison of density ratio effects on plume fingering.

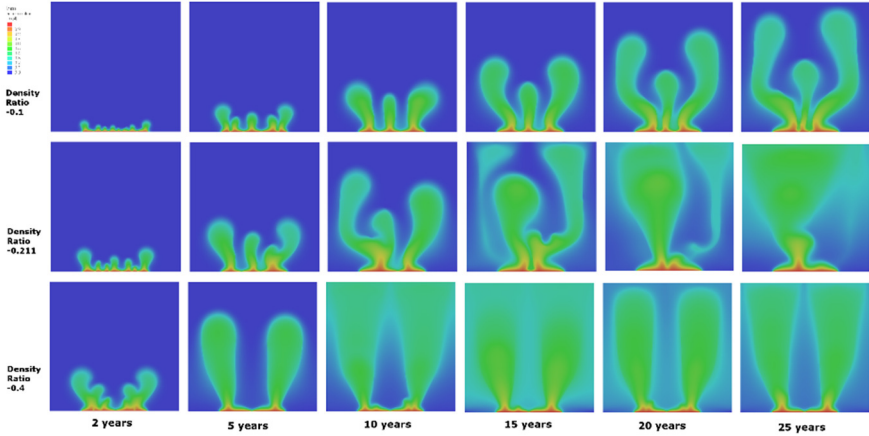
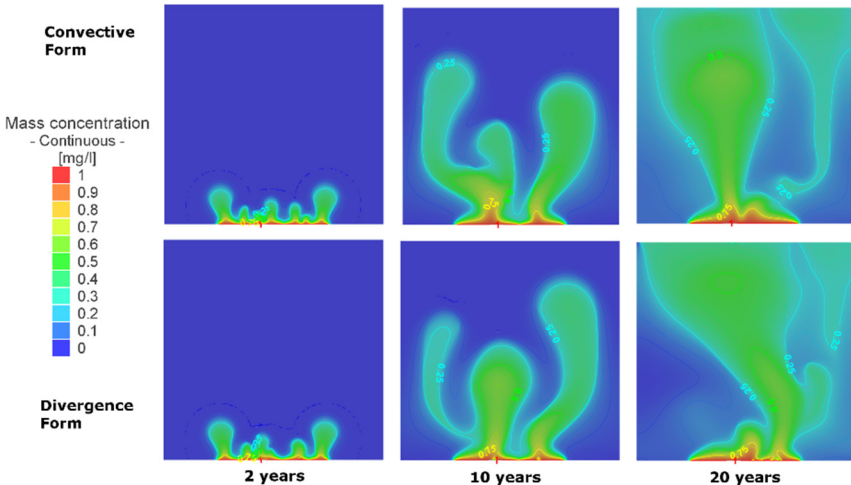


Figure 51 - Comparison of fingers behavior with convective and divergence formulation of ADE solved by FEFLOW.



Changing the characteristics of the free convection process results in a variation of the onset of plume generation, the rate of plume descent and the plume dimensions (Post and Prommer, 2007). Therefore, to test model with similar blobs velocities, two runs use a constant Ra (of about $9 \cdot 10^6$) obtained by proportional changes in density ratio (0.211 and 4.22) and hydraulic conductivity (2 and 0.5). However, results exhibit only unimportant differences in fingers behavior (Supporting Material – Fig.SM3), confirming that Ra value controls the density-driven flow. Finally, by testing convective and divergence form of advection-dispersion equation (Eq.19), quite different solutions are showed for the same parameters (Fig. 51). This fact underlines that only in absence of normal advective flux the two solution coincide (Diersch, 2014), since the meaning of BC in the two formulation are quite different. Divergence form allows the input of the total (advective and dispersive) mass flux at the boundary while convective form prioritize the advective flux (Diersch, 2014).

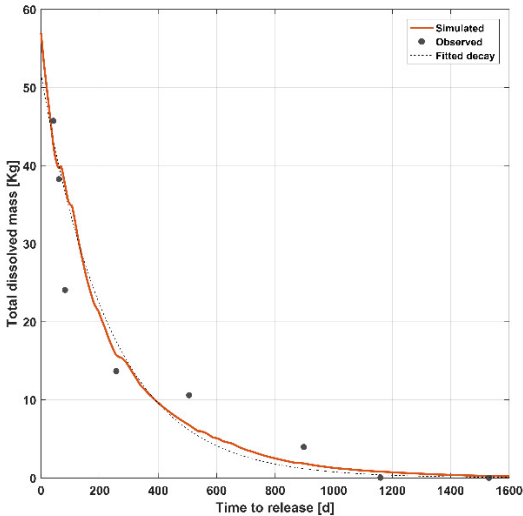
3.5.3.6 Model D

The model D analyzed reactive and conservative solute transport in a highly variable flow field with density and viscosity gradient effects. Its objective was to determine the differences in plume transport between steady and transient prescribed-head type boundary conditions.

Model D represents a numerical experiment based on the MNA_E85 field experiment conditions. A 3D domain defines a triangular portion of Ressacada Farm between piezometers PE03, PE02 and PM01 where MNA_E85 experiment is included (Fig. 44). This portion coincides with domain used to investigate the influence of variable flow conditions on solutes transport derived from a gasohol spill (Rama et al., 2019). The hypothesis was a pseudo-planar water table in the triangular area, which vertices are defined by hydraulic head records from piezometers. Richard's equation was preferred to simulate flow including vadose zone dynamics, while convective formulation of transport problem was used for contaminant migration. More information about model D are available in Quad.4. Head-prescribed type conditions along the three boundary faces of triangular prism describe water-table fluctuations and changes in flow direction during the field experiment (08/09/2010 to 30/11/2014). These conditions describe actual groundwater flow variations by the interpolation of piezometers level records over the boundary nodes of selected mesh. A Python sub-routine carries out this task, creating an organized temporal series of head records for all nodes of boundaries

(Supporting Material). In order to simulate a product mass consistent with a pulse release in the field experiment, source is set as an initial condition of concentration in the source nodes. Such concentration is estimated previously as a function of source volume (0.1 m^3) and assumed porosity (0.38). A manual trial-and-error approach is used to calibrate plume migration rate and concentration in the multi-level wells along the main direction of flow, showing a reasonable accordance between field data and numerical results (Fig.52).

Figure 52 – Comparison of Model D simulation (*red solid line*) and observed evolution (*black dots*) of total dissolved mass in the field experiment MNA_E85 (Rama et al., 2019).

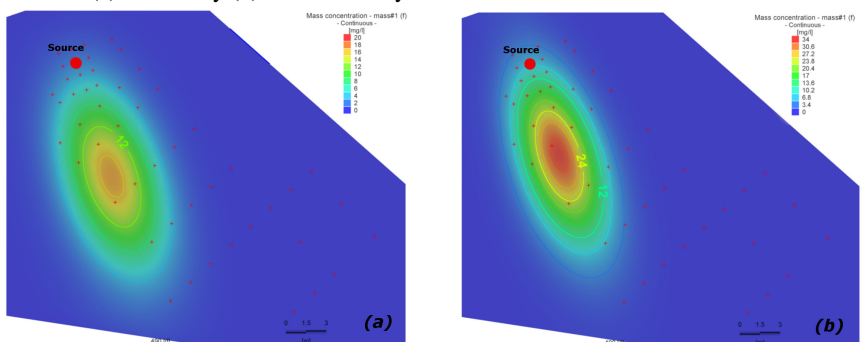


In addition, to assess implications of a chosen temporal behavior of the model on the plume transport, a test with stationary water table is presented. Such numerical experiment presents constant BCs based on the average head values in the simulated period, also respecting average water-table gradient and direction. It worth stressing that steady-state models are inherently simpler to create, run and post-process than transient models. They need a single set of calibration data and produce one set of results, while transient models require multiple calibration data sets and produce more outputs (Anderson et al. 2015). Furthermore, transient models require additional inputs (i.e. storage parameters, initial conditions). However, in many cases transient models are clearly required or need for the modelling objective. In the model D, having forcing

function period of 1 to 5 day (i.e. time-step for head records), a transient model is required to describe groundwater flow dynamics and sure enough the non-dimensional “aquifer response time” exhibits a value of about 0.6 [-]. This is a simple calculation used to assess when steady-state conditions can approximate transient system response to periodic stresses (Haitjema, 2006), prescribing for values between 0.1 and 1 to use transient models to describe flow phenomena. Moreover, “groundwater system time constant” (Domenico and Schwartz, 1998, p.173) showed a values of 7.7 days, suggesting for stresses of 1 to 5 days using transient flow models. Therefore, this steady test with Model D focus on the differences in plume migration, conscious that in any case a stationary groundwater simplification dropped out important flow field dynamics, but perhaps not affecting solute transport.

Results show differences in the dispersion of simulated plumes. Coherently with the averaged values of hydraulic head used to define the stationary BCs, both plumes move along a similar main direction. Conversely, transport appears to be affected even by fast transient changes in groundwater flow, resulting in a slightly different solute spreading (Fig. 53). Indeed, recurrent changes in head-prescribed BCs implicate a variable flow field within the domain, enhancing plume dispersion (Bellin et al. 1996; Rama et al. 2019). However, the plume distance in the two runs result less than supposed, likely due to the time of BC stresses to modify the whole domain. Instead of a pseudo-planar water table, the perturbation of levels along the boundary defines a curve aquifer surface within the domain that take 1 to 3 days to stabilize in a planar water table.

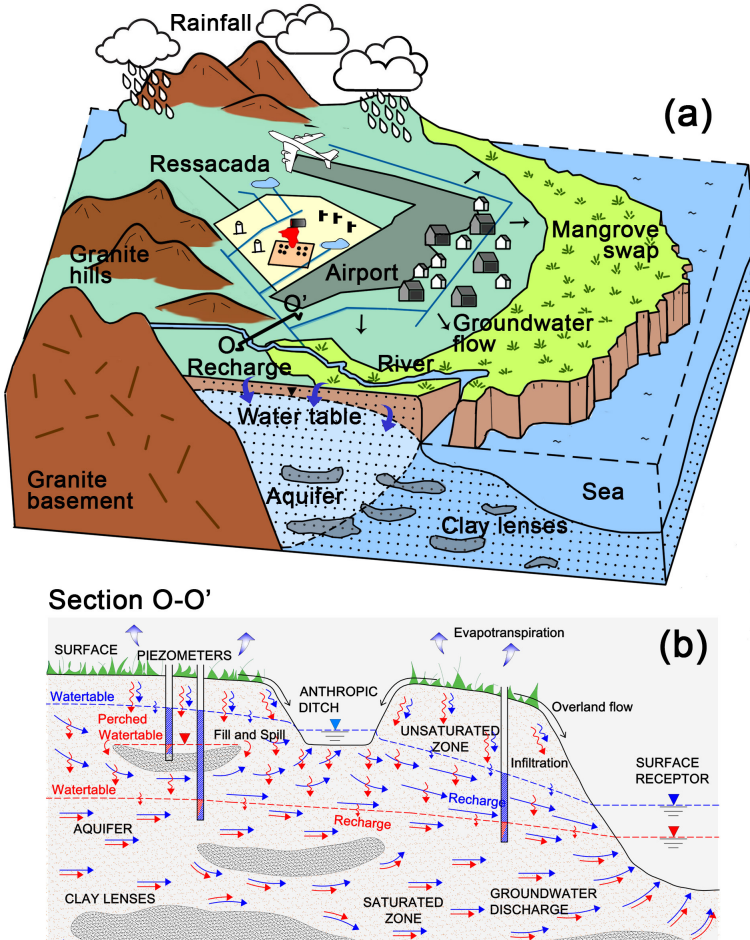
Figure 53 - Comparison of conservative plumes dispersion after 490 days with transient (a) and steady (b) head boundary conditions.



3.5.3.7 Hydrogeological conceptual model of Ressacada Aquifer

A multi-model approach was implemented in the development of hydrogeological conceptual model. An ensemble of numerical experiments at different scale was used to verify field information and main phenomena affecting aquifer water balance. Each model addressed specific conceptual issues, reducing total uncertainty of final assumptions on groundwater flow.

Figura 54 – (a) 3D sketch of hydrogeological conceptual model of the Ressacada plain. (b) 2D conceptual sketch of a soil transect (O-O') showing active processes affecting groundwater flow at local scale under different groundwater regimes.



In the model of Ressacada aquifer (Fig.54a), groundwater flow is a result of a low hydraulic gradient variation driven by precipitation recharge. The aquifer flow is radial diverging from the domain center (i.e. International Airport area) to the boundaries (i.e. Tavares River system and South Bay). The rapid fluctuation of water-table level results markedly more pronounced in the domain center (far from surface receptors) even with a uniform recharge stress (43% of precipitation). However, spatial variability of recharge along with preferential flow in the vadose zone and heterogeneity of porous medium entails transient changes in local flow directions (Rama et al. 2018). Surface receptors that represent domain boundaries are constantly subject to transient fluctuations of water level (e.g. tidal oscillations, flood events), which modify surface-subsurface interactions over the time. In addition, in the mangrove swamps low permeable layers along with density-driven effects of brackish water results in a complex hydrodynamic of first layers of soil that affect the water discharge of the aquifer. Conversely, runoff contribution from outcropping granite hills resulted negligible in the aquifer water budget, having only a local influence on the hydraulic head.

At local scale, close the field experiment, four mechanisms and their variation affect mostly flow field and water budget in the aquifer (Fig.54b):

- (1) irregular fluctuation of water table even for a uniform recharge in a homogeneous medium. Water-table fluctuations increase with the distance to the surface receptors (e.g. river, sea) and reach their maximum at the aquifer watershed;
- (2) transient drainage network activation. impacts infiltration process and local flow net, maintaining water-table position under the ground and avoiding permanent inundation of the plain
- (3) recurrent variation of hydraulic head at surface receptors (e.g. seasonal regime, isolated rainfall event). Such boundary fluctuations affects groundwater flow velocities and total discharge volumes from the aquifer, mainly for long-term variations
- (4) presence of irregular clay lenses with unknown position. These geological features modifies the local flow net and causes uncertainty in the measurements of hydraulic head. However, given their heterogeneous nature, lenses are difficult to be characterized and modelled, requiring for this high field and computation efforts.

3.5.4 Conclusions

A systematic regional conceptual model of Ressacada aquifer is developed by using field data analysis and numerical experiments. It is a coastal groundwater basin in which a number of complexities were highlighted, including (a) large water-table fluctuations, (b) transient changes in groundwater flow direction, (c) variations in boundary conditions, (d) strong reaction to precipitation recharge and, (e) surface drainage networks. The models showed that subsurface flow in the aquifer is driven by differential recharge over time and space, surface receptors levels and anthropic drain activation. The groundwater flow is mainly radial from the center of the plain. However, there are significant local deviations due to the combined effect of geological heterogeneities and transient hydrological processes. More importantly, the modelling showed that (a) direct influence of tidal oscillation on water table levels as well as (b) subsurface runoff from the granite hills in the south have a local influence only and do not affect hydraulic head and groundwater velocity distribution at the Experimental Farm.

This contribution underlines the importance of simple numerical models to verify and summarize our understanding of natural full-scale phenomena described by field data. In many practical cases, numerical models represent the key tool to integrate limited field data and explore the processes related with water resources. However, complex models may be too slow in the transient state, which suggests a need for a proper problem conceptualization to maintain strictly the necessary information and processes. On the other hand, the Model C1 confirms the importance of parameter optimization, which is much easier to perform in simple models. By developing a 2D vertical model of a longitudinal transect, the influence of BC levels and ditches streambed topography in the Ressacada plain is highlighted.

FEFLOW proves to be an effective tool to manage density-driven flow with negative density ratios (e.g. ethanol spills), despite some incongruences in pollutant mass estimation due to sudden variations in the considered water volume. Moreover due to impossibility to define a fixed mass of contaminant in the source, initial concentration within the source nodes have to be prior calculated as a function of source volume and total porosity.

Finally, the boundary level fluctuations result in a differential, although limited, solute plume migration between steady and transient run. However, hydraulic head perturbation at boundaries with temporal series results in a slow propagation towards the center of domain, which

may be related with hydraulic conductivity value. The expectation of obtaining a 'pseudo-instantaneous' change of water table direction in the model with no transient effects on the velocities caused by storage volume was proved to be unrealistic. Thus, it was not possible to dissociate propagation of boundary level information from conductivity value, which is a calibration parameter affecting solute transport, and thereby cannot be freely modified to enhance this propagation.

Acknowledgments

The authors want to acknowledge FEESC and Petróleo Brasileiro (Petrobras) for the financial and material support that made this study possible and DHI Group for providing a MIKE Powered by DHI license file to use FEFLOW. We thank also the Institute of Airspace Control (ICEA) and National Institute of Meteorology (INMET) for providing valuable precipitation data, all the technicians of Agrarian Sciences Center (CCA) and REMA for their support in the field data collection, Dr. Luis H.P. Garbossa for help obtaining sea-level records from the EPAGRI/CIRAM gauge station in the South Bay and Prof. Davide Franco (LaHiMar, ENS/UFSC) to provide the ultrasonic propeller current-meter. Finally we thank PhD Martina Pacifici (USP, PPGEC) for her crucial help with the figure design.

References

- Acharya, S., Jawitz, J.W., Mylavarapu, R.S., 2012. Analytical expressions for drainable and fillable porosity of phreatic aquifers under vertical fluxes from evapotranspiration and recharge. *Water Resour. Res.* 48, 1–15. <https://doi.org/10.1029/2012WR012043>
- Anderson, M.P., Woessner, W.W., Hunt, R.J. 2015. *Applied Groundwater Modeling - 2nd Edition - Simulation of Flow and Advective Transport*, Elsevier Inc., Academic Press, ISBN: 9780120581030, p.630
- Barnett, B., Townley, L.R., Post, V., Evans, R.E., Hunt, R.J., Peeters, L., Richardson, S., Werner, A.D., Knapton, A., Boronkay, A. 2012 *Australian groundwater modelling guidelines*. National Water Commission, Australia. ISBN: 978-1-921853-91-3, p.203
- Bear, J. 2018. *Modeling Phenomena of Flow and Transport in Porous Media*, Springer Nature, ISSN 2213-6940, p.761
- Bear, J., Cheng, A.H.-D., 2010. *Modeling Groundwater Flow and Contaminant Transport*, Springer Science, Vol. 23, ISBN 978-1-4020-6681-8, p.850
- Bellin, A., Dagan, G., Rubin, Y., 1996. The impact of head gradient transients on transport in heterogeneous formations: Application to the Borden Site. *Water Resour. Res.* 32, 2705–2713. <https://doi.org/10.1029/96WR01629>
- Boano, F., Harvey, J.W., Marion, A., Packman, A.I., Revelli, R., Ridolfi, L., Worman, A., 2014. Hyporheic flow and transport processes: Mechanisms, models, and biogeochemical implications *F. Rev. Geophys.* 52, 603–679. <https://doi.org/10.1002/2012RG000417>.Received
- Bredehoeft, J.D., 2005. The conceptualization model problem - Surprise. *Hydrogeol. J.* 13, 37–46. <https://doi.org/10.1007/s10040-004-0430-5>
- Brunner, P., Cook, P.G., Simmons, C.T., 2009. Hydrogeologic controls on disconnection between surface water and groundwater. *Water Resour. Res.* 45, 1–13. <https://doi.org/10.1029/2008WR006953>
- Cardenas, M.B., 2008. Surface water-groundwater interface geomorphology leads to scaling of residence times. *Geophys. Res. Lett.* 35, 1–5. <https://doi.org/10.1029/2008GL033753>
- CCA/UFSC. Centro de Ciências Agrárias da UFSC. Main page of Ressacada Experimental Farm project. Available at: <<http://fazenda.ufsc.br/>>. Accessed: March 2016

- Chaminé, H.I., Carvalho, J.M., Teixeira, J., Freitas, L., 2015. Role of hydrogeological mapping in groundwater practice: back to basics. *Eur. Geol.* 40, 34–42.
- Cherry J.A., Barker J.F., Feenstra S., Gillham R.W., Mackay D.M., Smyth D.J.A. (1996) The Borden Site for Groundwater Contamination Experiments: 1978–1995. In: Kobus H., Barczewski B., Koschitzky HP. (eds) *Groundwater and Subsurface Remediation*. Environmental Engineering. Springer, Berlin, Heidelberg
- Clement, T.P., 2011. Complexities in Hindcasting Models — When Should We Say Enough Is Enough? *Ground Water* 49, 620–629. <https://doi.org/10.1111/j.1745-6584.2010.00765.x>
- Corseuil, H.X., Fernandes, M., 1999. Efeito do etanol no aumento da solubilidade de compostos aromáticos presentes na gasolina brasileira. *Rev. Eng. Sanitária e Ambient.* 4, 71–75.
- Corseuil, H.X., Gomez, D.E., Schambeck, C.M., Ramos, D.T., Alvarez, P.J.J., 2015. Nitrate addition to groundwater impacted by ethanol-blended fuel accelerates ethanol removal and mitigates the associated metabolic flux dilution and inhibition of BTEX biodegradation. *J. Contam. Hydrol.* 174C, 1–9. <https://doi.org/10.1016/j.jconhyd.2014.12.004>
- Corseuil, H.X., Kaipper, B.I.A., Fernandes, M., 2004. Cosolvency effect in subsurface systems contaminated with petroleum hydrocarbons and ethanol. *Water Res.* 38, 1449–1456. <https://doi.org/10.1016/j.watres.2003.12.015>
- Corseuil, H.X., Monier, A.L., Fernandes, M., Schneider, M.R., Nunes, C.C., 2011a. BTEX Plume Dynamics Following an Ethanol Blend Release: Geochemical Footprint and Thermodynamic Constraints on Natural Attenuation - Supporting Information. *Environ. Sci. Technol.* 23. <https://doi.org/10.1117/1111.2794018.2>
- Corseuil, H.X., Monier, A.L., Fernandes, M., Schneider, M.R., Nunes, C.C., Do Rosario, M., Alvarez, P.J.J., 2011b. BTEX plume dynamics following an ethanol blend release: Geochemical footprint and thermodynamic constraints on natural attenuation. *Environ. Sci. Technol.* 45, 3422–3429. <https://doi.org/10.1021/es104055q>
- De Schepper, G., Therrien, R., Refsgaard, J.C., Hansen, A.L., 2015. Simulating coupled surface and subsurface water flow in a tile-drained agricultural catchment. *J. Hydrol.* 521, 374–388. <https://doi.org/10.1016/j.jhydrol.2014.12.035>
- Devos, A., Bollot, N., Chalumeau, L., Fronteau, G., Lejeune, O., 2015. Impact of lateral variations of geologic facies on water resources in homogeneous basins: example of tertiary plateaus in the Paris Basin. *Geodin. Acta* 27, 15–24. <https://doi.org/10.1080/09853111.2014.979531>
- Dewandel, B., Lachassagne, P., Wyns, R., Marechal, J.C., Krishnamurthy, N.S., 2006. A generalized 3-D geological and hydrogeological conceptual model of granite aquifers controlled by single or multiphase weathering. *J. Hydrol.* 330, 260–284. <https://doi.org/10.1016/j.jhydrol.2006.03.026>
- Diersch, H. J. G., 2014. *FEFLOW - Finite Element Modeling of Flow, Mass and Heat Transport in Porous and Fractured Media*, Springer, ISBN 978-3-642-38738-8, p.1018
- Diersch, H.J.G., Kolditz, O., 2002. Variable-density flow and transport in porous media; approaches and challenges. *Adv. Water Resour.* 25, 899–944. [https://doi.org/10.1016/S0309-1708\(02\)00063-5](https://doi.org/10.1016/S0309-1708(02)00063-5)
- Doherty, J., 2015. *Calibration and Uncertainty Analysis for Complex Environmental Models*. Watermark Numerical Computing, Brisbane, Australia. ISBN: 978-0-9943786-0-6.
- Doherty, J.E., Hunt, R.J., 2010. Approaches to highly parameterized inversion—A guide to using PEST for groundwater-model calibration: U.S. Geological Survey Scientific Investigations Report 2010–5169, 59 p.
- Doherty, J., Simmons, C.T., 2013. Groundwater modelling in decision support: reflections on a unified conceptual framework. *Hydrogeol. J.* 21, 1531–1537. <https://doi.org/10.1007/s10040-013-1027-7>
- Doherty, J., Welter, D., 2010. A short exploration of structural noise. *Water Resour. Res.* 46, 1–14. <https://doi.org/10.1029/2009WR008377>
- Domenico, P.A., Schwartz, F.W., 1998. *Physical and Chemical Hydrogeology*. John Wiley & Sons.
- Duke, H.R., 1972. Capillary properties of soils - Influence upon specific yield. *Trans. ASAE* 15, 688–691.
- Eberhardt, R.W., Latham, R.E., 2000. Relationships among Vegetation, Surficial Geology and Soil Water Content at the Pocono Mesic Till Barrens. *J. Torrey Bot. Soc.* 127, 115–124.

- Enemark, T., Peeters, L.J.M., Mallants, D., Batelaan, O., 2019. Hydrogeological conceptual model building and testing: A review. *J. Hydrol.* 569, 310–329. <https://doi.org/10.1016/j.jhydrol.2018.12.007>
- Esteves, M.B. Levantamento geofísico –Potencial espontâneo (SP). Documento não publicado. UFSC. Florianópolis. 2002.
- Esteves, M.B. Levantamento topo-geofísico e construção de piezômetros (informe sobre fluxo preferencial da água subterrânea). Documento não publicado. Laboratório de Geologia, Departamento de Geociências da UFSC. 2000
- Francés, A. P., Lubczynski, M. W., Roy, J., Santos, F. A. M., Ardekani, M. R. 2014. Hydrogeophysics and remote sensing for the design of hydrogeological conceptual models in hard rocks - Sardón catchment (Spain). *J. Appl. Geophys.* 110, 63–81.
- Freeze, R.A., Witherspoon, P.A., 1967. Theoretical Analysis of Regional Groundwater Flow. 2.Effect of Water-Table Configuration and Subsurface Permeability Variation. *Water Resour. Res.* 3, 623–634.
- Garbossa, L.H.P., Vanz, A., Fernandes, L., Souza, R.V. de, Vianna, L.F., Rupp, G., 2014. Modelling and Validation of the Santa Catarina Island Bays Hydrodynamics Based on Astronomic Tides and measured Tides. 11th Int. Conf. Hydroinformatics 8. <https://doi.org/10.13140/2.1.5123.6163>
- Guillaume, J.H.A., Hunt, R.J., Comunian, A., Blakers, R.S., Fu, B. 2016. Methods for Exploring Uncertainty in Groundwater Management Predictions. Chapter of: *Integrated Groundwater Management: Concepts, Approaches and Challenges*. Springer Open. DOI 10.1007/978-3-319-23576-9, p.711-737
- Haitjema, H.M. 2006. The role of hand calculations in ground water flow modeling. *Groundwater*, 44(6), 786-791. <http://dx.doi.org/10.1111/j.1745-6584.2006.00189.x>.
- Haitjema, H.M., Mitchell-bruker, S., 2005. Are Water Tables a Subdued Replica of the Topography ? *Ground Water* 43, 781–786. <https://doi.org/10.1111/j.1745-6584.2005.00090.x>
- Harrington, G.A., Payton Gardner, W., Munday, T.J., 2013. Tracking Groundwater Discharge to a Large River using Tracers and Geophysics. *Groundwater* 52, 837–852. <https://doi.org/10.1111/gwat.12124>
- Herkenrath, D., Langevin, C.D., Doherty, J., 2011. Predictive uncertainty analysis of a saltwater intrusion model using null-space Monte Carlo. *Water Resour. Res.* 47, 1–16. <https://doi.org/10.1029/2010WR009342>
- Hunt, R.J., Feinstein, D.T., Pint, C.D., Anderson, M.P., 2006. The importance of diverse data types to calibrate a watershed model of the Trout Lake Basin, Northern Wisconsin, USA. *J. Hydrol.* 321, 286–296. <https://doi.org/10.1016/j.jhydrol.2005.08.005>
- Jamshidzadeh, Z., Tsai, F.T., Ahmad, S., Ghasemzadeh, H., 2013. Fluid dispersion effects on density-driven thermohaline flow and transport in porous media. *Adv. Water Resour.* 61, 12–28. <https://doi.org/10.1016/j.advwatres.2013.08.006>
- Johnston, K., Ver Hoef, J.M., Krivoruchko, K., Lucas N. 2001. *Using ArcGIS™ Geostatistical Analyst*. ESRI, New York, p.306
- Kirsch R., Yaramanci U. (2009) *Geoelectrical methods*. In: Kirsch R. (eds) *Groundwater Geophysics*. Springer, Berlin, Heidelberg
- Konikow, L.F., 2011. The Secret to Successful Solute-Transport Modeling. *Ground Water* 49, 144–159. <https://doi.org/10.1111/j.1745-6584.2010.00764.x>
- Konikow, L. F., 1978. Calibration of ground-water models. In: *Verification of Mathematical and Physical Models in Hydraulic Engineering*. American Society of Civil Engineers, New York, p.87-93
- Konikow, L. F., Bredehoeft, J. D. “Computer Model of Two Dimensional Solute Transport and Dispersion in Groundwater,” U.S. Geological Survey, *Techniques of Water Resources Investigation Book 7, Chapter C2*, 1992, p. 90.
- Lage I de C (2005) *Avaliação de metodologias para determinação da permeabilidade em meios porosos: Fazenda Ressacada (Evaluation of methodologies for determination of permeability in porous media: Ressacada Farm)*. UFRJ. Rio de Janeiro. MSc Thesis.

LEBAC/FUNDUNESP. Laboratório de Estudos de Bacias/Fundação para o desenvolvimento (DGA/UNESP). Caracterização Geométrica do Campo Experimental da Fazenda Ressacada em Florianópolis: Resultados Preliminares. Documento não publicado. 2007

Li, Y., Oldenburg, D.W., 1996. 3-D inversion of magnetic data. *Geophysics* 61, 394–408.

Linde, N., Renard, P., Mukerji, T., Caers, J., 2015. Advances in Water Resources Geological realism in hydrogeological and geophysical inverse modeling: A review. *Adv. Water Resour.* 86, 86–101. <https://doi.org/10.1016/j.advwatres.2015.09.019>

Mckenna, S.A., Doherty, J., Hart, D.B., 2003. Non-uniqueness of inverse transmissivity field calibration and predictive transport modeling. *J. Hydrol.* 281, 265–280. [https://doi.org/10.1016/S0022-1694\(03\)00194-X](https://doi.org/10.1016/S0022-1694(03)00194-X)

Miotlinski, K., Dillon, P.J., Pavelic, P., Cook, P.G., Page, D.W., Levett, K., 2011. Recovery of injected freshwater to differentiate fracture flow in a low-permeability brackish aquifer. *J. Hydrol.* 409, 273–282. <https://doi.org/10.1016/j.jhydrol.2011.08.025>

Motyka, J., 1998. A conceptual model of hydraulic networks in carbonate rocks, illustrated by examples from Poland. *Hydrogeol. J.* 6, 469–482.

Nilsson, B., Højberg, A.L., Refsgaard, J.C., Troldborg, L., 2007. Uncertainty in geological and hydrogeological data. *Hydrol. Earth Syst. Sci.* 11, 1551–1561.

Ophori, D.U., 1998. The significance of viscosity in density-dependent flow of groundwater. *J. Hydrol.* 204, 261–270.

Ormsby, T.J. et al. 2004. Getting to know ARCGIS – 2nd Edition. ESRI Press, New York, ISBN 97&1-58948-260-9, p.597

Post, V.E.A., Prommer, H., 2007. Multicomponent reactive transport simulation of the Elder problem: Effects of chemical reactions on salt plume development. *Water Resour. Res.* 43, 1–13. <https://doi.org/10.1029/2006WR005630>

Prasad, A., Simmons, C.T., 2003. Unstable density-driven flow in heterogeneous porous media: A stochastic study of the Elder [1967b] “short heater” problem. *Water Resour. Res.* 39, 1–21. <https://doi.org/10.1029/2002WR001290>

Rama, F., Franco, D., Corseuil, H.X., 2017. Spatial and Temporal Analysis of Natural Drainage in the Ressacada Aquifer (Florianópolis, Brazil). *Int. J. Environ. Sci. Dev.* 8, 653–660. <https://doi.org/10.18178/ijesd.2017.8.9.1033>

Rama, F., Miotlinski, K., Franco, D., Corseuil, H.X., 2018. Recharge estimation from discrete water-table datasets in a coastal shallow aquifer in a humid subtropical climate. *Hydrogeol. J.* 26, 1887–1902. <https://doi.org/10.1007/s10040-018-1742-1>

Rama, F., Ramos, D.T., Müller, J.B., Corseuil, H.X., Miotlinski K., 2019. Flow field dynamics and high ethanol content in gasohol blends enhance BTEX migration and biodegradation in groundwater, *J. Contam. Hydrol.*, <https://doi.org/10.1016/j.jconhyd.2019.01.003>

Ramos, D.T., da Silva, M.L.B., Chiaranda, H.S., Alvarez, P.J.J., Corseuil, H.X., 2013. Biostimulation of anaerobic BTEX biodegradation under fermentative methanogenic conditions at source-zone groundwater contaminated with a biodiesel blend (B20). *Biodegradation* 24, 333–341. <https://doi.org/10.1007/s10532-012-9589-y>

Randle, C.H., Bond, C.E., Lark, R.M., Monaghan, A.A., 2018. Can uncertainty in geological cross-section interpretations be quantified and predicted? *Geosphere* 14, 1087–1100. <https://doi.org/10.1130/GES01510.1>

Renard, P., 2005. The future of hydraulic tests. *Hydrogeol. J.* 13, 259–262.

Riva, M., Guadagnini, L., Guadagnini, A., 2010. Effects of uncertainty of lithofacies, conductivity and porosity distributions on stochastic interpretations of a field scale tracer test. *Stoch. Environ. Res. Risk Assess.* 24, 955–970. <https://doi.org/10.1007/s00477-010-0399-7>

Sanchez-Vila, X., Guadagnini, A., Carrera, J., 2006. Representative hydraulic conductivities in saturated groundwater flow. *Rev Geophys* 44:RG3002. <https://doi.org/10.1029/2005RG000169>

- Skempton, A.W., 1953. SOIL MECHANICS IN RELATION TO GEOLOGY. Proc. Yorksh. Geol. Soc. 29, 33–62. <https://doi.org/10.1144/pygs.29.1.33>
- Steiner, L.V., Ramos, D.T., Liedke, A.M.R., Serbent, M.P., Corseuil, H.X., 2018. Ethanol content in different gasohol blend spills influences the decision-making on remediation technologies. J. Environ. Manage. 212, 8–16. <https://doi.org/10.1016/j.jenvman.2018.01.071>
- Sudicky, E.A., 1986. A natural gradient experiment on solute transport in a sand aquifer: Spatial variability of hydraulic conductivity and its role in the dispersion process. Water Resour. Res. 22, 2069–2082. <https://doi.org/10.1029/WR022i013p02069>
- Toth, J., 1962. A Theory of Groundwater Motion in Small Drainage Basins in central Alberta, Canada. J. Geophys. Res. 67, 4375–4387.
- Trefry, M.G., Muffels, C., 2007. FEFLOW: A Finite-Element Ground Water Flow and Transport Modeling Tool. Ground Water 525–528. <https://doi.org/10.1111/j.1745-6584.2007.00358.x>
- Voss, C.I., Souza, W.R., 1987. Variable density flow and solute transport simulation of regional aquifers containing a narrow freshwater–saltwater transition zone. Water Resour. Res. 23 10, 1851–1866.
- Wade, A., 1935. The Relationship between Topography and Geology. Aust. Surv. 5, 367–371. <https://doi.org/10.1080/00050326.1935.10436440>
- Winter, T.C. 1976. Numerical Simulation Analysis of the Interaction of Lakes and Ground Water. USGS Professional Papers 1001, p.45
- Woessner, W.W., 2000. Stream and fluvial plain ground water interactions: rescaling hydrogeologic thought. Ground Water 38, 432–429.
- Wooding, R. A. (1969), Growth of fingers at an unstable diffusing interface in a porous medium or Hele-Shaw cell, J. Fluid Mech., 39, 477–495.
- Xie, Y., Simmons, C.T., Werner, A.D., Ward, J.D., 2010. Effect of transient solute loading on free convection in porous media. Water Resour. Res. 46, 1–16. <https://doi.org/10.1029/2010WR009314>

4 PRINCIPAIS CONTRIBUIÇÕES

A partir da revisão do Capítulo 3.1 foi possível:

- Entender o transporte de solutos em um campo de fluxo variável.
 - Apresentou-se a formulação matemática do problema de fluxo e transporte, e os parâmetros de interesse
 - Foram descritos os principais fenômenos ativos as diferentes escalas em ambiente subterrâneo e as questões de pesquisas mais atuais sobre o problema
 - Destacaram-se as peculiaridades dos aquíferos costeiros e as condições de elevada variabilidade da hidrodinâmica subsuperficial

A partir do desenvolvimento dos Capítulos 3.2 e 3.3 foi possível:

- Analisar as escalas dos fenômenos de resposta às forçantes de precipitação e maré do aquífero da Ressacada, um aquífero costeiro, livre, em clima subtropical úmido (OBJ1 – OBJ2)
 - A variabilidade na descarga na porção investigada do aquífero da Ressacada foi caracterizada no espaço e no tempo
 - Dois grupos de piezômetros foram destacados na Ressacada, mostrando uma variação relevante no comportamento das taxas de rebaixamento do lençol freático (em média $47.3 - 87.7 \text{ mm}\cdot\text{d}^{-1}$)
 - Uma função exponencial foi usada para explicar as taxas de descarga no tempo, destacando dois regimes de fluxo típicos a partir do último evento pluviométrico
 - A recarga do aquífero foi estimada aplicando o método WTF a series de dados descontinuas e tendo em consideração a variabilidade no tempo e no espaço da infiltração
 - Uma abordagem inédita baseada em series descontinuas de cargas hidráulica e informações pluviométricas foi desenvolvida e aplicada ao banco de dados do REMA
 - O valor de recarga médio na Ressacada foi estimado com base 10 anos (43%), avaliando ao mesmo tempo sua variabilidade anual, sazonal e mensal (em média 35.9-51.6%)

- O valor plurianual de recarga foi verificado a partir da construção de um modelo numérico de fluxo 2D calibrado com 10 anos de medições em 2 piezômetros, que representa um perfil longitudinal do aquífero
- A contribuição da oscilação periódica de maré na alteração dos níveis freáticos na Fazenda foi considerada desprezível, por ser da ordem do centímetro

A partir da análise e das considerações do Capítulo 3.4 foi possível:

- Descrever os efeitos conjuntos do teor de etanol e da velocidade local do fluxo na migração e atenuação das plumas de contaminantes em aquíferos contaminados com gasolina e etanol (OBJ3)
 - Destacou-se uma direta relação entre as altas quantidade de etanol na fonte e as concentrações de BTEX nas águas subterrâneas (5 e 20 mg·L⁻¹, respectivamente nas áreas E24 e E85), cujo contato na fonte foi favorecido pelas intensas flutuações do lençol freático (60 cm)
 - Evidenciou-se que concentrações elevadas de BTEX implicaram taxas de degradação dos mesmos contaminantes em médias mais altas (respectivamente 0.401 e 0.816 y⁻¹ nas áreas E24 e E85)
 - Mostrou-se uma relação direta entre velocidade de fluxo subterrânea e taxa de migração dos BTEX dissolvidos, que portanto interessam áreas maiores na E85 respeito a E24
 - Destacou-se uma forte componente vertical no transporte das plumas (até 1.5 m em 250 dias), que deveria ser considerada em áreas contaminadas

A partir dos resultados apresentados no Capítulo 3.5 foi possível:

- Desenvolver um modelo conceitual do escoamento e dos fenômenos ativos no aquífero da Ressacada, mostrando o uso de experimentos numéricos na racionalização de dados e no entendimento das dinâmicas de campo (OBJ4)
 - Investigaram-se as diferentes escalas das forçantes hidrológicas e das respostas em termos de carga hidráulica e velocidade de escoamento

- Construiu-se um modelo conceitual hidrogeológico da região que incluísse os principais fenômenos que caracterizam o balanço hídrico do aquífero e seus efeitos no transporte de compostos na escala local
- Destacaram-se potencial e limitações do código FEFLOW na simulação de plumas em um campo de fluxo variável com efeito de densidade e viscosidade
- Desenvolveu-se uma rotina em Python de interpolação espacial de series de cargas hidráulicas para inclusão em FEFLOW de condições de contorno variáveis no tempo. Assim, avaliaram-se as diferenças no transporte de plumas entre condições de contorno estacionarias e transientes.

5 CONCLUSÕES

O objetivo principal deste trabalho foi analisar as relações entre a hidrodinâmica do fluxo subterrâneo e o transporte de compostos orgânicos em áreas contaminadas com gasolina e etanol. A partir deste objetivo se quis destacar a importância de uma adequada caracterização hidrogeológica das áreas contaminadas para escolha de tecnologias de remediação específicas. Na prática se sugeriu a integração de todas as informações disponíveis em uma área para contextualizar os fenômenos locais de circulação subterrânea adentro da hidrodinâmica e do balanço hídrico regional. O caso de estudo específico foi o aquífero da Ressacada, um aquífero granular não confinado de origem deposicional, localizado em uma região costeira de clima subtropical úmido. O trabalho se destacou por abranger um amplo conjunto de fatores na definição do campo de fluxo natural, que podem ser representativos de muitas áreas contaminadas no Brasil e no mundo. Este fato contribuiu a dúplici utilidade da pesquisa, que de um lado destacou metodologias, análises e aplicações inéditas para a setor científico (teoria) e por outro vislumbrou processos na escala de campo importantes na tomada de decisões em áreas contaminadas (prática).

De um ponto de vista geral, os resultados apresentados no trabalho confirmaram a elevada influência das condições de fluxo no comportamento das plumas nas áreas contaminadas da Ressacada. As peculiaridades em termo de clima, maré e circulação subterrânea da região contribuíram a qualidade do trabalho, resultando em um campo de fluxo fortemente variável no tempo e no espaço. Estas condições permitiram investigar as causas últimas das variações do nível freático em um aquífero costeiro, e com isso as velocidades, direções e gradientes hidráulicos. Foram portanto descritos os mecanismos ativos no subsolo que podem resultar importantes nas tomadas de decisões para áreas contaminadas (Ex. interação entre campo de fluxo e heterogeneidades, recarga variável, flutuação das condições de contorno). O processo de elaboração culminou na construção do modelo conceitual do aquífero da Ressacada, com destaque da influência das forças regionais sobre o fluxo e o comportamento dos contaminantes na escala local. De fato, a partir das informações disponíveis de carga hidráulica, das series pluviométricas e do mapeamento da rede de drenagem foram definidos os mecanismos de recarga e descarga do aquífero, e justificadas as irregularidades no transporte de contaminantes observados no campo. Ao mesmo tempo, foram desenvolvidas novas metodologias para estudo e

gerenciamento de áreas contaminadas (Ex. método WTF discreto, construtor de harmônicas de maré, taxas de migração das plumas).

Assim, resultaram atendidos os 4 objetivos específicos do trabalho (Capítulo 1.2.2). Ao mesmo tempo, as três hipóteses principais de pesquisa (Capítulo 1.1) foram verificadas ao longo do texto. No específico, foram relevadas importantes variações espaciais e temporais nas forçantes que influenciaram a carga hidráulica do aquífero. Também foi confirmado que estas variações do campo de fluxo subterrâneo impactaram a migração das plumas de brometo, BTEX e etanol. Ao contrário, não foi possível verificar totalmente a terceira hipótese, a presença de “divergências significativas na migração e atenuação das plumas simuladas em condições de fluxo estacionário e transiente”. De fato, mostrou-se uma diferenças significativas somente na dispersão entre as plumas simuladas, enquanto a migração média resultou parecida nas duas condições (Capítulo 3.5). Além disso, não foi possível estabelecer em que medida estas diferenças estavam ligadas à dispersão numérica devida à propagação das condições de contorno ou dependiam de reais diferenças nos processos físicos.

Cabe resumir nestas conclusões os principais achados práticos do trabalho, já discutidos em forma extensa ao longo do texto. Trata-se de pequenos “tijolos” de conhecimento, que constituem a base sobre a qual construir as futuras pesquisas na região. Por exemplo foi demonstrado no texto que o fluxo do aquífero da Ressacada é radial e veiculado pelo processo de recarga e pela carga hidráulica dos receptores superficiais. Porém, a eficiência da recarga resulta ligada ao regime pluviométrico e constantemente variável no tempo e no espaço em toda a planície. Além disso, a resposta as precipitações em termo de carga hidráulica do lençol freático é sempre muito rápida (8-12h) e dependente da posição do poço respeito aos receptores. O aquífero mostrou em geral um comportamento mais uniforme em épocas seca (taxas e velocidades de fluxo), resultando marcadamente impactado em época de chuva pela ativação da rede de drenagem superficial. Tratando-se de um aquífero costeiro, o lençol freático é controlado também pela oscilação periódica do nível do mar (maré astronômica), mas na ordem de ± 1 cm em até 300 m do receptor. Se demonstrou que tal perturbação de maré entra pelo estuário do Rio Tavares, procedendo ao longo do rio até as áreas experimentais (3 km de distância do mar). Nestas foi destacado que, sem um estudo hidrogeológico com adequada abrangência espacial e temporal, pode ser transcurada a componente vertical do transporte, resultando em tomadas de decisões erradas. Portanto, seria importante incluir na análise das áreas contaminadas os fatores que facilitam o contato entre as substancias,

como por exemplo as flutuações do lençol freático em casos de contaminação com gasolina e etanol. Por outro lado, para derramamentos de etanol, o efeito da viscosidade sobre o transporte resultou desprezível respeito à variação de densidade. O trabalho salientou que ao desconsiderar a contribuição do fluxo na diminuição das concentrações (transporte advectivo) pode-se sobrestimar as taxas de biodegradação dos contaminantes. Assim, uma tecnologia de remediação deveria ser escolhida com base no entendimento de migração e degradação dos compostos no local.

Finalizando com algumas recomendações para as próximas pesquisas na área, se destaca a necessidade de esforços adicionais para coletas de campo abrangentes e integradas. Visando uma melhor compreensão dos fenômenos naturais, para algumas variáveis (Ex. carga hidráulica, velocidade) se sugere o uso de equipamentos automáticos em lugar da clássica coleta manual. De fato a superioridade dos equipamentos automáticos para monitoramento de campo foi salientada no presente trabalho. Assim, na prossecução dos experimentos citados, sugere-se a adoção de acelerômetros e fluxímetros em contínuo para monitoramento de series temporais robustas. Ao mesmo tempo, foi comprovada a necessidade de obter parâmetros representativos dos fenômenos físicos com boa abrangência espacial, para desenvolver modelos numéricos eficazes. Assim, se auspica o estudo da capacidade de armazenamento do aquífero da Ressacada através de testes de bombeamento, a caracterização de detalhe da geologia local (disposição das lentes de argila) e o monitoramento dos volumes drenados pelas valas da Fazenda. Estudos com traçadores e isótopos, em conjunto ao monitoramento constante das taxas de drenagem, podem favorecer a compreensão das condições específicas de ativação da rede de drenagem nas diferentes condições pluviométricas. Para complementar o presente trabalho, estudos poderiam avaliar a contribuição da componente aperiódica de maré (meteorológica) na flutuação dos níveis freáticos. Também seria útil reconstruir em detalhe o sinal de maré ao longo do rio, para estimar a distância máxima de propagação do mesmo. Finalmente, o estudo das interações entre superfície e subsolo nas áreas de mangue, e contextualmente de seus impactos no balanço hídrico, contribuiriam para o entendimento geral do escoamento da bacia costeira.

REFERÊNCIAS

- ABNT - ASSOCIAÇÃO BRASILEIRA DE NORMAS TÉCNICAS. ABNT NBR 15515-3:2013. Avaliação de passivo ambiental em solo e água subterrânea - Parte 3: Investigação detalhada. Rio de Janeiro, 2013. p.18
- ANDERSON, M.P.; WOESSNER, W.W.; HUNT, R.J. Applied Groundwater Modeling - 2nd Edition - Simulation of Flow and Advective Transport, Elsevier Inc., Academic Press, p.630, 2015.
- ANP-BG. Agência Nacional do Petróleo, Gás Natural e Biocombustíveis. Abastecimento em números – 47º Boletim Gerencial. Fevereiro 2015. Disponível em < www.anp.gov.br/?dw=75634>.
- ANP-BMQP. Agência Nacional do Petróleo, Gás Natural e Biocombustíveis. Boletim de monitoramento da qualidade dos combustíveis. Junho 2018. Disponível em < www.anp.gov.br/>.
- AST - AMERICAN SOCIETY FOR TESTING MATERIALS. ASTM D5447-04(2010), Standard Guide for Application of a Groundwater Flow Model to a Site-Specific Problem, ASTM International, West Conshohocken, PA, 2010, www.astm.org
- AST - AMERICAN SOCIETY FOR TESTING MATERIALS. ASTM D5490-93(2014)e1, Standard Guide for Comparing Groundwater Flow Model Simulations to Site-Specific Information, ASTM International, West Conshohocken, PA, 2014, www.astm.org
- AST - AMERICAN SOCIETY FOR TESTING MATERIALS. ASTM D5609-16, Standard Guide for Defining Boundary Conditions in Groundwater Flow Modeling, ASTM International, West Conshohocken, PA, 2016, www.astm.org
- AST - AMERICAN SOCIETY FOR TESTING MATERIALS. ASTM D5981-96(2008), Standard Guide for Calibrating a Groundwater Flow Model Application, ASTM International, West Conshohocken, PA, 2008, www.astm.org
- ATAIE-ASHTIANI, B.; VOLKER, R. E.; LOCKINGTON, D. A. Tidal effects on groundwater dynamics in unconfined aquifers. Hydrological Processes, v. 15, n. 4, p. 655–669, 2001.
- BACHMAT, Y.; BEAR, J. The general equations of hydrodynamic dispersion in homogeneous, isotropic, porous mediums, Journal of Geophysical Research, v.69, n.12, p.2561–2567, 1964.
- BARRY, D. A. et al. Modelling the fate of oxidisable organic contaminants in groundwater. Advances in Water Resources, v. 25, n. 8–12, p. 945–983, 2002.
- BEAR, J. Modeling Phenomena of Flow and Transport in Porous Media, Springer Nature, p.761, 2018.
- BEAR, J.; CHENG, A.H.-D. Modeling Groundwater Flow and Contaminant Transport, Springer Science, Vol. 23, ISBN 978-1-4020-6681-8, p.850, 2010.

BOGGS, J. M. et al. Field study of dispersion in a heterogeneous aquifer - 1. Overview and site description. *Water Resources Research*, v. 28, n. 12, p. 3281–3291, 1992.

BOGGS, J. M.; ADAMS, E. E. Field Study of Dispersion in a Heterogeneous Acquifer 4. Investigation of Adsorption and Sampling Bias. *Water Resources Research*, v. 28, n. 12, p. 3325–3336, 1992.

BRUNNER, P. et al. Advances in understanding river-groundwater interactions. *Reviews of Geophysics*, v. 55, n. 3, p. 818–854, 2017.

BURR, D. T.; SUDICKY, E. A.; NAFF, R. L. Nonreactive and reactive solute transport in three-dimensional heterogeneous porous media: Mean displacement, plume spreading, and uncertainty. *Water Resources Research*, v. 30, n. 3, p. 791–815, 1994.

CEDAP/EPAGRI. Síntese informativa da maricultura 2014. Florianópolis, Santa Catarina, Brasil. p.7, 2015

CETESB. Companhia Ambiental do Estado de São Paulo. Áreas contaminadas - Apresentação. Disponível em: < <https://cetesb.sp.gov.br/areas-contaminadas/apresentacao/>> Acesso em: Abril 2016

CETESB-MGAC. Companhia Ambiental do Estado de São Paulo. Manual de Gerenciamento de áreas contaminadas. 2001 Disponível em: <<http://areascontaminadas.cetesb.sp.gov.br/>> Acesso em: Abril 2016

CETESB-RAC. Companhia Ambiental do Estado de São Paulo. Relação de áreas contaminadas. Dezembro 2017 Disponível em: <<http://areascontaminadas.cetesb.sp.gov.br/relacao-de-areas-contaminadas/>> Acesso em: Dezembro 2018

CHIARANDA, H. S. Alterações biogeoquímicas em águas subterrâneas impactadas por biodiesel de soja e misturas de diesel/biodiesel (B20). Florianopolis, UFSC, 2011.

COLOMBANI, N. et al. Inferring the interconnections between surface water bodies, tile-drains and an unconfined aquifer-aquitard system: A case study. *Journal of Hydrology*, v. 537, p. 86–95, 2016.

CONAMA - Resolução CONAMA Nº 420/2009 - "Dispõe sobre critérios e valores orientadores de qualidade do solo quanto à presença de substâncias químicas e estabelece diretrizes para o gerenciamento ambiental de áreas contaminadas por essas substâncias em decorrência de atividades antrópicas." - Data da legislação: 28/12/2009 - Publicação DOU nº 249, de 30/12/2009, págs. 81-84

COOK, P. G.; HERCZEG, A. L. Environmental tracers in subsurface hydrology. Springer Science+Business Media, LLC, New York. p.529, 2000

CORSEUIL, H. X. et al. The influence of the gasoline oxygenate ethanol on aerobic and anaerobic btx biodegradation. *Water Research*, v. 32, n. 7, p. 2065–2072, 1998.

- CORSEUIL, H. X. et al. BTEX Plume Dynamics Following an Ethanol Blend Release: Geochemical Footprint and Thermodynamic Constraints on Natural Attenuation. *Environmental Science and Technology*, v. 45, p. 3422–3429, 2011.
- CORSEUIL, H. X. et al. Nitrate addition to groundwater impacted by ethanol-blended fuel accelerates ethanol removal and mitigates the associated metabolic flux dilution and inhibition of BTEX biodegradation. *Journal of contaminant hydrology*, v. 174C, p. 1–9, 2015.
- CORSEUIL, H. X.; FERNANDES, M. Efeito do etanol no aumento da solubilidade de compostos aromáticos presentes na gasolina brasileira. *Revista Engenharia Sanitária e Ambiental*, v. 4, n. 1, p. 71–75, 1999.
- COSTA, R. A. H. Bioestimulação com injeção de nitrato em águas subterrâneas impactadas por derramamento de gasolina com etanol. [s.l.] UFSC, 2008.
- CUTHBERT, M. O. An improved time series approach for estimating groundwater recharge from groundwater level fluctuations. *Water Resources Research*, v. 46, n. 9, p. 1–11, 2010.
- D’AFFONSECA, F. M. et al. Field scale characterization and modeling of contaminant release from a coal tar source zone. *Journal of Contaminant Hydrology*, v. 102, n. 1–2, p. 120–139, 2008.
- DAVIS, G. B. et al. The variability and intrinsic remediation of a BTEX plume in anaerobic sulphate-rich groundwater. *Journal of Contaminant Hydrology*, v. 36, n. 3–4, p. 265–290, 1999.
- DE LOUW, P. G. B. et al. Rainwater lens dynamics and mixing between infiltrating rainwater and upward saline groundwater seepage beneath a tile-drained agricultural field. *Journal of Hydrology*, v. 501, p. 133–145, 2013.
- DENTZ, M.; CARRERA, J. Effective solute transport in temporally fluctuating flow through heterogeneous media. *Water Resources Research*, v. 41, n. 8, p. 1–20, 2005.
- DIERSCH, H. J. G. FEFLOW - Finite Element Modeling of Flow, Mass and Heat Transport in Porous and Fractured Media, Springer, p.1018, 2014.
- ESSAID, H. I.; BEKINS, B. A.; COZZARELLI, I. M. Organic contaminant transport and fate in the subsurface: Evolution of knowledge and understanding. *Water Resources Research*, v. 51, n. 7, p. 4861–4902, 2015.
- FEDRIZZI, F. et al. A Modified Approach for in Situ Chemical Oxidation Coupled to Biodegradation Enhances Light Nonaqueous Phase Liquid Source-Zone Remediation. *Environmental Science and Technology*, v. 51, n. 1, p. 463–472, 2017.
- FERNANDES, M. Atenuação natural de aquífero contaminado por derramamento de gasolina. Florianópolis, UFSC, 2002.

FIORI, A. et al. Stochastic modeling of solute transport in aquifers: From heterogeneity characterization to risk analysis. *Water Resources Research*, v. 51, n. 8, p. 6622–6648, 2015.

FREYBERG, D. L. A Natural Gradient Experiment on Solute Transport in a Sand Aquifer: 2. Spatial Moments and the Advection and Dispersion of Nonreactive Tracers. *Water Resources Research*, v. 22, n. 13, p. 2031–2046, 1986.

GARABEDIAN, S. P. et al. Large-scale natural gradient tracer test in sand and gravel Cape Cod, Massachusetts - 2. Analysis of spatial moment for a non-reactive tracer. *Water Resources Research*, v. 27, n. 5, p. 14, 1991.

GOODE, D. J.; KONIKOW, L. F. Apparent dispersion in transient groundwater flow. *Water Resources Research*, v. 26, n. 10, p. 2339–2351, 1990.

GREEN, D. W. et al. Numerical modeling of unsaturated groundwater flow and comparison of the model to a field experiment, *Water Resources Research*, v.6, n.3, p.862–874, 1970.

GROUNDWATER FOUNDATION, Sources of groundwater contamination. Disponível em: <<https://www.groundwater.org/>>. Acesso em: 28/12/2018.

HAGGERTY, R. et al. What controls the apparent timescale of solute mass transfer in aquifers and soils? A comparison of experimental results. *Water Resources Research*, v. 40, n. 40, p. 1–13, 2004.

HEALY, R.W.; COOK, P.G. Using groundwater levels to estimate recharge. *Hydrogeology Journal*, v.10, p.91–109. 2002.

HESS, K. M.; WOLF, S. H.; CELIA, M. A. Large-Scale natural gradient tracer test in sand and gravel, Cape Cod, Massachusetts - 3. Hydraulic Conductivity Variability and Calculated Macrodispersivities. *Water Resources Research*, v. 28, n. 8, p. 18, 1992.

INSTITUTO BRASILEIRO DE GEOGRAFIA E ESTATÍSTICA. IBGE. Censo demográfico 2010–Florianópolis. Disponível em: <<http://cidades.ibge.gov.br/xtras/perfil.php?codmun=420540/>> Acesso em: Fevereiro 2016

KAO, C. M.; WANG, Y. S. Field investigation of the natural attenuation and intrinsic biodegradation rates at an underground storage tank site. *Environmental Geology*, v. 40, n. 4–5, p. 622–631, 2001.

KITANIDIS, P. K. Persistent questions of heterogeneity, uncertainty, and scale in subsurface flow and transport. *Water Resources Research*, v. 51, n. 8, p. 5888–5904, 2015.

LAGE, I. DE C. Avaliação de metodologias para determinação de permeabilidade em meios porosos: Fazenda Ressacada. Rio de Janeiro, UFRJ, 2005.

- LAPINSKIENE, A.; MARTINKUS, P.; REBŽDAITE, V. Eco-toxicological studies of diesel and biodiesel fuels in aerated soil. *Environmental Pollution*, v. 142, n. 3, p. 432–437, 2006.
- LEBLANC, D. R. et al. Large-Scale Natural Gradient Tracer Test in Sand and Gravel, Cape Cod, Massachusetts - 1. Experimental Design and Observed Tracer Movement. *Water Resources*, v. 27, n. 5, p. 895–910, 1991.
- MACKAY, D. M. et al. A natural gradient experiment on solute transport in a sand aquifer - 1. Approach and overview of plume movement. *Water Resources Research*, v. 22, n. 13, p. 2017–2029, 1986.
- MACKAY, D. M. et al. Impact of Ethanol on the Natural Attenuation of Benzene, Toluene, and o -Xylene in a Normally Sulfate-Reducing Aquifer. *Environmental Science & Technology*, v. 40, n. 19, p. 6123–6130, 2006.
- MAO, X. et al. Tidal influence on behaviour of a coastal aquifer adjacent to a low-relief estuary. *Journal of Hydrology*, v. 327, n. 1–2, p. 110–127, 2006.
- MASETTI, M. et al. Impact of a Storm-Water Infiltration Basin on the Recharge Dynamics in a Highly Permeable Aquifer. *Water Resources Management*, v. 30, n. 1, p. 149–165, 2016.
- MCCRAY, J. E. et al. Remediation of NAPL source zones: Lessons learned from field studies at Hill and Dover AFB. *Ground Water*, v. 49, n. 5, p. 727–744, 2011.
- MCKNIGHT, T.; HESS, D.L. Climate Zones and Types. *Physical Geography: A Landscape Appreciation*. Upper Saddle River, NJ: Prentice Hall, p. 200-206, 2000.
- MOLZ, F. J. et al. Comment on “investigating the Macrodispersion Experiment (MADE) site in Columbus, Mississippi, using a three-dimensional inverse flow and transport model” by Heidi Christiansen Barlebo, Mary C. Hill, and Dan Rosbjerg. *Water Resources Research*, v. 42, n. 6, p. 1–5, 2006.
- MOLZ, F. J. Advection, Dispersion and Confusion. *Groundwater*, v. 54, n. 1, p. 2–3, 2015.
- MULLIGAN, C. N.; YONG, R. N. Natural attenuation of contaminated soils. *Environment International*, v. 30, n. 4, p. 587–601, 2004.
- NADIM, F. et al. Detection and remediation of soil and aquifer systems contaminated with petroleum products: An overview. *Journal of Petroleum Science and Engineering*, v. 26, n. 1–4, p. 169–178, 2000.
- NELSON, R. W. Evaluating the Environmental Consequences of Groundwater Contamination Location / Arrival Time and Location / Outflow Quantity Distributions for Steady Flow Systems. *Water Resources Research*, v. 14, n. 3, p. 416–428, 1978.
- OOSTERWOUD, M. et al. Variation in hydrologic connectivity as a result of microtopography explained by discharge to catchment size relationship. *Hydrological Processes*, v. 31, n. 15, p. 2683–2699, 2017.

ORGE, M. D. R. et al. Assessment of oil refinery waste on *Rhizophora mangle* L. Seedling growth in mangroves of Todos os Santos Bay, Bahia, Brazil. *Aquatic Ecosystem Health & Management*, v. 3, p. 471-477, 2000.

POOL, M.; DENTZ, M. Effects of Heterogeneity, Connectivity, and Density Variations on Mixing and Chemical Reactions Under Temporally Fluctuating Flow Conditions and the Formation of Reaction Patterns. *Water Resources Research*, v. 54, p. 186-204, 2018.

POOL, M.; POST, V. E. A.; SIMMONS, C. T. Effects of tidal fluctuations and spatial heterogeneity on mixing and spreading in spatially heterogeneous coastal aquifers. *Water Resources Research*, v. 51, p. 1570-1585, 2015.

POWERS, S. E. et al. The Transport and Fate of Ethanol and BTEX in Groundwater Contaminated by Gasohol. *Critical Reviews in Environmental Science and Technology*, v. 31, n. 1, p. 79-123, 2001.

RAMOS, D. T. et al. Biodiesel presence in the source zone hinders aromatic hydrocarbons attenuation in a B20-contaminated groundwater. *Journal of Contaminant Hydrology*, v. 193, p. 48-53, 2016.

REHFELDT, K. R.; BOGGS, K. M.; GELHAR, L. W. Field Study of Dispersion in a Heterogeneous Aquifer - 3. Geostatistical Analysis of Hydraulic Conductivity. *Water Resources Research*, v. 28, n. 12, p. 16, 1992.

RIVETT, M. O.; FEENSTRA, S.; CHERRY, J. A. A controlled field experiment on groundwater contamination by a multicomponent DNAPL: Creation of the emplaced-source and overview of dissolved plume development. *Journal of Contaminant Hydrology*, v. 49, n. 1-2, p. 111-149, 2001.

ROBERTS, P. V.; GOLTZ, M. N.; MACKAY, D. M. A Natural Gradient Experiment on Solute Transport in a Sand Aquifer - 3. Retardation Estimates and Mass Balances for Organic Solutes. *Water Resources Research*, v. 22, n. 13, p. 2047-2058, 1986.

SCHIRMER, M. et al. Influence of transient flow on contaminant biodegradation. *Groundwater*, v. 39, 2001.

SCHIRMER, M.; BUTLER, B. J. Transport behaviour and natural attenuation of organic contaminants at spill sites. *Toxicology*, v. 205, n. 3, p. 173-179, 2004.

SCHNEIDER, M. R. Intemperismo de fontes de contaminação em aquíferos impactados por derramamentos de gasolina e álcool e a influência sobre o risco à saúde humana. [s.l.] UFSC, 2005.

SEBOK, E. et al. Spatial variability in streambed hydraulic conductivity of contrasting stream morphologies: Channel bend and straight channel. *Hydrological Processes*, v. 29, n. 3, p. 458-472, 2015.

SINGH, R. N.; RAI, S. N.; RAMANA, D. V. Water table fluctuation in a sloping aquifer with transient recharge. *Journal of Hydrology*, v. 126, n. 3-4, p. 315-326, 1991.

SOGA, K.; PAGE, J. W. E.; ILLANGASEKARE, T. H. A review of NAPL source zone remediation efficiency and the mass flux approach. *Journal of Hazardous Materials*, v. 110, n. 1–3, p. 13–27, 2004.

SUDICKY, E. A.; ILLMAN, W. A. Lessons Learned from a Suite of CFB Borden History of the CFB Borden Site. *Ground water*, v. 49, n. 5, p. 630–648, 2011.

US CENSUS BUREAU. Economic Data of Gas Station Industry (2014). Disponível em: <<https://www.census.gov/econ/isp/sampler.php?naicscode=4471&naicslevel=4#>> Acesso em: Junho 2016

US EPA. United States Environmental Protection Agency. Underground Storage Tanks. Disponível em: <<https://www.epa.gov/ust/frequent-questions-about-underground-storage-tanks>> Acesso em: Abril 2016

VAN DER KAMP, G.; HAYASHI, M. Groundwater-wetland ecosystem interaction in the semiarid glaciated plains of North America. *Hydrogeology Journal*, v. 17, n. 1, p. 203–214, 2009.

WALKER, G. R. et al. Predicting aquifer response time for application in catchment modeling. *Groundwater*, v. 53, n. 3, p. 475–484, 2015.

WILSON, S. et al. Leaking Underground Storage Tanks and Environmental Injustice: Is There a Hidden and Unequal Threat to Public Health in South Carolina? *Environmental Justice*, v. 6, n. 5, p. 175–182, 2013.

ZHU, J.; SYKES, J. F. The influence of NAPL dissolution characteristics on field-scale contaminant transport in subsurface. *Journal of Contaminant Hydrology*, v. 41, n. 1–2, p. 133–154, 2000.

APÊNDICE A – Electronic supplementary material – Recharge estimation from discrete water-table datasets in a coastal shallow aquifer in a humid subtropical climate - Hydrogeology Journal

Fig. ESM1 - Transient cumulative groundwater balances: (a) scenario 1 with transient Sya for layer 1; (b) scenario 3; (c) scenario 4. Storage volume curves exhibit storage contribution to flow and discharge.

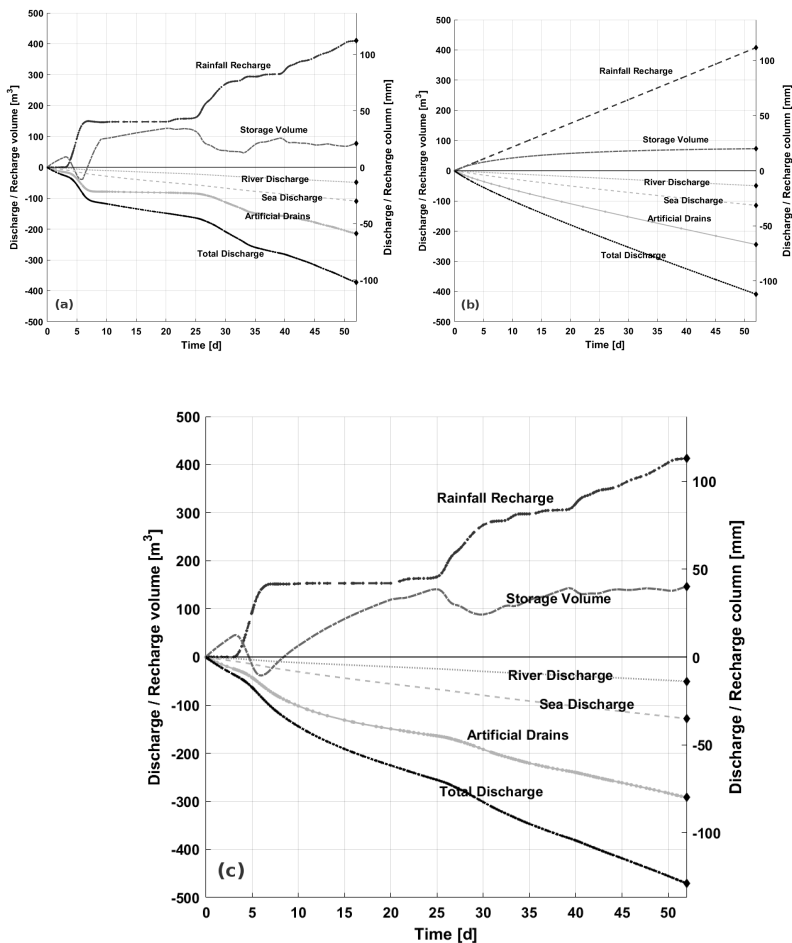


Fig. ESM2 - Combined plot showing water level fluctuations in the 51-day period. Dashed lines represent continuously monitored piezometer levels while solid lines are different scenarios. The bar plots show recorded precipitation (dark purple bars) and daily estimated recharge values (lilac bars). (a) Scenario 1 with transient Sya for layer 1; (b) scenario 3; (c) scenario 4.

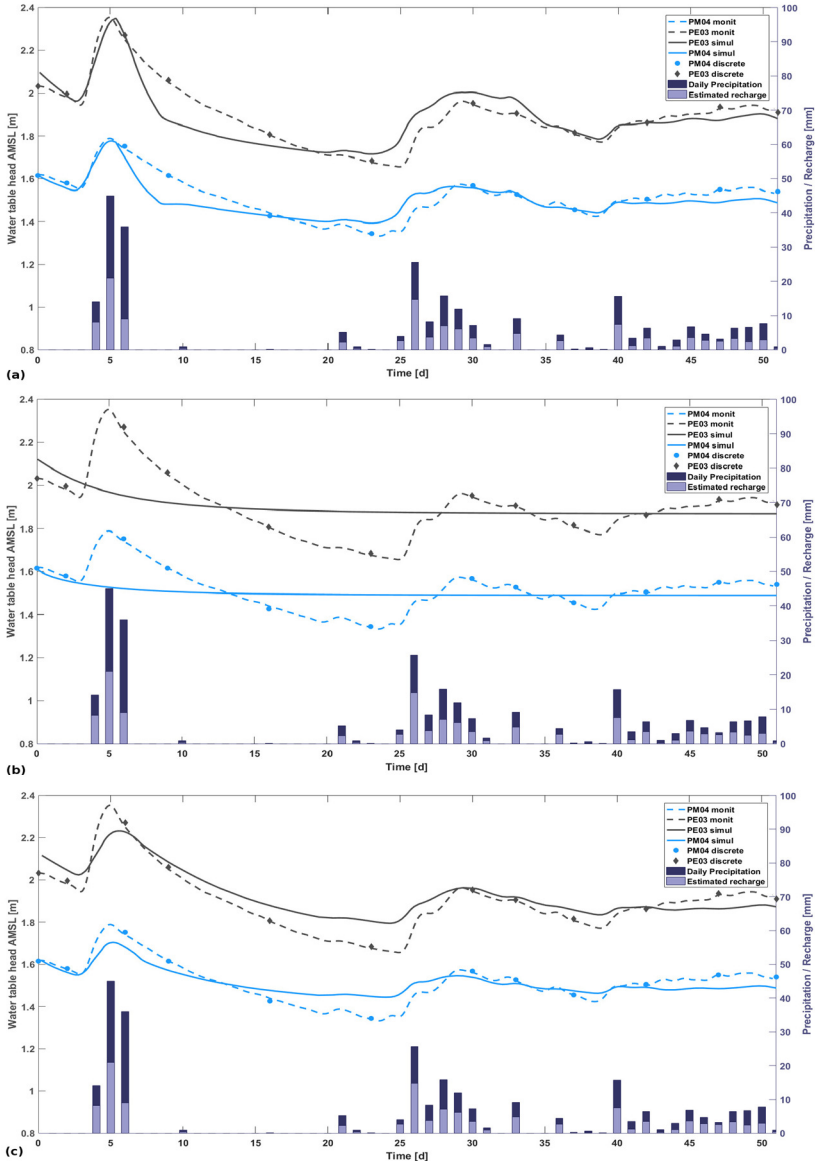
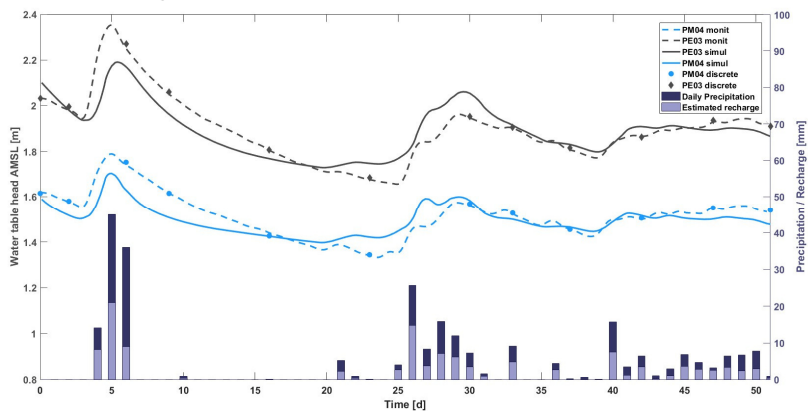


Fig. ESM3 - Combined plot showing water level fluctuations in the 51-day period. Dashed lines represent continuously monitored piezometer levels while solid lines are the scenario 2. Bar plot shows recorded precipitation (dark purple bars) and daily estimated recharge values (lilac bars)



APÊNDICE B – Supporting Information - Flow field dynamics and high ethanol content in gasohol blends enhance BTEX migration and biodegradation in groundwater – Journal of Contaminant Hydrology

Table S1 – Electron acceptors concentrations over time in E85 experimental site.

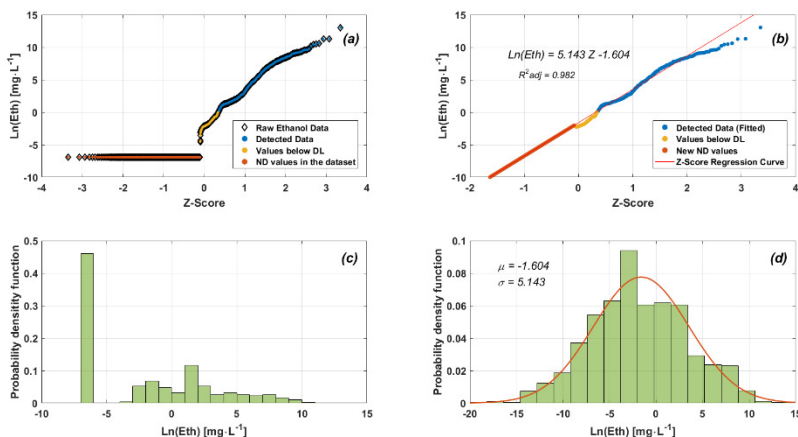
MW	Time [d]	Dissolved oxygen [mg L ⁻¹]	Nitrite [mg L ⁻¹]	Nitrate [mg L ⁻¹]	Fe II [mg L ⁻¹]	Sulfide [µg L ⁻¹]	Sulphate [mg L ⁻¹]	Methane [mg L ⁻¹]
MW-S	0	3.144 ± 0.886	ND	1.440 ± 0.187	NA	NA	2.129 ± 1.297	NA
MW-S	83	1.628 ± 0.593	1.453 ± 2.316	2.883 ± 0.426	5.958 ± 9.954	22.000 ± 9.940	2.268 ± 0.442	0.520 ± 0.188
MW-S	258	1.860 ± 1.456	0.045 ± 0.044	1.026 ± 0.713	1.216 ± 1.343	NA	2.437 ± 0.978	0.396 ± 0.147
MW-S	460	1.995 ± 2.122	ND	1.816 ± 0.959	0.100 ± 0.141	4.250 ± 7.361	3.459 ± 0.730	0.125 ± 0.024
MW-S	911	1.014 ± 0.338	ND	3.517 ± 1.705	1.036 ± 2.072	NA	3.390 ± 0.857	0.013 ± 0.001
MW-S	1161	2.446 ± 0.461	ND	2.735 ± 0.269	0.050 ± 0.100	3.600 ± 5.426	5.743 ± 1.666	ND
MW-S	1540	2.384 ± 1.207	ND	2.811 ± 1.059	0.548 ± 0.699	9.200 ± 12.624	3.889 ± 0.919	0.067 ± 0.003
MW-11	0	4.052 ± 0.345	ND	1.130 ± 0.581	NA	NA	2.041 ± 0.811	NA
MW-11	83	1.090 ± 0.726	ND	2.565 ± 0.459	6.542 ± 5.280	69.000 ± 46.943	1.594 ± 0.774	1.039 ± 0.395
MW-11	258	0.684 ± 0.337	0.039 ± 0.016	1.061 ± 1.056	20.280 ± 28.251	23.600 ± 25.216	0.809 ± 0.722	16.680 ± 4.181
MW-11	460	0.884 ± 0.542	ND	0.933 ± 1.144	6.980 ± 8.127	13.600 ± 15.794	1.426 ± 1.586	19.372 ± 5.069
MW-11	911	1.118 ± 1.231	ND	1.700 ± 1.763	4.048 ± 4.286	51.600 ± 56.102	3.209 ± 2.307	16.019 ± 4.441
MW-11	1161	1.966 ± 1.922	ND	3.507 ± 2.427	2.560 ± 3.521	41.000 ± 23.206	5.156 ± 2.827	2.303 ± 0.992
MW-11	1540	2.076 ± 1.180	ND	2.399 ± 0.718	0.248 ± 0.404	17.400 ± 16.548	3.329 ± 0.999	0.139 ± 0.067
MW-23	0	1.478 ± 0.311	0.016 ± 0.033	1.865 ± 1.151	NA	NA	2.557 ± 1.000	NA
MW-23	258	NA	NA	NA	NA	NA	NA	NA
MW-23	460	0.946 ± 1.050	0.085 ± 0.060	10.093 ± 12.186	3.346 ± 3.851	26.200 ± 51.901	1.462 ± 1.017	1.674 ± 2.345
MW-23	911	0.980 ± 1.126	ND	55.234 ± 67.572	5.304 ± 6.491	138.400 ± 156.587	4.627 ± 3.277	12.772 ± 10.942
MW-23	1161	1.662 ± 2.100	0.060 ± 0.008	44.829 ± 53.233	3.306 ± 4.329	24.000 ± 17.754	3.577 ± 2.436	3.524 ± 3.732
MW-23	1540	0.793 ± 0.180	ND	68.347 ± 91.902	1.930 ± 1.702	19.250 ± 15.594	3.031 ± 1.513	0.241 ± 0.179
MW-25	0	2.236 ± 0.658	ND	1.680 ± 0.607	NA	NA	2.503 ± 0.812	NA
MW-25	258	1.732 ± 0.900	ND	11.203 ± 9.647	ND	9.600 ± 7.605	4.519 ± 1.284	0.009 ± 0.001
MW-25	460	1.568 ± 1.859	ND	13.344 ± 17.133	8.198 ± 8.363	125.200 ± 198.939	1.995 ± 1.284	0.214 ± 0.141
MW-25	911	0.390 ± 0.220	ND	8.196 ± 15.202	47.460 ± 44.672	154.800 ± 136.743	2.768 ± 2.605	14.487 ± 7.471
MW-25	1161	1.346 ± 1.754	ND	14.242 ± 17.512	7.664 ± 6.433	190.600 ± 338.965	2.460 ± 2.832	12.777 ± 10.623

MW-25	1540	1.686 ± 1.930	ND	9.070 ± 18.141	3.232 ± 2.654	14.200 ± 5.810	10.012 ± 13.531	0.989 ± 1.296
-------	------	------------------	----	-------------------	------------------	-------------------	--------------------	------------------

ND: not detected; NA: not analysed.

In order to deal with a large amount of non-detected values (ND) in the dataset, means and standard deviations for each compound were calculated from a linear regression of expected normal scores (Z-Score), using the methodology by Gineval and Splitstone, (2003). An example of application with ethanol concentration series was showed in Fig. S1.

Fig. S1. – The ethanol concentration in a function of the Z-score (expected normal value), generated by the statistical procedure: (a) raw data before the transformation; (b) ND value transformation with the regression method; (c) probability density function (pdf) of raw data; (d) pdf histogram of data after the ND values transformation. The inset histograms show that the dataset became more regular following the treatment. Ln(Eth) refers to natural logarithm of dissolved ethanol concentration.



The cosolvency model was described by a logarithmic law:

$$\log(s_m) = \log(s_w) + \sigma f$$

where s_m is the compound solubility in the mixture, s_w is the compound solubility in water, f is the co-solvent volume fraction (ethanol) and σ is the cosolvency energy that accounts for the co-solvent capacity to solubilize the BTEXs. Detailed information about BTEX at the E85 site are summarized in Table S1

Table S2 – BTEX saturation concentrations in E85 experiment based on Raoult's Law and cosolvency logarithmic Law.

Compound	Solubility [mg L ⁻¹]	Relative Density	Gasohol Molar Fraction	Total Initial Mass [gr]	Cosolvency Energy	Saturation Concentr. [mg L ⁻¹]
Benzene	1750	0.8765	0.0113	200	0.7888	3421.6
Toluene	515	0.8669	0.0418	873	1.2144	1445.8
Ethylbenzene	152	0.867	0.0097	234	1.5488	567.0
Xylenes	158	0.865	0.0521	1254	1.5868	608.7

The integration of mass in every sampling event represents the zero-order moments of concentration. Mathematically, it was defined for the whole domain as follows:

$$M = \sum_{i=0}^N UV_i \times C_i \times e$$

where M is the total calculated mass, e is the total porosity, UV is the unit volume and C is the interpolated concentration. Subscript i refers to the elements with concentrations higher than boundary values of a plume. It worth stressing that the ratio between the interpolated mass and released mass of conservative tracer (bromide) represented the total error of the method and included interpolation approximation, bias in laboratory procedures, degradation processes, and compound offsite migration.

Table S3 – Detailed comparison of water level, recharge and BTEX concentration in the source zone during the first 90 days. AMSL indicates elevation above mean sea level.

SEs	Days from spill	N° Sampled Wells	Accum. Rain [mm.d ⁻¹]	AMSL Average Water Table Head [m]	Water Table Variation [cm]	Average BTEX Concentr. [µg.L ⁻¹]	N° FPS
SE-1	1	12	0.0	1.509	-3.0	266.1	0
SE-2	2	12	0.0	1.486	/	257.9	0
SE-3	5	12	28.3	1.550	+6.9	2264.9	0
SE-4	6	12	0.0	1.580	/	2965.9	0
SE-5	7	12	0.0	1.535	-1.5	1985.4	0
SE-7	20	17	139.2	1.934	+62.0	4388.7	1
SE-8	27	17	24.0	2.057	-4.7	6937.2	3
SE-10	42	17	56.9	1.971	+19.3	6731.9	7
SE-11	61	17	93	1.849	+16.7	8295.0	5
SE-12	76-85	20	77	1.789	-17.3	11655.8	9

In order to compare transients of flow field features and highlight differences between E24 and E85 sites, two figures were built on the temporal analysis of groundwater.

Fig. S2 – Temporal comparison of flow field features at E85 site: (a) bars shows daily recharge and numbers represent values above 60 mm; (b) exhibits water-table plane deviation from average direction, with zero degrees referring to the North direction; (c) is instantaneous seepage velocity, obtained from the Darcy's Law; (d) shows water-table levels above mean sea level for piezometers used in the triangulation process. Sampling events are underlined (blue dots).

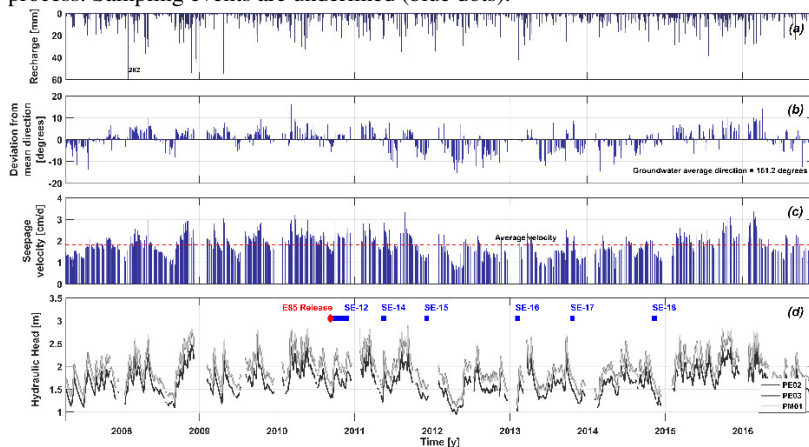


Fig. S3 – Temporal comparison of flow field features at E24 site: (a) bars shows daily recharge and numbers represent values above 60 mm; (b) exhibits water-table plane deviation from average direction in the area, with zero degrees referring to the North direction; (c) is instantaneous seepage velocity, obtained from the Darcy's Law; (d) shows hydraulic head records used in the triangulation process. Sampling events are underlined in (d) plot (blue dots).

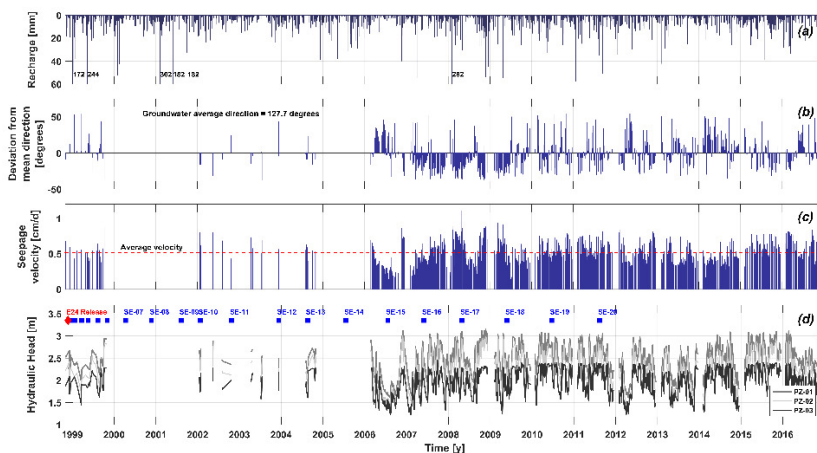


Table S4 - Metabolic characteristics of the microbial genera found in groundwater source-zone in E85 experimental site.

Genus	Class	Respiration	Substrates	References
<i>Candidatus koribacter</i>	Acidobacteriia	Nitrate or nitrite-reducer	Sugars, amino acids, alcohols, organic acids and cellulose,	Ward et al. (2009)
<i>Candidatus methanoregula</i>	Methanomicrobia	Methanogenic or anaerobic	Hydrogen, carbon dioxide	Bräuer et al. (2011, 2006), Imachi et al. (2008)
<i>Candidatus methyloirabilis</i>	Candidate division NC10	Anaerobic methanotroph, aerobic, nitrate and nitrite reduction	Methane	Wu et al., 2015; Kool et al., 2012; Ettwig et al., 2010
<i>Candidatus nitrososphaera</i>	Nitrososphaeria	Aerobic	Ammonia, nitrate, aminoacids, pyruvate, urea, cyanate	Spang et al., 2012
<i>Candidatus solibacter</i>	Acidobacteria	Nitrate or nitrite-reducer	Sugars, amino acids, alcohols, organic acids, cellulose, pectin	Ward et al. (2009)
DA 101	Spartobacteria	Aerobic	Amino acids	Brewer et al., 2016
<i>Geobacter</i>	δ -Proteobacteria	Iron-reducer, fermentative	Short-chain fatty acids, alcohols, monoaromatic compounds	Lovley et al., 1993; Cord-Ruwisch et al., 1998
<i>Gouta 19</i>	Nitrospira	Sulfate reduction	Chlorinated organic compounds, Aromatic compounds	Alfreider; Vogt; Babel, 2002, Müller et al., 2017
<i>Herbaspirillum</i>	β -Proteobacteria	Microaerophilic	Organic acids, sugars	Schmid et al., 2006
<i>Kaistobacter</i>	α -Proteobacteria	Aerobic	Aromatic compounds, organic compounds	Bardhan, 2010; Li et al., 2017; Kertesz et al., 2018
<i>Methanocella</i>	Methanobacteria	Methanogenic	H ₂ , CO ₂ , formate	Sakai et al., 2008; Sakai, Conrad, Imachi, 2014;
<i>Methanoregula</i>	Methanomicrobia	Methanogenic	H ₂ , CO ₂ ,	Bräuer et al., 2011; Bräuer et al., 2015
<i>Methanosaeta</i>	Methanomicrobia	Methanogenic	Acetate	Liu & Whitman, 2008; Rivière et al., 20090
<i>Methylobacter</i>	γ -Proteobacteria	Aerobic	Methane	Kallistova et al., 2013
<i>Mucilaginibacter</i>	Sphingobacteria	Aerobic	Sugars, organic acids	Männistö et al., 2010; Kämpfer et al., 2014
<i>Nevskia</i>	γ -Proteobacteria	Aerobic	Sugars, starch, cellulose, organic acids, ethanol, aminoacids, benzoate	Cypionka et al., 2006; Babenzien and Cypionka, 2015

<i>Nitrospira</i>	Nitrospira	Aerobic	Ammonia, nitrite	Kuypers, 2015; Madigan et al., 2011
<i>Opitutus</i>	Verrucomicrobiae	Anaerobic	Sugars	Chin, Leisack & Janssen, 2001
<i>Pantoea</i>	γ -Proteobacteria	Facultative anaerobic	Sugars and aromatic compounds	Brady et al., 2010; Vasileva-Tonkova & Gesheva, 2006
<i>Paracoccus</i>	α -Proteobacteria	Aerobic, facultative anaerobic	Sugars, organic acids, alcohols, amino acids	Kelly, Rainey & Wood, 2006
<i>Rhodoblastus</i>	α -Proteobacteria	Microaerophilic, or facultative anaerobic	Organic acids, alcohols	Imhoff, 2005
<i>Rhodoplanes</i>	α -Proteobacteria	Facultative	Organic acids	Okamura et al., 2009
<i>Sphingomonas</i>	α -Proteobacteria	Anaerobic, Sulfate-, nitrate-, thiosulfate-reducer	Organic acids, amino acids, alcohols	Pollock, 1993; Yabuuchi et al., 1990; Fang et al., 2007; Borde et al., 2003
<i>Syntrophobacter</i>	α -Proteobacteria	Anaerobic, fermentative	Propionate, lactate	McInerney, Stams and Boone, 2015
<i>Telmatospirillum</i>	α -Proteobacteria	Microaerophilic, or fermentative	Organic acids, ethanol	Sizova et al. (2007), Schmidt et al. (2016), Hausmann et al. (2016)
<i>Treponema</i>	Spirochaetia	Anaerobic or microaerophilic	Carbohydrates, amino acids	Abt et al. (2013), Krieg et al. (2010), Paster et al. (1991)
WCHB1-05	Anaerolineae	Anaerobic	Aromatic hydrocarbons, organochlorides, organic matter, lipids	Allen et al., 2007, Penfield, 2017, Petropoulos et al., 2018, Dojka et al., 1998

APÊNDICE C – Supporting Material - Numerical modelling as a tool to develop a conceptual hydrogeological model – Unpublished

Table SM1 – Details of field experiments in the Ressacada Farm

NAME	SOURCE AREA	EXP AREA	Nº MULTI LEVEL WELLS	EXP. SURFACE	RELEASE DATE	COLLECTION EVENTS
MNA_E24	(1 x 1,5) x 1,5m – 100 Lt	1	51	460 m ²	12/1998	21
MNA_E85	(1 x 1,5) x 0,25m – 200Lt	3	50	365 m ²	09/2010	18
MNA_D50	(1 x 1) x 1m – 40 Lt	1	32	72 m ²	12/2000	11
MNA_D100	(1 x 1) x 1m – 20 Lt	1	33	72 m ²	12/2000	15
MNA_B20	(1 x 1) x 1,5m – 100 Lt	3	47	310 m ²	06/2008	11
MNA_B100	(1 x 1) x 1,5m – 100 Lt	3	47	310 m ²	06/2008	11
BAA_B20	(1 x 1) x 1,7m – 100 Lt	3	42	310 m ²	07/2010	11
BAN_E25	(1 x 1) x 1m – 100 Lt	3	65	390 m ²	12/2004	17
BAS_E10	(1 x 1) x 1,6m – 100 Lt	3	58	585 m ²	05/2009	9
BAF_B20	(2 x 1,5) x 1,4m – 100 Lt	3	30	180 m ²	02/2014	7
BFM_B100	(1 x 2) x 1,8m – 100 Lt	3	30	180 m ²	02/2014	5

Table SM2 – Design information of piezometers in the Ressacada Farm

NAME	NOMINAL DEPTH (ATUAL)	GROUND ELEVAT.	WELL ELEVAT.	FILTER (TOP-BOTTOM)	MONITOR. DATE	POSITION	CONDITION/RELIABILITY
PE01	4.5 (4.5)	2.83	3.48	2.5-4.5 m	26/02/2007	Area III	Good
PE02	4.5 (4.5)	3.23	3.66	2.5-4.5 m	26/02/2007	Area III	Good
PE03	4.5 (3)	3.36	3.96	2.5-4.5 m	26/02/2007	Area III	Good
PE04	15 (13.45)	3.37	3.49	12-14 m	30/03/2007	Area III	Partially clogged
PE06	32 (26)	3.05	3.37	21-31 m	26/02/2007	Area III	Partially clogged
PE07	16 (10)	2.73	??	11-13 m	13/04/2007	Area III	Clogged/Bury
PM01	4.5 (4.4)	3.25	3.79	2.5-4.5 m	26/02/2007	Area III	Good
PM02	4.5 (4.4)	3.32	3.93	2.5-4.5 m	26/02/2007	Area III	Good
PM03	4.5 (2.95)	3.17	3.73	2.5-4.5 m	26/02/2007	Area III	Damaged
PM04	4.5 (4.4)	2.42	3.02	2.5-4.5 m	26/02/2007	Area III	Good
PM05	4.5 (4.35)	3.31	3.88	2.5-4.5 m	26/02/2007	Area III	Good
PM06	4 (2.65)	2.98	3.11	2-4 m	13/04/2007	Area III	Partially clogged
PM07	3 (2.16)	2.28	2.58	1-3 m	26/08/2016	Area III	Partially clogged
PM10	3 (2.5)	3.34	3.52	1-3 m	26/08/2016	Area III	Good
PM18	3 (2.15)	2.68	3.02	1-3 m	26/02/2007	Area III	Good
PZ01	16 (15)	3.01	3.45	10-15 m	26/02/2007	Area III	Good
PZ02	15 (10.85)	2.96	3.24	5-10 m	26/02/2007	Area III	Good
PZ03	15 (7.3)	3.23	3.18	5-10 m	22/03/2007	Area III	Damaged
PZ04	15 (15)	3.26	3.38	10-15 m	26/08/2016	Area III	Good
PZ05	2 (1.9)	3.08	3.73	ponteira	13/04/2007	Area III	Clogged/Bury
PZ07	2.5 (2.3)	3.09	3.31	ponteira	13/04/2007	Area III	Damaged
PZ08	2 (2)	3.04	3.42	ponteira	13/04/2007	Area III	Damaged
PZ-1	2.5 (2.6)	2.90	3.27	ponteira	02/07/1998	Area I	Good
PZ-2	3 (2.85)	3.09	3.56	ponteira	02/07/1998	Area I	Good
PZ-3	2.5 (2.5)	2.38	2.68	ponteira	02/07/1998	Area I	Good
PZ-4	1.5 (1.5)	2.38	2.63	ponteira	02/07/1998	Area I	Clogged/Bury
PZ-6	2 (1.8)	3.22	3.52	ponteira	22/11/2000	Area I	Good
PZ-7	1.5 (1.45)	3.16	3.49	ponteira	22/11/2000	Area I	Good
PZ-8	1.5 (1.15)	3.00	3.30	ponteira	22/11/2000	Area I	Partially clogged
PZ-9	1 (1)	2.98	3.30	ponteira	22/11/2000	Area I	Partially clogged
CCA1	1.5 (1.5)	3.171	3.521	ponteira	12/2011	Farm	Good
CCA2	1.5 (1.5)	2.451	2.761	ponteira	12/2011	Farm	Good
CCA3	1.5 (1.5)	2.429	2.759	ponteira	12/2011	Farm	Damaged

CCA4	1.5 (1.5)	3.200	3.460	ponteira	12/2011	Farm	Good
CCA5	1.5 (1.5)	3.500	3.765	ponteira	12/2011	Farm	Damaged
CCA6	1.5 (1.5)	2.800	3.060	ponteira	12/2011	Farm	Damaged
CCA7	1.5 (1.5)	3.400	3.690	ponteira	12/2011	Farm	Damaged
CCA8	1.5 (1.5)	3.083	3.413	ponteira	12/2011	Farm	Damaged
CCA9	1.5 (1.5)	3.600	4.000	ponteira	12/2011	Farm	Damaged
CCA10	1.5 (1.5)	3.500	3.745	ponteira	12/2011	Farm	Damaged
CCA11	1.5 (1.5)	3.467	3.777	ponteira	12/2011	Farm	Good
CCA12	1.5 (1.5)	3.465	3.865	ponteira	12/2011	Farm	Damaged
CCA13	1.5 (1.5)	3.356	3.626	ponteira	12/2011	Farm	Good
CCA14	1.5 (1.5)	3.300	3.870	ponteira	12/2011	Farm	Damaged
CCA15	1.5 (1.5)	3.306	3.586	ponteira	12/2011	Farm	Good
CCA16	1.5 (1.5)	3.100	3.470	ponteira	12/2011	Farm	Good
R1	3 ^b	1.037	3.407 ^a	staff gauge	18/05/2016	Pond	Good
R2	3 ^b	0.805	3.407 ^a	staff gauge	18/05/2016	Pond	Good
R-L	3 ^b	0.083	3.407 ^a	staff gauge	18/05/2016	Pond	Stolen

^a the equipment elevation for the staff (head) gauges is referred to the local elevation reference in the Ressacada Farm

^b the depth represents the nominal length of the aluminum staff (3 m) installed in the surface reservoirs

Fig. SM1 – Details of Farm Creek characterization

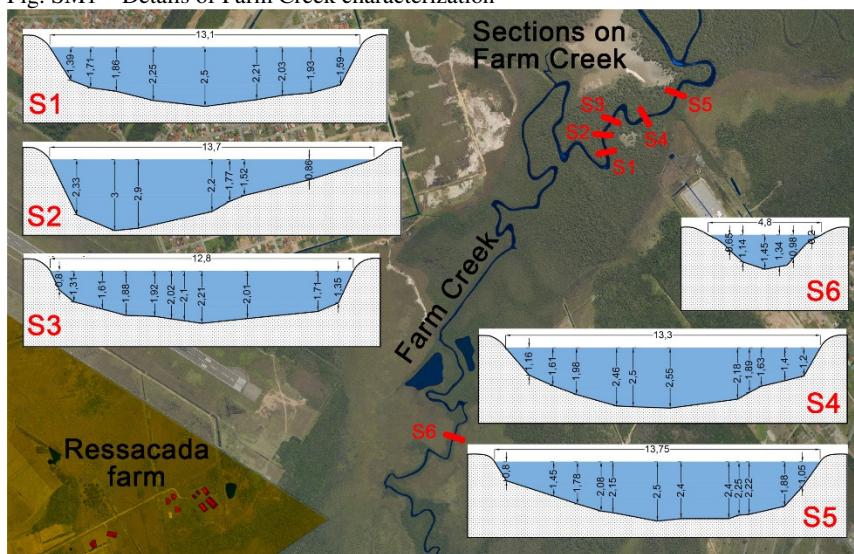


Table SM3 – Complete results of Slug Test campaigns

WELL NAME	1 ST CAMP. 2004	2 ND CAMP. ^a 2005		3 RD CAMP. ^b 12/2016		4 TH CAMP. ^b 04/2017	
		(Hvorsev)	(Bower-Rice)	(Hvorsev)	(Bower-Rice)	(Hvorsev)	(Bower-Rice)
PE01	2.12E-03	1.34E-04	1.00E-04	1.25E-03	1.41E-03	1.00E-03	6.70E-04
PE02	3.92E-03	5.11E-04	4.27E-04	1.68E-03	1.83E-03	1.52E-03	1.09E-03
PE03	1.53E-03	4.45E-04	3.70E-04	1.20E-03	1.60E-03	9.41E-04	6.12E-04

PE04	1.76E-03					3.30E-03	3.60E-03		1.82E-03	1.53E-03
PE06	1.85E-03					2.00E-03	2.80E-03		2.65E-03	2.05E-03
PE07	6.93E-04					1.20E-03	1.34E-03		1.23E-03	9.15E-04
PM01	9.55E-04	7.87E-04	6.68E-04			1.48E-03	2.00E-03		1.23E-03	9.40E-04
PM02	2.03E-03	1.44E-03	1.15E-03			5.55E-03	7.50E-03		4.81E-03	3.17E-03
PM03		1.00E-03	8.08E-04			1.00E-04	1.50E-04		1.27E-04	7.72E-05
PM04	8.98E-03	6.64E-03	5.84E-03			1.10E-02	1.66E-02		1.15E-02	8.85E-03
PM05	8.56E-04	3.32E-04	2.56E-04			5.50E-04	7.60E-04		4.42E-04	2.96E-04
PM06	1.34E-04					2.15E-02	3.30E-02			
PM07						6.93E-04	9.16E-04		1.38E-04	1.20E-04
PM10						1.79E-03	2.45E-03		9.79E-04	8.60E-04
PM18						1.60E-02	1.82E-02			
PZ01	6.64E-03					9.55E-03	1.49E-02		1.08E-02	9.33E-03
PZ02	3.21E-03					2.54E-03	4.12E-03		2.73E-03	2.01E-03
PZ03	3.48E-04					5.00E-04	8.13E-04		7.27E-05	6.94E-05
PZ04						4.82E-03	8.51E-03		4.50E-03	3.54E-03

^a detailed information about equipment and methods available in Lage (2005)

^b test executed by the author, employing automatic water-level loggers and interpreted with Winslug® software (Serendip)

Table SM4 - Statistics of hydraulic head records from piezometers

Name	N° val	% Val.	Mean	Median	Min	Max	Var.	Std. Dev.	Skewness	Kurtosis
PE01	834	71	1.61±0.01	1.61	0.93	2.26	0.06	0.25	-0.06±0.08	-0.24±0.17
PE02	856	72.9	1.71±0.01	1.69	0.96	2.58	0.09	0.3	0.24±0.08	-0.14±0.17
PE03	871	74.1	2.03±0.01	2.01	1.19	2.98	0.12	0.34	0.14±0.08	-0.31±0.17
PE04	811	69	2.49±0.01	2.47	0.62	3.35	0.13	0.36	-0.05±0.09	0.10±0.17
PE06	831	70.7	1.80±0.01	1.79	1.03	2.6	0.07	0.27	0.12±0.08	-0.11±0.17
PE07	795	67.7	1.63±0.01	1.64	0.99	2.31	0.06	0.24	0.05±0.09	-0.25±0.17
PM01	871	74.1	2.03±0.01	2.01	0.84	2.98	0.13	0.37	0.14±0.08	-0.23±0.17
PM02	866	73.7	1.70±0.01	1.69	0.97	2.52	0.08	0.28	0.13±0.08	-0.14±0.17
PM03	866	73.7	1.69±0.01	1.68	0.95	2.54	0.08	0.28	0.08±0.08	-0.31±0.17
PM04	831	70.7	1.59±0.01	1.58	0.91	2.27	0.06	0.25	-0.01±0.08	-0.21±0.17
PM05	934	79.5	1.97±0.01	1.96	1.14	2.93	0.12	0.34	0.21±0.08	-0.25±0.16
PM06	795	67.7	1.79±0.01	1.78	1.12	2.65	0.07	0.27	0.36±0.09	-0.13±0.17
PM18	831	70.7	1.62±0.01	1.61	0.92	2.37	0.07	0.27	0.12±0.08	-0.21±0.17
PZ01	828	70.5	1.76±0.01	1.75	1.04	2.8	0.08	0.28	0.25±0.08	0.07±0.17
PZ02	831	70.7	1.78±0.01	1.77	1.06	2.65	0.08	0.29	0.21±0.08	-0.11±0.17
PZ03	817	69.5	1.97±0.01	1.94	1.04	3.23	0.13	0.36	0.63±0.09	0.69±0.17
PZ05	812	69.1	2.94±0.01	3.01	2.26	3.66	0.07	0.27	-0.35±0.09	-0.37±0.17
PZ07	721	61.4	1.91±0.01	1.86	1.21	3.37	0.14	0.37	0.93±0.09	1.30±0.18
PZ08	841	71.6	1.70±0.01	1.69	0.89	3.08	0.08	0.28	0.37±0.08	1.24±0.17
PZ-1	954	81.2	2.35±0.01	2.39	1.4	3.06	0.14	0.38	-0.36±0.08	-0.59±0.16
PZ-2	948	80.7	2.14±0.02	2.2	0.63	3.42	0.31	0.55	-0.16±0.08	-0.68±0.16
PZ-3	953	81.1	1.98±0.01	2.01	0.69	2.54	0.1	0.31	-0.45±0.08	-0.63±0.16
PZ-4	946	80.5	1.96±0.01	1.99	-0.09	2.53	0.1	0.31	-0.68±0.08	0.95±0.16
PZ-6	905	77	2.36±0.01	2.42	1.09	3.7	0.19	0.44	-0.37±0.08	-0.36±0.16
PZ-7	875	74.5	2.30±0.01	2.29	1.45	3.6	0.12	0.35	0.32±0.08	-0.39±0.17
PZ-8	896	76.3	2.39±0.01	2.38	0.8	3.04	0.14	0.37	-0.26±0.08	-0.39±0.16
PZ-9	847	72.1	2.30±0.01	2.26	1.57	2.96	0.07	0.27	0.34±0.08	-0.11±0.17
CCA1	51	-	2.20±0.01	2.04	2.021	3.071	0.07	0.260	NaN	NaN
CCA2	51	-	1.66±0.01	1.631	1.241	2.381	0.11	0.325	NaN	NaN
CCA3	45	-	1.62±0.01	1.569	1.249	2.399	0.09	0.293	NaN	NaN
CCA4	50	-	2.18±0.01	2.050	1.910	3.070	0.08	0.289	NaN	NaN
CCA5	45	-	2.43±0.01	2.305	2.245	3.765	0.10	0.319	NaN	NaN
CCA6	45	-	1.96±0.01	1.950	1.570	2.710	0.05	0.232	NaN	NaN
CCA7	45	-	2.76±0.01	2.800	2.170	3.470	0.15	0.390	NaN	NaN
CCA8	45	-	2.45±0.01	2.413	1.903	3.063	0.11	0.331	NaN	NaN
CCA9	45	-	2.99±0.01	3.020	2.505	4.000	0.12	0.346	NaN	NaN

CCA10	45	-	2.75±0.01	2.765	2.230	3.565	0.13	0.364	NaN	NaN
CCA11	47	-	2.80±0.01	2.767	2.277	3.417	0.13	0.361	NaN	NaN
CCA12	40	-	2.96±0.01	2.955	2.395	3.865	0.16	0.397	NaN	NaN
CCA13	50	-	2.79±0.01	2.746	2.176	3.446	0.14	0.377	NaN	NaN
CCA14	45	-	2.87±0.01	2.880	2.370	3.870	0.16	0.405	NaN	NaN
CCA15	51	-	2.57±0.01	2.561	2.086	3.326	0.12	0.340	NaN	NaN
CCA16	51	-	2.40±0.01	2.350	1.940	3.100	0.11	0.330	NaN	NaN

Fig. SM2 – Comparison of dynamic viscosity effects on plume fingering

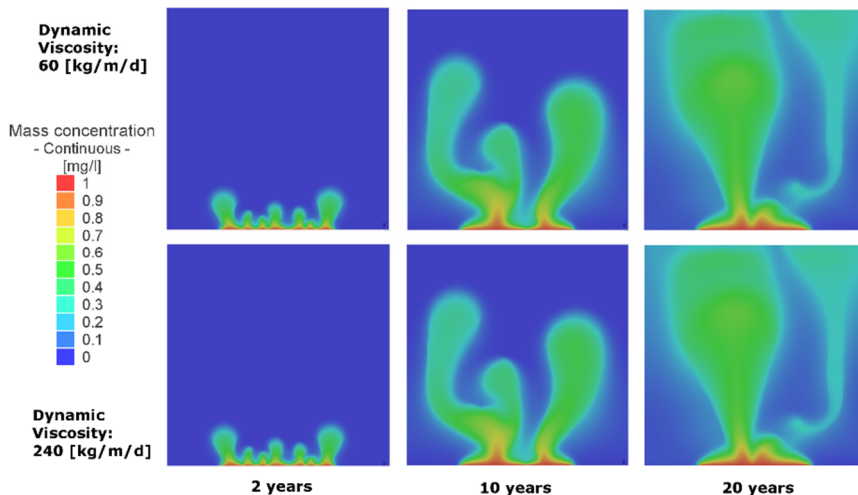
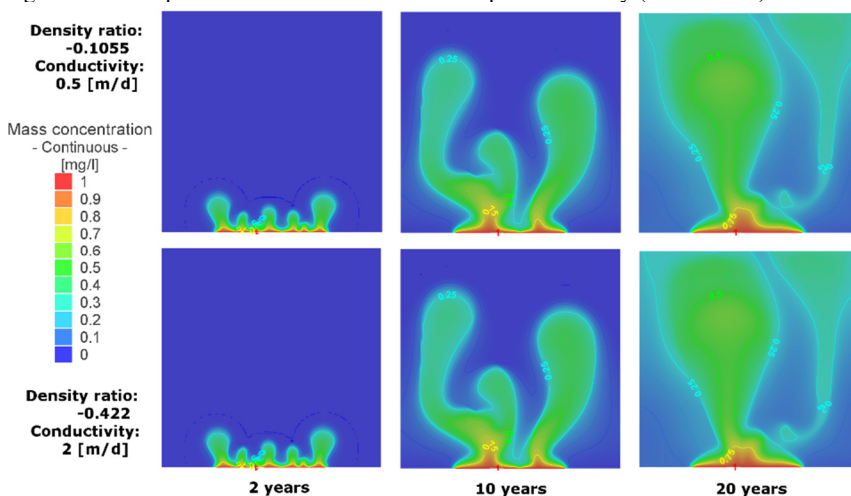


Fig. SM3 – Comparison of two test with the same plume velocity (constant Ra)



Finally we provide commands, developed in Python 2.7, to interpolate head time-series from piezometers along boundary nodes in a 3D FEM model, creating a .pow file with BC for every node over the time.

```
## VarInterpBC.py (beta_release) - Author: Fabrizio Rama - 05/04/2018

# import libraries
import sys; import os; import numpy as np; import pandas as pd; import xlrd; import xlwt;
import time; import calendar; import datetime; sys.path.append(r'C:\Program Files\DH\2017\FEFLOW 7.1\bin64');
import ifm; import scipy; from scipy.interpolate import griddata; import matplotlib.pyplot as plt;
import xml.etree.ElementTree as ET

# define locations on the drive
femdir = r'E:\AtWork\feflow\femdata'
importexportdir = r'E:\AtWork\feflow\import-export'
resultsdir = r'E:\AtWork\feflow\results'

#change directory and open fem (doc)
os.chdir(femdir)
fem = 'Transient_E85-fem'
doc = ifm.loadDocument(fem)
#change directory
os.chdir(importexportdir)

# Load xls created with matlab: file contains datavector,datetime,
# and measures of the vertex,only in the studied period,with no NAN
# load a dataframe with pandas library
file_loc = r'E:\AtWork\matlab\piezoE85.xlsx'
xls = pd.ExcelFile(file_loc)
df1 = pd.read_excel(xls, 'Piezo')

# load a workbook with xlrd library
workbook = xlrd.open_workbook(file_loc)
sheet = workbook.sheet_by_index(1)

## anticlockwise organization of piezometers (columns) starting from PE03 (PE03/PE02/PM01)
data = [[sheet.cell_value(r, c) for c in range(sheet.ncols)] for r in range(sheet.nrows)] #importa per righe

# some useful definitions
def zerolist(n):
    listofzeros = [0] * n
    return listofzeros

def roundTime(dt=None, roundTo=60):
    """Round a datetime object to any time laps in seconds
    dt : datetime.datetime object, default now.
    roundTo : Closest number of seconds to round to, default 1 minute.
    Author: Thierry Husson 2012 .
    """
    if dt == None : dt = datetime.datetime.now()
    seconds = (dt.replace(tzinfo=None) - dt.min).seconds
    rounding = (seconds+roundTo/2) // roundTo * roundTo
    return dt + datetime.timedelta(0,rounding-seconds,-dt.microsecond)
# print roundTime(dt,roundTo=30*60)

def XLSgen_toFEFLOW(filename, aba, varnum, list1, list2, list3, list4, list5, list6):
    """Spreadsheet writing with TS_ID for every transient head BC, assigned to
    every node of the domain
    Author: Fab 2018.
    """
    book = xlwt.Workbook()
    sh = book.add_sheet(aba)
    n=0
```

```

col_name = ['ID','X','Y','Z','Node','TS_ID']
list=[list1,list2,list3,list4,list5,list6]
# col2_name = 'X'
# col3_name = 'Y'
# col4_name = 'Z'
# col5_name = 'Node'
# col6_name = 'TS_ID'
for i in range(varnum):
    sh.write(0, i, col_name[i])
# sh.write(0, 1, col2_name)
# sh.write(0, 1, col2_name)
for i in range(varnum):
    for m, e1 in enumerate(list[i], n+1):
        sh.write(m, i, e1)
# for m, e2 in enumerate(list2, n+1):
# sh.write(m, 1, e2)
book.save(filename)

# -----
# TIME SERIES IMPORT from excell and matlab: IMPORTANT variable order, PE03/PE02/PM01 anticlockwise,
# to maintain validity in line 250: h_tuple
# variables estimation: TIMEPROG, DATEHEAD, HYDHEAD
hydhead={}
# datehead={}
datehead=[]
pzcol=[8,9,10]
for i in range(len(data)):
    temp=[]
    dt = datetime.datetime(int(data[i][0]),int(data[i][1]),int(data[i][2]),
                           int(data[i][3]),int(data[i][4]))
    for c in pzcol:
        temp.append(data[i][c])
    hydhead[i]=temp
# datehead[i-1]=dt #se volessi un dictionary invece di una list
datehead.append(dt)

#progressive time from spill (t=0) with approximated values (days)
timeprog=[]
for t in range(len(datehead)):
    dist=datehead[t]-datehead[0]
    tx = int(round(dist.total_seconds()/datetime.timedelta(days=1).total_seconds()))
    timeprog.append(tx)

timestep=range(len(timeprog))

# -----
# FEFLOW EXPORT
# start importing nodes from all selections (saved files xml from FEFLOW),
# in a dictionary of array and a dictionary of list, and save them in separated files.
# selection needed: all_bounds (all slices), boundary (just slice1), segmentAB, segmentBC, segmentCA,
# vertex (3 points in this case) and, A (PE03), B (PE02), C (PM01) separated
# A, B, C choice have to be made anticlockwise (nuple: AB, BC, CA)
node_solut_d = {}
selections = ['all_bounds', 'boundary', 'segmentAB', 'segmentBC', 'segmentCA', 'vertex', 'A','B','C']

for chars in selections:
    tree = ET.parse(chars + '.xml')
    root = tree.getroot()
    xml = []
    for r in root.findall('range'):
        st_node = r.get("start")
        sp_node = r.get("end")
        xml.append((st_node, sp_node))
    xml = np.array(xml)
    xml = xml.astype(np.int)
    temp = []
    for i in range(len(xml)):

```

```

    for i in range(xml[i,0],xml[i,1]):
        temp.append(i)

node_solut_d[chars] = np.array(temp)
np.savetxt(resultsdir + r'\list-'+ chars + '.sel', node_solut_d[chars], fmt= '%i', header='nodes')

#if you prefer we can do also a list of list instead of a dictionary of lists
node_solut_l = {}
for chars in selections:
    node_solut_l[chars] = np.ndarray.tolist(node_solut_d[chars])

# obtain info about position of nodes of the fem by ifm
X0=doc.getOriginX()
Y0=doc.getOriginY()
Z0=doc.getOriginZ()

# Create dictionaries with spatial information
Xcoord = {}
Ycoord = {}
Zcoord = {}
for chars in selections:
    temp=[]
    temp2=[]
    for n in node_solut_l[chars]:
        temp=doc.getX(n)
        temp2.append(temp)
    Xcoord[chars]=temp2
for chars in selections:
    temp=[]
    temp2=[]
    for n in node_solut_l[chars]:
        temp=doc.getY(n)
        temp2.append(temp)
    Ycoord[chars]=temp2
for chars in selections:
    temp=[]
    temp2=[]
    for n in node_solut_l[chars]:
        temp=doc.getZ(n)
        temp2.append(temp)
    Zcoord[chars]=temp2

# Notes:
# the methodology works for streight boundaries, where max distance is equal to distance between
# vertex, for curve boundaries we must estimate maxdist as sum of distances between each node
# and proportionally integrate the nodes
# useful: doc.getBorderNode(0,78) to get ordinated nodes
# ordina A, B, C sempre antiorario, con coppie ordinate di valori da interpolare AB, BC, CA

#-----
# variables estimation: SOLUT_HEAD, SOLUT_ID (list with ID of slice 1 for all nodes),
# SOLUT_ALL (dict of all nodes with all time steps)
solut_all={}
segments=['segmentAB', 'segmentBC', 'segmentCA']
# sorted lists of temp variable used in loop for
vertX=[Xcoord['A'][0],Xcoord['B'][0],Xcoord['C'][0]]
vertY=[Ycoord['A'][0],Ycoord['B'][0],Ycoord['C'][0]]
maxdist_seg = [np.sqrt((Xcoord['B'][0] - Xcoord['A'][0])**2 + (Ycoord['B'][0] - Ycoord['A'][0])**2),
               np.sqrt((Xcoord['C'][0] - Xcoord['B'][0])**2 + (Ycoord['C'][0] - Ycoord['B'][0])**2),
               np.sqrt((Xcoord['A'][0] - Xcoord['C'][0])**2 + (Ycoord['A'][0] - Ycoord['C'][0])**2)]
iniz_seg = np.zeros(len(maxdist_seg))
# nested loops in time and space to create an organized list of list of BCs information
for t in timestep:
    head=hyhead[t]
    solut_head=zerolist(len(Ycoord['all_bounds']))
    solut_id=zerolist(len(Ycoord['all_bounds']))
    # sorted lists of temp variable used in loop for
    h_tuple = [[head[0],head[1]], [head[1],head[2]], [head[2],head[0]]]

```

```

#create empty dictionaries
interp_segm={}
interp_dist={}

for chars in segments:
    segX = np.asarray(Xcoord[chars])
    segY = np.asarray(Ycoord[chars])
    xval = vertX[segments.index(chars)]
    yval = vertY[segments.index(chars)]
    xinit = xval * np.ones(len(segX))
    yinit = yval * np.ones(len(segY))
    nodes_dist = np.sqrt((segX - xinit)**2 + (segY - yinit)**2)
    segm = np.array([iniiz_seg[segments.index(chars)], maxdist_seg[segments.index(chars)]])
    hd = np.array([h_tuple[segments.index(chars)]])
    f = scipy.interpolate.interp1d(segm, hd, kind='linear', axis=-1, copy=True,
        bounds_error=True, assume_sorted=False)

    interp_head = f(nodes_dist) # use interpolation function returned by `interp1d`
    #np.transpose(interp_head)
    # interp_head = f(nodes_dist).T
    interp_dist[chars]=np.ndarray.tolist(nodes_dist)
    interp_segm[chars]=np.ndarray.tolist(interp_head[0])
# plt.plot(interp_dist[chars],interp_segm[chars], 'o')
# plt.ylabel(chars+'head')
# plt.show()

for n in Xcoord[chars]:
    indices = [i for i, x in enumerate(Xcoord['all_bounds']) if x == n]
    for i in indices:
        solut_head[i] = interp_segm[chars][Xcoord[chars].index(n)]
        solut_id[i] = node_solut_[chars][Xcoord[chars].index(n)] # control list da fare meglio

solut_all[t]=solut_head

# -----
# POW writing with proper information for every node, with data organized per time (cronological)
e=('END','')
temp2=[]
for n in range(len(node_solut_['boundary'])):
    for t in timestep:
        temp=solut_all[t][n]
        temp2.append(temp)
    open(r'E:\AtWork\feflow\import+export\BCinterp_syn.pow', 'a').close()
    f_handle = file(r'E:\AtWork\feflow\import+export\BCinterp_syn.pow', 'a')
    np.savetxt(f_handle, np.c_[np.asarray(timeprog),np.asarray(temp2)], fmt= ['%i','%7.3f'],
        header = str(solut_id[n]+1), newline='\n')
    np.savetxt(f_handle, [e], fmt= ['%s','%s'], newline='\n')
    f_handle.close()
    temp2=[]
f_handle = file(r'E:\AtWork\feflow\import+export\BCinterp_syn.pow', 'a')
np.savetxt(f_handle, [e], fmt= ['%s','%s'], newline='\n')
f_handle.close()

# -----
# Spreadsheet writing with TS_ID assigned for every node
# hdom = 3.35
list1 = range(1,len(solut_id)+1)
list2 = Xcoord['all_bounds']
list3 = Ycoord['all_bounds']
list4 = Zcoord['all_bounds']
# list4 = np.ndarray.tolist(np.ones(len(solut_id))*hdom)
list5 = np.ndarray.tolist(np.array(node_solut_['all_bounds']+1))
list6 = np.ndarray.tolist(np.array(solut_id)+1)

XLGen_toFEFLOW('ts_id_BC.xls','ts_id_ALL',6,list1,list2,list3,list4,list5,list6)

```